

Master's Thesis in Materials,  
Energy and Nanotechnology

**Kristian Blindheim Lausund**

**Adhesion between  
ceramic and composite  
materials for use in  
lightweight ballistic  
armour**

**DEPARTMENT OF  
CHEMISTRY/PHYSICS**  
Faculty of Mathematics and Natural  
Sciences

**UNIVERSITETET I OSLO**

**01/06/2014**





# Adhesion between ceramic and composite materials for use in lightweight ballistic armour

Kristian Blindheim Lausund



Master's thesis at the Department of Chemistry/Physics  
Faculty of Mathematics and Natural Sciences

UNIVERSITY OF OSLO

01/06/2014

© Kristian Blindheim Lausund

2014

Adhesion between ceramic and composite materials for use in lightweight ballistic armour

Kristian Blindheim Lausund

<http://www.duo.uio.no/>

Print: Reprosentralen, Universitetet i Oslo

# Preface

The work with this thesis has been carried out at the Norwegian Defence Research Establishment (FFI), under the supervision of Bernt Brønmo Johnsen, PhD, and Professor Finn Knut Hansen, and is a part of a master's degree in materials energy and nanotechnology (MENA) at the department of chemistry/physics at the University of Oslo (UiO). The work was done during the autumn of 2013 and the spring of 2014. The topic for the thesis was suggested by Bernt Brønmo Johnsen, PhD.

I would like to thank Bernt Brønmo Johnsen, PhD, Professor Finn Knut Hansen and Dennis Bo Rahbek, PhD, for all their help and support, their good ideas, and the interesting discussions we have had.

I would also like to thank Lasse Sundem-Eriksen and Ole Andreas Haugland for their help with ballistic testing, Ferdinand Männle and Britt Sommer at SINTEF for their help with the POSS particles, Spyros Diplas for help with the XPS measurements and Sissel Jørgensen for comments on the interpretation of the XPS results, Grazyna Jonski for help with the profilometer measurements, Helge Steen and Runar Wattum Hansen for help with microscopy, Kai Frode Grythe for help with the plasma chamber, and, last but not least, all other FFI employees who have been very welcoming and supportive and who have taken a genuine interest in my work.

Kjeller, June 2014.



Kristian Blindheim Lausund



# Summary

In lightweight ballistic armour, ceramics are used in combination with a metal or composite backing plate. These two materials are adhesively bonded to each other. This work has been focused on improving this adhesive bond with the aim to improve the ballistic performance of these lightweight armours.

Several different surface treatments were applied to an alumina ceramic in order to attempt to improve the adhesion to a glass fibre reinforced polyester composite. The ceramic was washed in acetone before surface treatments. The surface treatments which were used are sandblasting, plasma treatment, silane treatment, and chromic sulphuric acid etching, some of which were tested in multiple variants. The surfaces were analysed after the various treatments using techniques such as XPS, contact angle measurements, profilometer measurements, and SEM.

After surface treatment, the adhesive bond between the two materials was made by heating the materials in a vacuum oven and allowing the composite matrix to melt and cover the ceramic. Test samples were made in order to perform peel tests, and thus record the level of adhesion for each surface treatment. These peel tests show that the as-received sample has a peel strength of 9.6 N/mm, while the peel strength for the control sample which was washed in acetone was 13.8 N/mm. The silane treated sample showed the highest level of adhesion with a peel strength of 19.9 N/mm. The silane treatment was done in several ways. The peel strength above is for the most effective silane treatment process.

In addition to the various surface treatments, an attempt was made to improve the adhesion by adding a type of nanoparticles called POSS particles to the composite matrix near the interface between the materials. The technique used for adding the POSS particles to the system should be reconsidered since the current technique lowered the peel strength of the control samples drastically. The POSS particles themselves improved the adhesion at low concentrations, but higher concentrations caused brittleness in the composite matrix.

Ballistic tests were also performed. Test samples were made of the as-received, acetone washed and silane treated ceramics tiles bonded to the composite material. In addition, some ceramic tiles were wrapped in a Teflon film before adding the composite in order to test a system with no adhesion between the materials. The ballistic tests were done at different projectile velocities, and the amount of delamination between the materials, and the amount of damage to the ceramic were compared for the different samples.

Based on the results from these ballistic tests, it is believed that there is an ideal level of adhesion in order to get the optimum ballistic performance. However, more work has to be done in order to confirm this.



# Contents

Preface .....	v
Summary .....	vii
1 Introduction .....	1
2 Literature survey and theory.....	3
2.1 Ballistic protection systems.....	3
2.2 Relevant materials .....	5
2.2.1 Metals .....	6
2.2.2 Ceramics .....	7
2.2.3 Composites .....	8
2.3 Adhesion theory .....	9
2.4 The effect of adhesion on the ballistic performance .....	10
2.5 Surface treatment of ceramic.....	12
2.6 Techniques for surface analysis .....	16
2.6.1 Contact angle.....	16
2.6.2 Profilometer.....	19
2.6.3 X-ray photoelectron spectroscopy.....	21
2.6.4 Scanning electron microscopy.....	23
2.7 Mechanical tests of adhesive bond performance.....	25
2.7.1 Butt joint test .....	25
2.7.2 Double lap shear joint test.....	25
2.7.3 Peel test .....	26
2.8 Ballistic tests .....	28
2.9 Effects of nanoparticles on ballistic performance .....	31
3 Experimental .....	33
3.1 Materials and chemicals .....	33
3.1.1 Ceramics.....	33
3.1.2 Composite.....	37
3.1.3 Silane coupling agent .....	40
3.1.4 Polyhedral oligomeric silsesquioxanes .....	40
3.2 Surface treatment.....	41
3.2.1 Sandblasting .....	42
3.2.2 Plasma treatment .....	42

3.2.3	Silane treatment.....	43
3.2.4	Chromic sulphuric acid etch.....	44
3.3	Surface analysis.....	45
3.3.1	Contact angle.....	45
3.3.2	Profilometer.....	46
3.3.3	X-ray photoelectron spectroscopy.....	47
3.3.4	Scanning electron microscopy.....	48
3.4	LPET films containing POSS.....	49
3.5	Production of test samples.....	54
3.6	Peel testing .....	59
3.7	Ballistic testing .....	61
3.8	Microscopy.....	63
4	Results.....	65
4.1	Surface analysis.....	65
4.1.1	Contact angle measurements.....	72
4.1.2	Profilometer measurements.....	76
4.1.3	X-ray photoelectron spectroscopy.....	83
4.2	Peel tests.....	91
4.2.1	Effect of silane concentration.....	96
4.2.2	Failure modes .....	98
4.3	Ballistic tests .....	102
4.4	POSS particles.....	107
5	Discussion.....	117
5.1	Adhesion.....	117
5.1.1	As-received.....	117
5.1.2	Acetone washed.....	118
5.1.3	Sandblasted.....	119
5.1.4	Plasma treated .....	119
5.1.5	Silane treated .....	120
5.1.6	Chromic sulphuric acid etched.....	122
5.1.7	Contact angle measurements.....	123
5.2	Ballistic properties.....	124
5.3	Interlayer film of POSS/LPET .....	126

5.3.1	Acetone washed ceramic .....	126
5.3.2	Silane treated ceramic .....	127
6	Conclusion.....	129
7	Future work .....	131
	References .....	133
Appendix A	XPS tables .....	I
Appendix B	XPS survey scans .....	V
Appendix C	Profilometer images .....	IX
Appendix D	Peel test results .....	XIX
Appendix E	Composite data sheet.....	XXXI
Appendix F	Silane data sheet .....	XXXIII
Appendix G	Projectile data sheet.....	XXXV
Appendix H	Investigation of small particles on the alumina surface .....	XXXVII



# 1 Introduction

In order to protect personnel and vehicles from ballistic threats one has to use armour of some kind. Traditionally, armours were made from metal. However, more recently complex, lightweight ballistic protection systems have been developed. These are often made of ceramics combined with metal or fibre-composite backing materials. The materials are arranged in a layered structure.

A lot of work has been done on testing various materials for making these ballistic protection plates. However, not nearly as much work has been put into finding out how the adhesion between these materials affects the performance of the plates. This thesis is aimed at studying methods for improving this adhesion, and studying the effects of improved adhesion on the ballistic performance of armour plates. The level of adhesion after these surface treatments was found by a peel test, where the force needed to peel the composite off the ceramic was measured.

In this thesis, alumina ceramic plates were used together with a glass fibre-reinforced polyester composite backing material. The ceramic tiles were exposed to various surface treatments in order to improve the adhesion between the two materials, and the surfaces were analysed with techniques such as XPS, contact angle measurements, profilometer measurements, and SEM.

When the level of adhesion was found for each surface treatment, ballistic tests were performed. The tests were done on plates where the ceramic had been exposed to different surface treatments, in order to investigate the effect the adhesion had on the ballistic performance.

In addition, nanoparticles were added to the interlayer between the ceramic and the composite in various concentrations. This was done in order to investigate what effect they would have on the adhesion. The nanoparticles were used in combination with two of the surface treatments. The nanoparticles which were used are a type of polyhedral oligomeric silsesquioxane (POSS) particles.

This thesis consists of seven chapters. After this introduction comes Chapter 2 which is a literature survey combined with some theory. In that chapter, previous work done on adhesion and ballistic armour will be presented alongside some important theory. In Chapter 3, the experimental methods, and the materials that were used are described. The

results from all experimental tests are presented in Chapter 4, and these are discussed further in Chapter 5. The conclusion of the thesis is given in Chapter 6, and some ideas for future work are listed in Chapter 7.

## **2 Literature survey and theory**

In order to get a better understanding of the previous work done with respect to adhesion between ceramic materials and composite materials for use in ballistic protection systems, a literature survey was conducted.

The aim was to get an overview of relevant materials, methods for surface treatment of the ceramic, methods for surface analysis of the treated surfaces, and methods for testing adhesion. In addition to this, it is interesting to learn more about the effects of adding nanoparticles to the adhesive with respect to adhesion, and what effects increased adhesion has on the ballistic performance of the armour plates.

This chapter will be focused on presenting what was found by this literature survey along with some theory on lightweight ballistic armour, mechanisms for adhesion, and the theory behind some relevant techniques.

### **2.1 Ballistic protection systems**

As mentioned above, lightweight ballistic armours combine a ceramic tile with a metal or fibre composite backing material. The ceramics make up the main body of the armour, and have a few important functions to fulfil. When the projectile hits the ceramic, it will break apart and be eroded by the hard ceramic. Crushing of the ceramic takes place, and the ceramic distributes the force of the projectile over a larger area of the backing plate. When the ceramic is struck by the projectile, cracks propagate through the ceramic in such a way that they form a hard cone in front of the projectile as shown in the illustration in Figure 2.1. This cone is pushed in front of the projectile, and strikes a larger area of the backing plate compared to the original area of the ceramic which was struck by the projectile [1;2].

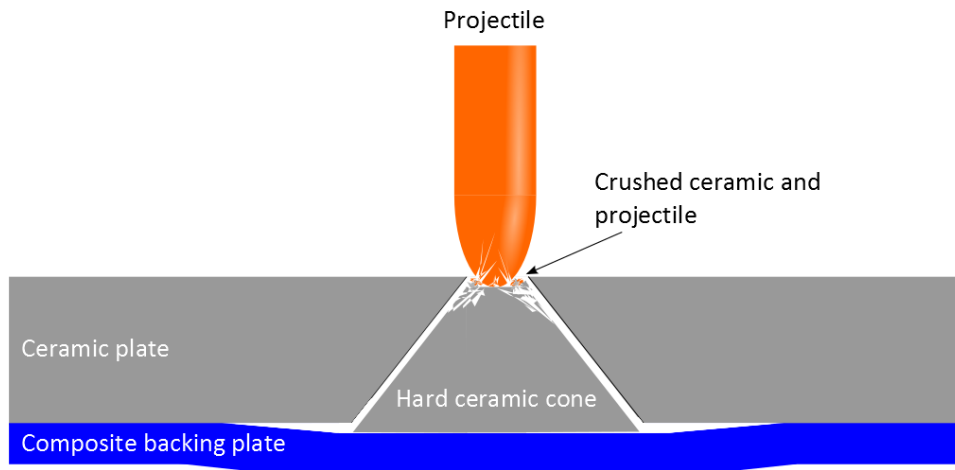


*Figure 2.1: Illustration of a ceramic armour with a composite backing plate being struck by a projectile. The projectile is crushed when it hits the ceramic, and eroded by the hard ceramic. The ceramic also distributes the force of the impact over a larger area by forming a cone in front of the projectile.*

However, as discussed by Sarva et al. [3] and Sherman [1], the ceramic plate needs to be confined by either metals or composite materials in order to reduce the damage to the ceramic. Confinement by a material with similar acoustic impedance is favourable since that reduces the amount of stress waves that are reflected back into the ceramic at the interface between the materials, and reduces the breakage of the ceramic. The confinement can be in the form of a backing plate, or both a backing plate and a strike face plate. The backing plate is important not only because of confinement, but also because it takes the load of the ceramic cone and prevents fragments of the projectile or the ceramic from penetrating through the armour.

There are also vests that only consist of many layers of a tough fibre such as Kevlar® (poly aramid) or similar fibres, and not ceramics or metals. These are very lightweight and flexible, but can only protect against splinters, slower projectiles, knife stabs, etc.

When protecting personnel, the layered armour is usually made into one relatively large plate, which covers vital organs, and placed into a vest. One such plate for use in a bulletproof vest is shown in Figure 2.2. There are also other ways to arrange the protective plates, such as in Dragon skin® where small, round tiles are placed in an overlapping way in order to protect the user at the same time as it is flexible, but these are less common. [4].



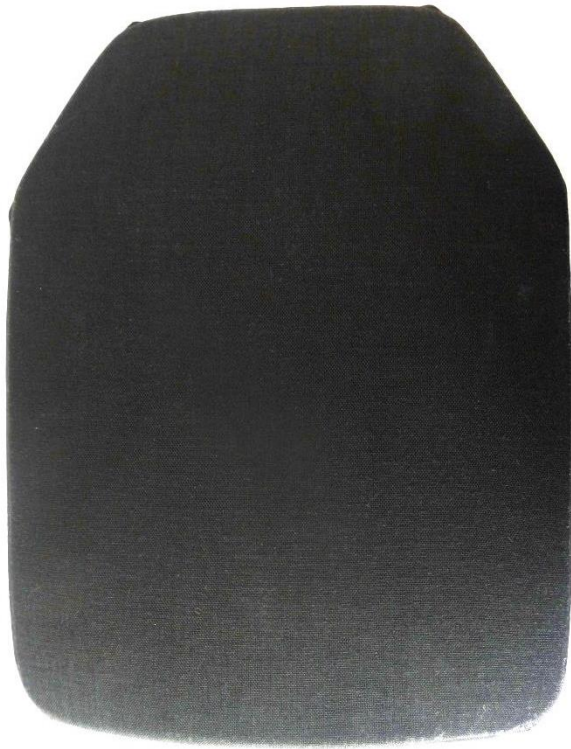


*Figure 2.2: A ceramic insert plate for bulletproof vests.*

## **2.2 Relevant materials**

In ballistic protection systems, there are a number of factors to consider with respect to the choice of materials. The materials should have high bulk and shear moduli, high yield stress, and high dynamic tensile stress [5;6]. The reasons for these requirements are to prevent large deformations, to insure a high resistance to failure, and to prevent rupture in the material when exposed to tensile stress waves.

It is important that the final product has the lowest possible area density in order to be as light as possible. This is of course most important when protecting personnel but it is also important for vehicle protection.

Traditionally, metals have been used as armour materials because they meet most of the demands for a good protective material. They do, however, fail when it comes to the area density. In order to overcome the weight issue of metals, other materials and combinations of materials have been used. Today, ceramics are frequently used for protection but due to their low dynamic tensile strength, they are used in combination

with either metals or polymer-based composite materials. In the work done by Übeyli et al. [7] and Zaera et al. [5], ceramic armour plates with a metal backing plate were investigated, while Navarro et al. [2] performed their work on ceramic armour with a fibre-based composite as backing plate. Grujicic et al. [8] chose a system where a polymer-matrix composite was used as backing plate as the basis for simulations.

An adhesive such as epoxy or polyurethane is often used in order to bond the materials together [7]. However, adhesives will not be used in this work, and will therefore not be discussed in much detail.

### **2.2.1 Metals**

Metals have, as before mentioned, traditionally been used as protective materials, and they are still used for many applications such as vehicles. In addition to serving as armour, they will provide structural strength. The most frequently used metal for armour is steel. This is among other reasons because of its high toughness and hardness, and because it is relatively cheap to produce. Steel, however, is not the only metal used for armour [9].

Different alloys of aluminium have been used for armour because of their low density which is about a third of that of steel. These alloys perform as well as certain types of steel against shell fragments but not as well against armour-piercing ammunition. Some titanium alloys also perform well as armour. However, they are quite expensive and they tend to fail by adiabatic shear. Some research is also done on the use of magnesium for armour [9;10].

As mentioned above, metals do not meet the demands for area density. This is a problem especially with respect to personnel protection, it is simply too heavy to carry a massive steel plate around for protection. Still, metals are useful as backing plates for complex armour systems.

In the work done by Übeyli et al. [7], the aluminium alloy AA2024 was used as backing plate. The aim of this particular study was to investigate the ballistic behaviour of laminated armour systems of aluminium and alumina. In order to investigate the role of the adhesive in layered armour of metal and ceramic, Zaera et al. [5] modelled a system

where low calibre projectiles hit an alumina tile backed by an aluminium plate. Gao et al. [11] investigated the ballistic performance of ceramic armour systems with different adhesives, and used alumina bonded to an armour steel backing plate.

## 2.2.2 Ceramics

This thesis will focus on ceramic armour with a glass fibre reinforced polymer composite backing plate. However, there are a large number of possible material combinations. In this section, the most common ceramics for armour are presented.

Some commonly used ceramics for ballistic protective systems are alumina ( $\text{Al}_2\text{O}_3$ ), boron carbide ( $\text{B}_4\text{C}$ ) and silicon carbide ( $\text{SiC}$ ). There are also other ceramic materials that are used for armour such as titanium diboride ( $\text{TiB}_2$ ), tungsten carbide ( $\text{WC}$ ), or silicon nitride ( $\text{Si}_3\text{N}_4$ ). Navarro et al. [2] also used a mix of boron nitride ( $\text{BN}$ ) and silicon nitride ( $\text{Si}_3\text{N}_4$ ). Some of these ceramics have disadvantages that make them less used for ballistic protection. For example, titanium diboride has a rather high density which makes it perform worse than boron carbide and silicon carbide per weight, it is also quite expensive compared to the others. Tungsten carbide has an even higher density and is very brittle. Silicon nitride performs approximately as well as titanium diboride per weight, and is therefore outperformed by silicon carbide and boron carbide [12;13].

According to Kaufmann et al [14], alumina is outperformed by boron carbide and silicon carbide in a depth of penetration test. This is due to the fact that silicon carbide and boron carbide show higher values for almost all relevant material properties. They have higher Young's modulus and shear modulus; higher compressive strength and Hugoniot elastic limit; and they are harder. The bulk modulus and the density are higher for alumina.

Even though silicon carbide and boron carbide are more effective at stopping a projectile, alumina will mostly be used for this thesis. One reason is that we need to be able to cut ceramic plates into smaller pieces for the experimental work. The two other ceramics are much harder, and are therefore more difficult to handle when it comes to cutting. In addition to this, alumina is relatively cheap. Boron carbide, for example, is ~16 times more expensive than alumina.

### 2.2.3 Composites

Composites used for armour are usually fibre-reinforced, polymer-based materials. Different polymer matrices and reinforcement fibres are used.

The first composite materials used for armour were typically enforced by either E-glass fibres or nylon fibres [15]. These fibres are still used today because they are relatively cheap but it is more common to use so called high-performance polymeric fibres such as poly-aramid (Kevlar®, Twaron®, Technora®), ultra high molecular weight poly ethylene (UHMWPE)(Dynema®, Spectra®) and to some extent poly-benzobis-oxazole (PBO)(Zylon®).

An example of composite materials that are used for armour is aramid fibres in a vinyl ester matrix. This was used by Navarro et al. [2], who also used a composite where a fabric of polyethylene was embedded in a polyethylene matrix. These fibres are most likely UHMWPE such as Dynema® or Spectra®. Naik et al. [16] modelled a glass fibre composite in order to see how well it performed against a ballistic impact on its own, and Guden et al. [17] did a series of experiments on a woven glass fibre reinforced epoxy-based composite for use as a backing material in ceramic armour plates, in order to find its failure mechanisms.

The arrangement of the fibres in the composite may also affect the properties of the composite. The most common ways of arranging the fibres are to weave them into fabrics, or to arrange them in a 0°/90° cross-ply which means stacking layers where all the fibres lay parallel to each other in such a way that one layer is rotated 90° compared to the layers above and below [15].

In this thesis, a woven glass fibre composite was used. This material is described further in Section 3.1.2.

## 2.3 Adhesion theory

There are quite a few different mechanisms of adhesion. This section will be focused on describing the most common adhesion mechanisms. Some of the most important mechanisms are mechanical interlocking, physical adsorption, chemical bonding, electrostatics, diffusion, and acid-base interaction [18;19].

The first and perhaps simplest mechanism is *mechanical interlocking*. It is based on the fact that surfaces normally have micro-sized pores or other irregularities into which the adhesive can penetrate, resulting in mechanical interlocking. In order for this to occur, the adhesive must wet the surface, and it must have a sufficiently low viscosity in order to penetrate the pores in a reasonably short amount of time [18;19].

The second mechanism is *physical adsorption*. This is caused by intermolecular forces at the interface. These forces include Van-der-Waals forces and hydrogen bonds. It is important that the adhesive is able to wet the surface in order to achieve good contact. This mechanism can explain how adhesion can be achieved without the adhesive penetrating pores on the surface of the material it is bonding to [18;19].

*Chemisorption* is in many ways an extension of the physical adsorption. When the adhesive makes strong chemical bonds (covalent, ionic or metallic) to the bonded surface in addition to the Van-der-Waals forces of the physical adsorption, the adhesion strength can increase a lot. One reason why surface treatments before adhesion can be very effective, is because they can change the surface chemistry and enable chemisorption [18;19].

*Electrostatic attraction* as a mechanism for adhesion is slightly controversial. Some say it is not significant. However, it is useful to explain some special cases of adhesion [18]. The theory is that electrostatic charges with opposite sign on the two surfaces attract each other and cause adhesion. The electrostatic charges are formed by the electrical double layer [18;19].

*Diffusion* can also be an important factor for adhesion. This is especially true for adhesion between polymer materials which have the ability to diffuse into each other in such a way that the molecule chains get entangled. In order to enable diffusion, the two polymers must be solvable in each other, the temperature must be above the glass transition

temperature  $T_g$  for the polymers, and the polymers must not be too crystalline or too highly cross-linked [18;19].

*Acid-base interaction* is also a mechanism which could be of importance especially when considering adhesion between a polymer and an oxide surface. It is based on the Bronsted acid-base concept, and can be used to predict to what extent hydrogen bonds form between the polymer and the oxide in a moist environment [18].

An important concept to grasp when discussing adhesion is the *weak boundary layer*. This is not a mechanism of adhesion, but rather a theory for explaining failure. If the interface between the materials which are bonded together is contaminated, the adhesion can be lower than expected. This is because the contaminant may have a low coherent strength, causing the fracture to propagate inside the contamination layer. This is the reason why bonding to a moist surface is difficult [18;20].

It is important to realise that not all mechanisms are present in every case of adhesion. For example, if the adhesive is unable to penetrate pores in the substrate surface, mechanical interlocking will not happen. In order to improve the adhesion, it is important to facilitate as many of the mechanisms as possible. This can be done by altering surface chemistry and topology by different surface treatment which will be described further in Section 2.5.

## **2.4 The effect of adhesion on the ballistic performance**

As will be discussed in Section 2.5, there are many surface treatments which can improve the adhesion between the ceramic tile and the backing plate of an armour system. But before looking into that, the effect the improved adhesion has on the ballistic performance of the armour system will be discussed.

First off all, it is important to realise that when an adhesive layer is used in armour, its function is not only that of holding the two segments together. Using the “right” adhesive can be crucial since its function includes transferring shock waves from the ceramic to the backing plate in order to minimise the damage to the ceramic caused by the reflected

shock waves. In other words, it is important to match the acoustic impedance of the ceramic, adhesive layer and backing plate as good as possible. In order for shock waves to propagate from the ceramic to the backing plate, it is important that the adhesive bond does not break apart. If the damage of the ceramic is minimised, and the adhesive bond to the backing plate is intact, the armour may be able to better withstand multiple hits [21]. This has been shown by Harris et al. [22] who arranged many small, hexagonal, silicon carbide tiles onto a backing plate. With no surface treatments on the tiles, all tiles detached from the backing plate upon impact, while only a few tiles detached when the surface was laser treated to improve adhesion. This allowed the armour to better withstand multiple hits. In addition to laser treatment, some SiC tiles were re-fired in air. While these showed improved adhesion, they did not show improved ballistic performance. This may be because there is a rather small increase in the tensile strength [21].

Two common adhesives used in armour are epoxy and polyurethane. Epoxy is stiffer than polyurethane, and is able to transfer 13 times the energy from ceramic to backing plate compared to polyurethane [21]. However, the adhesive bond between polyurethane and the ceramic is less likely to break apart, which makes polyurethane the preferred adhesive of the two. Harris et al. [21] argue that increasing the bond strength between epoxy and ceramic could improve ceramic armour. They tested a few different surface treatments which are further described in Section 2.5.

Übeyli et al. [7] also found that there was less debonding when polyurethane was used instead of epoxy. However, they did not find any significant difference in ballistic performance between armours where these two adhesives were used.

As will be further described in Section 2.9, Gao et al. [11] improved both the adhesion strength and the acoustic impedance of their adhesive by adding nano SiO<sub>2</sub> particles. This reduced the damage during ballistic testing which shows that increased adhesion strength, increased acoustic impedance or both will improve the ballistic performance.

Both Grujicic et al [8] and Zaera et al. [5] have done simulations on the adhesive layer between the ceramic and the backing plate in ballistic armour, but their focus has not been so much on the adhesive strength as on the adhesive layers ability to transfer the energy to the backing plate.

## 2.5 Surface treatment of ceramic

There are many different surface treatments that can improve the adhesion between the ceramic and the composite. This is done by altering the chemistry, the topology and/or the wettability of the surface.

The work done by Harris et al. [21] shows that surface treatment can be very effective in this respect. They chose to test two different surface treatments of silicon carbide (SiC): reheating of the ceramics to 1100° C in air for 1.5 hours, and a laser treatment with a 248 nm krypton fluoride (KrF) laser. Both of these surface treatments oxidised the SiC surface, and the laser treatment also altered the topography of the surface. With these two surface treatments they managed to increase the tensile strength of the adhesion relative to the control by 18% and 109%, respectively (from 11 MPa (control) to 13 MPa (reheating) and 23 MPa (laser)), and the shear strength was increased by 417% and 367%, respectively (from 6 MPa (control) to 31 MPa (reheating) and 28 MPa (laser)). The tensile strengths in this article were found by the butt joint method, and the shear strength was measured by the double lap shear joint method. Both of these test methods will be described further in Section 2.7. This example shows that some sort of surface treatment prior to adhesive bonding may dramatically improve the adhesion strength. Surface treatments can also be done to the composite, but for this thesis, the focus was on surface treatments of the ceramics.

The surface treatments studied in this thesis are done in order to increase the adhesion between the ceramic and the backing plate, but achieving better adhesion is important in other fields as well. When repairing broken teeth, dentists often use ceramics to restore teeth. These ceramic teeth need to be glued to the remaining part of the tooth, and in order to optimise the adhesion, a lot of research has been done on different surface treatments of the ceramic. These surface treatment methods may be useful in the production of ceramic armour as well.

One of the methods that are investigated for use in dental restoration is etching the surface of the ceramic before gluing. Typically hydrofluoric acid (HF) is used with varying concentration [23-26]. According to Madani et al [23], etching with a too concentrated of HF solution (9.5%) gave worse results than etching with a more diluted HF solution (5%). Other acids are sometimes also used for etching the ceramic.

Another method for surface treatment is abrasion. This is also studied for use in dental restoration. Typically, the surface is grit blasted with alumina particles of different sizes



in order to affect the topology of the surface. The size of the alumina particles can typically be between 1  $\mu\text{m}$  and 110  $\mu\text{m}$  [23-27]. Of all the surface treatment studied by Madani et al [23], grit blasting proved most effective. Grit blasting, or other kinds of abrasion may be beneficial in the production of ceramic armour as well.

In the many of the above mentioned articles related to dental restoration, the ceramic surface was silane treated. In some of these articles, this silane treatment was done in addition to the other surface treatments that were used [23;24;26], and in some articles it was investigated as a separate surface treatment [24;27]. Treating surfaces with a silane as a method to improve adhesion has been used and studied by many others as well, and the aim of this treatment is to enable chemical bonding, or chemisorption, between the adhesive and the substrate.

Johnsen et al. [28] used the  $\gamma$ -glycidoxypropyltrimethoxysilane (GPS) in order to treat an aluminium surface, and then further treated the surface with different amines in order to study the chemical bonds that were made between the silane film and the amines. They also treated the GPS film with an epoxy adhesive, and found that the epoxy forms covalent bonds to the GPS film. Rodrigues and Broughton [29] used the same silane in order to treat boron carbide particles before they were used as filler in an epoxy matrix. The strength of this boron carbide reinforced epoxy-based composite material was improved by somewhere between 24% and 56% by silane treating the boron carbide particles before they were mixed into the epoxy matrix. Tanoglu et al. [30] used two different silanes to treat alumina before gluing it to a vinyl-ester resin this resulted in higher mechanical properties. They also observed that they got a uniform silane coating only with the right concentration of silane in the solution used for the treatment. In their case, a concentration of 0.35-0.50 wt% proved most effective, and higher concentrations gave non-uniform coatings.

Another common surface treatment for aluminium is etching in chromic-sulphuric acid, such as the FPL-etch (named after the Forest Products Laboratory). This technique was used in the aerospace industry on aluminium with very good results. Not only did it oxidise organic contaminants, it also affected the aluminium electrochemically [20]. As mentioned by Johnsen et al. [28], scientists have been trying to replace FPL-etch due to the fact that the hexavalent chromium is quite toxic, and thereby an environmental hazard. One alternative is the silane treatment. However, the FPL-etch, and other chromic-sulphuric acid treatments can be investigated for use in armour production, if only for comparison. It has already been used in armour production, for example by Übeyli et al. [7], who used the FPL-etch on the aluminium backing plate before gluing this to the alumina ceramic.

Even though the FPL-etch is developed for aluminium treatment, it may be effective on alumina ceramic as well. The surface of aluminium metal is covered in aluminium oxide, so it should be chemically quite similar to alumina. Even though the chromic-sulphuric acid may not electrochemically react with the alumina as it does with aluminium, it will certainly clean the surface thoroughly.

Treating the surface with plasma is also a way of increasing adhesion to the surface. Plasma is an ionised gas, and it affects the surface chemistry of the material by the interaction between the surface and the ions and electrons in the plasma. The plasma can be generated using many different gases. Originally noble gasses such as argon and xenon were used, but later many other gases such as nitrogen and oxygen have been used. [20].

There are many ways of producing plasma, and it can be produced at low pressure or at ambient pressure. A couple of the most common ways of producing plasma for surface treatment are Capacitively Coupled Plasma (CCP) and Inductively Coupled Plasma (ICP) [20;31]. Both of these methods work at low pressure, and need a radio frequency (RF) generator to work. The CCP-method consists of two metallic plates arranged like a capacitor with a RF electric field between them; typically this field has a frequency of 13.56 MHz [31]. In the ICP-method, a conductive coil is wrapped around a vessel. After the vessel has been evacuated, and the active gas has been added to the chamber, the RF-generator applies a signal to the coil in order to induce plasma in the vessel [20].

Asai et al. [32] treated AlN with an oxygen plasma, an aqueous solution of  $K_2O$  ( $B_2O_3$ ), and combinations of the two treatments in order to improve adhesion. Bujanda et al. [33] used plasma at atmospheric pressure as surface treatment of three different polymers and alumina in order to functionalize the surface and improve adhesion with good results.

A summary of all the surface treatments mentioned in this section, and the ceramics on which they were used is given in Table 2.1.

Table 2.1: An overview of the surface treatments mentioned in this section and the different ceramics on which they were used.

Surface treatment	Ceramic	Reference
Reheating in air	SiC	Harris et al. [21]
KrF laser	SiC	Harris et al. [21]
Etching with HF	Al <sub>2</sub> O <sub>3</sub>	Kim et al. [25] Madani et al. [23] Özcan et al. [26]
	Li <sub>2</sub> Si <sub>2</sub> O <sub>5</sub> ZrO <sub>2</sub>	Kim et al. [25]
	K[AlSi <sub>2</sub> O <sub>6</sub> ]-based ceramic Li <sub>2</sub> O-based ceramic	Della Bona et al. [24]
Abrasion	Al <sub>2</sub> O <sub>3</sub>	Kim et al. [25] Madani et al. [23] Özcan et al. [26]
	Li <sub>2</sub> Si <sub>2</sub> O <sub>5</sub> ZrO <sub>2</sub>	Kim et al. [25]
	K[AlSi <sub>2</sub> O <sub>6</sub> ]-based ceramic Li <sub>2</sub> O-based ceramic	Della Bona et al. [24]
Silane treatment	Al <sub>2</sub> O <sub>3</sub>	Tanoglu et al. [30] Madani et al. [23] Özcan et al. [26] Valandro et al. [27]
	B <sub>4</sub> C	Rodrigues and Broughton [29]
	K[AlSi <sub>2</sub> O <sub>6</sub> ]-based ceramic Li <sub>2</sub> O-based ceramic	Della Bona et al. [24]
FPL-etch	Mostly used on aluminium metal, not on ceramics.	Übeyli et al. [7]
Plasma	Al <sub>2</sub> O <sub>3</sub>	Bujanda et al. [33]
	AlN	Asai et al. [32]

## 2.6 Techniques for surface analysis

In order to understand what has happened to the ceramic during the surface treatments discussed in the previous section, a set of techniques for surface analysis is required. The aim is to understand how the surface free energy changes, which changes there are in the surface chemistry, and how the surface treatment affects the topology of the ceramic. The reason why these changes are interesting is that they can all affect the adhesion to the ceramic.

### 2.6.1 Contact angle

The surface free energy can be calculated from the measured values of contact angles of water and other liquids on the surface of the ceramic. This technique has, for example, been used by Bujanda et al. [33] in order to investigate the effect of plasma treatment on polymer surfaces. They discovered that the contact angles of water on UHMWPE, PET and PTFE films were dramatically decreased after exposure to He-H<sub>2</sub>O plasma. This indicates that the surface energy has increased.

Figure 2.3 shows an illustration of a drop of a liquid on a solid surface. The contact angle is defined as the angle between the solid surface and the liquid surface inside the liquid face.

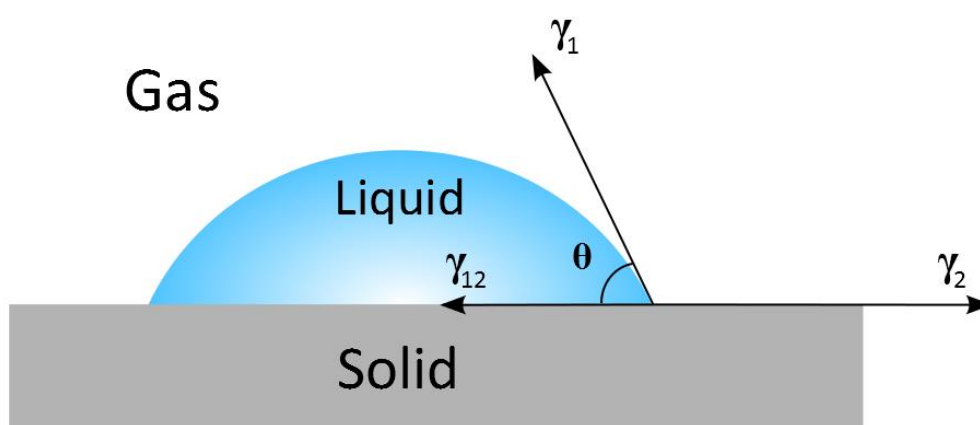


Figure 2.3: Illustration of a liquid drop on a solid surface. The contact angle is marked as  $\theta$ , and the vectors  $\gamma_1$ ,  $\gamma_2$  and  $\gamma_{12}$  are the surface energies or surface tensions of the liquid surface, the solid surface and the solid-liquid interface, respectively.

The vectors shown in the illustration represent the surface energies or surface tensions of the liquid surface, the solid surface and the solid-liquid interface. These surface energies have the following correlation:

$$\gamma_2 = \gamma_{12} + \gamma_1 \cos \theta \quad (2.1)$$

This equation is known as Young's equation. This can also be expressed by the work of adhesion which gives the Young-Dupree equation (the work of adhesion is defined as  $W_a = \gamma_1 + \gamma_2 - \gamma_{12}$ ) [34]:

$$W^a = \gamma_1 (1 + \cos \theta) \quad (2.2)$$

The work of adhesion can also be written as:

$$W^a = 2\Phi(\gamma_1\gamma_2)^{1/2} \quad (2.3)$$

where  $\Phi$  is the so-called interaction parameter:  $0.5 < \Phi < 1.15$

Inserting this into the Young-Dupree equation gives:

$$2\Phi(\gamma_1\gamma_2)^{1/2} = \gamma_1(1 + \cos \theta) \Rightarrow \gamma_2 = \gamma_1 \frac{(1 + \cos \theta)^2}{4\Phi^2} \quad (2.4)$$

Kwok and Neumann have used the following expression for  $\Phi$ , allowing  $\gamma_2$  to be calculated when  $\gamma_1$  for the liquid is known.

$$\Phi = e^{\left[ \beta(\gamma_1 - \gamma_2)^2 \right]} \quad (2.5)$$

With this method, the surface energy of the material can be measured with only one liquid. However, if two liquids are used, one can get a much more reliable result. In that case, the so-called two-liquid method must be used, and the polar and dispersive parts of the surface energy can be calculated [34].

The basis for the two-liquid method is Fowkes theory. This theory assumes that surface energies are additive, and that a geometric mean can be used for the work of adhesion for each part of the surface energy ( $\Phi = 1$ ).

In other words  $\gamma$  can be written as:

$$\gamma = \gamma^d + \gamma^p + \gamma^i + \dots \quad (2.6)$$

where  $\gamma^d$ ,  $\gamma^p$  and  $\gamma^i$  are the contributions from the dispersive, polar, and induction forces, which are some of the forces that affect the surface energy. The different parts of  $W^a$  can be written as:

$$\begin{aligned} W^{a,d} &= 2(\gamma_1^d \gamma_2^d)^{1/2} \\ W^{a,p} &= 2(\gamma_1^p \gamma_2^p)^{1/2} \\ &\dots \end{aligned} \quad (2.7)$$

Using these two assumptions,  $W^a$  can be expressed as:

$$W^a = \gamma_1 (1 + \cos \theta) = 2(\gamma_1^d \gamma_2^d)^{1/2} + 2(\gamma_1^p \gamma_2^p)^{1/2} \quad (2.8)$$

When two liquids, A and B, are used, the following set of equations can be written:

$$\begin{aligned} W^a_A &= \gamma_{1,A} (1 + \cos \theta_A) = 2(\gamma_{1,A}^d \gamma_2^d)^{1/2} + 2(\gamma_{1,A}^p \gamma_2^p)^{1/2} \\ W^a_B &= \gamma_{1,B} (1 + \cos \theta_B) = 2(\gamma_{1,B}^d \gamma_2^d)^{1/2} + 2(\gamma_{1,B}^p \gamma_2^p)^{1/2} \end{aligned} \quad (2.9)$$

This can be linearized in order to get the following set of equations. Since the surface energies of the liquids ( $\gamma_{1A}^d, \gamma_{1A}^p, \gamma_{1B}^d, \gamma_{1B}^p$ , and  $\gamma_{1B}$ ) and the contact angles ( $\theta_A$  and  $\theta_B$ ) are known, the values of  $\gamma_2^d$  and  $\gamma_2^p$  can be found from these equations:

$$\frac{(\gamma_{1,A}^d)^{1/2}}{\gamma_{1,A}}(\gamma_2^d)^{1/2} + \frac{(\gamma_{1,A}^p)^{1/2}}{\gamma_{1,A}}(\gamma_2^p)^{1/2} = \frac{1 + \cos \theta_A}{2}$$

$$\frac{(\gamma_{1,B}^d)^{1/2}}{\gamma_{1,B}}(\gamma_2^d)^{1/2} + \frac{(\gamma_{1,B}^p)^{1/2}}{\gamma_{1,B}}(\gamma_2^p)^{1/2} = \frac{1 + \cos \theta_B}{2}$$
(2.10)

This is the method which will be used to calculate surface energies in this thesis [20;34].

The measured contact angle is also affected by the roughness of the surface. This effect was described by Robert N. Wenzel in 1936, and can be expressed by the following equation:

$$\cos \theta_m = r \cos \theta_Y$$
(2.11)

Where  $\theta_m$  is the measured contact angle,  $\theta_Y$  is the so-called Young contact angle which corresponds to the contact angle on a completely flat surface, and  $r$  is the roughness ratio. This surface ratio can be calculated based on some of the results from the profilometer measurements. This will be described in Section 2.6.2 [35].

## 2.6.2 Profilometer

A profilometer is used in order to get information about the roughness and topology of a surface. There are a number of different types of profilometers, ranging from contact profilometers where a diamond tipped stylus is dragged across the surface and the height of the sample is measured, to non-contact profilometers which use light to scan the surface [36]. There are multiple techniques used for non-contact profilometry, some of these are laser triangulation, confocal microscopy, phase-shift interferometry and vertical scanning interferometry [37;38].

In addition to giving beautiful three-dimensional scans of the surface, a profilometer can give a set of parameters which give useful information about the surface. There are quite a lot of different parameters that can be calculated, but some of the most important ones are  $S_a$ ,  $S_q$ ,  $S_p$ ,  $S_v$ ,  $S_z$  and  $S_{dr}$ . The  $S$  indicates that the entire three dimensional surface was

used to calculate the parameter as opposed to  $R_a$ ,  $R_q$ , etc., which are calculated from a two-dimensional profile of the surface [35].

$S_a$  is the average deviation of the surface and is defined as:

$$S_a = \frac{1}{MN} \sum_{j=1}^N \sum_{i=1}^M |\eta(x_i, y_j)| \quad (2.12)$$

where  $M$  and  $N$  are the number of points in  $y$  and  $x$  direction respectively, and  $\eta$  is the height of each point relative to a defined plane [35].

$S_q$  is the root-mean-square deviation of the surface, and is defined as:

$$S_q = \sqrt{\frac{1}{MN} \sum_{j=1}^N \sum_{i=1}^M \eta^2(x_i, y_j)} \quad (2.13)$$

$S_p$  and  $S_v$  are the maximum height of the peaks and the minimum height of the valleys respectively, and  $S_z$  is the total height of the surface ( $S_z = S_p + S_v$ ).

$S_{dr}$  is the increase in surface area from a completely flat surface to the actual rough surface given in percent.  $S_{dr}$  is given by:

$$S_{dr} = \frac{(A_{rough}) - (A_{flat})}{(A_{flat})} \cdot 100\% \quad (2.14)$$

$S_{dr}$  can be used to calculate the roughness ratio which is used in Equation 2.11 in Section 2.6.1. This is done by the following equation:

$$r = 1 + \frac{S_{dr}}{100} \quad (2.15)$$



In addition to these parameters, the profilometer measurements can be used to calculate a number of parameters which describe the shape of the peaks and valleys, such as  $S_{ku}$  and  $S_{sk}$  [35].

### 2.6.3 X-ray photoelectron spectroscopy

X-ray photoelectron spectroscopy (XPS) is a technique of surface analysis which can give valuable information about the surface chemistry. It is very surface sensitive, and can detect which elements are present in the surface of the material, the amount of each element, and their chemical state.

In XPS, low energy X-rays are sent towards the sample. When these X-rays hit the surface, photoelectrons are emitted. Based on the kinetic energy of the emitted photoelectrons, the binding energy of the electrons can be calculated from the following equation [39]:

$$E_B = h\nu - E_{kin} - \phi \quad (2.16)$$

Here  $E_B$  is the binding energy of the electron,  $h\nu$  is the energy of the X-ray photon, and  $\phi$  is the work function of the spectrometer as shown in Figure 2.4.

The binding energy  $E_B$  is characteristic for the element the electron came from, and the bonds this atom shares with other atoms.

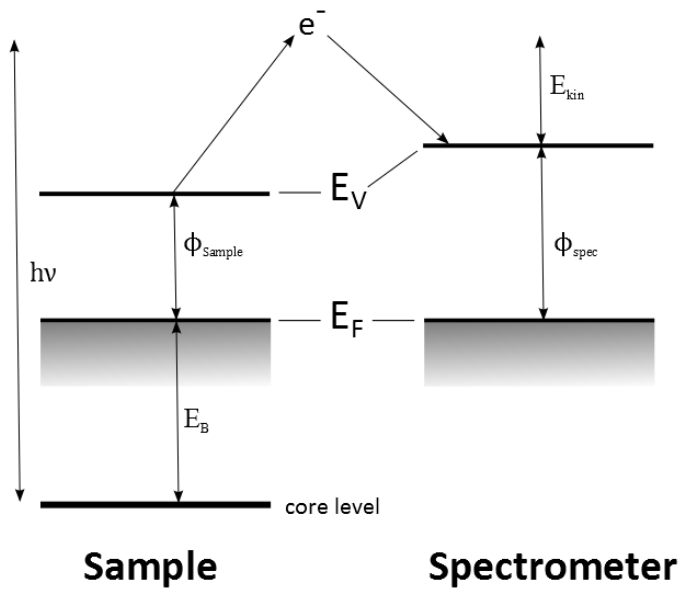


Figure 2.4: Illustration of the energy levels in the sample and the spectrometer.  $E_F$  is the Fermi level, and  $E_V$  is the vacuum level. This illustration explains the equation above:  $E_B = h\nu - E_{kin} - \phi$  (where  $\phi = \phi_{spec}$  is the work function of the spectrometer)

When the emitted photoelectrons leave the surface of the sample, they enter a velocity analyser, through which only electrons with a very narrow range of velocities can pass. In the other end of this velocity analyser, there is a detector which measures the number of electrons with each specific kinetic energy as is shown in Figure 2.5 [40].

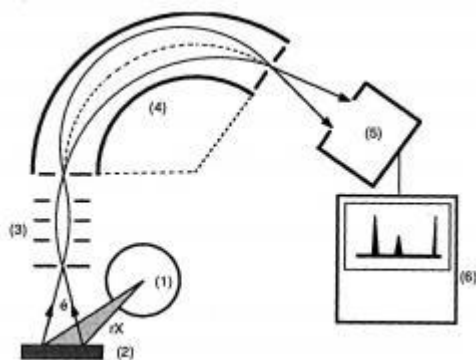


Figure 2.5: Illustration of the setup of an XPS. The item marked (1) is the X-ray source, (2) is the sample, (3) is a device for focusing the electrons, (4) is the velocity analyser, (5) is the detector, and (6) is the system for acquiring and treating the data [41].

In the end, the data is processed, and a graph of the intensity at each different binding energy is obtained. By analysing the size of the peaks in this graph, one can determine the amount of each element. By analysing the shape of the peak from a high resolution scan

one can determine in which chemical state the different elements are, and the amounts of each chemical state. The reason why the latter is possible is that the binding energy of the electrons shift to a higher or lower value depending on the chemical state the atom is in, this is called chemical shift [42].

Some examples of the application of XPS are the work done by Bujanda et al. [33], where they used XPS in order to investigate the changes in chemical groups on the surface of an UHMWPE film after plasma treatment; and the work done by Asai et al. [32] who used XPS for similar investigations on an AlN ceramic surface after treatment with a few different plasmas. Harris et al. [21] also used XPS, and found that their silicon carbide surface was oxidised after reheating in air and after a laser treatment.

#### **2.6.4 Scanning electron microscopy**

In scanning electron microscopy (SEM), an electron beam is swiped across the sample, scanning an area of interest. The secondary electrons are then collected in order to form an image of that area.

With SEM, one can get images with a very high resolution. In some cases a resolution of  $\sim 1$  nm can be achieved, but normally it is about 30 nm. For example, the SU6600 Schottky Field Emission Analytical SEM, which was used in this thesis, is capable of a resolution of 1.2 nm under certain conditions [43].

A SEM will give a very good depth of view when the signal from the secondary electrons is used. This good depth of view will give a good impression of the topology of the sample surface. When a backscatter detector is used, one will see the distribution of the mean atomic number on the surface [40].

A drawing of the most important parts of a SEM can be seen in Figure 2.6. The electrons are sent from the electron gun, focused by two magnetic lenses, and deflected by a coil in order to scan the sample. The secondary electrons are detected by the detector at the bottom right in Figure 2.6 in order to get an image of the surface. A backscatter detector would have been close to the second magnetic lens in order to detect primary electrons which are scattered back the way they came from, but it is not shown in this figure.

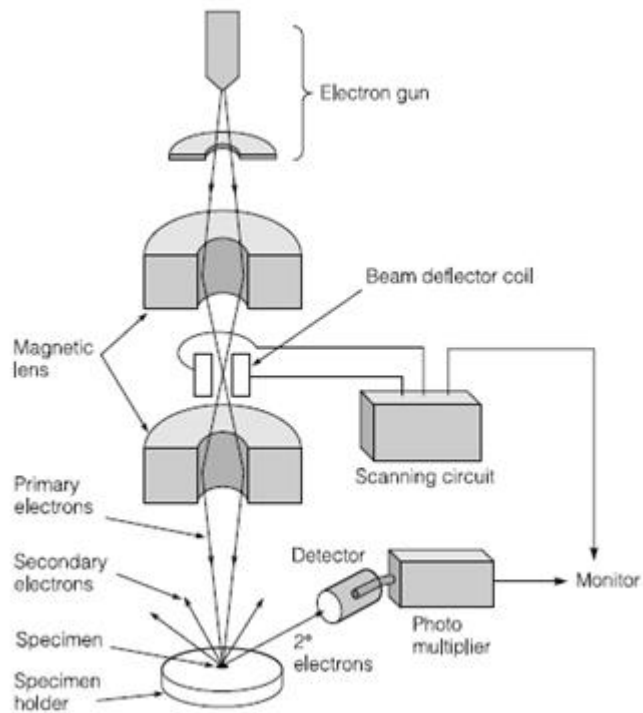


Figure 2.6: An illustration of a scanning electron microscope (SEM) showing the electron gun, magnetic lenses, beam deflector coil (scanning coil) and secondary electron detector [44].

SEM is widely used in order to obtain good images. One example is Rodrigues and Broughton [29], who conducted SEM of boron carbide particles. Another example is Della Bona et al. [24] who used SEM imaging to study the effect of etching a ceramic in either HF or acidulated phosphate fluoride (APF).

## 2.7 Mechanical tests of adhesive bond performance

In order to see how well the composite is adhesively bonded to the ceramic a mechanical test is required. Three possible tests to measure adhesive strength of ceramics are the butt joint, double lap shear, and peel tests. These will be presented in this section.

### 2.7.1 Butt joint test

The butt joint test is perhaps the most simple of these tests. It measures tensile strength in the bond, and is performed as shown in Figure 2.7.



*Figure 2.7: An illustration of the butt joint test.*

Two pieces of a material are bonded together with an adhesive. These are then pulled apart in order to see how well the adhesive is bonded to the material. The force it takes to pull them apart is measured, and this force is then divided by the contact area in order to get the tensile strength.

The butt joint test was used by Harris et al. [21] to investigate how well silicon carbide was bonded to an epoxy adhesive after a few different surface treatments. Della Bona et al. [24] also used a variant of the butt joint test where they glued two pieces on top of each other, and then cut them into smaller bars which were then pulled apart to measure the strength.

### 2.7.2 Double lap shear joint test

The double lap shear joint test is in many ways similar to the butt joint test since pieces of the material of interest are bonded together with an adhesive and then pulled apart. The

difference is that, in the double lap shear joint test the pieces are pulled apart along an axis parallel to the bonded surfaces instead of perpendicular to this surface.

As the name implies, this test measures the shear strength of the bond, again by measuring the force it takes to pull the pieces apart. An illustration of the test is shown in Figure 2.8



Figure 2.8: An illustration of the double lap shear test.

Harris et al. [21] used the double lap shear joint test in addition to the butt joint test in order to measure both tensile strength and shear strength. This test can also be done in compression. In that case, the two material pieces on the far left and far right of the figure above would be pushed towards each other until the bonds break instead of being pulled apart [22].

### 2.7.3 Peel test

A third way of testing the strength of the adhesive bond is the peel test. There are many ways of performing a peel test some of the most common configurations are shown in Figure 2.9, the fixed arm peel test is also shown in Figure 2.10.

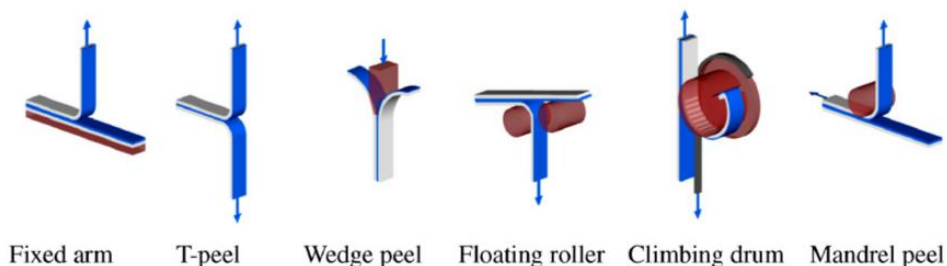
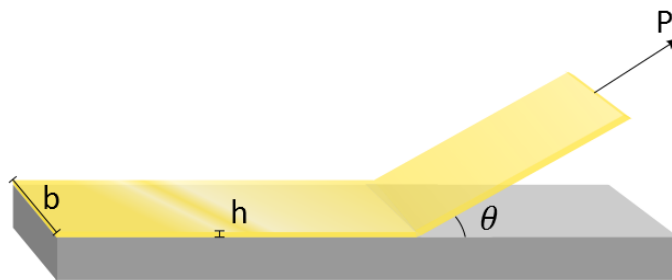


Figure 2.9: Different configurations of peel testing [45].

In all of the peel tests, a rectangular sample where two materials are adhesively bonded together is used. As the name implies, one of the materials is peeled off the other in order to get a measurement of the strength of the adhesive bond between them. The difference lies in how this peeling is performed. In order to perform these tests (with exemption of the wedge peel test) at least one of the materials that are bonded together needs to be relatively flexible.

The fixed arm peel test can be performed at a wide range of angles, usually  $45^\circ$  to  $180^\circ$ . A few methods have been developed in order to maintain a  $90^\circ$  peel angle throughout the test. For example, mounting the base substrate to a movable fixture that works as a pendulum in order to keep the peel front directly below the crosshead of the testing machine at all times. Another method is bending the sample into a semi-cylindrical shape, and then peeling from the inside and allowing the semi-cylinder to rotate so that the angle between the peel arm and the substrate is  $90^\circ$  at all times [45].

The different types of peel testing are useful for different purposes. For example, the T-peel is good when two flexible materials are bonded together, and the floating roller is often used for rigid to rigid bonding such as metals bonded to metals [45].



*Figure 2.10: An illustration of a fixed arm peel test showing the peel angle  $\theta$ , peel arm thickness  $h$ , peel arm width  $b$  and peel force  $P$ .*

In a peel test, the peel strength is measured. This is given by a force per unit of width of the peel arm. However, it can often be useful to also find the adhesive fracture toughness which tells how well the two layers are bonded together, and not just how difficult it is to peel one off the other [46].

When performing a peel test, it is common to differentiate between adhesive and cohesive fractures. An adhesive fracture is when the fracture propagates through the interface

between the materials and a cohesive fracture is when the fracture propagates through one of the materials which are bonded together. In Figure 2.11, an example of the results from a peel test in the literature is shown. The two black lines mark the value for the cohesive and the adhesive peel forces.

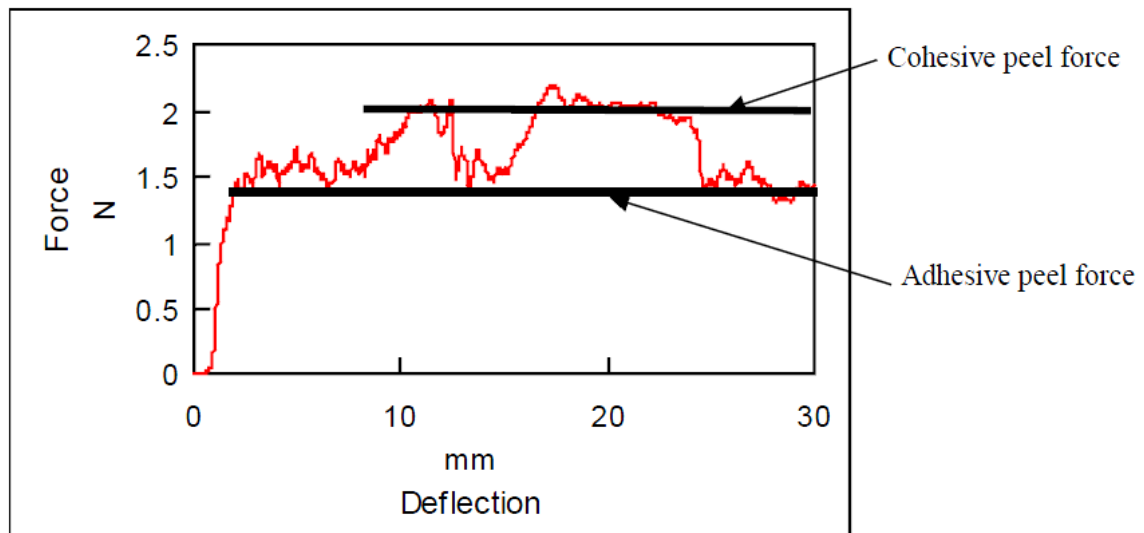


Figure 2.11: An example of a graph from a peel test showing the force (N) versus the deflection (mm). The adhesive and cohesive peel forces are shown [46].

A number of people have used peel testing. Bujanda et al. [33] used a T-peel test to investigate adhesion to their plasma treated UHMWPE, PET and PTFE films. Karbhari and Engineer [47] and Karbhari et al. [48], tested the bonding of composite materials to concrete for use in rehabilitation of concrete structures. And Asai et al. [32] used a peel test in order to test the adhesion between aluminium nitride (AlN) and an adhesive called polyaminobismaleimide (PABM) after surface treatments.

## 2.8 Ballistic tests

In order to see how well a ballistic protection system performs, a few standard tests are used.

One of the most frequently used ballistic tests is the so-called ballistic-limit test. This is well suited for testing complete ballistic protection systems. In this test, a series of shots are fired into the same material at different velocities. In some cases, the projectile will



perforate the target, and in other cases it will only partly penetrate the target. The aim is to find a velocity where the projectile has a 50% chance of perforating the target. This particular velocity is called  $V_{50}$ . Alternatively, one can find  $V_{100}$ , which is the minimal velocity where all projectile perforate the target; or  $V_0$ , which is the maximum velocity where none of the projectiles perforate the target [9].

With this ballistic limit test, one should be aware that there might be two different  $V_{50}$  values for the same material. This phenomenon is called the “shatter-gap”. If the projectile is able to perforate the target at a velocity which is too low for it to break, increasing the velocity might cause the projectile to be stopped by the target because it is shattered. By further increasing the velocity, even the shattered projectile will perforate the target, giving two different  $V_{50}$  values [9].

Another important ballistic test is the depth of penetration (DOP) test. DOP tests are useful for investigating how well one material, for example one type of ceramic tile, performs. In this test, a semi-infinite metal block is used as a witness material. One shot is fired into the bare metal block in order to form a baseline reference, and another shot is fired into the material of interest which is backed by a similar semi-infinite metal block. The depth of penetration is compared for the two cases, which will give information on how well the armour material performs. In Figure 2.12, an illustration of the DOP test is shown. The advantages of this test method are that it is relatively simple, and in principle only two shots need to be fired. The main disadvantage is that the semi-infinite backing material performs differently than a normal backing plate, which could affect the results [9].

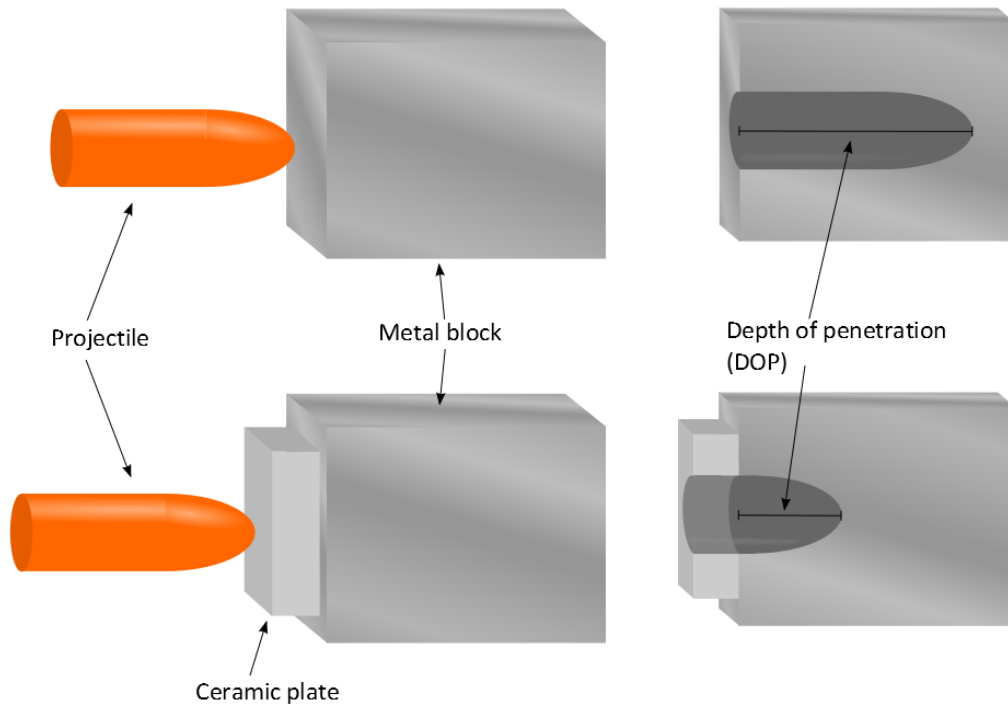


Figure 2.12: An illustration of a depth of penetration (DOP) test showing both the actual test (bottom) and the control (top).

A third, and less frequently used, test method is called the ballistic pendulum test. In this test, a box is suspended from the ceiling behind the target in order to catch the projectile after it has perforated the target. The impact of the projectile will make the suspended box swing like a pendulum, and by measuring the swing of the pendulum, the momentum of the projectile after perforation can be calculated. By comparing this to the momentum before hitting the target, which is found by weighing the projectile and measuring its velocity, one can calculate the momentum transferred to the armour. The energy transferred to the armour can also be calculated if it is possible to retrieve and weigh the projectile after perforation [9].

In all of these ballistic tests, it is important that the test tiles are large enough. This is in order to ensure that stress waves which are reflected from the edges of the tile do not interfere with the penetration process of the projectile. Using the following equation, one can calculate the velocity of the stress wave  $c_0$ :

$$c_0 = \sqrt{\frac{E}{\rho}} \quad (2.17)$$

Here  $E$  is the elastic modulus of the ceramic, and  $\rho$  is the density.

When the time it takes for the projectile to penetrate the target is known, one can calculate the minimum distance needed between the impact point and the tile edge. As a rule of thumb, the tile should be at least 15 times the size of the projectile calibre [9].

In the following paragraph, a few different examples of applications of ballistic testing are presented.

Übeyli et al. [7] used a variant of the ballistic limit test where they fired several shots with the same velocity into many different test samples. The test samples were made with varying thickness of the alumina ceramic and the aluminium backing plate. In order to determine which combination worked best, they compared the probability for perforating each of the sample types.

Gao et al. [11] fired bullets with a velocity of 800 m/s at different test samples in order to investigate how adding different amounts of nano-SiO<sub>2</sub> particles to the adhesive between ceramic and metal affects the ballistic performance. The result was analysed by comparing the amount of damage on the different test samples.

Kaufmann et al. [14] used a DOP test in order to compare alumina, modified alumina, silicon carbide, and boron carbide. They found that for the same impact velocity both alumina and modified alumina had a higher depth of penetration than silicon carbide. At impact velocities of 850 m/s and 910 m/s alumina and modified alumina had a depth of penetration which was approximately five times as high as both silicon carbide and boron carbide.

Harris et al. [22] have also tested the effect of adhesion between the ceramic and the backing material on ballistic performance. The tests were performed on plates consisting of many small hexagonal ceramic tiles bonded to a large backing plate. Either one or four projectiles were fired into the plates. The ballistic performance of the plates on the second, third and fourth hits was studied, and the plates were investigated in order to see how many of the tiles that were detached.

## **2.9 Effects of nanoparticles on ballistic performance**

Adding nanoparticles to the adhesive layer between the ceramic plate and the backing plate may improve the ballistic properties. The nanoparticles can improve the adhesive properties which, as discussed in Section 2.4, can improve the ballistic properties. Adding nanoparticles can also change the acoustic impedance of the adhesive layer, and in that

way insure that more energy from the shock wave is transferred to the backing plate, and that less is reflected back into the ceramic [11].

One specific type of nanoparticles which can improve adhesion is polyhedral oligomeric silsesquioxanes (POSS). POSS particles consist of an inorganic core of silicon and oxygen, with organic groups attached to each silicon atom. The general formula for POSS particles is  $(\text{RSiO}_{1.5})_n$  where the number of Si atoms,  $n$ , can be 8, 10 or 12, and R is the organic groups attached to the silicon vertices. In the most common type of POSS particles,  $n = 8$ . This type is called T8-POSS, and is shown in Figure 2.13 (The “T” in T8-POSS comes from a common nomenclature from silicon nuclear magnetic resonance, denoting three oxygen atoms bound to the silicon atom) [18].

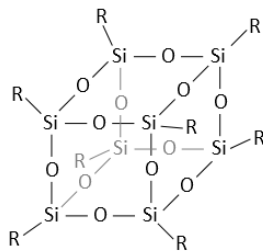


Figure 2.13: An illustration of a general T8-POSS molecule.

Nguyen et al. [49] mixed a certain type of POSS particles (octa-(ethyl octadeca-10,13 dienoamide) silsesquioxane or bio-POSS) into polyethylene (PE) in varying concentrations in order to test the adhesive properties of these mixtures to paperboard. They found that, depending on the temperature when applying the coat to the paperboard, either 3 wt% (at 300 °C/20 °C) or 5 wt% (at 200 °C/20 °C) gave the best adhesion (the two different temperatures are the temperature on the top and bottom of the paperboard). For concentrations above 10 wt%, the adhesion decreased compared to pure PE.

An example of nanoparticles being used to modify adhesives for armour applications is Gao et al. [11], who performed ballistic tests on alumina plates which were adhesively bonded to an armour steel backing plate by an epoxy based adhesive. They added varying amounts of nano-SiO<sub>2</sub> particles, and found that both the adhesive strength and the acoustic impedance of the adhesive increase with increasing amount of nano-SiO<sub>2</sub> particles. The adhesive with the highest amount of nano-SiO<sub>2</sub> particles (20 g added to a mix of 100 g of epoxy resin and 30 g of curing agent) also showed the least damage after ballistic testing.

# 3 Experimental

In this chapter, the materials and some important chemicals that were used will be presented. The process for all of the different surface treatments will be explained, and all techniques and equipment used for surface analysis of the treated surfaces will be presented. The production of test samples for the mechanical and ballistic tests, and the test methods are also described.

A part of this thesis is focused on attempting to improve the adhesion by adding POSS particles to the composite matrix close to the interface between the composite and the ceramic. Section 3.4 explains how this was done.

## 3.1 Materials and chemicals

In this section, the ceramic and composite materials which were used for making test samples will be described. In addition to this, the silane and the POSS nanoparticles which were used in order to increase the adhesion will be presented.

### 3.1.1 Ceramics

The ceramics which was used was alumina ( $\text{Al}_2\text{O}_3$ ). The alumina was Alotec 98 SB from CeramTec, for which some of the material properties are shown in Table 3.1. The size of the tiles was 150 mm x150 mm x10 mm. For some of the surface analysis, it was necessary to cut the tiles into smaller pieces.

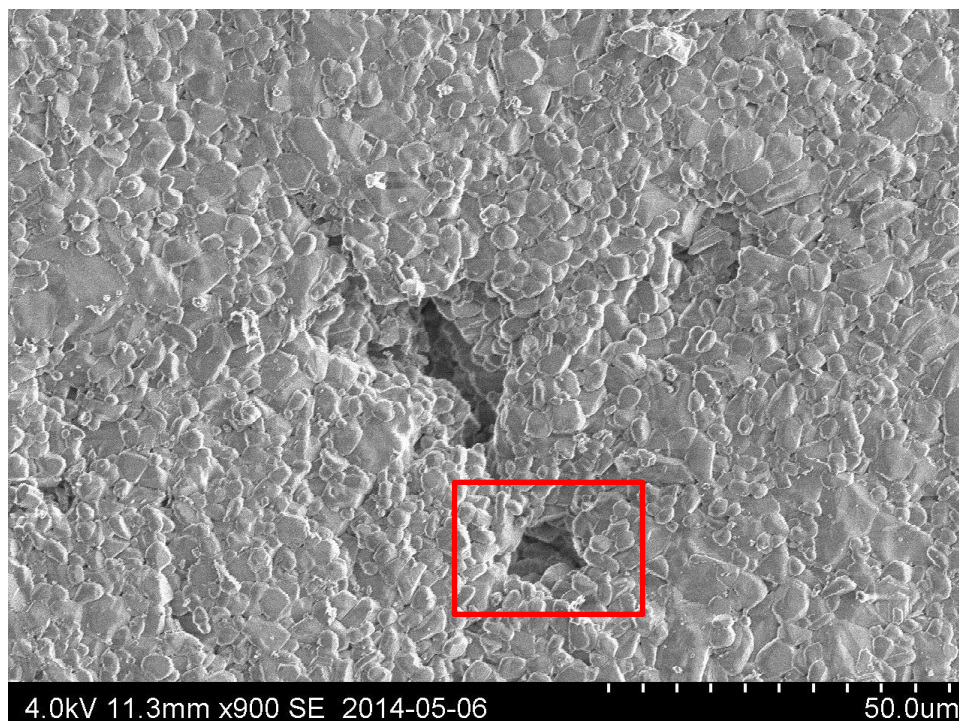
*Table 3.1: Material properties for the Alotec 98 SB from CeramTec given by the manufacturer.*

Property	Value
Density	3.80 g/cm <sup>3</sup>
Medium grain size	6 μm
Vickers hardness	13.5 GPa
Young's modulus	335 GPa
Sound velocity ( $V_L$ )	10200 m/s

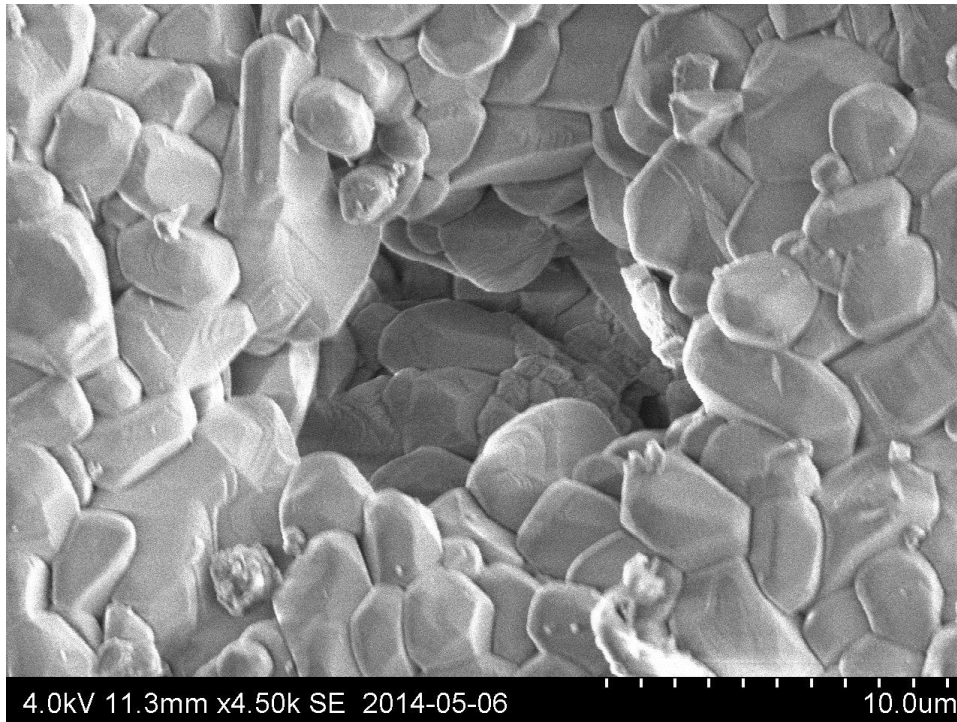
Figure 3.1 to Figure 3.3 show SEM images of different parts of the alumina surface. In the two first images, one can clearly see that there are a few pores in the surface. These may be an advantage with respect to the adhesion. If the composite matrix (or the adhesive) is able to penetrate into these pores, they could facilitate mechanical interlocking between the composite and the ceramic. If this is not the case, these pores could be a disadvantage since they would reduce the contact area between the two materials. A polished cross section of the ceramics shows these pores more clearly. This cross section can be seen in Figure 3.4.

Figure 3.3 show the alumina grains in more detail, showing that the grains vary in diameter. The smallest ones seem to be well under 1  $\mu\text{m}$  while the largest ones can be almost 20  $\mu\text{m}$  across. This seems to correspond well with the data in Table 3.1, which states that the medium grain size is 6  $\mu\text{m}$ .

The fact that the alumina has such a rough surface can affect the wettability and the adhesion to the composite in many different ways. This will be more apparent after the results of mechanical tests and contact angle measurements are compared to SEM images of the surface after various surface treatments.



*Figure 3.1: SEM-image showing the overview of the alumina surface before any surface treatment. The surface is relatively rough, and there are a few deeper pores. The red square marks the area which is shown in Figure 3.2.*



*Figure 3.2: Higher magnification SEM image of one of the pores in the surface. This pore is approximately 10-15  $\mu\text{m}$  wide.*

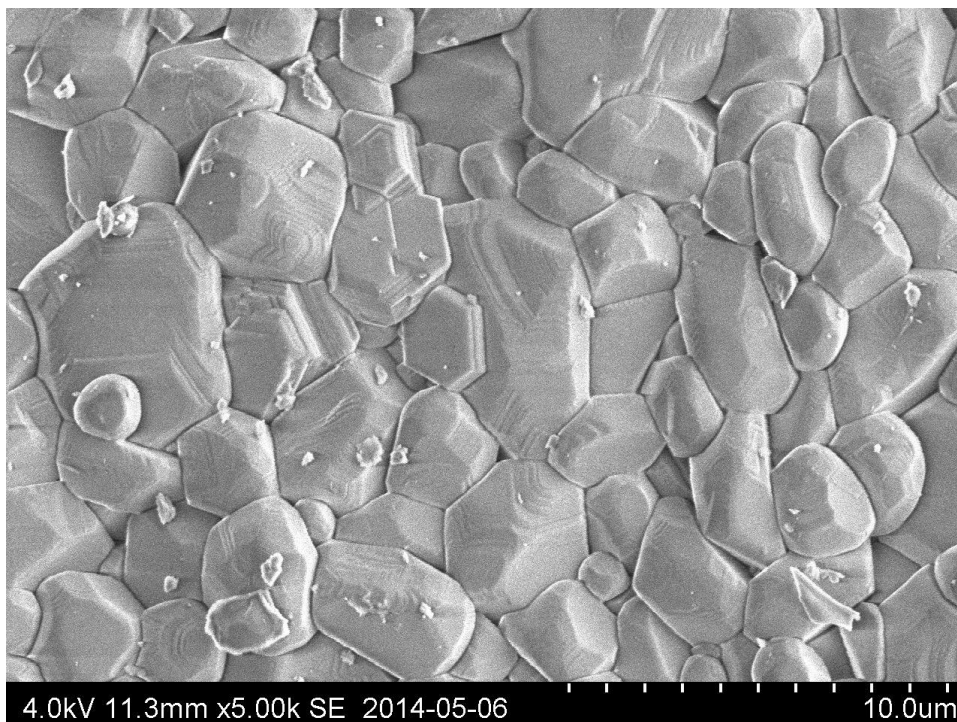


*Figure 3.3: SEM image showing the grains at the surface of the alumina ceramic. The grain size varies a lot. In this image, the smallest grains are approximately 1  $\mu\text{m}$  and the largest ones are between 5 and 10  $\mu\text{m}$ . However, grains as large as 20  $\mu\text{m}$  have been observed.*

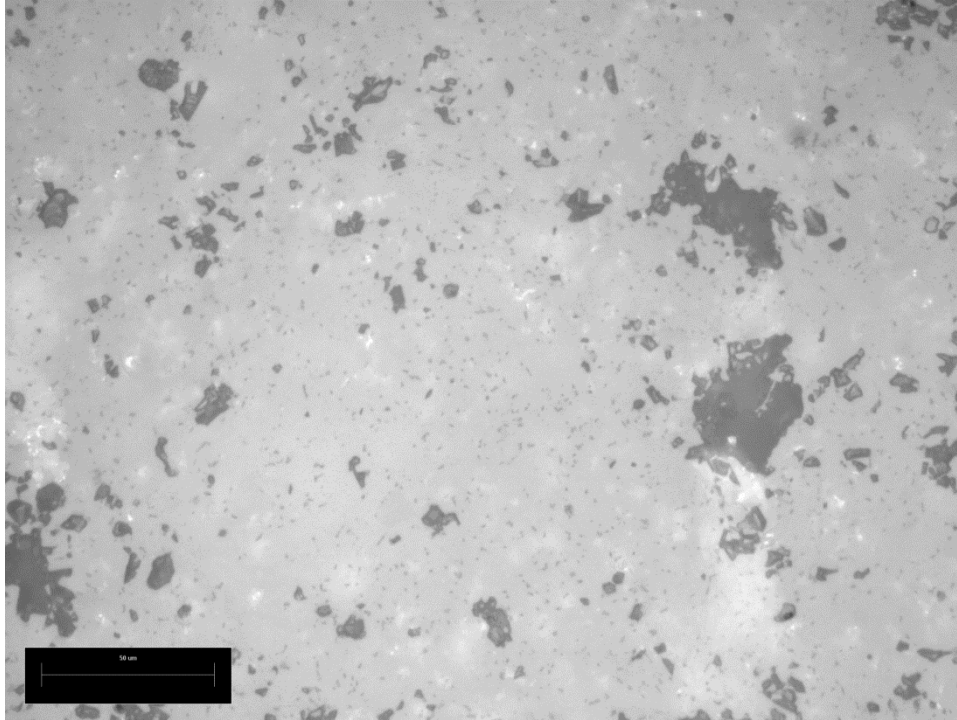


*Figure 3.4: A polished cross-section of the ceramic showing that the material is quite porous.  
(The scale bar is 50  $\mu\text{m}$ )*



### 3.1.2 Composite

The composite that was used was glass fibre (GF) in a low-melting temperature polyethylene terephthalate (LPET) matrix. The repeating unit of polyethylene terephthalate (PET) which is the basis for LPET can be seen in Figure 3.5. The composite was delivered as a woven fabric of LPET fibres and glass fibres. The SEM image in Figure 3.6 shows the glass fibres along with the LPET fibres. As can be seen from this image, the glass fibres have a diameter of approximately 12-13  $\mu\text{m}$ . This fabric was then heat treated in order to form the finished composite. Regular PET has a melting point of 255  $^{\circ}\text{C}$ . However, LPET has been modified to melt at 160-180 $^{\circ}\text{C}$  [50]. The GF-LPET fabric was produced by COMFIL<sup>®</sup>, and some of its properties are shown in Table 3.2. More information is found in the data sheet in Appendix E.

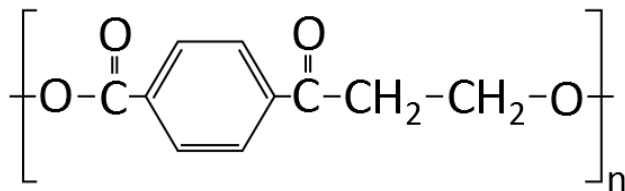


Figure 3.5: The chemical structure of the repeating unit of polyethylene terephthalate (PET). The chemical structure for LPET is a trade secret, but it is similar to the PET structure.

Table 3.2: The specifications of the GF-LPET fabric. The values are taken from the data sheet provided by COMFIL<sup>®</sup>. This data sheet is shown in Appendix E.

Property	Value
Area density	750 $\text{g}/\text{m}^2$
Glass fibre content	57 wt.%
Glass fibre content	42 vol.%
Thickness of consolidated fabric	0.4 mm
Density of consolidated material	1.87 $\text{g}/\text{cm}^3$

During the production of test samples, the composite fabric is heated so that the LPET fibres melt, cover the glass fibres, and become the matrix of the composite. A microscope image of the cross-section of the finished composite is shown in Figure 3.9. The production method will be described further in Section 3.4.

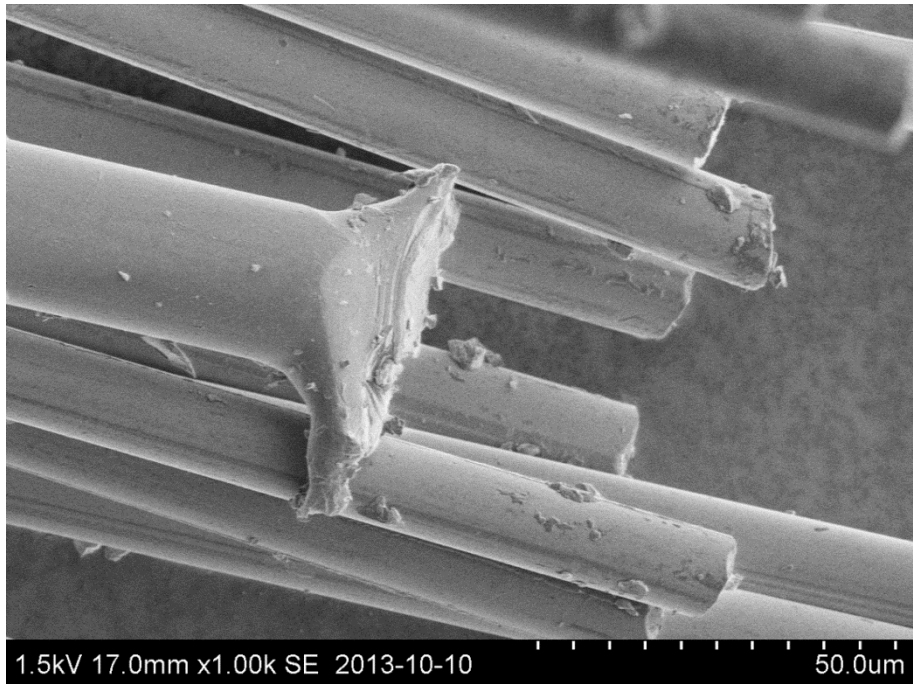


Figure 3.6: SEM image of the fibres from the edge of an untreated GF-LPET fabric which was cut with a pair of scissors. The largest fibre with the broad end is the LPET, and the smaller, clean cut fibres are glass fibres. When heated, the LPET melts and form the matrix that surrounds the glass fibres.

The GF-LPET fabric is woven from yarn where LPET fibres and glass fibres are commingled. This means that the fibres are mixed together, but not necessarily ideally. The illustration in Figure 3.7 shows the difference between the cross-sections of ideal yarns, commingled yarns, and yarns where the two types of fibre are just put together. An SEM image of the two different fibres can be seen in Figure 3.8. This shows that the fibres in the composite fabric are commingled.

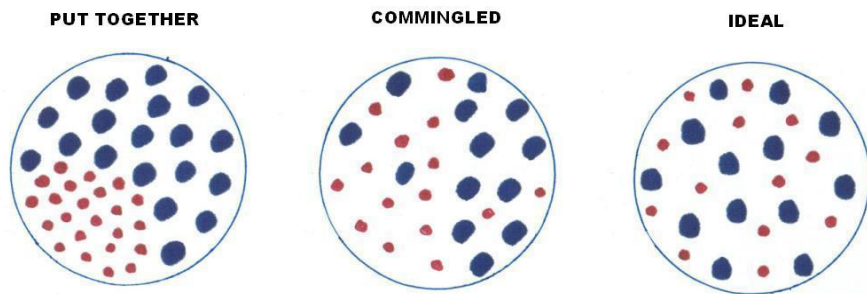
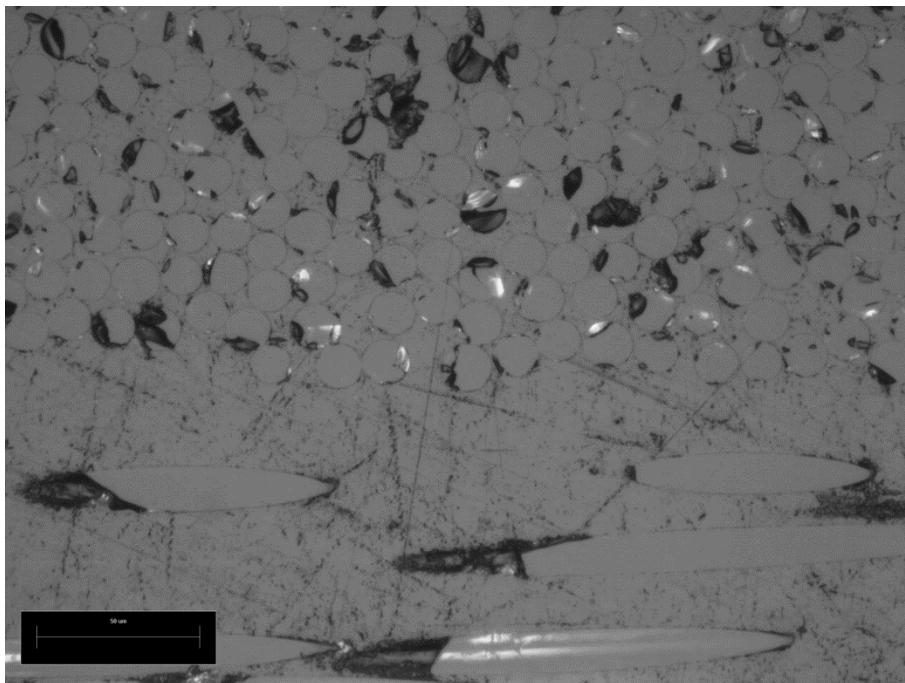


Figure 3.7: A drawing of the cross-section of the fibres in three different kinds of yarn: put together, commingled, and ideal [50].



*Figure 3.8: SEM image of the fibres in the GF-LPET fabric showing clearly that the glass fibres and the LPET fibres are commingled. Again, the fibres were cut with a pair of scissors, so the LPET fibres have a broad end but the glass fibres have a clean cut. (The fibres that are not parallel to the others have been displaced during cutting)*



*Figure 3.9: A cross-section image showing the composite after the LPET fibres are melted. The circles in the top half of the image are glass fibres perpendicular to the image. In the bottom half of the image, the glass fibres are cut at an angle. (The scale bar is 50  $\mu\text{m}$ ).*

### 3.1.3 Silane coupling agent

For silane treatment, the silane called 3-glycidyloxypropyl trimethoxysilane (GPS), delivered by Sigma-Aldrich, was used. The chemical structure of this silane is shown in Figure 3.10. This silane is the same as the one used by Johnsen et al. [28]. The molecular formula of the silane is  $C_9H_{20}O_5Si$ , and the molecular weight is then 236.3 g/mol [51;52]. More information about the silane coupling agent is found in Appendix F.

The silane comes in liquid form, and in order to treat the ceramic, a solution is made with water. The ceramic tiles are then immersed in this solution for a given amount of time. The procedure is described in further detail in Section 3.2.3.

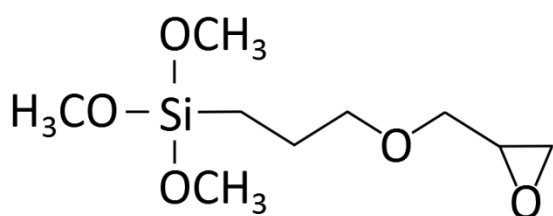


Figure 3.10: The chemical structure of the silane that was used. This silane is known as 3-glycidyloxypropyl trimethoxysilane or  $\gamma$ -glycidoxypropyltrimethoxysilane and is abbreviated GPS.

### 3.1.4 Polyhedral oligomeric silsesquioxanes

The polyhedral oligomeric silsesquioxanes (POSS) particles used in this thesis are FunzioNano AMS-656 Delivered by SINTEF Materials and Chemistry. The structure of these POSS particles is shown in Figure 3.11. Unfortunately, it turns out that the AMS-656 has some impurities due to some previously unknown side reactions.

In order to get these particles added to the matrix of the composite, films of LPET (the same material as the composite matrix) were made with varying concentrations of POSS particles. These films were then placed between the GF-LPET fabric and the ceramic before applying heat so that the LPET fibres in the fabric and the POSS-containing LPET films melt together. The process of adding POSS particles to the LPET, and making the POSS-containing LPET films will be further described in Section 3.4.

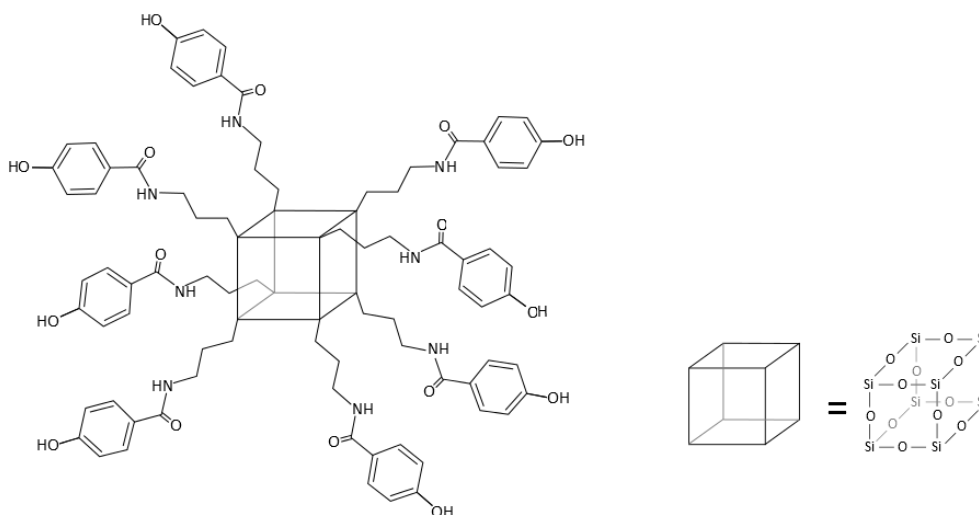


Figure 3.11: An illustration of the FunzioNano AMS-656 particles.

## 3.2 Surface treatment

In this thesis, four different types of surface treatment were tested on the ceramic. These are sandblasting, plasma treatment, silane treatment and etching in chromic-sulphuric acid. Each of these techniques will be explained below.

All samples were washed in acetone before surface treatment. Most of the samples made for investigation with SEM, and all samples made for XPS were also washed in an ultrasonic bath. The reason for this ultrasonic washing is that the cooling water used when cutting the ceramic into smaller pieces contained crushed alumina particles that ended up in pores and in-between grains on the alumina surface. This is described in further detail in Appendix H.

Since all samples were washed in acetone before the surface treatment, a series of test samples were made of acetone-washed ceramic without further surface treatment as a control. A series of tests was also performed on the as-received ceramic which was not washed in acetone in order to see to what extent the washing and surface treatment improves the adhesion.

### 3.2.1 Sandblasting

Some of the ceramic tiles were sandblasted in order to alter their topography. The sand which was used is shown in Figure 3.12. As can be seen from the image, the grains vary in size and shape, and they have a rather rough surface. The grains are a lot larger than the grains on the surface of the alumina ceramic. The sand is Svarco aluminium oxide OSO K40 supplied by Trond T. Wikant AS. This aluminium oxide seems to be polluted by various other elements due to differences in colour between the grains. All the sandblasted samples were washed in acetone after sandblasting in order to remove sand and dust from the surface.

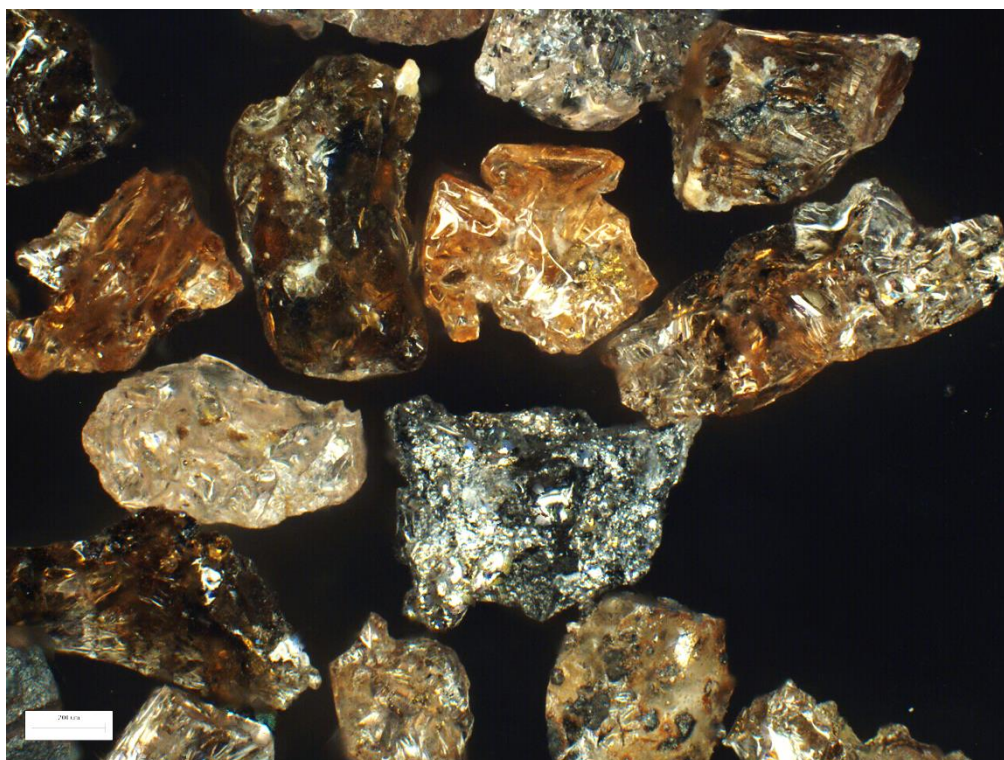


*Figure 3.12: A microscope image of the sand used for the sandblasting. (The scale bar is 200  $\mu\text{m}$ .)*

### 3.2.2 Plasma treatment

The plasma treatment was done in a Piccolo plasma chamber produced by Plasma Electronic. The chamber pressure was lowered to 15 Pa, before 50 sccm (standard cubic centimetres per minute) of argon (Ar) was let into the chamber for 60 seconds. After this, the gas flow of Ar was set to 10 sccm, and kept at that level for three minutes before generating the plasma in order to allow the pressure in the chamber to stabilise (the

vacuum pump was running continuously during this process). The reason for doing this procedure before generating the plasma is to replace most of the air in the chamber with Ar.

When the plasma was generated, the pressure in the chamber was approximately 20 to 25 Pa and the gas flow of Ar was still 10 sccm. The power of the RF generator was 100 W, and the frequency was 13.56 MHz.

Small test samples of the ceramic were exposed to this plasma for 25, 50 or 100 seconds in order to ensure that the plasma treatment was complete, and no changes would happen with longer exposure. The full scale ceramic tiles used to make test samples for peel testing were plasma treated for 100 seconds.

### 3.2.3 Silane treatment

The silane treatment was done following the procedure described by Johnsen et al. [28]. First, the pH of water was adjusted to 5 by adding acetic acid, and then the appropriate amount of 3-glycidyloxypropyl trimethoxysilane was added in order to get a concentration of 0.25%, 0.5%, or 1 wt%. After this, the solution was stirred for one hour with a magnetic stirrer in order for a hydrolysis reaction, as shown in Figure 3.13, to occur.

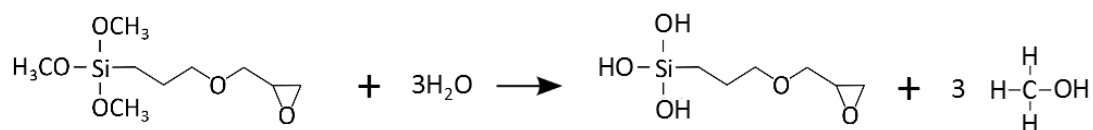


Figure 3.13: The hydrolysis reaction of silane.

The alumina samples, which had already been washed in acetone and dried, were immersed in the solution for 10 minutes. After removal from the bath, they were dried at 93°C for 60 minutes. Some of the samples from the 1 wt% solution were rinsed in water before they were dried in order to see if that would remove excess silane which had not adsorbed properly to the ceramic surface. In Figure 3.14, the condensation reaction where the silane attaches to the ceramic is shown.

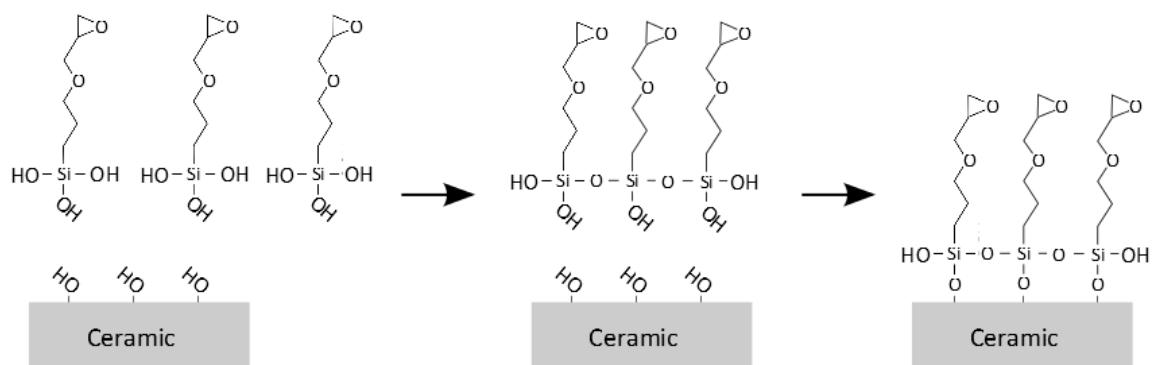


Figure 3.14: The condensation reaction of the silane. This figure is the ideal case, and may not be true for all cases.

### 3.2.4 Chromic sulphuric acid etch

Two different recipes were followed in order to test two different chromic-sulphuric acids.

The first recipe is the one known as the FPL-etch. Two parts of sodium dichromate, ten parts of sulphuric acid, and 30 parts of water by weight were used [20]. The sodium dichromate was dissolved in the water, and then the sulphuric acid was added little by little to prevent large increases in temperature. The chromic-sulphuric acid made by this recipe was held at 55-60°C during the treatment.

The same procedure was followed with the second recipe, but with 20 g sodium dichromate, 20 ml water, and 400 ml sulphuric acid (this corresponds to one part  $\text{Na}_2\text{Cr}_2\text{O}_7 \cdot 2\text{H}_2\text{O}$ , one part  $\text{H}_2\text{O}$  and approximately 36.8 parts  $\text{H}_2\text{SO}_4$ ) [53]. The chromic sulphuric acid made by this recipe was held at room temperature during the treatment.

In both cases, the following procedure was followed. The alumina samples were washed in acetone and dried. They were then immersed in one of the chromic-sulphuric acids for 10 or 60 minutes after which they were rinsed in distilled water, air dried for 10 minutes, and dried at 55-60°C for another 10 minutes.



### 3.3 Surface analysis

After surface treatment, the samples were analysed by different techniques in order to see how the surfaces were affected by the treatments. The techniques which were used were contact angle measurements, profilometer measurements, X-ray photoelectron spectroscopy (XPS) and scanning electron microscopy (SEM). In this section, the equipment, settings and methods used for these surface analyses will be presented.

#### 3.3.1 Contact angle

The contact angle measurements were done with water and diiodomethane. A 5  $\mu\text{l}$  drop of the liquid was placed on the surface, and the contact angle was measured. After that, the drop size was increased with a step size of 5  $\mu\text{l}$ , and new measurements were made after each step. This stepwise procedure was repeated until the standard deviation was sufficiently low, or until the drop was too big to measure. In that case, new drops were placed on the surface. Measurements were in all cases made at three or more places on the surface. The goniometer which was used for the contact angle measurements is shown in Figure 3.15.



*Figure 3.15: The goniometer used for contact angle measurements. The goniometer is supplied by Ramé-Hart, and is equipped with a light source (SCHOTT ACE<sup>®</sup> I) and a video camera (also supplied by Ramé-Hart).*

When all contact angle measurements were made, a geometric model was used in order to calculate the total surface energy and its polar and dispersive components.

### 3.3.2 Profilometer

A SENSOFAR PL $\mu$  2300 profilometer was used in order to investigate the topography, and to measure the roughness of the samples. A photograph of the profilometer is shown in Figure 3.16. Each sample was scanned at three different places on the surface. Two such sets of scans were performed, one where the light intensity was quite low and one with higher light intensity. Every scan consisted of 201 planes in the z-direction with a step length of 0.1  $\mu\text{m}$  between the planes.



*Figure 3.16: A photograph of the profilometer, SENSOFAR PL $\mu$  2300.*

The first set of scans, where the light was less intense, did not give a complete scan of each sample. Some areas on the surfaces lacked information. In the second set of scans, the light intensity was increased in order to get a more complete scan of each surface. However, this may have caused false, sharp peaks to occur due to light reflecting off the surface and causing interference. These false peaks may have influenced the height sensitive parameters such as  $S_a$ ,  $S_q$ ,  $S_p$ ,  $S_v$  and  $S_z$ ; but they do not seem to have a large effect on the surface area ratio  $S_{dr}$ .

### 3.3.3 X-ray photoelectron spectroscopy

For chemical analysis of the surfaces, a “KRATOS Axis Ultra<sup>DLD</sup>” XPS instrument, as shown in Figure 3.17, was used. For each sample, a survey scan was done in addition to high resolution scans of a few select peaks (oxygen, carbon, aluminium, and silicon peaks).

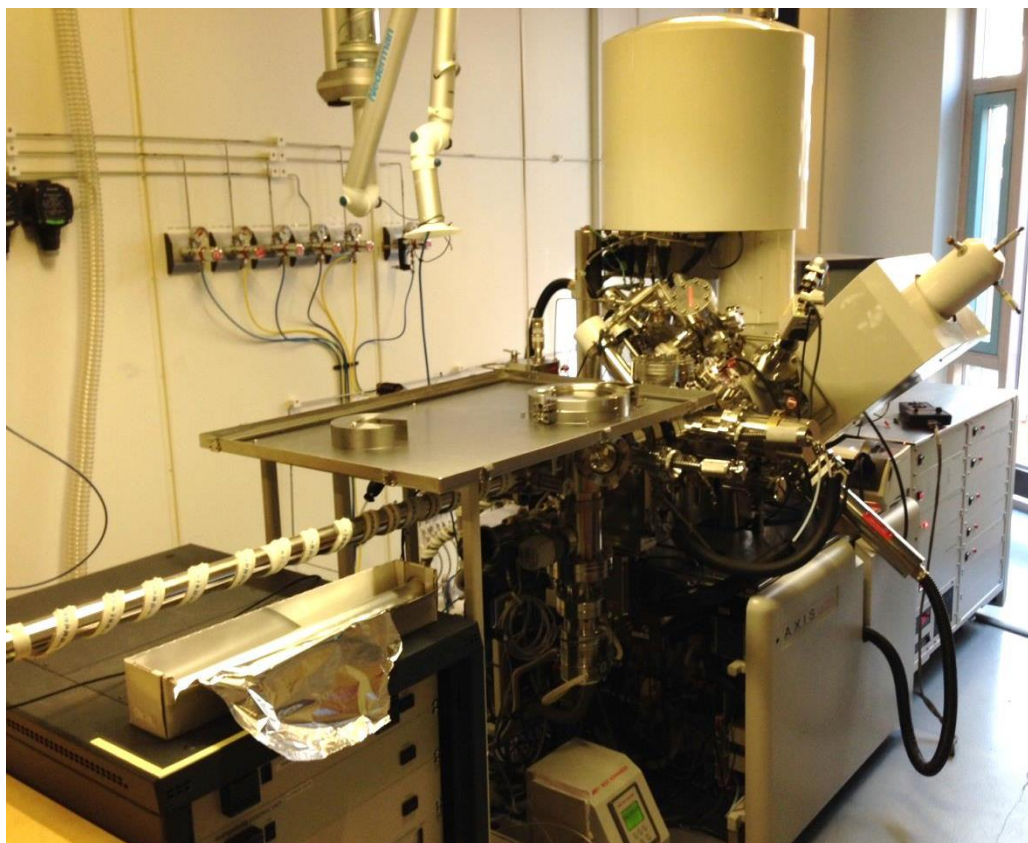


Figure 3.17: The XPS instrument, KRATOS Axis Ultra<sup>DLD</sup>.

The XPS instrument was used with a monochromatic Al K $\alpha$  anode with  $h\nu = 1486.69$  eV. The emission was set to 10 mA, and the pass energy was set to 160 eV with a step size of 1eV for the survey scans and 20 eV with a step size of 0.1 eV for the high resolution scans. The lens was used in hybrid mode meaning that both the magnetic and the electrostatic lens were used. Charge neutralisation was applied since the samples are poor conductors.

### 3.3.4 Scanning electron microscopy

The scanning electron microscope used in this thesis is the SU6600 Schottky Field Emission Analytical SEM, which is shown in Figure 3.18.

The settings used varied somewhat from sample to sample in order to get good images of each sample, and prevent charging of the sample. The working distance (WD) was normally ~12 mm, but in some cases it was lower. For most of the uncoated samples, accelerating voltages of 4 kV or 1 kV were used. However, some of the samples were coated with a 10 nm thick layer of a Pt/Pd alloy, allowing the accelerating voltage to be as high as 10 kV. The coater which was used is shown in Figure 3.19.



*Figure 3.18: The scanning electron microscope used in this thesis, SU6600 Schottky Field Emission Analytical SEM.*



Figure 3.19: Cressington 208 HR sputter coater used to increase conductivity of samples for SEM imaging.

### 3.4 LPET films containing POSS

As mentioned in Section 3.1.4, the POSS particles were added to the matrix of the composite by adding interlayer LPET films containing POSS particles between the ceramic and the composite. These films were allowed to melt into LPET in the composite. The interlayer films were made with varying concentrations of POSS particles. In this section, the process of making these POSS containing films will be explained.

First, the LPET and the FunzioNano AMS-656 were mixed in a 15 cc micro extruder. The extruder is shown in Figure 3.20, and consists of a chamber with two rotating screws which mix the materials together. The mixing was done at 215 °C and the screws rotated at 70 rpm.



Figure 3.20: A photograph of the twin screw 15 cc micro extruder, DSM MIDI2000

When the materials were well mixed, the product was collected as a string from the bottom of the extruder. The amount of material collected was not the same as the amount of material inserted to the extruder since some of the material was left in the extruder. In order to calculate the concentration of the extruded material, the material was weighed before and after extrusion so that the amount of material left in the extruder could be taken into account. In Table 3.3, the input and output weights are shown along with the calculated POSS concentration of product.

The first four runs were done with pure LPET, and in run 5 some of the POSS particles were added. In runs 6, 7 and 8 the mixture of LPET and POSS was thinned down by adding only LPET in order to get a set of different POSS concentrations.

Table 3.3: The amount of LPET and POSS added to the extruder in each run, the amount of finished product which was collected in each run, and the calculated POSS concentration in the product.

Run number	Input LPET (g)	Input POSS (g)	Output (g)	wt% of POSS
Run 1	10.00	0	3.46	0.0
Run 2	10.00	0	9.64	0.0
Run 3	10.00	0	9.84	0.0
Run 4	10.00	0	9.83	0.0
Run 5	8.02	1.98	9.80	11.49
Run 6	8.97	0	8.50	5.21
Run 7	9.00	0	8.19	2.44
Run 8	9.00	0	8.70	1.20

The pure LPET from the run 2 to run 4 was pressed into films and used as controls. Runs 5 through 8 were used to test the effect of the concentration on the adhesion. The product from run 1 was discarded since it was polluted by residual material in the extruder.

The films were produced by arranging the extruded strings inside a thin metal frame between two Teflon-covered metal plates, as shown in Figure 3.21, and then applying heat and pressure in the hydraulic compressor shown in Figure 3.23. The dimensions of the frame were 150 mm x 180 mm x 0.1 mm. Approximately 4 - 4.5 g of extruded string was weighed in for each film depending on the amount of material available. These metal plates with the LPET-POSS mix between them were placed between two heaters and heated to 200 °C. When the material was melted (after approximately 2 minutes) a pressure equivalent to approximately 6-7 tons was applied, the pressure was increased a little after about 30 seconds. After a few minutes at high pressure, the plates were cooled down to temperatures below 60 °C, and the pressure was released. When the plates were sufficiently cold, they were taken apart, and the POSS containing LPET film was retrieved. Some of the finished films are shown in Figure 3.22.



*Figure 3.21: The arrangement of the extruded material before it is pressed into a film.*

After the production, the thickness of the films was measured. This showed that the finished interlayer films were  $0.16 \pm 0.04$  mm thick.

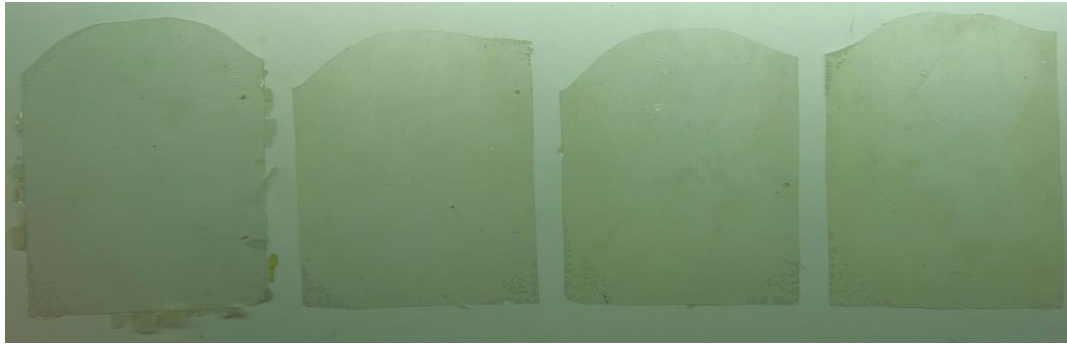


*Figure 3.22: Four of the finished LPET films. The POSS content of the films increases from left to right (0 wt%, 1.20 wt%, 2.44 wt% and 5.21 wt%)*



*Figure 3.23: A photograph of the hydraulic compressor used for pressing films, Fontijne TH200.*

With increasing concentration of POSS particles, the films became more brittle, and therefore more difficult to handle. This caused some of them to crack, but all of them were good enough to be used. One of the films with 11.49 wt% POSS is shown in Figure 3.24. The high POSS content in this film caused it to be so brittle that it broke into smaller pieces.



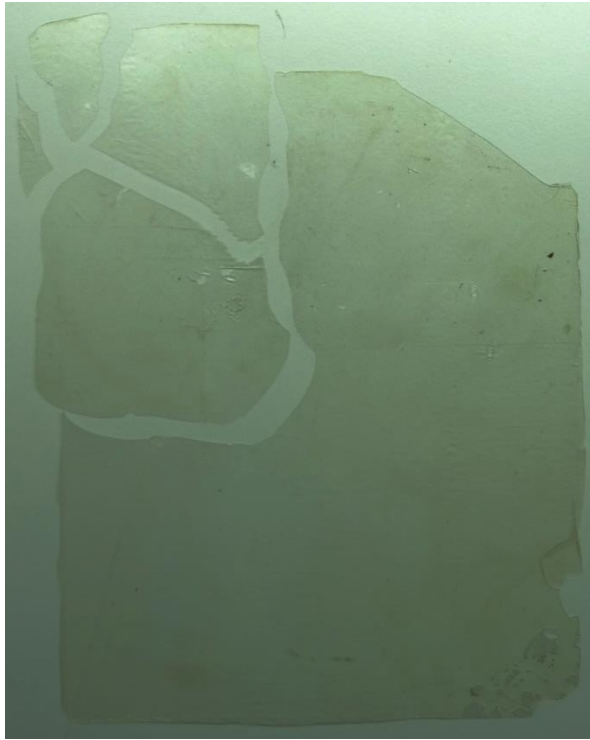


*Figure 3.24: One of the films with 11.49 wt% POSS particles. The film broke due to the brittleness caused by the high POSS content.*

The POSS containing films were used either with acetone washed ceramic tiles or silane treated ceramic tiles. The concentration of the silane solution was 0.5 wt% in an attempt to avoid getting peel strengths that were too high to measure.

### 3.5 Production of test samples

The test samples used for peel test and ballistic tests were made in a vacuum oven shown in Figure 3.25.

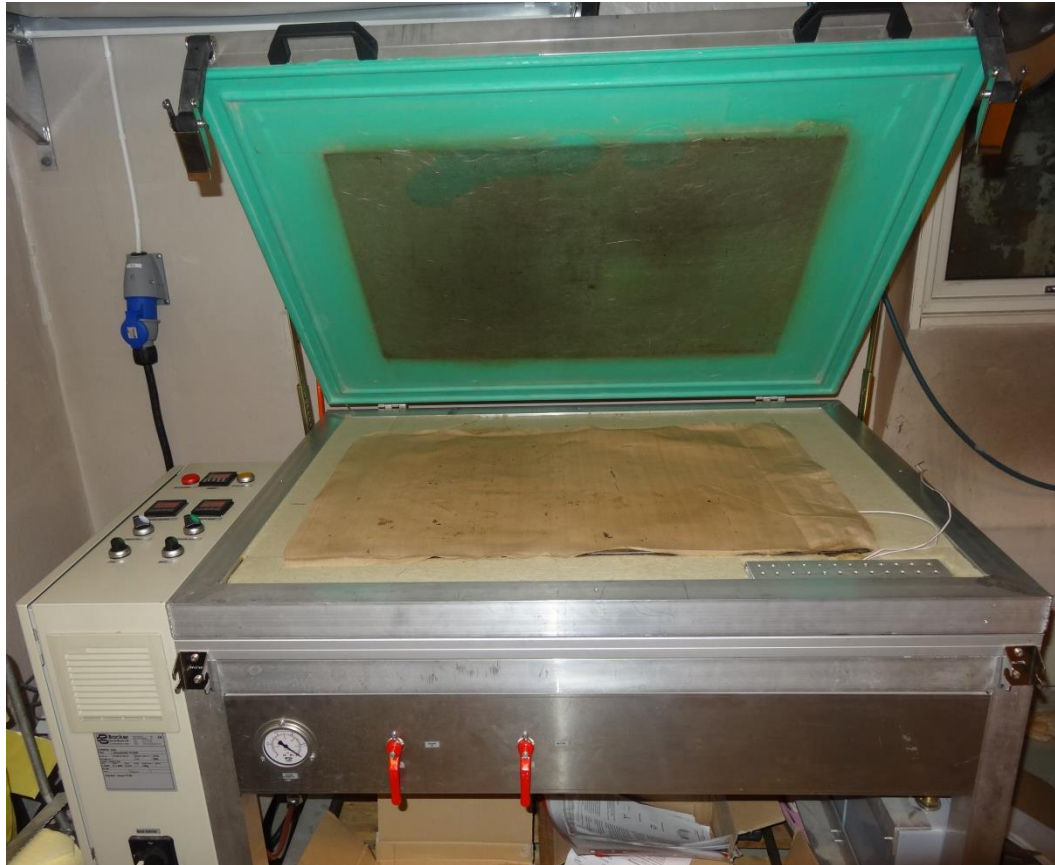


*Figure 3.25: The vacuum oven used for making test samples, Vacuumheater VT 75 x 50 supplied by Norske Backer A/S.*

The peel test samples were made with five layers of the GF-LPET fabric on the side of the ceramic facing down towards the heat source, and four layers of GF-LPET fabric on the side facing away from the heater. The only exemption from this was the POSS containing samples where an interlayer film was added between the five layers of composite fabric and the ceramic, and where only two layers of composite fabric were used on the side facing away from the heat source.

In order to get a good grip on the peel arm, a dummy tile was placed next to the surface treated tile with a Teflon film between the ceramic and the composite to prevent the two from adhering to each other. The Teflon film was placed 20 mm in on the surface treated tile from the edge in order to create a starter pre-crack for the crack growth. This can be

seen in Figure 3.26. A Teflon film and a metal plate were placed on top of the entire system in order to ensure a flat surface on the top. This was done in order to be able to test the side with four layers without the problems an uneven surface would give. The entire layup can be seen step by step in Figure 3.27.

The side where four layers of composite fabric were added was tested for some of the surface treatments. In these tests, the composite had a tendency to break when the adhesion was good. Because of this, the side where five layers were added is the one used for peel testing.



*Figure 3.26: The lay-up of the composite, Teflon film and ceramic before heating. The Teflon film is placed 20 mm in on the surface treated sample. The dummy tile would be placed on top of the Teflon film in the right part of this picture. This image corresponds to step two in Figure 3.27.*

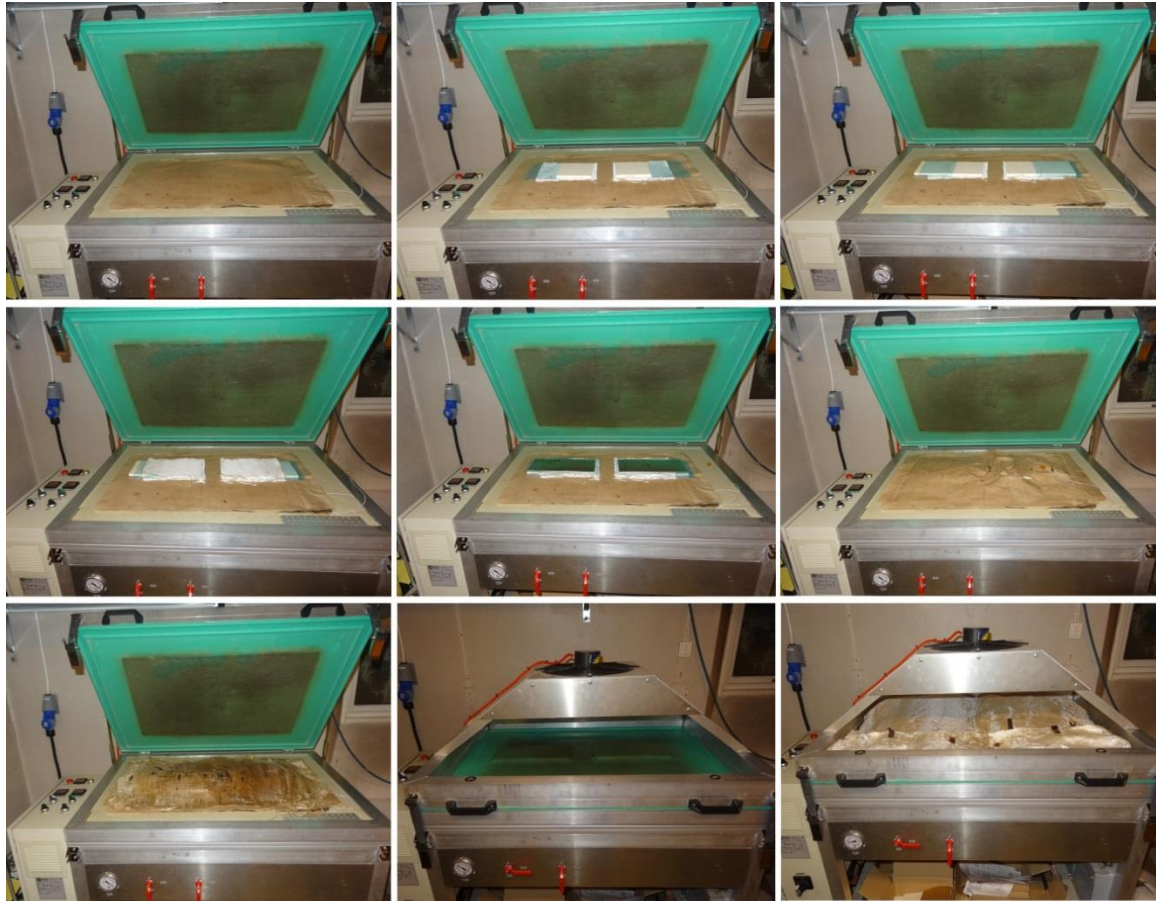


*Figure 3.27: A step by step illustration of the lay-up for production of the peel test samples. First, the ceramic is placed on top of five layers of the GF-LPET fabric with a Teflon film partly between them as shown in Figure 3.26. Then the dummy tile is placed as shown in picture three followed by a new Teflon film, four (or two) more layers of GF-LPET fabric and a metal plate. This is then covered in a Teflon fabric and a protective glass fibre fabric (without LPET). Vacuum is then applied, insulation put in place, and the heating is started.*

The test samples for ballistic testing were made without the dummy tile, and with two layers of composite on each side. Two long strips of the GF-LPET fabric were folded around the ceramic, as shown in Figure 3.28, in order to get as good contact as possible between the ceramic and the composite around the edges of the ceramic. There was a small overlap of GF-LPET fabric on one side of the ceramic, this overlap was placed as close to the edge of the tile as possible. The tiles were placed in the oven in such a way that the side where there was an overlap of the GF-LPET was up. This side was the front side during the ballistic tests.

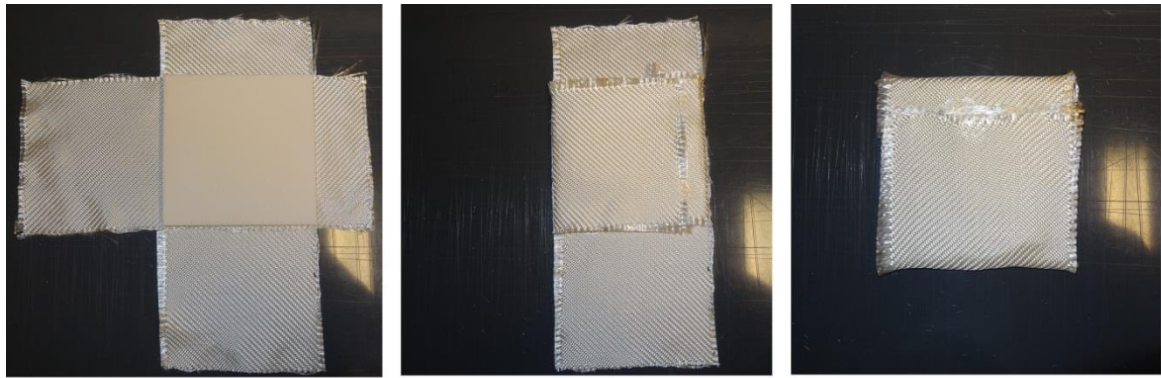


Figure 3.28: Photographs of how the glass fibre fabric was folded in order to make the ballistic test samples.

The tiles with the composite were heated to 215 °C under vacuum, and a timer was started. 90 minutes after turning on the heat, the oven was turned off, and a fan was turned on in order to cool the samples more efficiently. When the samples were cooled, air was let in, and they were removed. In Figure 3.29, the process window of the LPET is shown, this illustrates the amount of time the LPET must be kept at different temperatures in order for the composite to be acceptable.

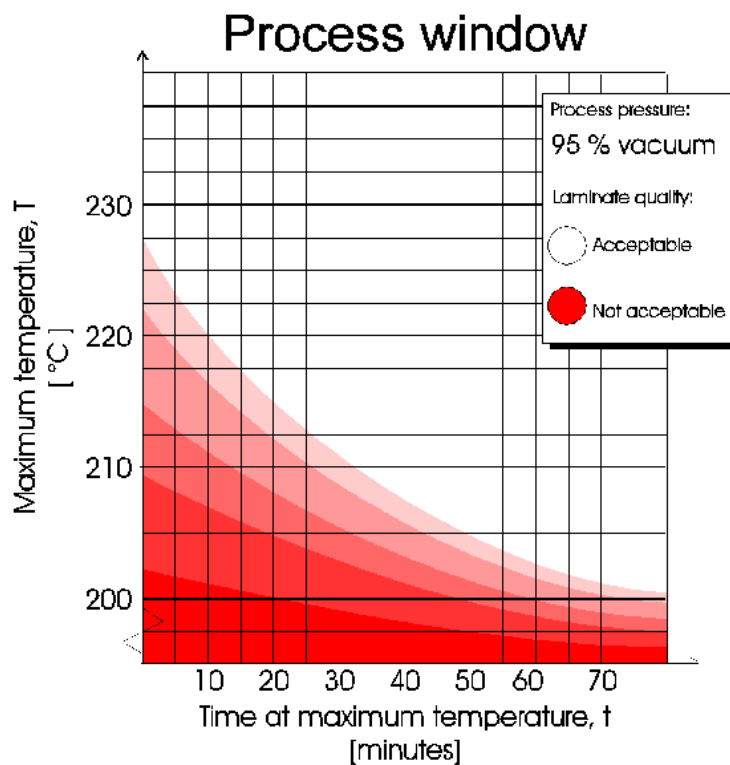


Figure 3.29: The process window for the LPET showing temperature versus exposure time. The white areas mark the time-temperature combinations that give an acceptable finished product, and the red areas mark the combinations which do not give an acceptable product [50].

Heating the vacuum oven to 215 °C took approximately 10 minutes, leaving 80 minutes of the production time at maximum temperature. This heating time can be seen from the graph in Figure 3.30.

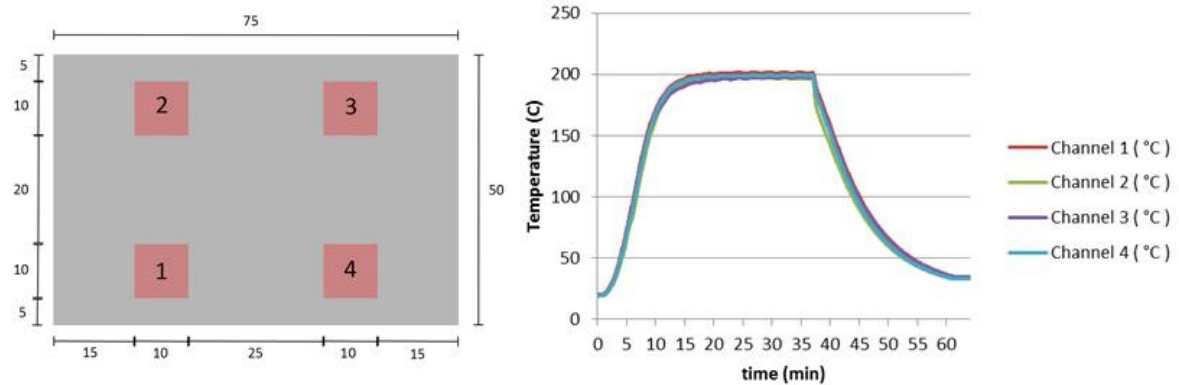


Figure 3.30: Graph of temperature vs. time during heating and cooling of the samples. These tests were done with a different type of ceramic tile, and the temperature was set to 200 °C, but the heating time is about the same. The temperature was measured in four different places in the oven as shown on the left side of the figure.

After removing the dummy tiles, the tiles for peel testing were cut into five, 20 mm wide test samples using a Rodia 600 tile saw, which is shown in Figure 3.31. The finished peel test samples are shown in Figure 3.32. An example of a finished ballistic test sample is shown in Figure 3.33.



Figure 3.31: The Rodia 600 tile saw used for cutting the ceramic plates into peel test samples.

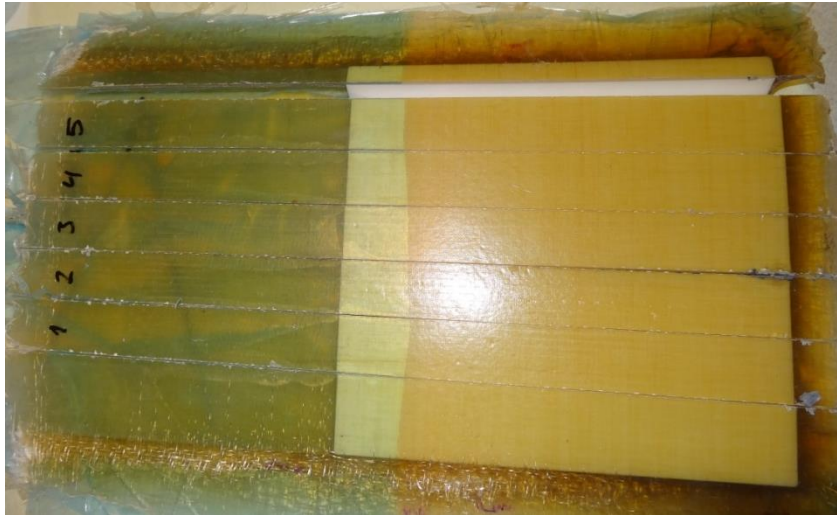


Figure 3.32: The finished peel test samples numbered 1 to 5. The edges of the ceramic tile were cut off.

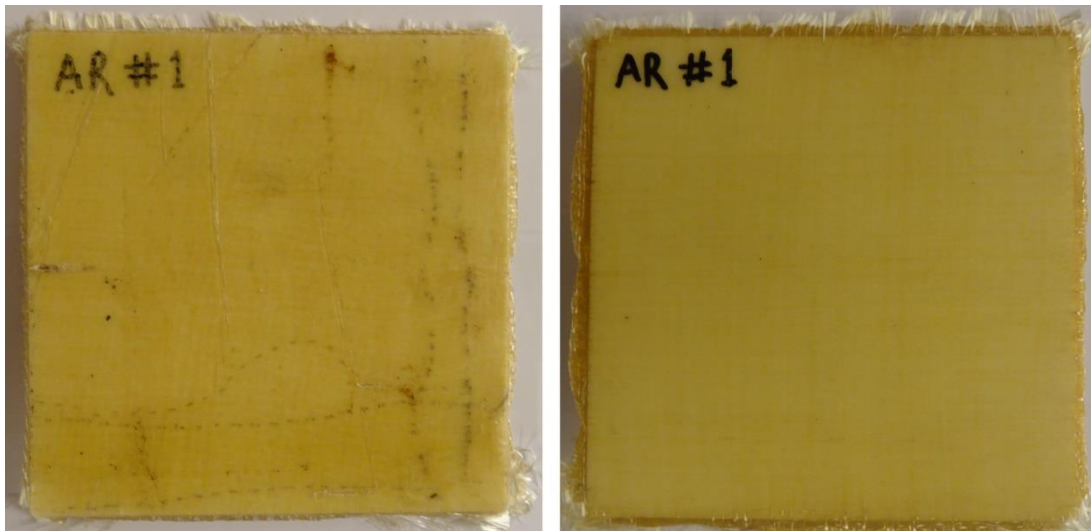
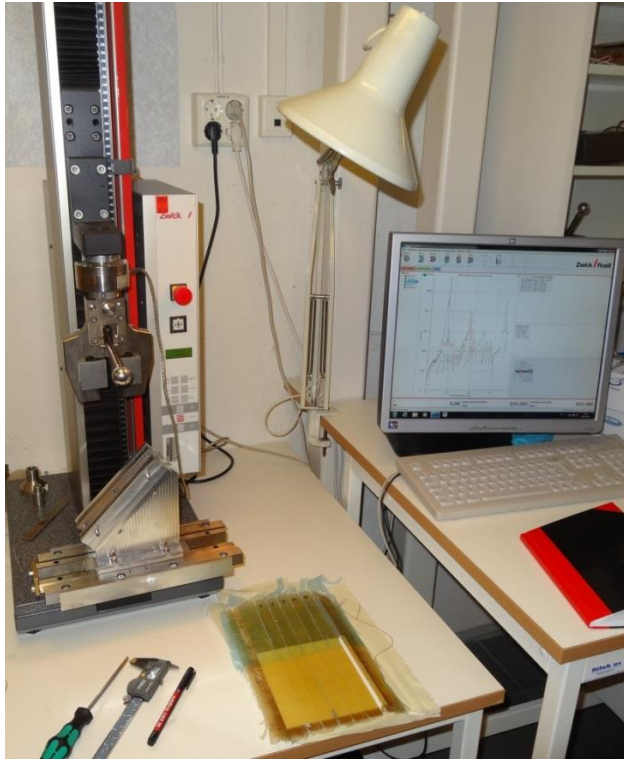


Figure 3.33: The finished ballistic test sample. Left: front side (facing up during production). Right: back side (facing down during production)

### 3.6 Peel testing

The peel testing was performed using a Zwick BZ 2.5/TN1S test machine together with a custom built fixture for peel testing. The purpose of this fixture was to maintain a peel angle of  $45^\circ$  by sliding the angled sample holder on linear bearings in order to keep the crack front below the crosshead of the test machine. This setup can be seen in Figure 3.34.



*Figure 3.34: The Zwick BZ 2.5/TN1S test machine with the custom built peel test fixture.*

Before the peel arm of the sample was attached in the grip on the testing machine, the measured force was zeroed. The crosshead speed was set to 2.93 mm/min in order for the crack growth to be 10.0 mm/min [46]. The bonded area of the test samples was approximately 20 mm wide as mentioned above, and about 130 mm long. Figure 3.35 shows the peel test in progress.

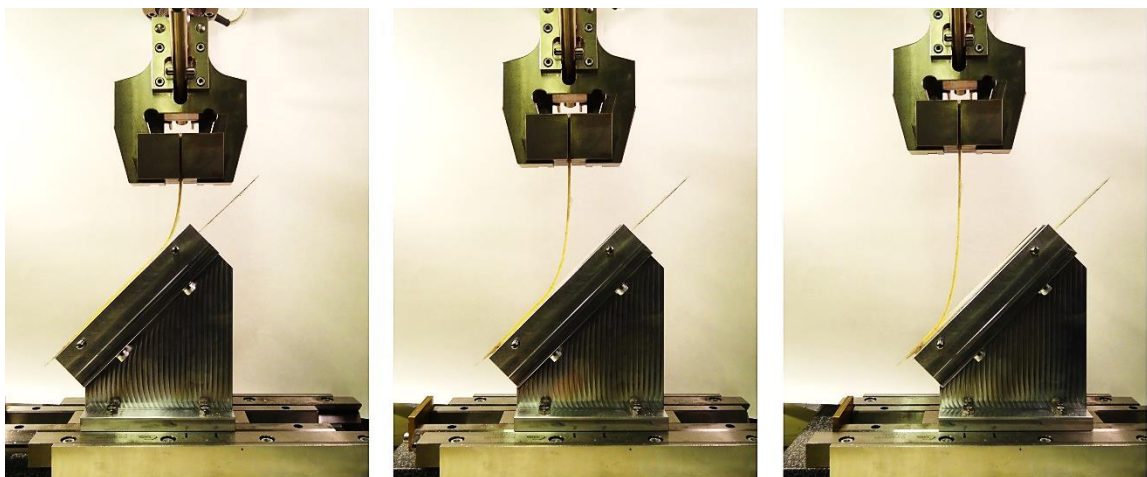


*Figure 3.35: The peel test in progress.*



The tests were conducted between 0 mm and 36 mm standard travel for the cross head. For some of the samples with the best adhesion, the composite peel arm would crack or break causing inaccurate results in some tests, and failure of others. This cracking would usually occur at the beginning of the test. In other tests, where the adhesion was not as good, the crack would reach the end of the ceramic before the cross head reached 36 mm standard travel. Because of these inaccuracies, the results from the beginning and end of each sample were discarded. However, there are still some inaccuracies in the result from cracking of the peel arm and uneven movement on the rails causing the peel angle to vary a little.

Normally, five parallel samples were tested. For each of these samples, a load-displacement curve was recorded and a width measurement was conducted on the position of the crack front along the sample for every 5 mm of standard travel. An average value was calculated for the measured force from the acceptable part of each sample, and this was divided by the average width of the sample in order to correct for varying sample widths. This corrected value is called the peel force, and is given in N/mm.

### **3.7 Ballistic testing**

Four sets of samples were made for the ballistic testing following the procedure which is described in Section 3.5. Each set consisted of four samples, one as-received, one acetone washed, one silane treated (1 wt%, not rinsed) and one Teflon wrapped sample.

The test samples were taped to a 20 cm x 20 cm large backing plate made from 20 layers of Twaron UD41, and then strapped to a clay block as shown in Figure 3.36.



Figure 3.36: The set-up of the sample before ballistic testing.

The projectile type which was used was a hardened steel core projectile (RUAG 7.62 x 51 HC). This projectile type is specifically designed to penetrate hard targets. Additional information about the projectile can be found in Appendix G. A photograph of the projectile and the stripped steel core, and an illustration of the projectile are shown in Figure 3.37.

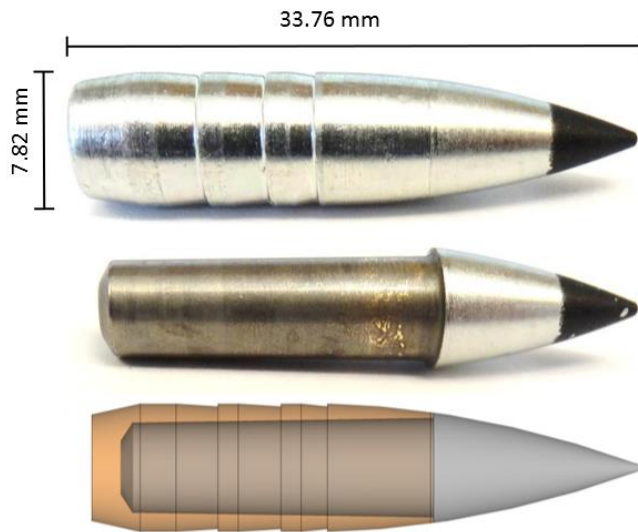


Figure 3.37: Photographs of the projectile and the stripped hardened steel core and an illustration of the projectile where the hardened steel core is shown.

The tests were done with different projectile velocities. For the first set of samples the projectile velocity was approximately 335-340 m/s, and for the second set the velocity was 480-485 m/s. The third and fourth sets were both tested with a projectile velocity of approximately 600 m/s. However, there were some variations in the velocities for these sets. The exact projectile velocity for all the tests can be seen in Table 4.10 in the results chapter.

After the shot was fired, a red penetrant (BYCOTEST RP20) was sprayed into the hole left by the projectile, and allowed to penetrate into the cracks in the ceramic in order to visually enhance them. Pictures were then taken of the front and back of the plates in order to compare the damage on the different samples.

### 3.8 Microscopy

Most of the microscopy in this thesis was done with the scanning electron microscope as mentioned in Section 3.3.4. However, in order to find out whether or not the composite matrix is able to penetrate into pores on the alumina surface, cross-section images were taken on a “ZEISS imager.M1m” microscope. Small samples were cut from the leftover of the peel test plates, and moulded into an epoxy. They were then polished in order to get a smooth cross-section. An overview image of the cross-section on the as-received sample is shown in Figure 3.38, the rest of the cross-section images are shown in Section 4.1.

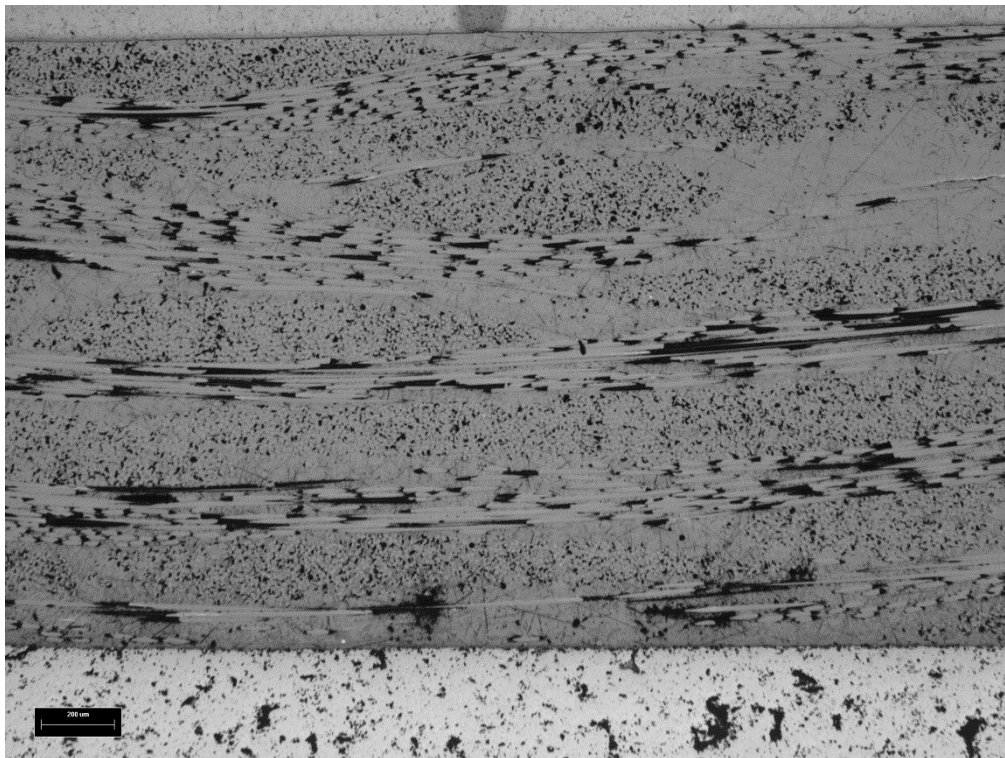


*Figure 3.38: An overview image of the cross-section of the as-received sample. The full thickness of the composite layer can be seen on top of the ceramic surface. (The scale bar in the bottom left corner is 200  $\mu\text{m}$ )*



## 4 Results

In this section, the results from all tests will be presented. The results from the surface analysis after various surface treatments will be presented first, followed by the results from the peel tests and the ballistic tests. After this, the results from the peel tests of the samples with POSS particles will be presented separately.

### 4.1 Surface analysis

After all the different surface treatments, the surfaces were analysed by contact angle measurements, profilometer and XPS in order to find out how the treatments affect the surfaces. The results from these tests will be presented in this section. In addition to this, images of the surfaces were taken using a scanning electron microscope. The SEM images are shown in Figure 4.1 to Figure 4.8.

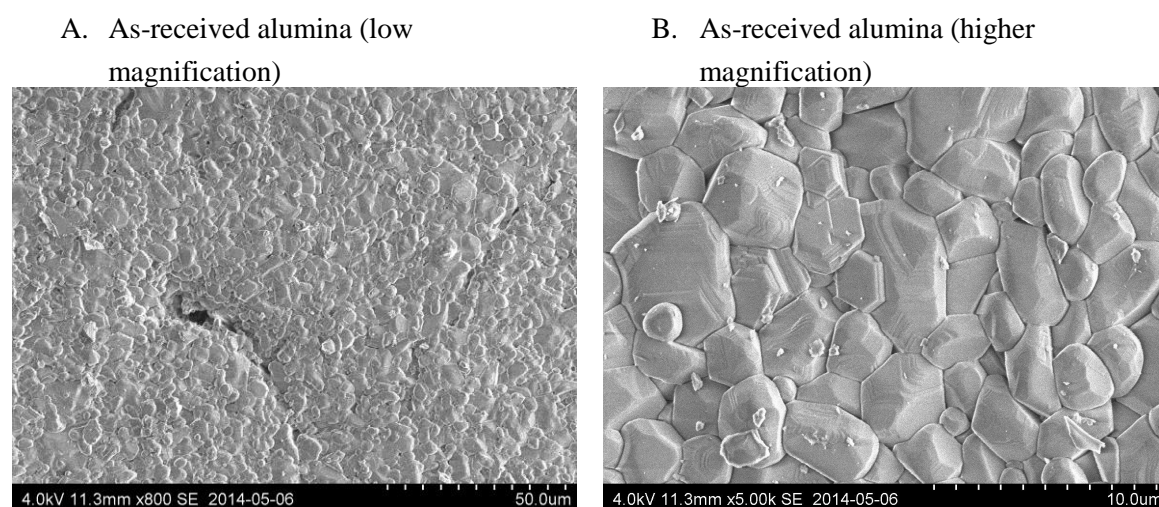
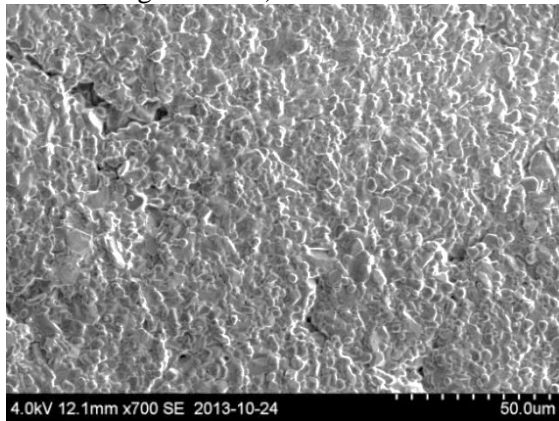


Figure 4.1: SEM images of the as-received alumina surface at two different magnifications.

A. Acetone washed alumina (low magnification)



B. Acetone washed alumina (higher magnification)

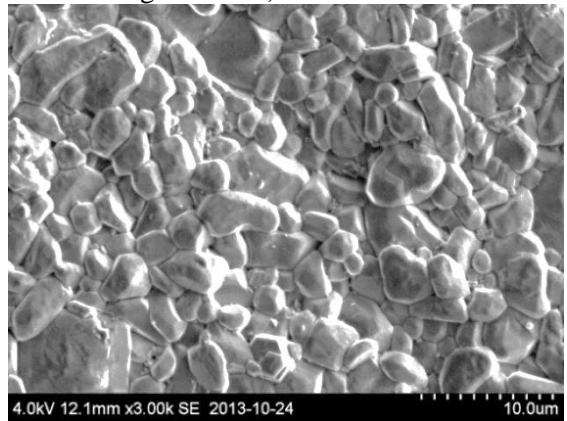
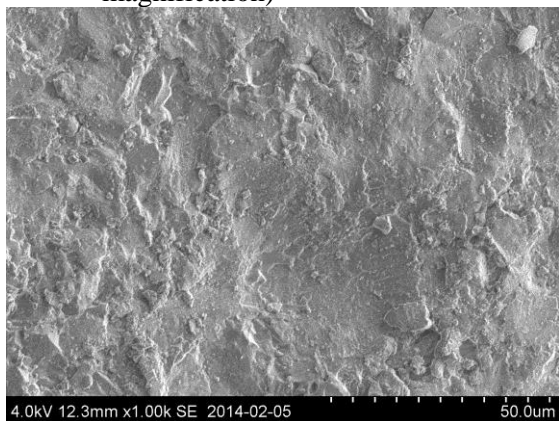


Figure 4.2: SEM images of the acetone washed alumina surface at two different magnifications.

A. Sandblasted alumina (low magnification)

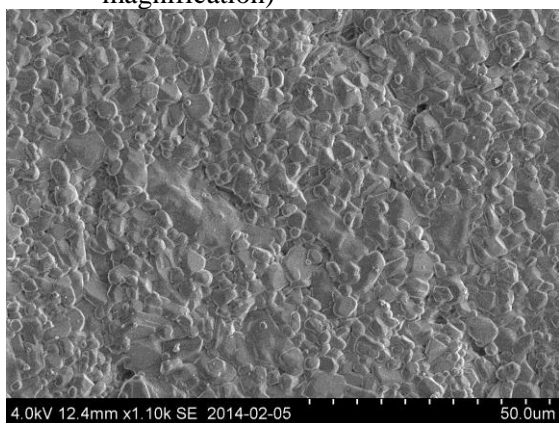


B. Sandblasted alumina (higher magnification)



Figure 4.3: The sandblasted surface at two different magnifications.

A. Plasma treated alumina (low magnification)



B. Plasma treated alumina (higher magnification)



Figure 4.4: The plasma treated surface at two different magnifications.

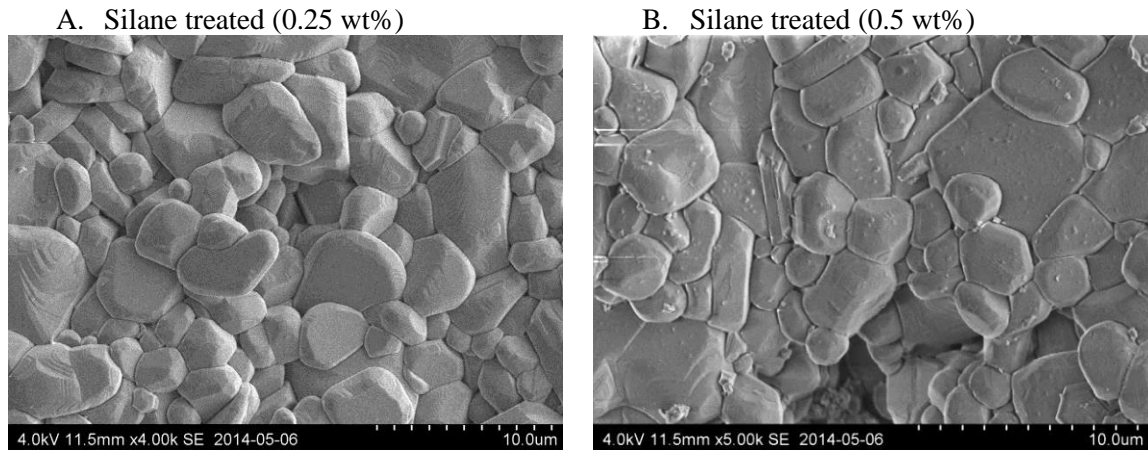


Figure 4.5: SEM images of the surface after silane treatment with a concentration of A.: 0.25 wt% and B.: 0.5 wt% on the silane solution.

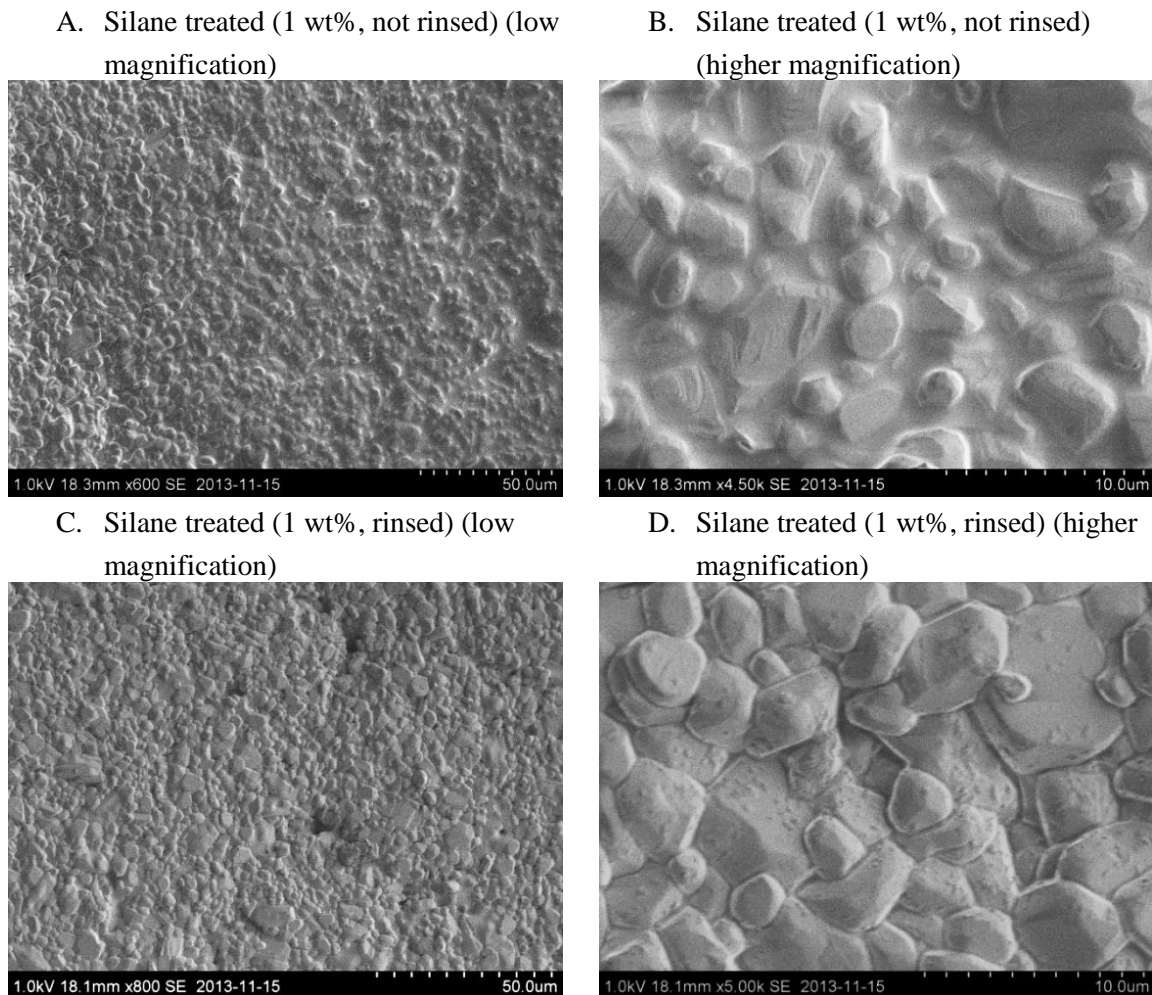
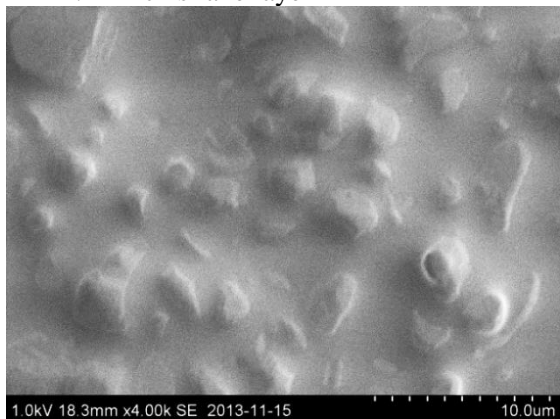
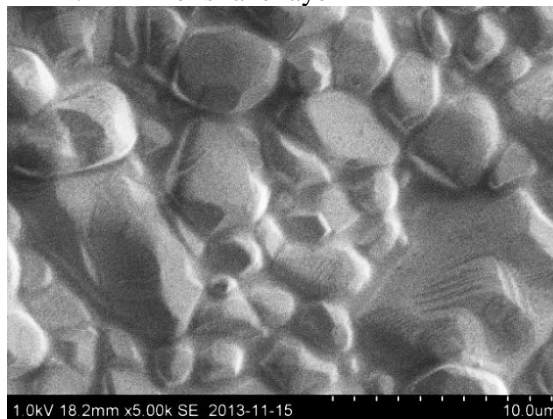


Figure 4.6: SEM images of the silane treated surfaces with a concentration of 1 wt% on the silane solution; with and without rinsing.

A. Thick silane layer



B. Thinner silane layer



*Figure 4.7: A comparison of two different areas of the surface of the silane treated (1%, not rinsed) alumina showing that the thickness of the silane layer varies a lot. This variation was not found on the surface of the silane treated alumina that was rinsed. In Figure 4.6 A, this variation can be seen between the left and the right part of the image.*



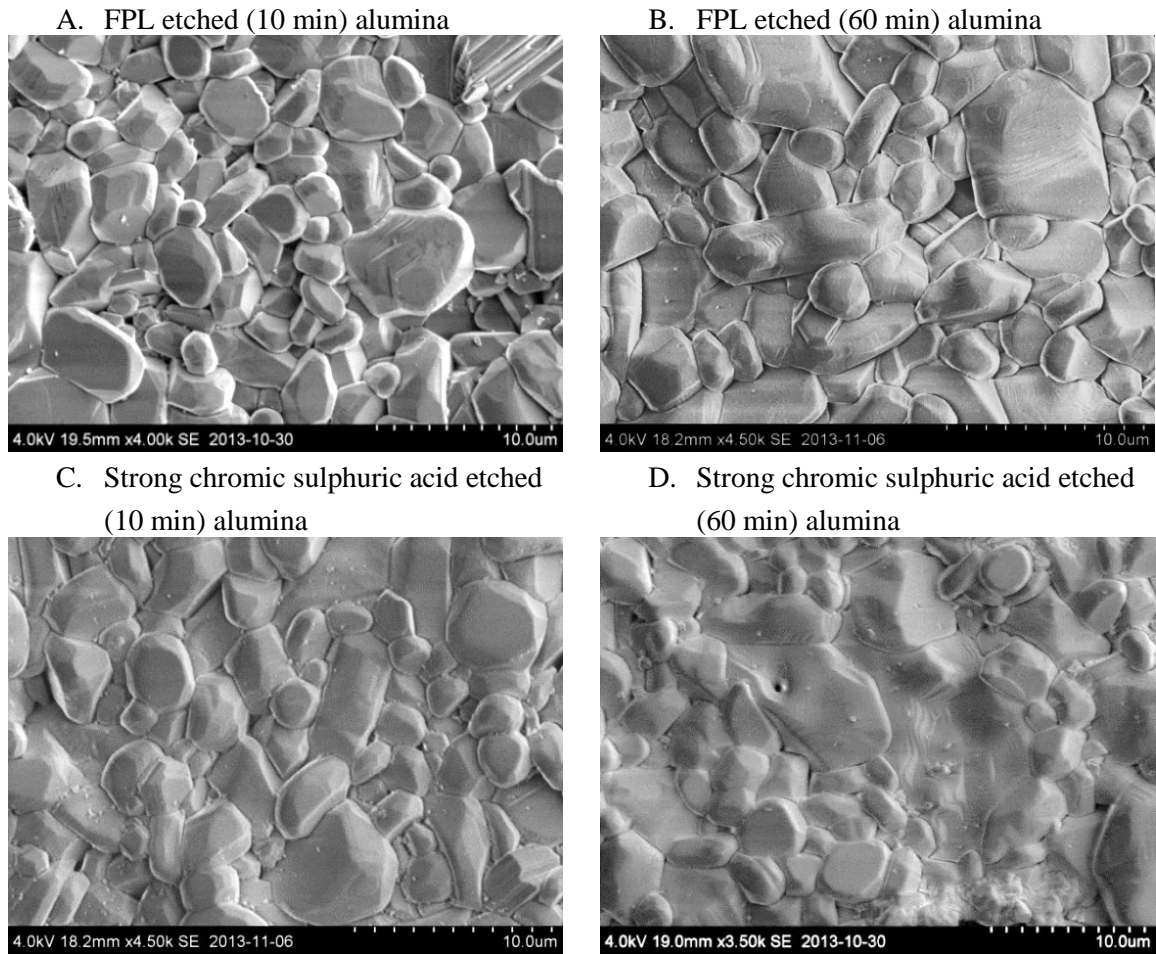


*Figure 4.8: A comparison of the alumina surface after different chromic/sulphuric acid treatments. A: the surface after 10 minutes of the FPL-etch; B: the surface after 60 minutes of the FPL-etch; C: the surface after 10 minutes of the strong chromic/sulphuric acid treatment; and D: the surface after 60 minutes of the strong chromic/sulphuric acid treatment.*

In addition to the SEM image, a set of cross-section images were taken of the ceramic with the composite attached to it. These images are shown in Figure 4.9 to Figure 4.12. The difference between these cross-section images may not be overwhelming, but it is quite clear that the surface of the sandblasted ceramic in Figure 4.11 is damaged from the treatment. This seems to result in less contact between the ceramic and the composite in that case. When comparing the as-received and the acetone washed samples in Figure 4.9 and Figure 4.10, it may seem that there is a slightly larger contact area on the acetone washed sample. On the silane treated (1 wt%, not rinsed) sample in Figure 4.12, the gap between the ceramic and the composite has both grey and black areas. It may be that the grey areas filling the pores on the ceramic surface is the silane layer, and that the black areas closer to the composite are similar to the holes seen in all the other samples. However, it is difficult to make any certain evaluations based on these images.

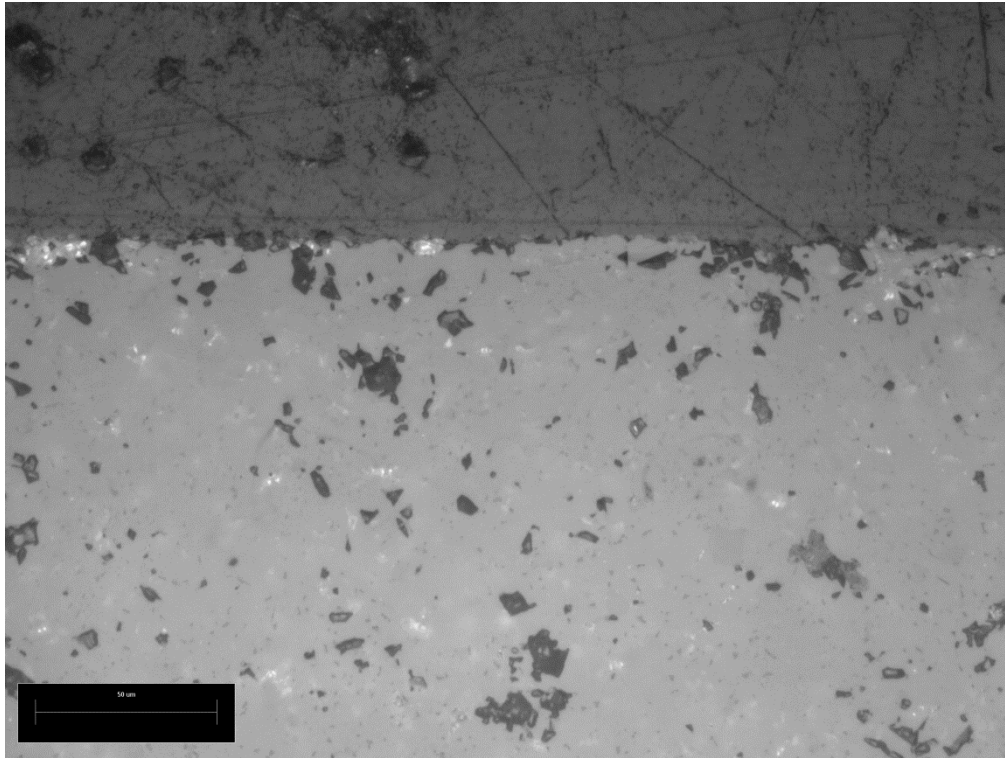


*Figure 4.9: A cross-section image of the interface between the composite and the as-received ceramic.*

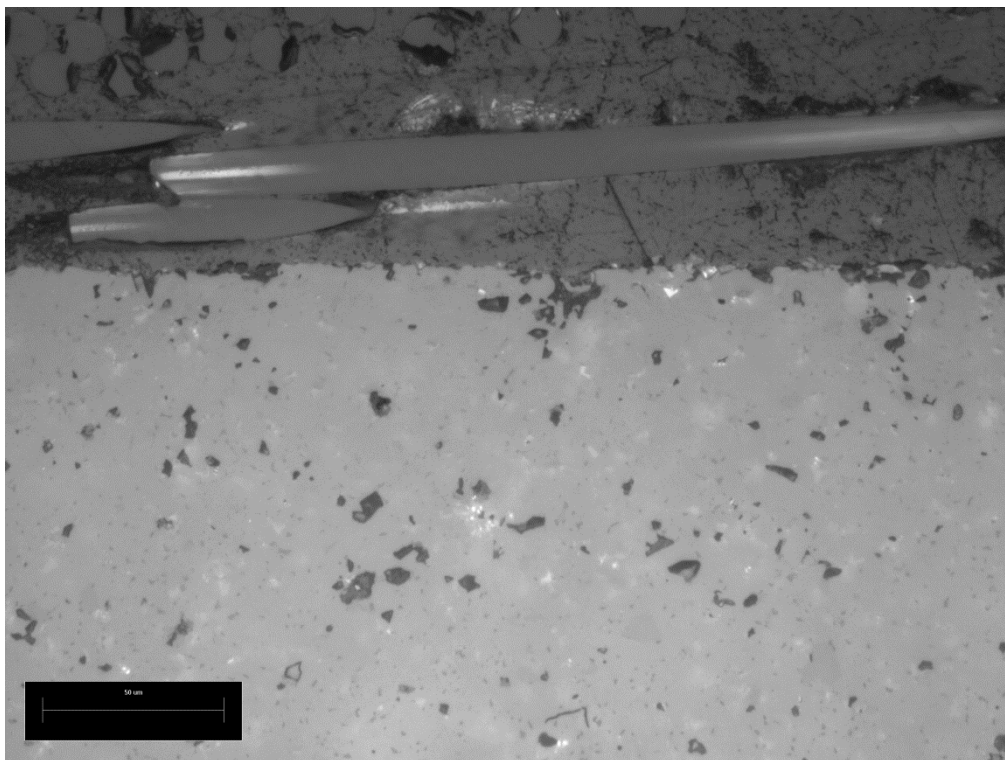


*Figure 4.10: A cross-section image of the interface between the composite and the acetone washed ceramic.*

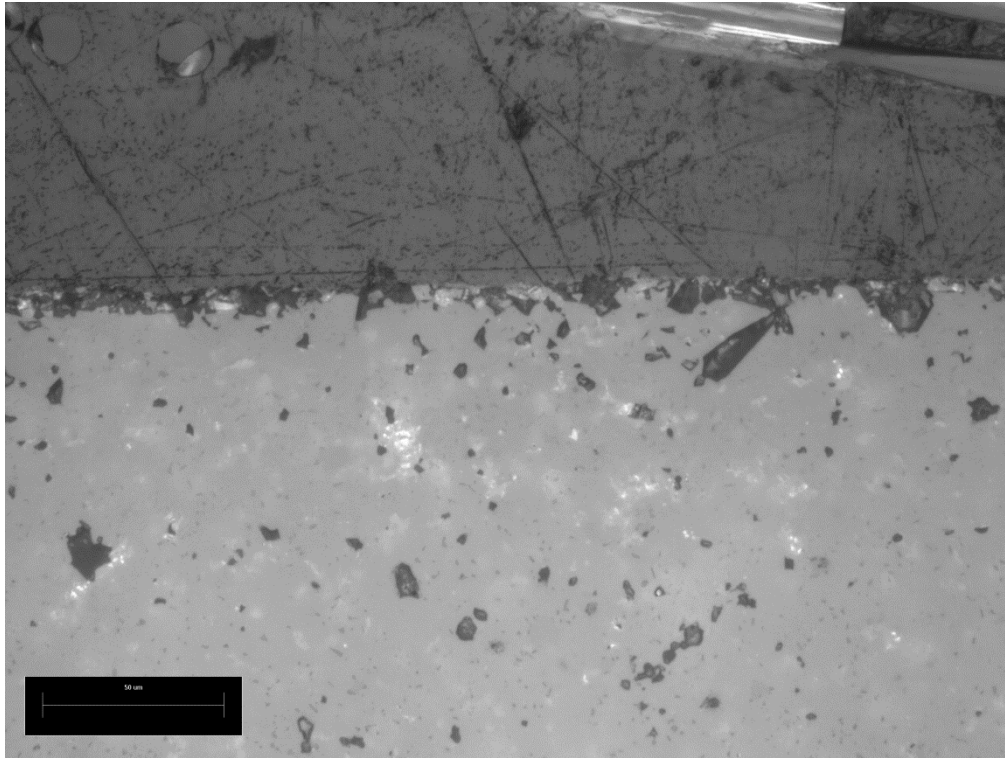


*Figure 4.11: A cross-section image of the interface between the composite and the sandblasted ceramic.*

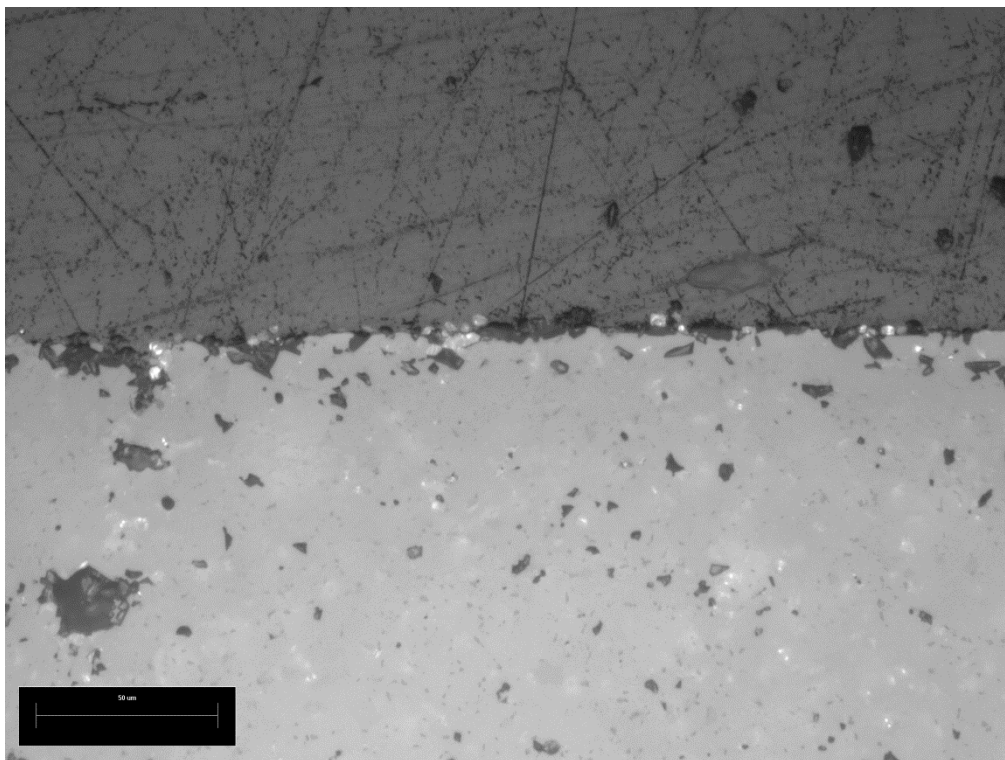


*Figure 4.12: A cross-section image of the interface between the composite and the silane treated (1 wt%, not rinsed) ceramic.*

### 4.1.1 Contact angle measurements

In this section, the results of the contact angle measurements and the calculated surface energies will be presented for all the different surface treatments. It should be mentioned that contact angles can be very difficult to reproduce from one sample to another, so some care should be taken when analysing the results.

The contact angles and calculated surface energies for the different samples are found in Table 4.1 and Table 4.2 respectively. In order to better understand the properties of the composite, two blocks of solid LPET were made, and contact angles were measured on their surfaces. The results from these measurements and calculated values for the surface energies can also be seen in these tables. Comparing this information to the measurements done on the alumina samples may help with the understanding of how well the composite matrix is able to wet the ceramic surface after the different surface treatments. The calculated surface energies in this table are also shown as a bar graph in Figure 4.13.

*Table 4.1: The measured contact angles for all the different samples.*

	Contact angle (deg.)	
	Water	Diiodomethane
As-received alumina	45.4 ± 1.0	70.4 ± 0.6
Acetone washed alumina	32.6 ± 0.3	48.9 ± 0.4
Sandblasted alumina	40.3 ± 0.7	30.3 ± 0.4
Plasma treated (25 sec)	18.1 ± 0.6	28.9 ± 0.4
Plasma treated (50 sec)	15.3 ± 0.4	35.2 ± 0.5
Plasma treated (100 sec)	16.7 ± 0.5	34.8 ± 0.4
Silane treated (0.25 wt%)	70.7 ± 0.6	47.6 ± 0.2
Silane treated (0.5 wt%)	56.8 ± 0.5	39.9 ± 0.4
Silane treated (1 wt%, not rinsed)	39.6 ± 0.4	25.6 ± 0.6
Silane treated (1 wt%, rinsed)	42.7 ± 0.8	38.5 ± 0.5
FPL-etch, (10 min)	25.6 ± 0.5	37.5 ± 0.6
FPL-etch, (60 min)	21.4 ± 0.4	30.6 ± 0.6
Strong chromic/sulphuric acid, (10 min)	20.3 ± 0.8	28.2 ± 0.5
Strong chromic/sulphuric acid, (60 min)	12.2 ± 0.7	40.6 ± 1.0
Solid LPET block	69.1 ± 0.4	28.9 ± 0.5

Table 4.2: The calculated total surface energy and the calculated polar and dispersive contributions to the surface energy for all the different samples.

	Surface energy (mJ/m <sup>2</sup> )		
	Polar	Dispersive	Total
As-received alumina	31.0 ± 0.2	22.6 ± 0.4	53.6 ± 0.7
Acetone washed alumina	30.6 ± 0.2	34.9 ± 0.2	65.5 ± 0.2
Sandblasted alumina	21.6 ± 0.4	44.1 ± 0.2	65.7 ± 0.4
Plasma treated (25 sec)	31.0 ± 0.2	44.7 ± 0.2	75.7 ± 0.2
Plasma treated (50 sec)	33.4 ± 0.2	41.9 ± 0.2	75.3 ± 0.2
Plasma treated (100 sec)	32.9 ± 0.2	42.1 ± 0.2	75.0 ± 0.2
Silane treated (0.25 wt%)	8.3 ± 0.3	35.6 ± 0.1	43.9 ± 0.3
Silane treated (0.5 wt%)	14.2 ± 0.3	39.7 ± 0.2	53.9 ± 0.3
Silane treated (1 wt%, not rinsed)	21.1 ± 0.3	45.9 ± 0.2	67.0 ± 0.3
Silane treated (1 wt%, rinsed)	22.0 ± 0.5	40.3 ± 0.2	62.3 ± 0.5
FPL-etch, (10 min)	30.4 ± 0.3	40.8 ± 0.3	71.3 ± 0.3
FPL-etch, (60 min)	30.4 ± 0.2	44.0 ± 0.2	74.3 ± 0.2
Strong chromic/sulphuric acid, (10 min)	30.2 ± 0.3	45.0 ± 0.2	75.1 ± 0.3
Strong chromic/sulphuric acid, (60 min)	35.8 ± 0.3	39.3 ± 0.5	75.1 ± 0.2
Solid LPET block	6.5 ± 0.2	44.7 ± 0.2	51.2 ± 0.5

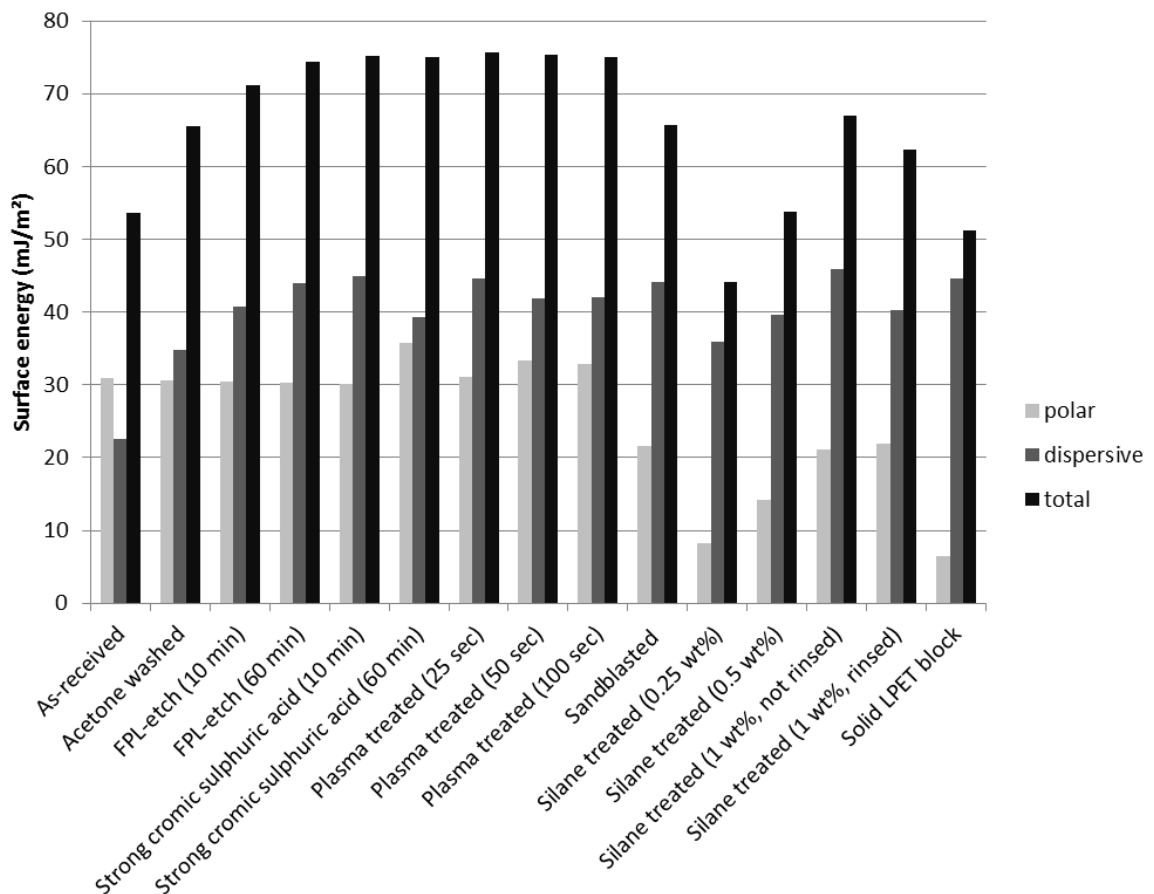


Figure 4.13: The calculated total surface energies, and the polar and dispersive contributions to the surface energies for the different samples.

The contact angles are affected by the surface chemistry and the surface roughness, so in order to better understand the contact angle measurements they should be compared with the XPS results in Section 4.1.3 and the results from the profilometer analysis in Section 4.1.2. Comparison of the contact angle measurements and the XPS results will be done in the discussion chapter. The effect of the different roughness of the samples however, can be corrected for quite easily. The values for the percentage increase in surface area due to roughness,  $S_{dr}$ , from the profilometer measurements were used to calculate the roughness ratio  $r$  in Equation 2.11. This equation was then used to calculate what the contact angles would be on a flat surface. These new contact angles were used to calculate the surface energies. A bar graph of these roughness-corrected surface energies is shown in Figure 4.14. The  $S_{dr}$  values used to calculate this are presented along with the rest of the profilometer measurements in Section 4.1.2.

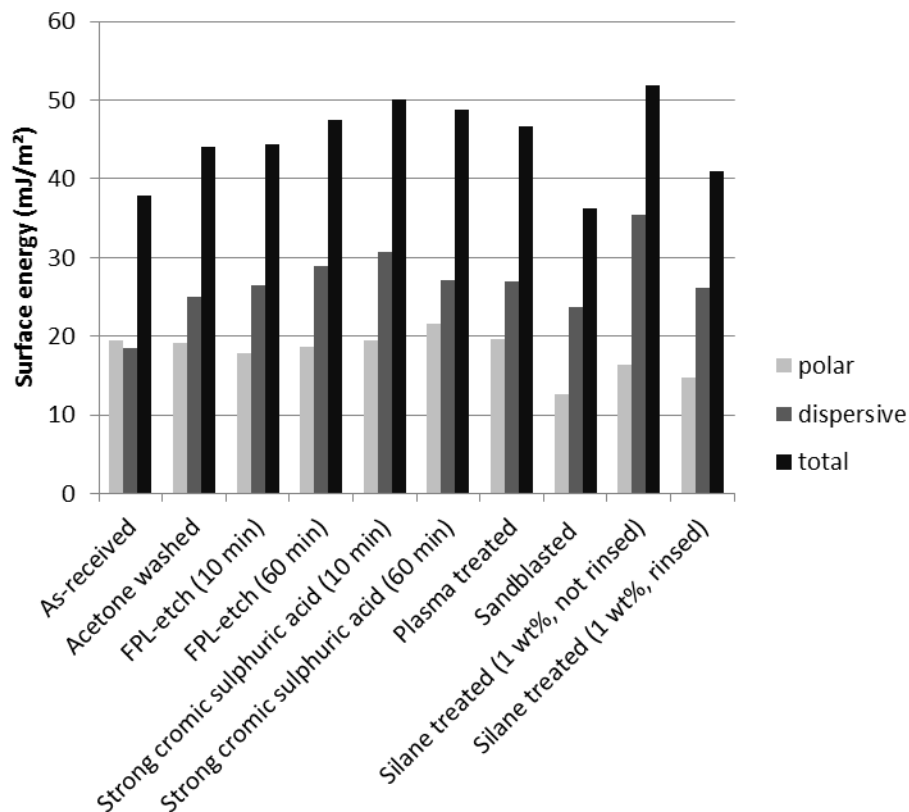


Figure 4.14: A bar graph of the surface energies calculated with contact angles which are corrected for differences in roughness between the samples.

One of the trends that can be seen in these results is that the surface energy increases when the surface is cleaned with either acetone or chromic sulphuric acid. It is interesting to note that it tends to be dispersive contribution which increases. Another trend is that the polar contribution of the surface energy for the silane treated samples, which is very low for the sample with the lowest concentration of silane in the solution, tends to increase when this silane concentration is increased. These trends will be discussed further in Chapter 5.

In Figure 4.15, photographs from different measurements are shown. It is clear that the surface treatment has a significant effect on the contact angle. It is also clear that it affects the contact angle of water and diiodomethane differently.

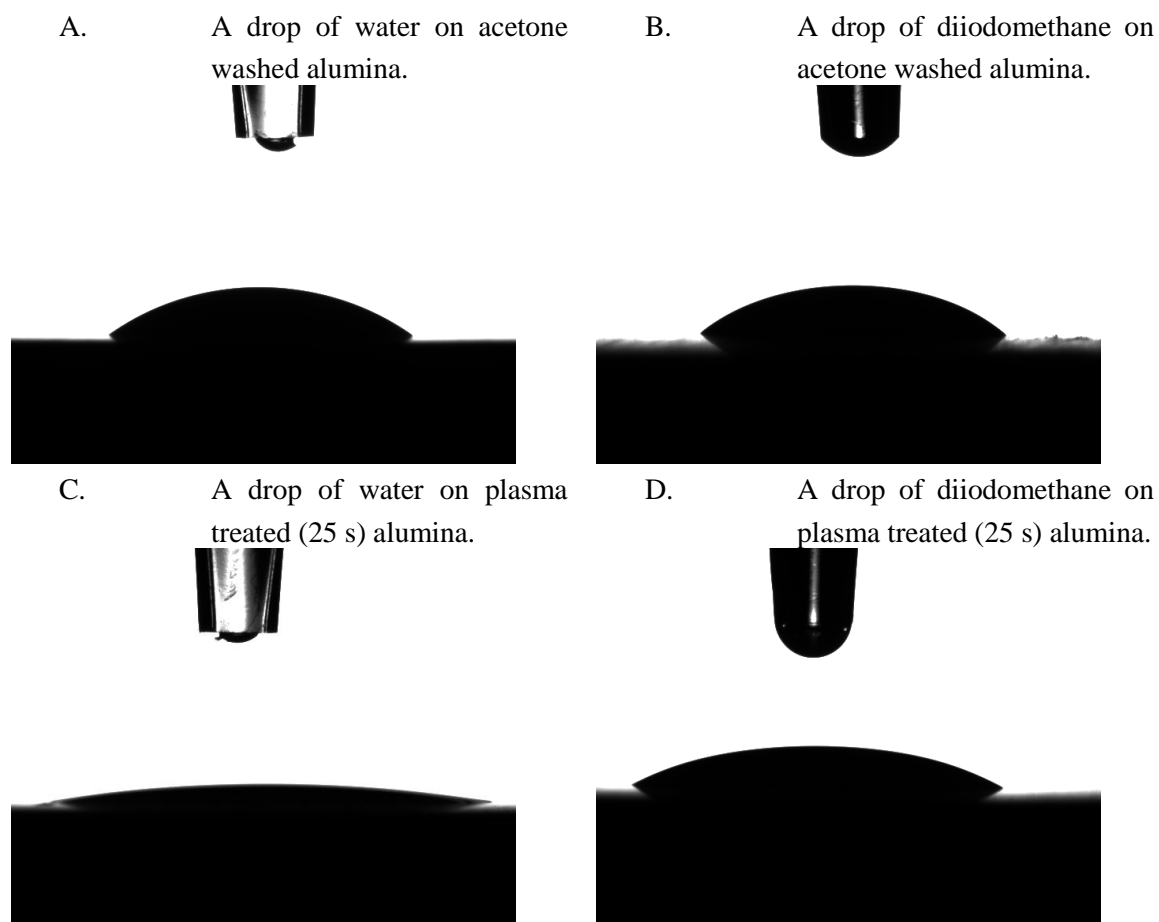


Figure 4.15: Photographs from four different contact angle measurements. Image A and B are from measurements on acetone washed alumina, while C and D are from plasma treated alumina. Image A and C are from measurements with water, and in image B and D, diiodomethane was used.

#### 4.1.2 Profilometer measurements

The profilometer analysis can give quite a few different parameters which give information about the surface. Some of them will be listed here for the different surface treatments for comparison. In addition to this, the profilometer takes three-dimensional images of the surface which show the topography.

The values of  $S_{dr}$  are shown in Table 4.3 and in Figure 4.16.  $S_{dr}$  is the percentage by which the surface area is increased compared to a flat surface due to increased roughness. Table 4.4 and Table 4.5 show average deviation ( $S_a$ ) of the surface and the root-mean-square deviation ( $S_q$ ) of the surface respectively. There seems to be some inaccuracies in these measurements, as an example, the values of  $S_q$  and  $S_a$  for the rinsed silane treated



surface is quite high. The  $S_{dr}$  parameter does not show the same high values, this may be because  $S_q$  and  $S_a$  are more height sensitive, and are more easily affected by false, sharp peaks on the surface as mentioned in Section 3.3.2. This might be due to the fact that the light intensity may have been too high, but this might also be due to differences in roughness between the alumina plates which were used.

*Table 4.3: The measured values for the developed interfacial area ratio ( $S_{dr}$ ). For this parameter, the sandblasted sample and the silane treated sample (1 wt%, not rinsed) are the only two surface treatments which show statistically significant differences compared to the acetone washed sample.*

	1 (%)	2 (%)	3 (%)	Average (%)	St. dev. (%)
Acetone washed	74.1	62.7	56.8	64.5	8.8
Ultrasound washed	60.3	68.8	54.0	61.0	7.4
Sandblasted	124	133	126	127.7	4.7
Plasma treated	77.3	80.8	72.0	76.7	4.4
Silane treated (1 wt%, rinsed)	62.5	88.6	71.3	74.1	13.3
Silane treated (1 wt%, not rinsed)	55.7	13.7	40.4	36.6	21.3
FPL-etch (10 min)	74.4	68.6	105	82.7	19.6
FPL-etch (60 min)	86.8	67.3	61.0	71.7	13.5
Strong chromic sulphuric acid (10 min)	61.0	62.2	50.8	58.0	6.3
Strong chromic sulphuric acid (60 min)	61.3	69.4	64.0	64.9	4.1

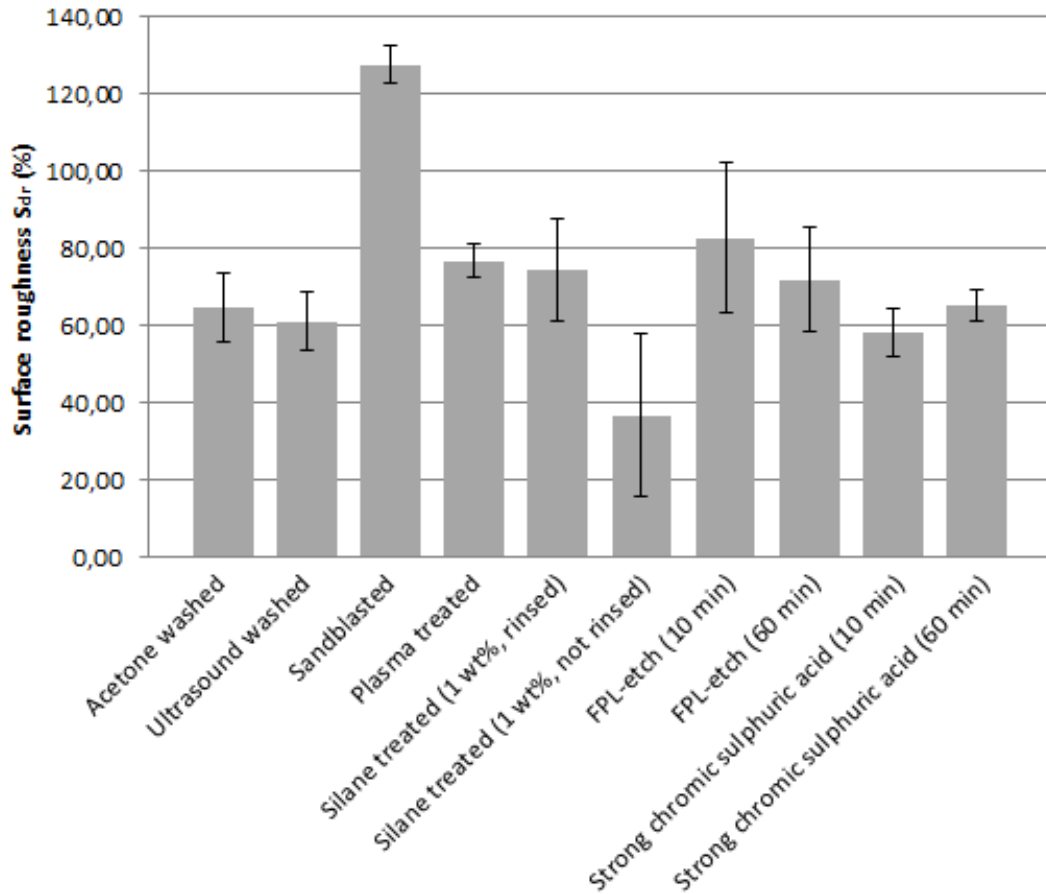


Figure 4.16: The roughness of the various samples represented by the  $S_{dr}$  value. The large error bar for the silane treated sample (1 wt%, not rinsed) is due to the unevenness of the silane layer. This can be seen in the SEM images in Figure 4.6 and Figure 4.7.

Table 4.4: The measured values for the average deviation of the surface ( $S_a$ ).

	1 ( $\mu\text{m}$ )	2 ( $\mu\text{m}$ )	3 ( $\mu\text{m}$ )	Average ( $\mu\text{m}$ )	St. dev. ( $\mu\text{m}$ )
Acetone washed	0.68	0.66	1.25	0.87	0.33
Ultrasound washed	0.81	0.86	0.53	0.73	0.18
Sandblasted	1.57	1.47	1.27	1.44	0.15
Plasma treated	0.88	0.71	0.51	0.70	0.19
Silane treated (1 wt%, rinsed)	1.19	1.49	1.21	1.30	0.17
Silane treated (1 wt%, not rinsed)	0.84	0.54	0.52	0.64	0.18
FPL-etch (10 min)	0.48	0.86	0.86	0.73	0.22
FPL-etch (60 min)	0.99	0.55	0.79	0.78	0.22
Strong chromic sulphuric acid (10 min)	0.95	0.73	0.66	0.78	0.16
Strong chromic sulphuric acid (60 min)	0.81	1.11	0.50	0.81	0.30

Table 4.5: The measured values for the root-mean-square deviation of the surface ( $S_q$ ).

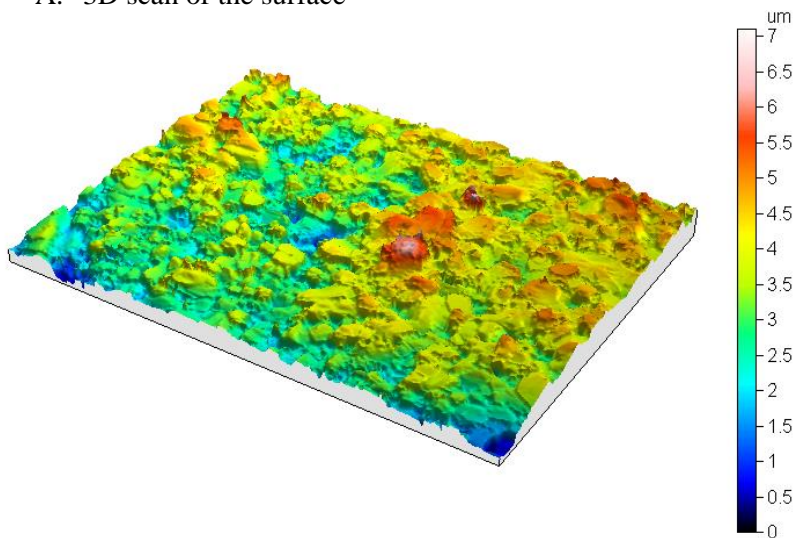
	1 ( $\mu\text{m}$ )	2 ( $\mu\text{m}$ )	3 ( $\mu\text{m}$ )	Average ( $\mu\text{m}$ )	St. dev. ( $\mu\text{m}$ )
Acetone washed	0.85	0.91	1.57	1.11	0.40
Ultrasound washed	1.06	1.10	0.69	0.95	0.23
Sandblasted	1.98	1.80	1.67	1.82	0.16
Plasma treated	1.14	0.89	0.67	0.90	0.23
Silane treated (1 wt%, rinsed)	1.44	1.79	1.55	1.59	0.18
Silane treated (1 wt%, not rinsed)	1.20	0.67	0.66	0.84	0.31
FPL-etch (10 min)	0.63	1.09	1.08	0.93	0.27
FPL-etch (60 min)	1.27	0.71	1.01	1.00	0.28
Strong chromic sulphuric acid (10 min)	1.25	0.94	0.84	1.01	0.22
Strong chromic sulphuric acid (60 min)	1.02	1.33	0.63	0.99	0.35

The silane treated (1 wt%, not rinsed) surface and the sandblasted surface are the only two samples that show a significant difference in the  $S_{dr}$  values measured compared to the acetone washed sample. They are therefore the most interesting cases to compare when it comes to roughness. The other parameters are as before mentioned more sensitive to inaccuracy in the measurements due to too bright light, so it makes sense to focus more on the  $S_{dr}$  values.

The silane treated (1 wt%, not rinsed) surface showed a lower roughness than the other samples with an  $S_{dr}$  of 36.6 %. This is most likely because the silane layer collects in between the grains on the alumina surface and fills the pores. This was also seen on the SEM images of this surface. These SEM images can be seen in Figure 4.6 in Section 4.1. The sandblasted surface showed a higher roughness than the rest with an  $S_{dr}$  of 127.7 %. This is because the grains on the alumina surface are crushed by the sandblasting, which creates many small cracks on the surface. This can be seen in the microscopy image in Figure 4.19, in the SEM image in Figure 4.3, and in the cross-section image in Figure 4.11. In comparison, most of the other samples had  $S_{dr}$  values around 60-80 % as can be seen in Table 4.3. As mentioned earlier, these  $S_{dr}$  values were used in order to calculate contact angles corrected for the roughness which were used to calculate corrected values for the surface energies.

As mentioned, the profilometer also takes three-dimensional pictures of the surfaces. One of these pictures is shown in Figure 4.17 along with a two-dimensional height map of the same surface; these figures show the acetone washed surface. The three-dimensional pictures and the two-dimensional height maps of the rest of the samples can be seen in Appendix C.

A. 3D scan of the surface



B. 2D height map of the surface

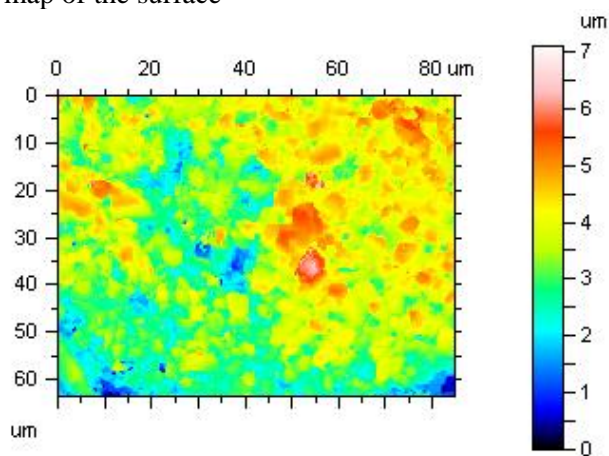


*Figure 4.17: Profilometer scans of the acetone washed surface. A. shows the 3D image, and B. shows a 2D height map of the same surface.*

In addition to these 3D images, the profilometer took microscopy images of the surfaces, some of which are shown in Figure 4.18 and Figure 4.19. In these figures, the colour shadings show the different heights on the surface.

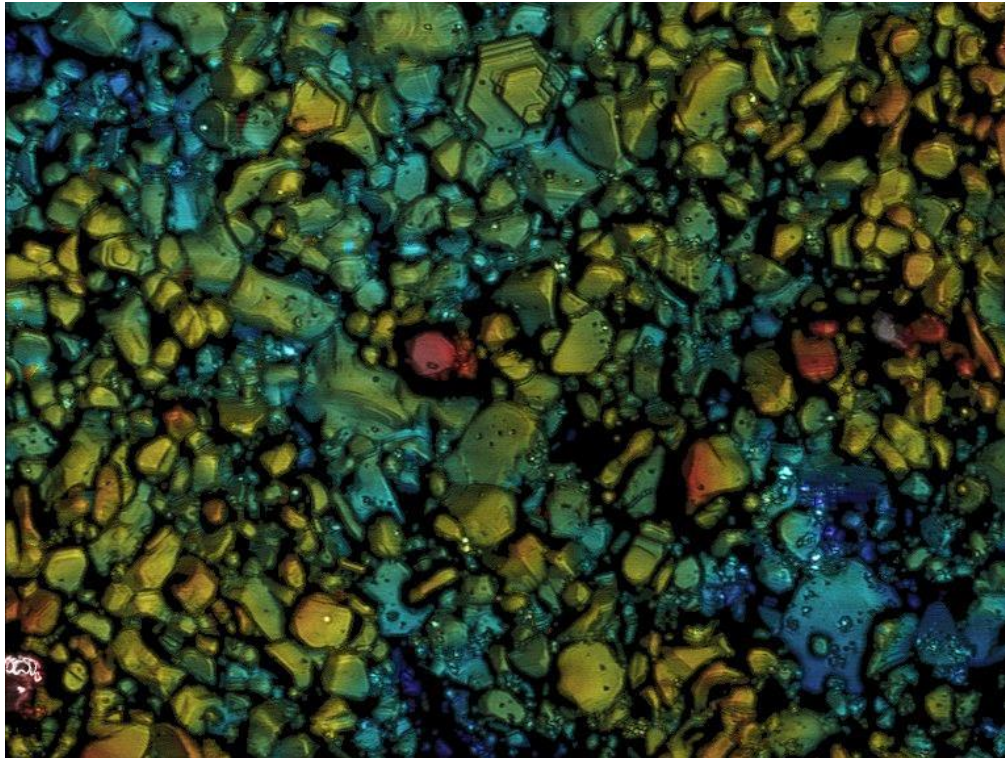


*Figure 4.18: Microscopy image of the acetone washed alumina surface taken with the profilometer*

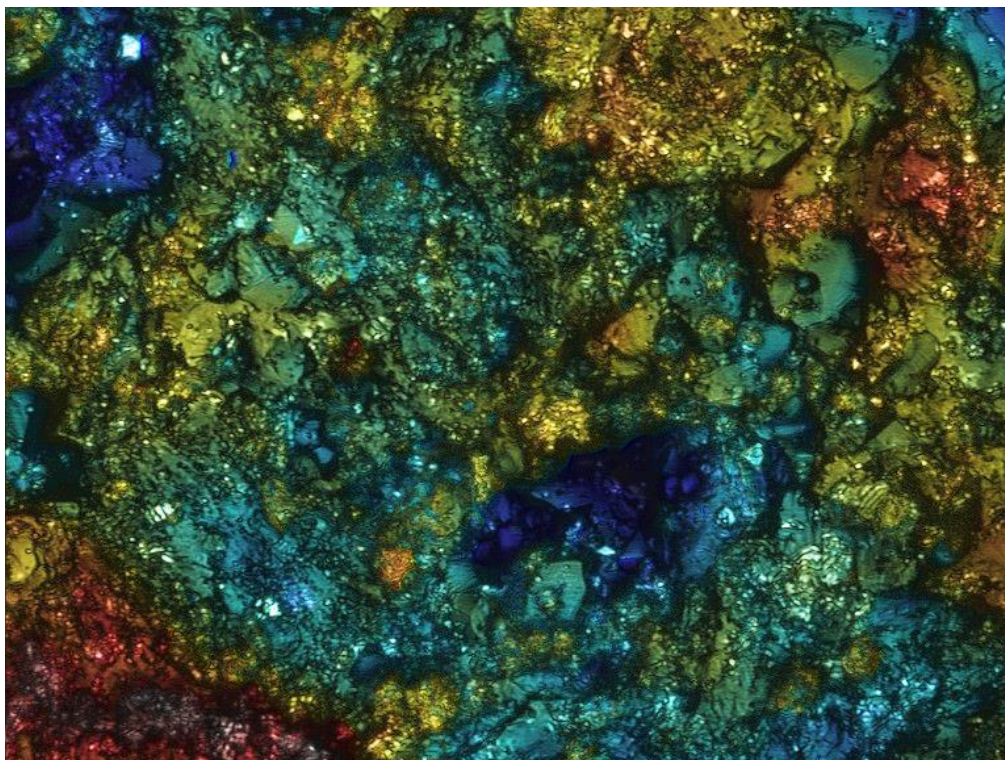


*Figure 4.19: Microscopy image of the sandblasted alumina surface taken with the profilometer*

### 4.1.3 X-ray photoelectron spectroscopy

By analysing the XPS survey scans of each sample, an overview of the concentration of each element found on the different surfaces is obtained. In Figure 4.20, an example of a survey scan is presented; all the survey scans can be found in Appendix B. A bar graph presenting the contents on each surface is displayed in Figure 4.21. Bear in mind that the percentage is relative to the total content on each surface. These results are also displayed in Table 4.6.

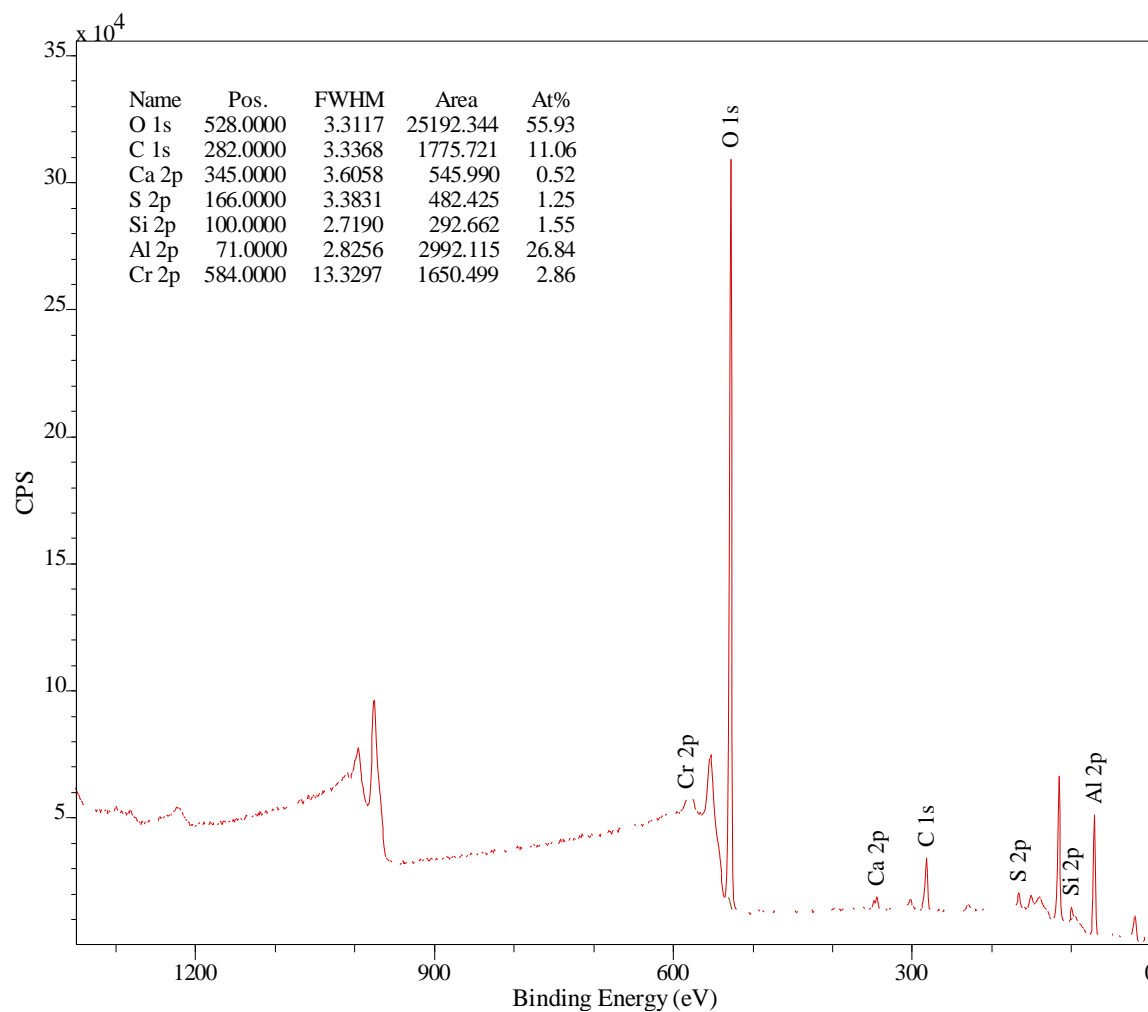


Figure 4.20: An example of an XPS survey scan. This is the scan for the FPL-etched surface.

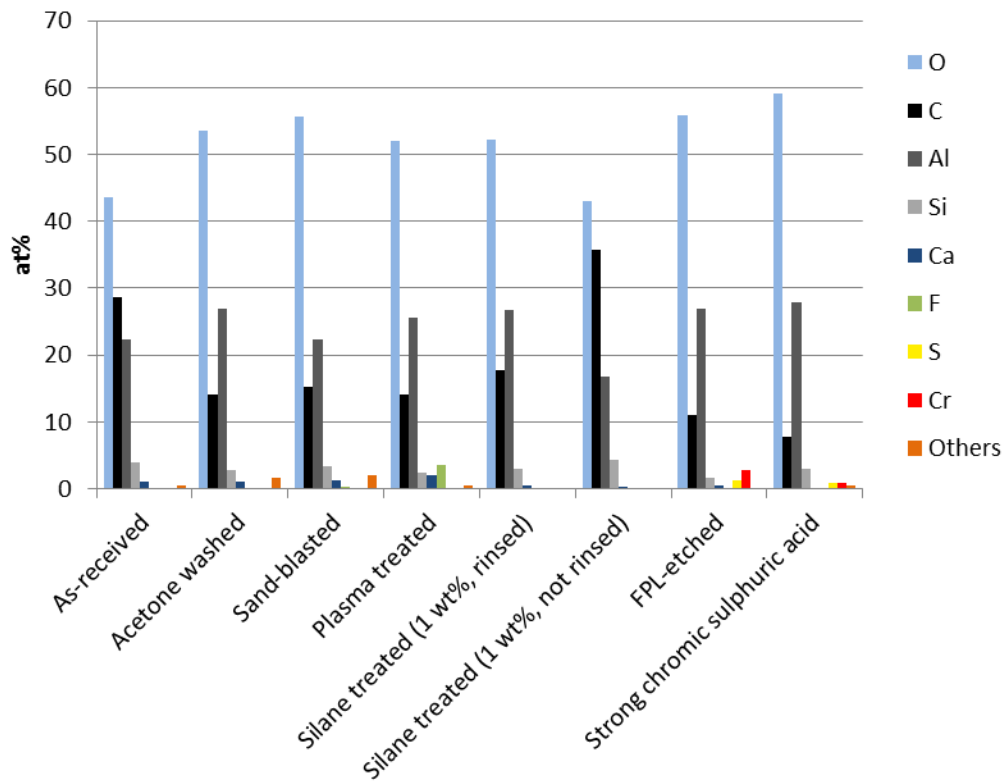


Figure 4.21: Overview of the element concentration on the surfaces. The values are also displayed in Table 4.6.

Table 4.6: Overview of the contents of the different elements on the surfaces given in at%.

	As-received	Acetone washed	Sand-blasted	Plasma treated	Silane treated (1%, rinsed)	Silane treated (1% not rinsed)	FPL-etched	Strong chromic sulphuric acid
O	43.59	53.47	55.56	52.01	52.30	42.95	55.93	59.08
C	28.67	14.14	15.17	14.00	17.63	35.71	11.06	7.67
Al	22.25	26.93	22.39	25.63	26.63	16.67	26.84	27.96
Si	3.92	2.79	3.31	2.34	2.95	4.37	1.55	3.06
Ca	1.01	1.04	1.23	2.02	0.49	0.30	0.52	-
F	-	-	0.34	3.58	-	-	-	-
S	-	-	-	-	-	-	1.25	0.95
Cr	-	-	-	-	-	-	2.86	0.85
Other	0.57	1.63	2.00	0.42	-	-	-	0.43

One of the most important trends that can be seen in these results is that the amount of carbon decreases when the surface is washed in either acetone or chromic sulphuric acid. It is also worth mentioning that the carbon concentration increases drastically when the surface is silane treated, and not rinsed. This indicates that there is in fact a silane layer on the sample. However, the carbon concentration on the silane treated sample that was



rinsed prior to drying, was about the same as for the acetone washed sample. This indicates that most of the silane was washed away in the rinsing step.

By analysing the high resolution scan of the carbon peak for the different samples, it is possible to see in which chemical states the carbon on the surface is found. This is done by a peak fitting, and shows that for all samples, except the silane treated (1 wt%, not rinsed) sample and the strong chromic sulphuric acid etched sample, the carbon peak seems to split into the same three peaks. The different samples show a varying degree of contribution from each of these three peaks. The sample which was etched with the strong chromic sulphuric acid show three similar peaks as the rest of the samples, but with a higher chemical shift between the peaks. This increase in the shift may indicate that there are other chemical groups present in the carbon compounds on that surface. This increase in shift may also be because there is a larger amount of secondary shift effects (see Table A-4 in Appendix A), which may indicate that there are shorter carbon chains on this surface compared with the other surfaces. In Figure 4.22 and Table 4.7, the difference in the composition of the carbon based compounds on some of these surfaces is shown by comparing the peak fitting of the carbon peak for the as-received, acetone washed, silane treated (1 wt%, rinsed), and strong chromic sulphuric acid-etched samples.

It is also interesting to note that the carbon peak for the silane treated (1 wt%, rinsed) sample (Figure 4.22-C) deviates slightly in shape from the rest of the samples, such as the acetone washed sample (Figure 4.22-B). This indicates that there may be some silane left on the surface. However, comparisons between the carbon peak for silane treated (1 wt%, rinsed) and silane treated (1 wt%, not rinsed) (Figure 4.23), combined with the overall carbon amount on the sample (see Table 4.6), indicate that most of the silane on the silane treated (1 wt%, rinsed) sample has been washed away.

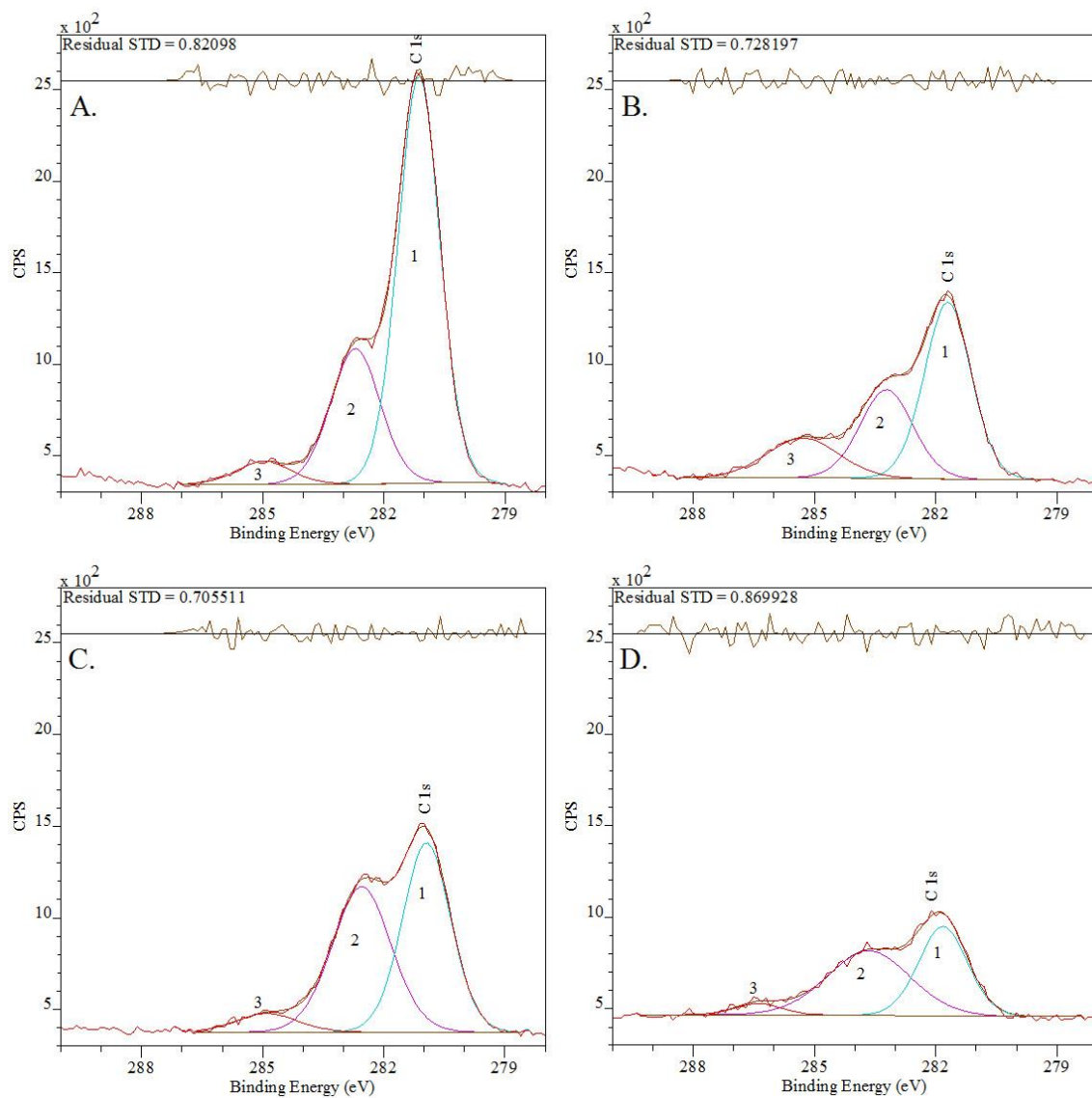


Figure 4.22: Peak fitting of the carbon peak for A: as-received, B: acetone washed, C: silane treated (1 wt%, rinsed), and D: strong chromic sulphuric acid-etched. The total amount of carbon and the contribution from the A, B and C peaks vary a lot between the samples.

*Table 4.7: The contribution from peak 1, 2, and 3 from the peak fitting of the carbon peak. The results are given in at% of the total composition on the surface. The chemical shift relative to peak 1 is included for the two other peaks.*

	Peak 1	Peak 2		Peak 3	
	Contribution (at%)	Contribution (at%)	Chemical shift relative to peak 1 (eV)	Contribution (at%)	Chemical shift relative to peak 1 (eV)
As-received	19.55	7.73	1.527	1.45	3.837
Sandblasted	7.75	5.01	1.365	2.41	4.056
Acetone washed	7.38	4.20	1.514	2.57	3.586
Plasma treated	8.67	3.79	1.306	1.55	3.999
Silane treated (1 wt%, rinsed)	8.54	8.01	1.608	1.08	3.950
FPL-etched	6.16	3.62	1.454	1.31	4.022
Strong chromic sulphuric acid	3.26	4.00	1.839	0.41	4.578

The carbon peak for the silane treated (1 wt%, not rinsed) sample is quite different from the rest of the carbon peaks. Since this peak has a rather complex shape, there are several possibilities for the peak fitting. The peak is shown in Figure 4.23 along with three options for peak fittings. The results from these peak fittings are also summarised in Table 4.8.

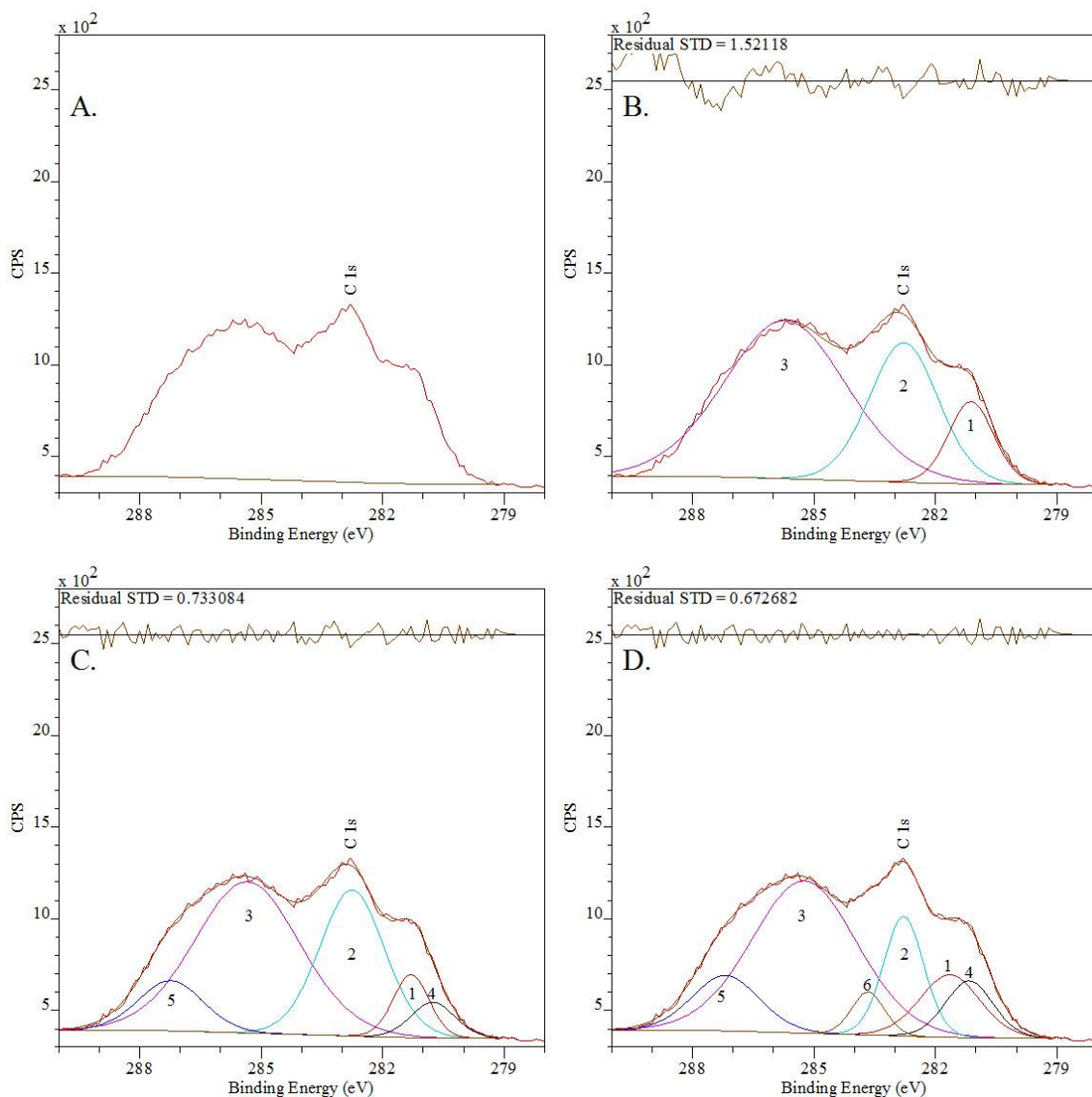


Figure 4.23: The carbon peak for the silane treated (1 wt%, not rinsed) sample. A. shows the unfitted peak, and B., C., and D. show the peak fitting with three, five, and six peaks respectively

Table 4.8: Table of the contribution (in at%) and chemical shift relative to peak 1 (in eV) for each of the peaks in the peak fitting. B, C and D are the three different peak fitting options in Figure 4.23.

	1	2		3		4		5		6	
	Con. at%	Con. at%	Ch. Shift	Con. at%	Ch. Shift	Con. at%	Ch. Shift	Con. at%	Ch. Shift	Con. at%	Ch. Shift
B	4.07	10.55	1.660	21.20	4.589	-	-	-	-	-	-
C	2.50	10.47	1.457	17.52	4.051	1.74	-0.539	3.59	5.945	-	-
D	4.19	5.28	1.137	17.64	3.595	3.01	-0.484	4.12	5.542	1.58	2.017

The peak fittings for the silane treated (1 wt%, not rinsed) sample are somewhat uncertain, and will not be discussed in much detail. They do, however, show that carbon is found in more chemical states on this sample compared to the rest. This corresponds well with there being a silane layer on this sample.

A peak fitting was also done for the oxygen peak. This is the same method as used by Harris et al. [54]. In Figure 4.24, the oxygen peaks for the as-received, acetone washed, plasma treated, and FPL etched samples are displayed.

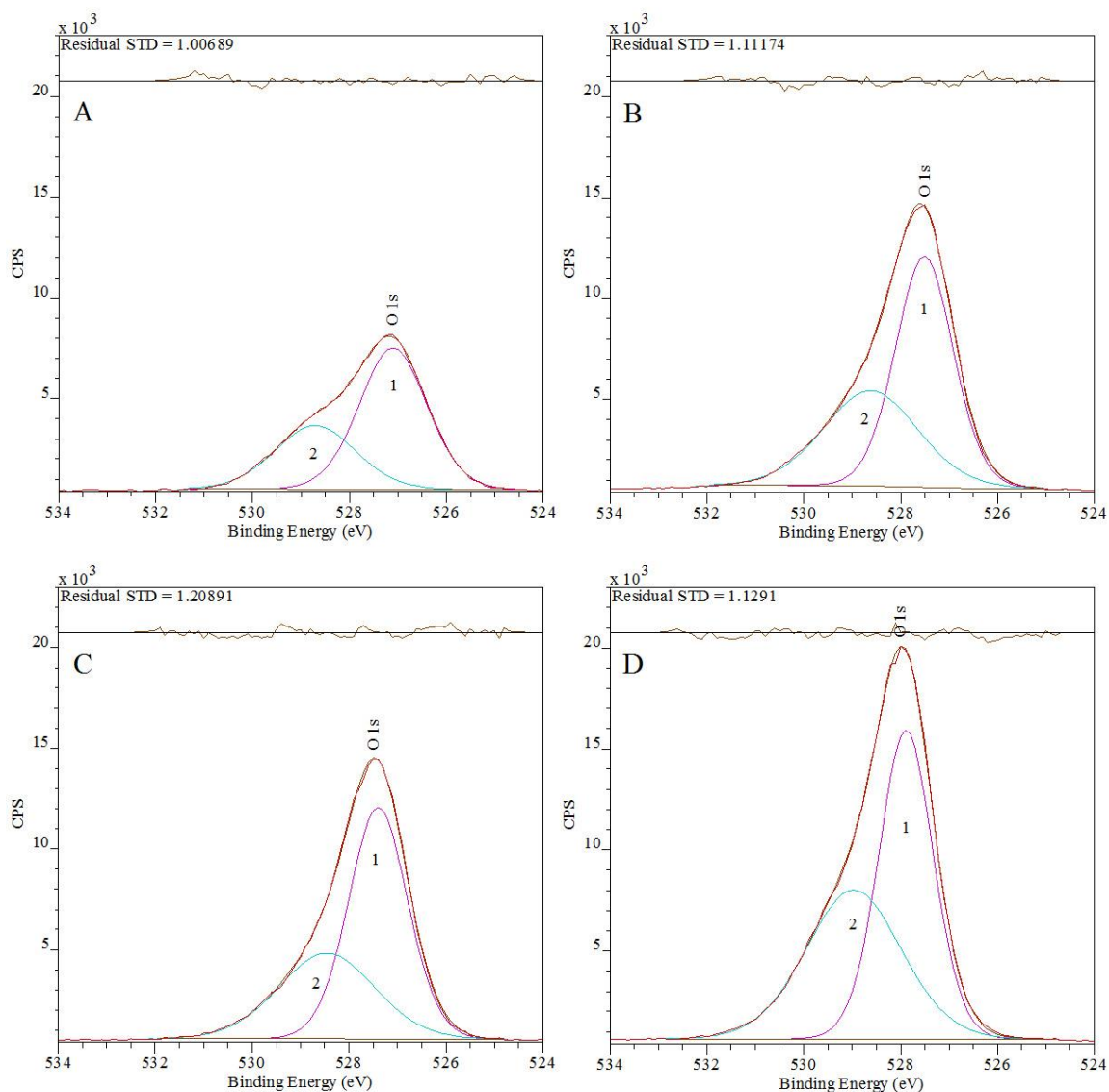


Figure 4.24: A comparison of the peak fitted oxygen results from the surfaces of A: as-received, B: acetone washed, C: plasma treated and D: FPL-etched.

The oxygen peak splits into two peaks. Peak 1 is most likely from the alumina lattice, and peak 2 corresponds to chemical groups such as OH-groups on the alumina surface and oxygen in the carbon based compounds. The contribution from these two peaks are summarised in Table 4.9.

*Table 4.9: The contributions from lattice oxygen and OH-groups on the XPS results for the different surfaces. The chemical shift between the two is included for each case.*

	Peak 1 (at%)	Peak 2 (at%)	Chemical shift (eV)
As-received	30.16	15.54	1.606
Acetone washed	31.86	21.61	1.102
Plasma treated	32.50	19.57	1.061
FPL-etch	30.32	25.71	1.082

The amount of lattice oxygen should be possible to calculate by multiplying the amount of aluminium found by the survey scan with 1.5 since the chemical formula for alumina is  $Al_2O_3$ . This fits reasonably well for the as-received sample, but not for the other samples where the amounts of aluminium multiplied by 1.5 give values in the range of 40 at% for the lattice oxygen (where Table 4.9 suggests it should be in the range of 30%). The peak fitting of the aluminium peak for the as-received and acetone washed samples is shown in Figure 4.25

When studying a peak fitting of the aluminium peak, the explanation for this may be found. As an example, the alumina peak for the acetone washed sample shows that only ~70% of the Al atoms are in the chemical state of  $Al_2O_3$ , the rest may have OH-groups or other groups attached. When taking this into account, the amount of lattice oxygen calculated from the amount of aluminium in the chemical state of  $Al_2O_3$  is in the range of 30%. The aluminium peak for the as-received sample, on the other hand, seems to consist of only one peak. This indicates that the alumina almost no chemical groups such as OH-groups on the surface for the as-received sample. In other words, the splitting of the aluminium peak combined with the increase in peak 2 on in the oxygen peak (see Figure 4.24 and Table 4.9), suggests that OH-groups or other chemical groups are found on the surface of the treated samples but not on the as-received sample. The amount of these chemical groups is difficult to determine since it is hard to say how much of peak 2 in the oxygen peak which corresponds to chemical groups on the alumina surface and how much is oxygen in carbon based compounds in the contamination layer.

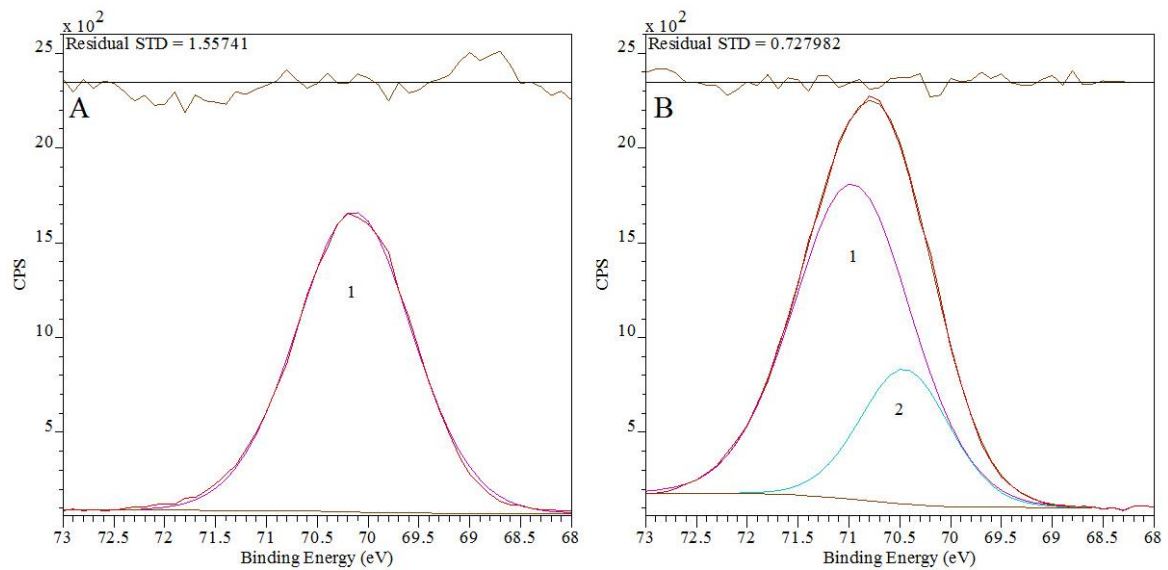


Figure 4.25: Peak fitting for the aluminium peaks of the A: as-received and B: acetone washed surfaces. The peak on the as-received surface is at a binding energy of 70.1405 eV, and the two peaks on the acetone washed surface are at 70.4611 eV and 70.9758 eV. Most likely, the peak at 70.9758 eV on the acetone washed surface corresponds to the peak on the as-received surface due to a shift of  $\sim 0.5$  eV of the two spectres relative to each other.

## 4.2 Peel tests

Typical results from the peel tests are displayed in Figure 4.26, the rest of the peel test results can be found in APENDIX D. The results from the peel tests on the samples with varying surface treatments are summarised in the bar graph in Figure 4.27. Usually, the results obtained between 10 mm and 30 mm standard travel were analysed. (The results from the peel test on the POSS-containing samples are presented in Section 4.4.)

From the bar graph in Figure 4.27, it is possible to see that the surfaces which were cleaned with acetone and chromic sulphuric acid show an improvement in peel strength compared to the as-received sample. The sandblasted and plasma treated samples perform a little worse than the acetone washed control. The silane treated sample which was rinsed after the silane treatment shows almost exactly the same peel strength as the acetone washed sample while the silane treated sample which was not rinsed show a substantial improvement in peel strength. These results correspond well with the results from the XPS analysis as will be discussed in Chapter 5.

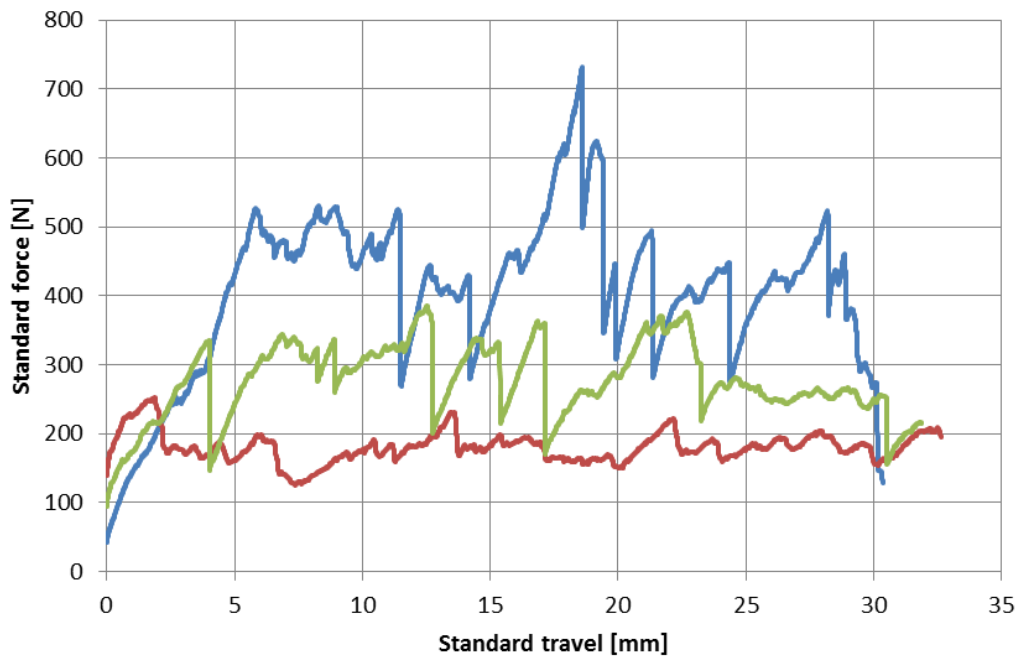


Figure 4.26: Typical results from the peel tests showing the measured standard force (N) as a function of the standard travel (mm) of the crosshead. These results are from an as-received sample (red), an acetone washed sample (green), and a silane treated (1 wt% not rinsed) sample (blue).

In Figure 4.28, SEM images of the fracture surface after peel testing is shown. These images are taken on the ceramic side of the fracture. The fracture propagated from left to right on the images during the peel test. From these images it is possible to see that the amount of composite matrix left on the ceramic surface varies. This indicates that there is a difference in the ratio between the amount of adhesive fracture and the amount of cohesive fracture among the different samples. It is clear that the amount of adhesive fracture, where the fracture propagates in the interface between the ceramic and the composite, is much higher for the as-received sample than the other samples. It can be seen that when the adhesion improves, the amount of cohesive fracture (fracture in the composite matrix) increases. However, when there is a lot of composite matrix left on the ceramic surface, there is also normally a lot of adhesive fracture between the composite matrix and the glass fibres, and not only cohesive fracture in the composite matrix. The amount of adhesive fracture in the interface between the ceramic and the composite can, to a certain degree, be quantified. On the as-received sample, this type of fracture makes up approximately 80 % of the fracture surface. On the acetone washed, silane treated (1 wt%, rinsed), and FPL-etched samples it is about 40 %; on the sandblasted and plasma treated surfaces it is about 20 %; and on the on the silane treated sample which was not rinsed it is almost 0 %.



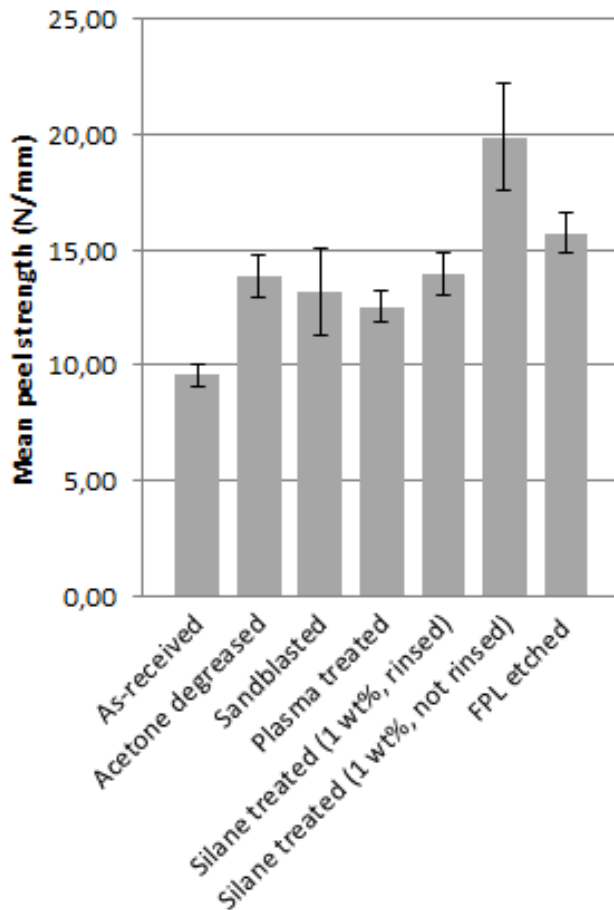
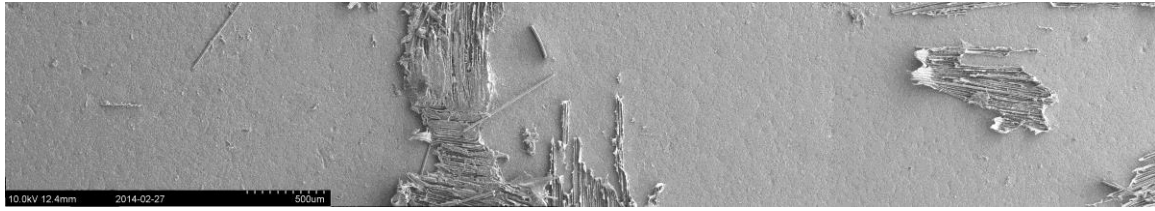


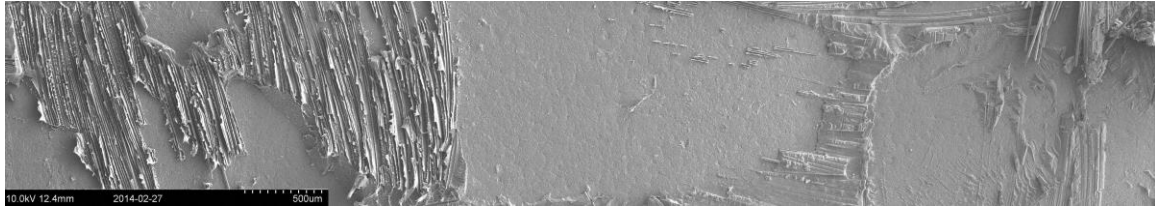
Figure 4.27: The results from the peel tests on the samples with different surface treatments. An error bar was added to each of the columns. This represents the standard deviation of the results.

The images in Figure 4.29 show the composite side of the fracture surface. Again, the fracture propagated from left to right in the image during the peel test. Here it is possible to see that in some areas of the composite, an imprint of the ceramic can be seen while in other areas, the glass fibres are exposed. This is again due to a decreasing amount of adhesive fracture in the interface between the ceramic and the composite when the adhesion is increased.

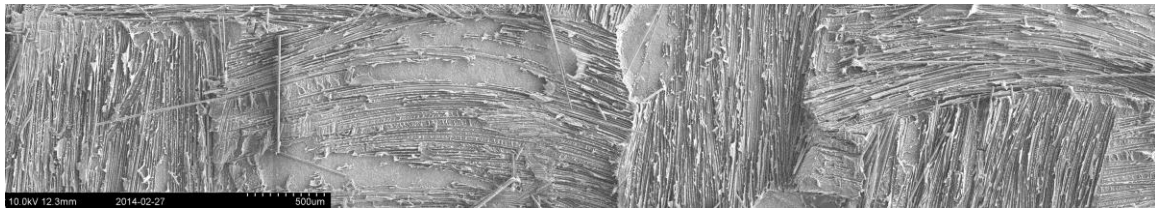
A. As-received



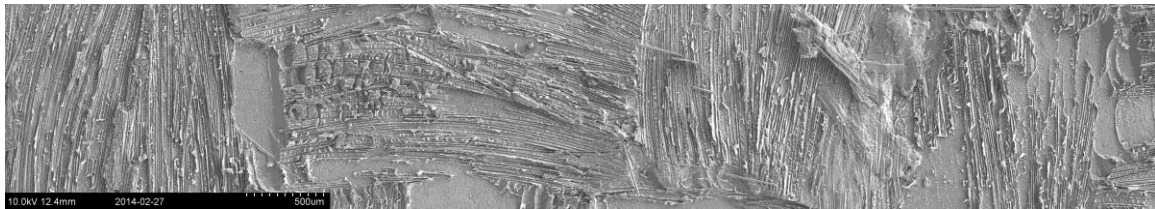
B. Acetone washed



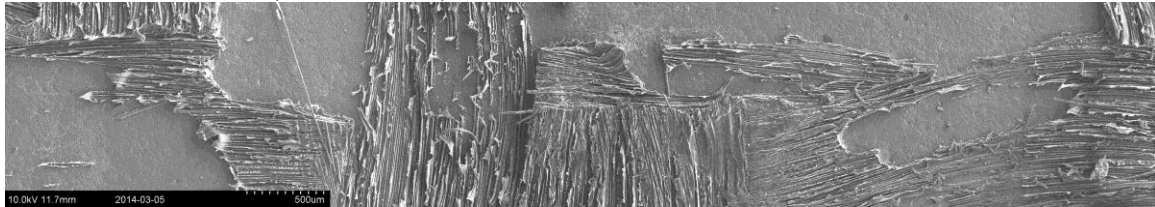
C. Sandblasted



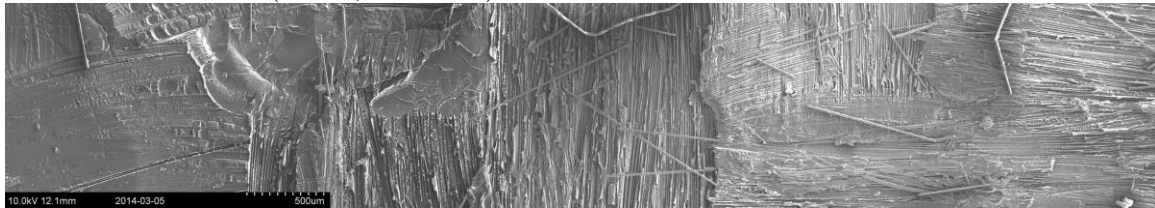
D. Plasma treated



E. Silane treated (1 wt%, rinsed)



F. Silane treated (1 wt%, not rinsed)



G. FPL etched

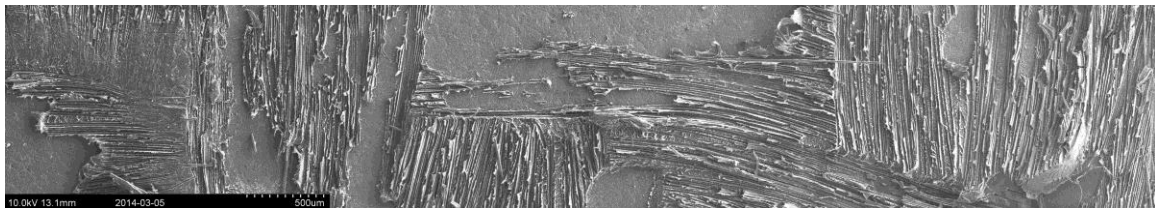
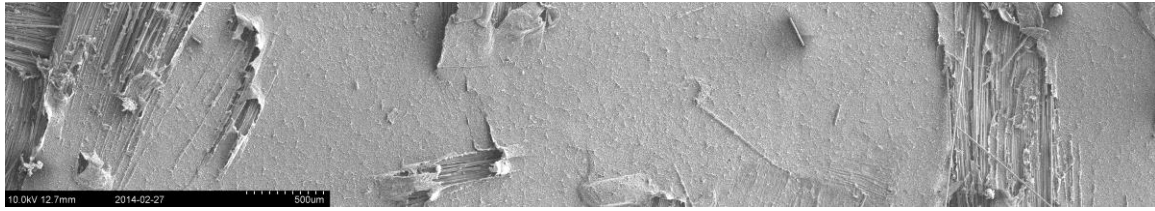
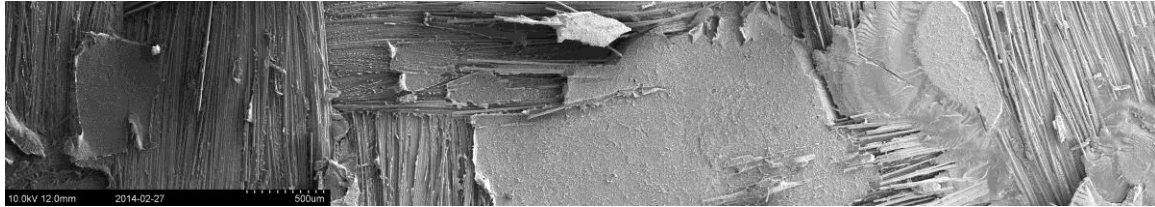


*Figure 4.28: The ceramic side of the fracture surfaces for the samples with varying surface treatments after peel testing.*

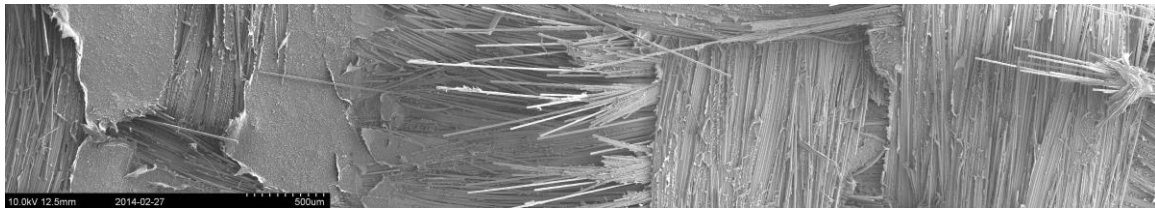
A. As-received



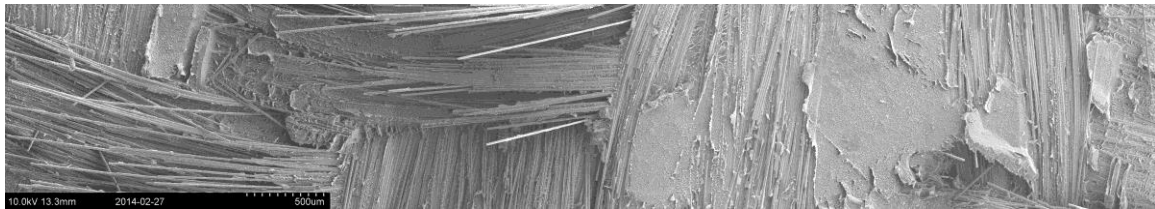
B. Acetone washed



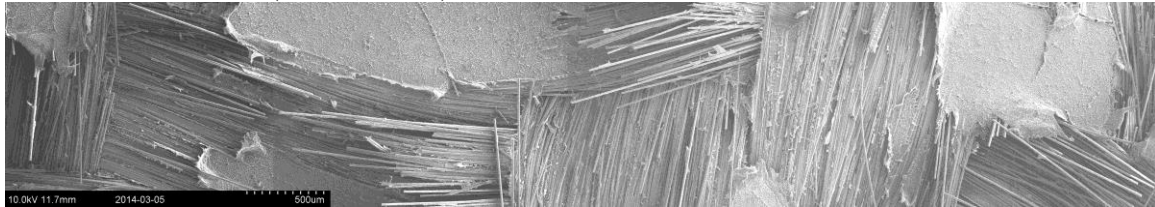
C. Sandblasted



D. Plasma treated



E. Silane treated (1 wt%, rinsed)



F. Silane treated (1 wt%, not rinsed)



G. FPL etched

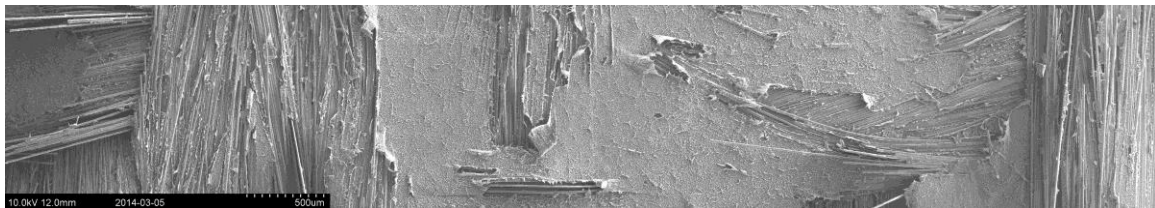


Figure 4.29: The composite side of the fracture surfaces for the samples with varying surface treatments after peel testing.

## 4.2.1 Effect of silane concentration

In addition to the peel test series above, a series of tests were performed in order to investigate the effects of the concentration of the solution used in the silane treatment. Concentrations of 0.25 wt% and 0.5 wt% were tested in addition to the one with 1 wt% which is shown in the series above. The results from all tests are shown in Figure 4.30, along with the acetone washed sample for comparison. From these results it can be seen that the peel strength increases with an increasing concentration of the silane solution up to 1 wt%. It seems that 0.25 wt% silane is not enough to get an improvement in the peel strength, however, when the concentration is increased to 0.5 wt% there may be a slight improvement. As mentioned before, when the silane treatment is performed with a silane concentration of 1 wt%, the peel strength is dramatically improved compared with the acetone washed sample.

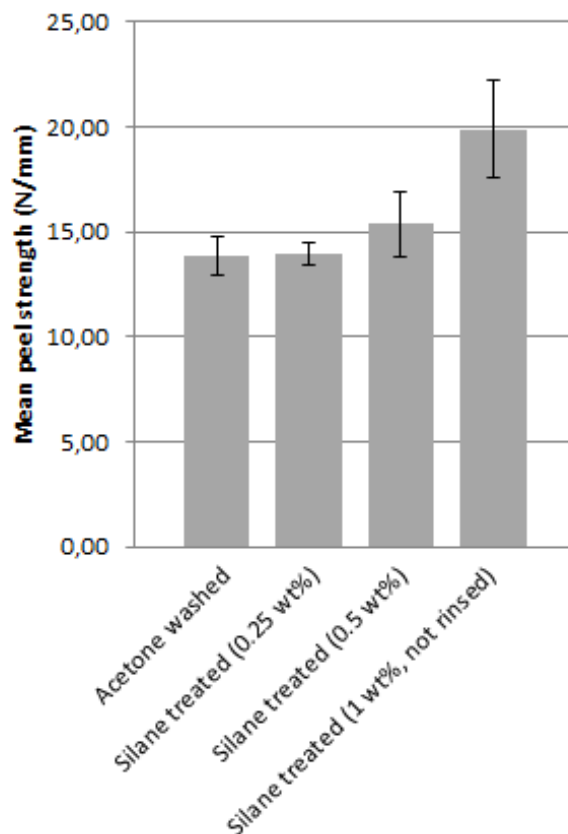
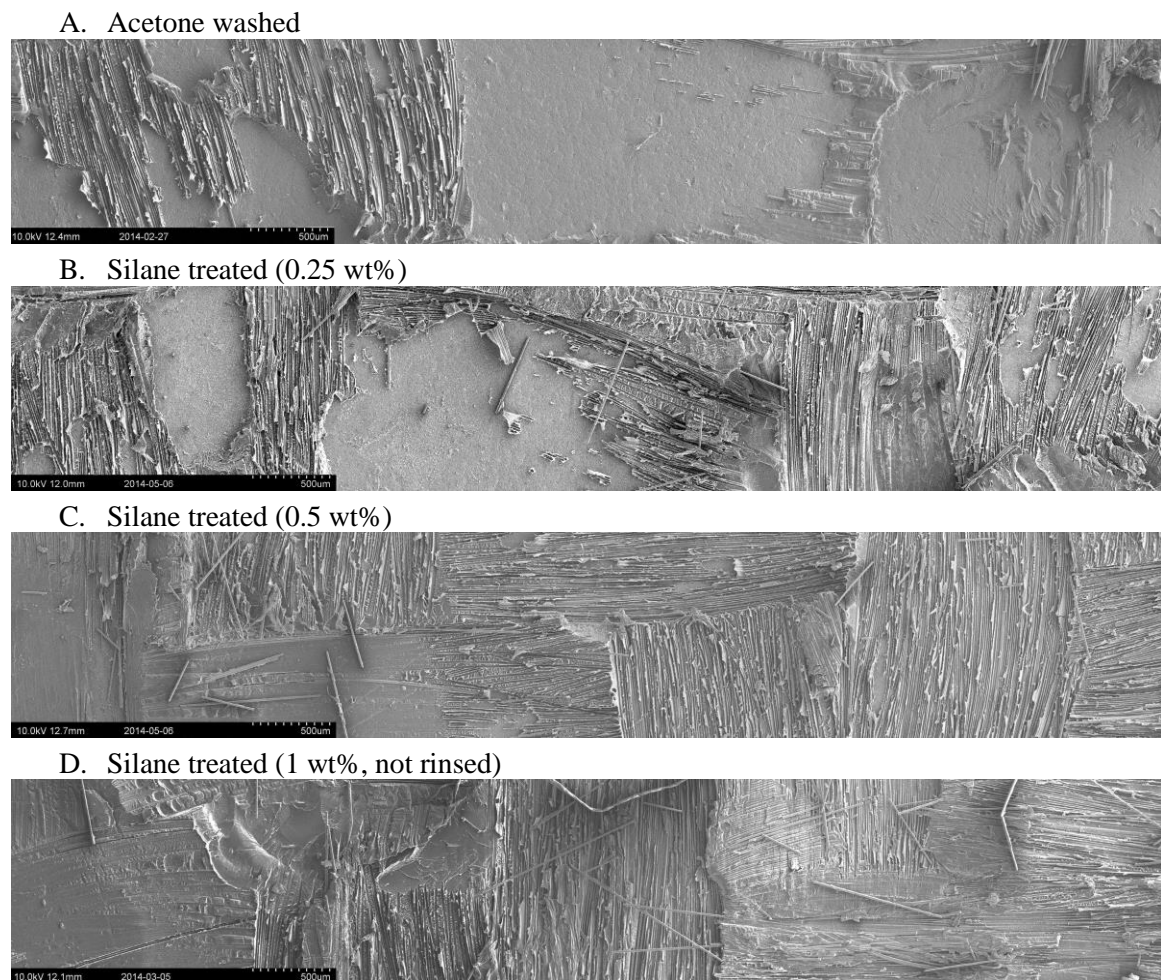


Figure 4.30: The results from the peel test on the samples which were silane treated with different concentrations of the silane solution. The acetone washed sample is included for comparison.

SEM images of the fracture surfaces of these samples can be seen in Figure 4.31 and Figure 4.32 which show the ceramic side and the composite side of the fracture surface

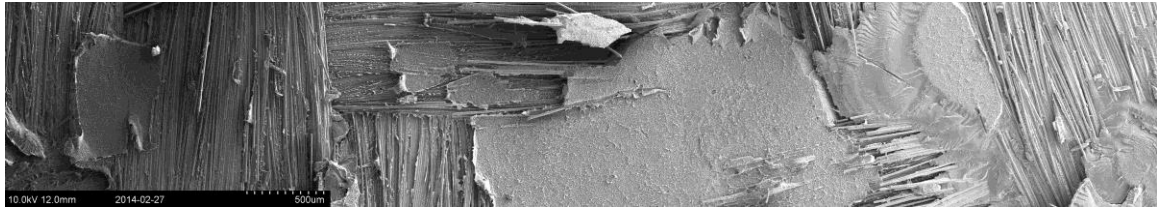
respectively. The SEM images of the acetone washed sample and the sample which was silane treated with the highest concentration are included here as well for comparison.

In the same way as for the fracture surfaces shown above, there is a difference in the amount of adhesive fracture in the ceramic-composite interface among these samples. The acetone washed sample, which is included here for comparison has a fracture surface of approximately 40 % interfacial fracture. When the silane treatment was performed with a 0.25 wt% solution, this amount was reduced to about 30 %, and when the concentration of the silane solution was 0.5 wt%, the amount of adhesive fracture in the ceramic-composite interface was reduced to about 10 %. Again, the silane treated (1 wt%, not rinsed) showed almost no adhesive fracture in this interface.

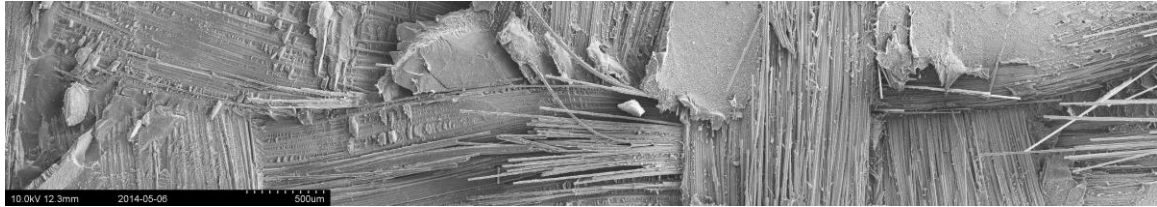


*Figure 4.31: The ceramic side of the fracture surface for the silane treated samples with varying concentration of the silane solution after peel testing. The acetone washed sample is included for comparison.*

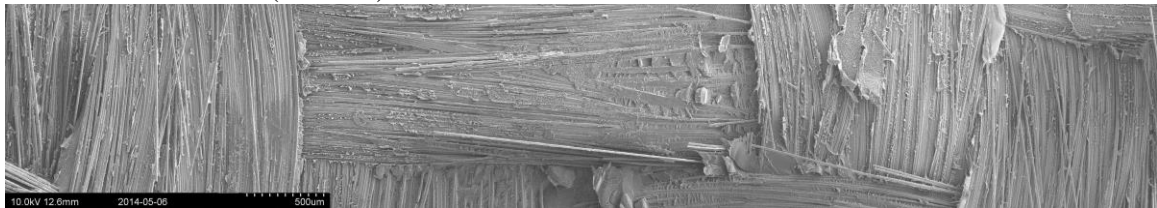
A. Acetone washed



B. Silane treated (0.25 wt%)



C. Silane treated (0.5 wt%)



D. Silane treated (1 wt%, not rinsed)



*Figure 4.32: The composite side of the fracture surface for the silane treated samples with varying concentration of the silane solution after peel testing. The acetone washed sample is included for comparison.*

## 4.2.2 Failure modes

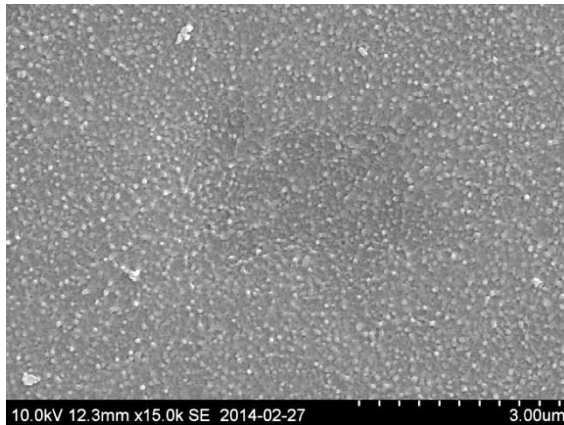
A lot of information about where the fracture has propagated, and in what manner it has propagated can be obtained by looking at a few SEM images with a higher magnification. Figure 4.33 shows a section of the composite side of the fracture surface for the acetone washed sample. A high build-up in the measured force, followed by rapid crack movement and a big drop in the force was quite typical for the acetone washed samples. This section is from an area where this occurred. The same section can also be seen on the right side of Figure 4.29 B, and the ceramic side of a similar area of the fracture surface can be seen on the right side of Figure 4.28 B.

Another example where the high magnification SEM images can give additional useful information is in the case of the sandblasted sample, where these images show that some ceramic grains and crushed ceramic particles are left on the composite side of the fracture surface. This may be because the sandblasting has created a lot of cracks in the ceramics where the crack front can propagate during the peel test. One such image is shown in Figure 4.34.

A. Section of the composite side of the fracture surface for the acetone washed sample.



B. Zoomed in on the smooth area



C. Zoomed in on the rough area

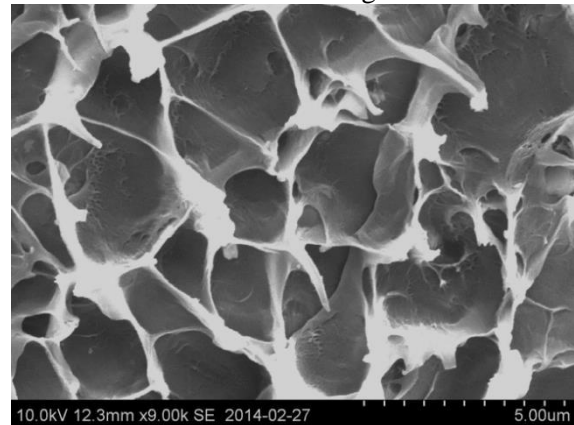


*Figure 4.33: Comparison of the smooth and rough areas on the composite side of the fracture surface for the acetone washed surface. The smooth area (B) is where the fracture has moved fast inside the composite matrix causing a substantial drop in the measured force, and the rough area (C) is where the fracture has moved slowly along the interface between the composite and the matrix. The imprint of the ceramic grains can be seen.*



*Figure 4.34: An SEM image of the composite side of the fracture surface from the sandblasted sample. Grains and crushed particles from the ceramic can be seen in the composite.*

The crack front can propagate along the interface between the ceramic and the composite, inside the composite matrix, or along the interface between the composite matrix and the glass fibres. Figure 4.35 to Figure 4.37 show SEM images of these different cases.

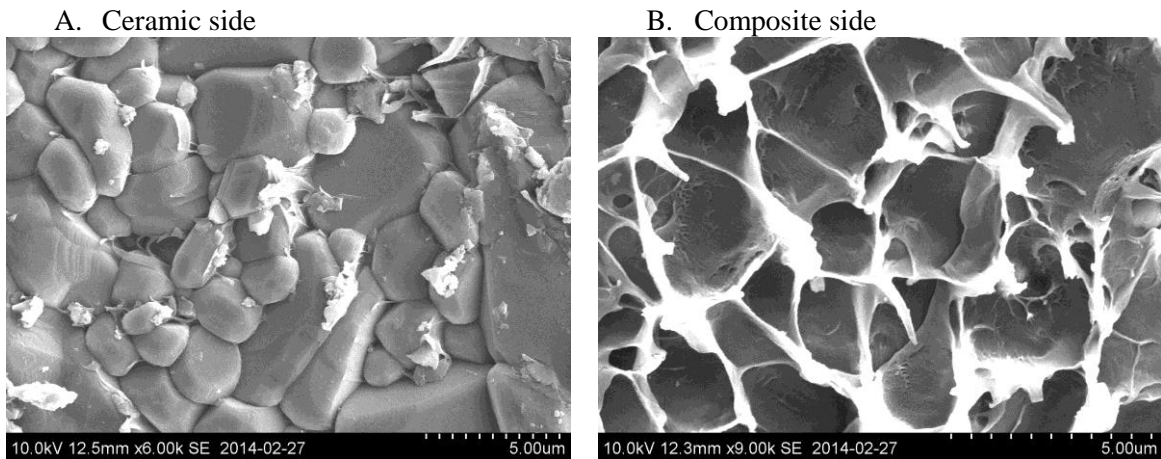


*Figure 4.35: SEM images from an area where the fracture has propagated along the interface between the ceramic and the composite. (The images are taken from the acetone washed sample.) A is from the ceramic side, and B is from the composite side.*



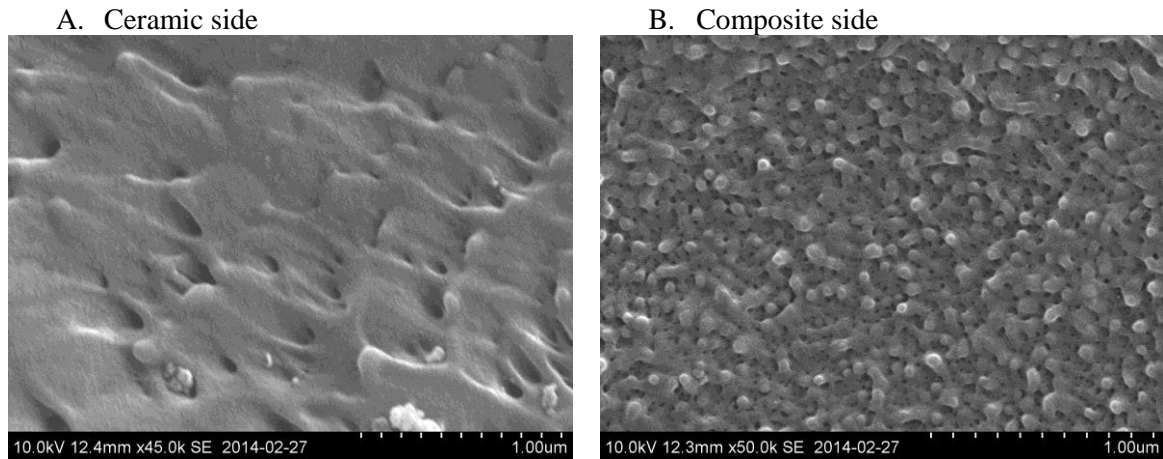


*Figure 4.36: SEM images from an area where the fracture has propagated inside the composite matrix. (The images are taken from the acetone washed sample.) A is from the ceramic side, and B is from the composite side.*

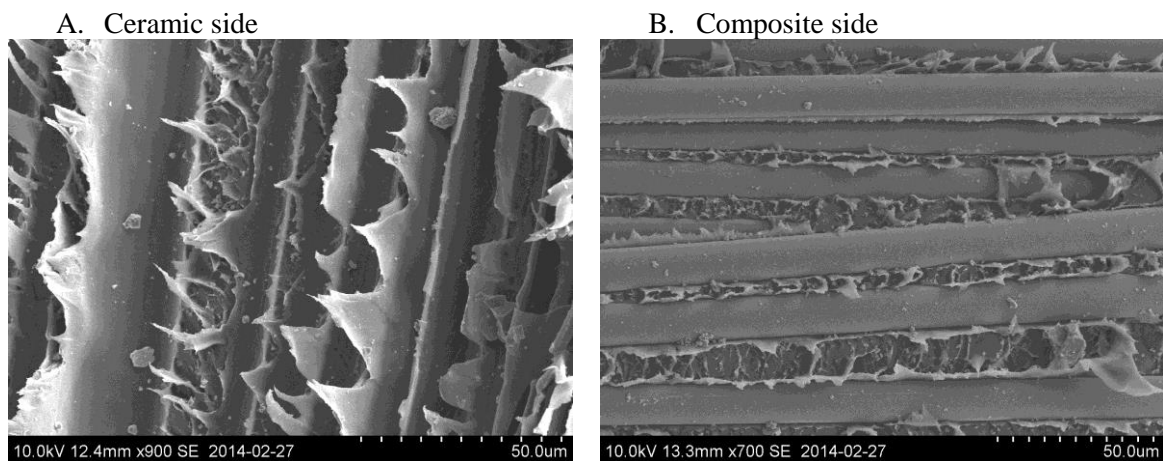


*Figure 4.37: SEM images from an area where the fracture has propagated along the interface between the composite matrix and the glass fibre. (The images are taken from the plasma treated sample.) A is from the ceramic side where the fibres have been perpendicular to the direction of the fracture growth, and B is from the composite side where the fibres have been parallel to the direction of the fracture growth.*

When determining where the fracture has propagated, one should be careful since the fracture may appear to have moved along one of the interfaces when it in fact has propagated inside the composite matrix close to one of the interfaces. This is illustrated by the SEM images in Figure 4.38.

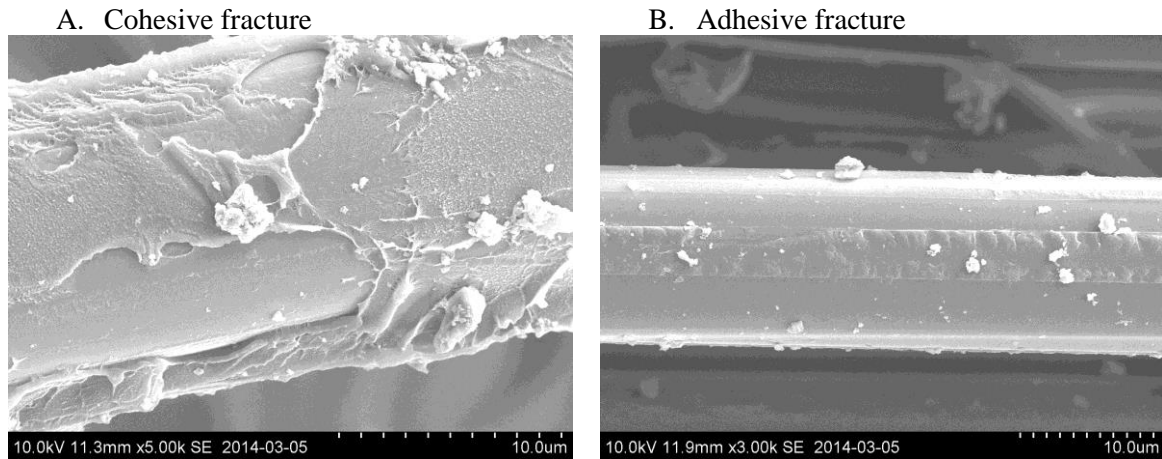


Figure 4.38: A: SEM image of a glass fibre from the composite side of the fracture surface for the silane treated (1 wt%, not rinsed) sample. Here, it is possible to see that there is some composite matrix (LPET) left on the glass fibre, and a “bumpy” structure similar to that in Figure 4.36 B is seen on the LPET. In other words, the fracture is cohesive inside the composite matrix. B: SEM image of a glass fibre from the composite side of the fracture surface for the FPL-etched sample. Here the glass fibre is clean, and the fracture adhesive in the interface between the fibre and the composite matrix.

### 4.3 Ballistic tests

In this section, the results from the ballistic tests will be presented. The velocity of the projectile was measured for every test, and the plates were photographed on both sides after a red penetrant was added.

The projectile velocity can be found in Table 4.10, and the photographs of the tested plates can be seen in Figure 4.39 to Figure 4.43. The first four of these pictures show the front and back sides of the as-received, acetone washed and silane treated samples for the four different sets, and Figure 4.43 shows the front side of the Teflon wrapped samples. The red penetrant was not added to these Teflon wrapped samples since it would flow freely and cover everything due to the complete delamination between the ceramic and the composite. Because of this, it was difficult to get good pictures of the back-side of these samples without removing the composite on the back-side. One such picture has been taken this can be seen in Figure 4.44. This was not done with the rest of these samples since the damaged ceramic plate had a tendency to break apart completely, and the crack pattern would be difficult to photograph.

When comparing the damage on each of the plates, bear in mind that the projectile velocities for the third and fourth set varied quite a lot. For example, the silane treated sample from the third set must be compared to the acetone washed sample from the fourth set and not the acetone washed sample from its own set in order to get the best comparison.

Table 4.10: The projectile velocity for each of the ballistic tests.

	The projectile velocity (m/s)			
	Set 1	Set 2	Set 3	Set 4
As-received (AR)	335	485	574	575
Acetone washed (AD)	337	483	581	631
Silane treated (1%, not rinsed) (SU)	339	484	627	641
Teflon wrapped (TW)	343	481	582	573

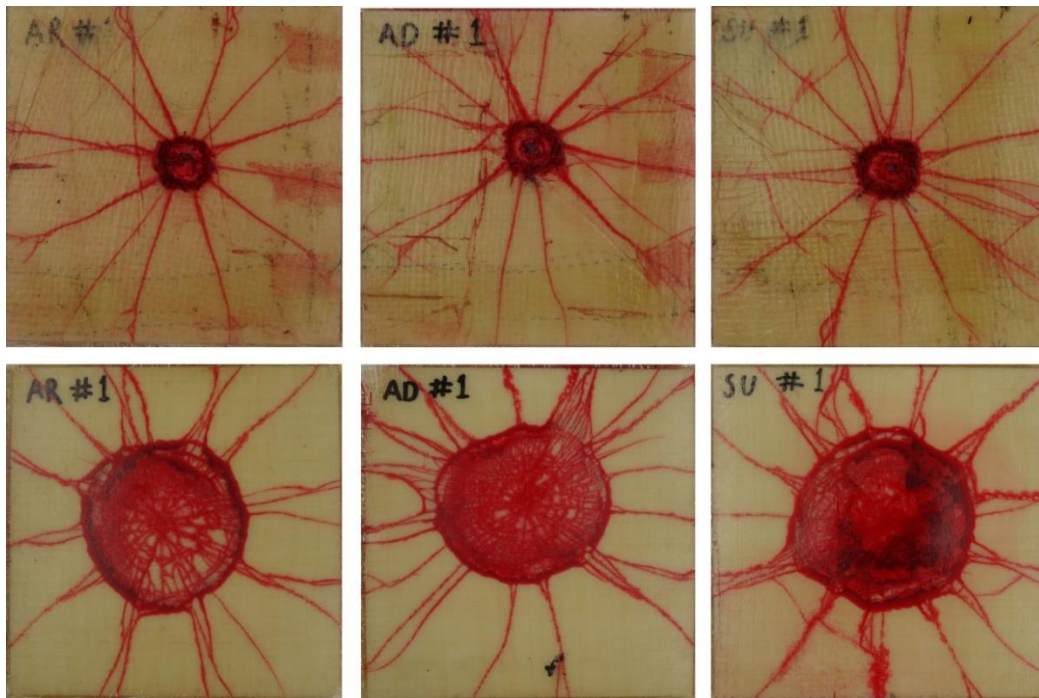


Figure 4.39: The first set of test samples after ballistic testing. The top row shows the front of the plates, and the bottom row shows the back side of the plates. The samples are, from left to right, the as-received, the acetone washed and the silane treated (1 wt%, not rinsed)

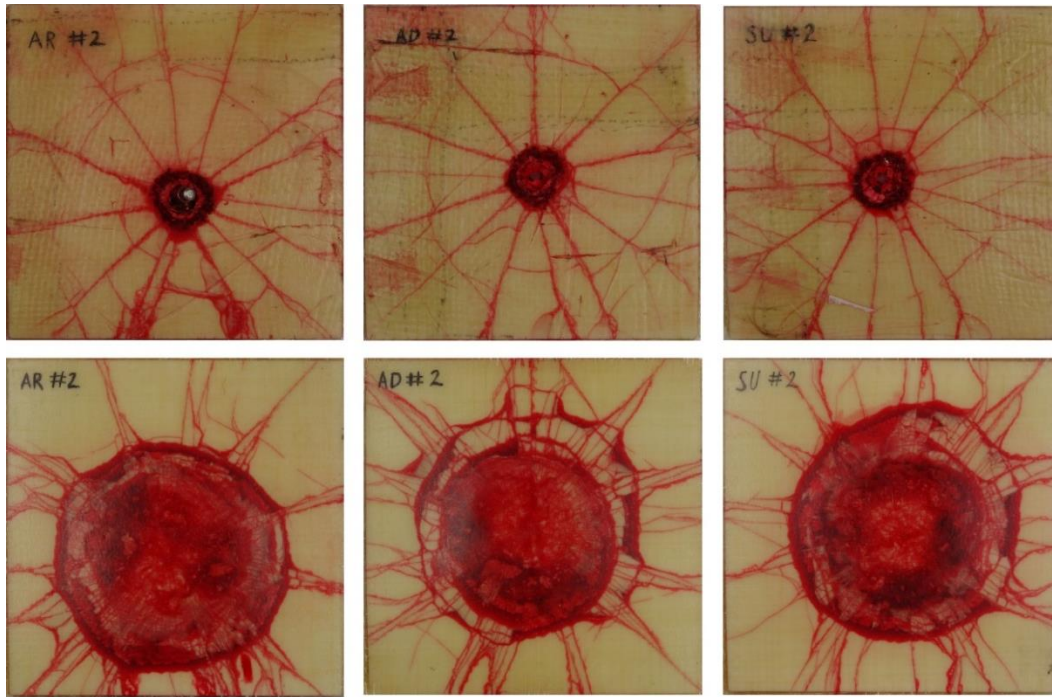


Figure 4.40: The second set of test samples after ballistic testing. The top row shows the front of the plates, and the bottom row shows the back side of the plates. The samples are, from left to right, the as-received, the acetone washed and the silane treated (1 wt%, not rinsed)

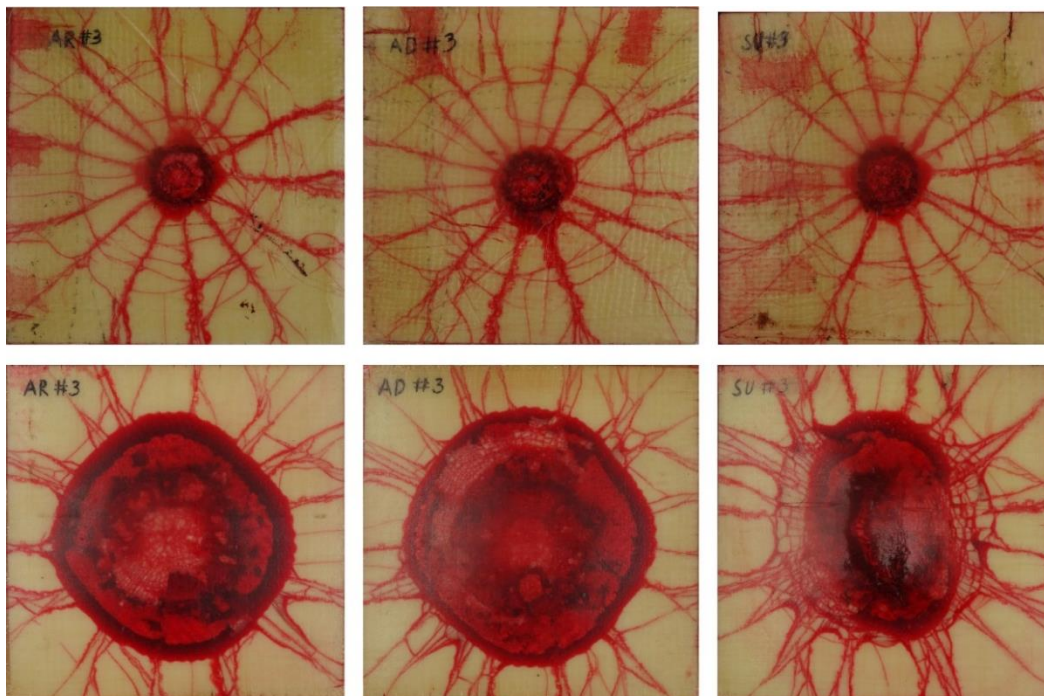


Figure 4.41: The third set of test samples after ballistic testing. The top row shows the front of the plates, and the bottom row shows the back side of the plates. The samples are, from left to right, the as-received, the acetone washed and the silane treated (1 wt%, not rinsed)

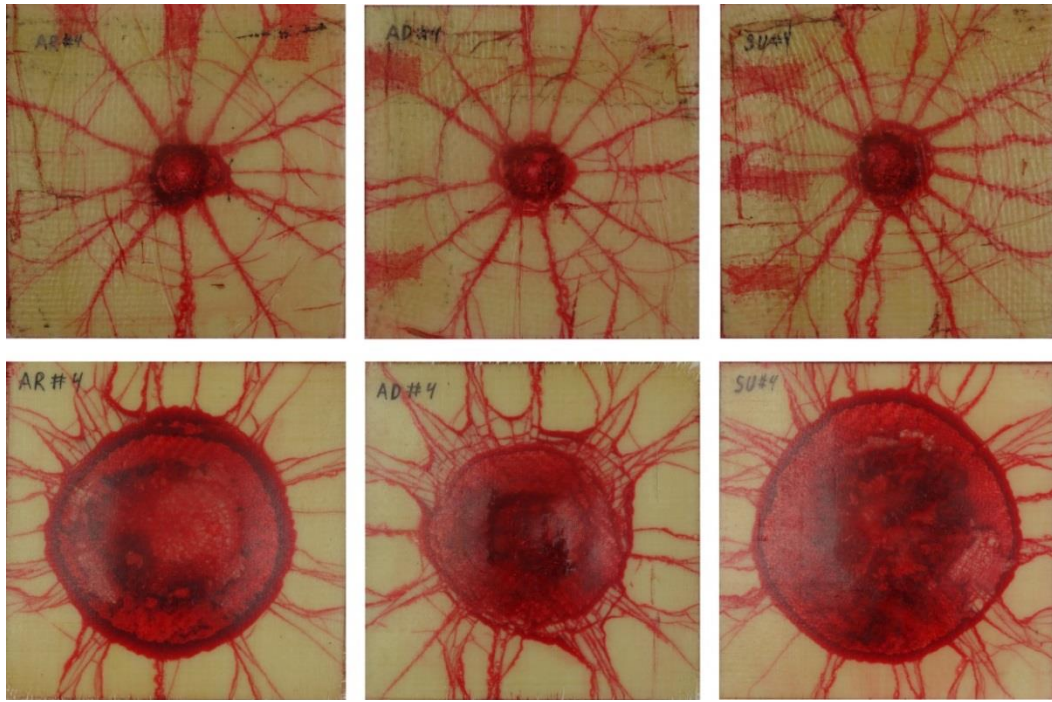


Figure 4.42: The fourth set of test samples after ballistic testing. The top row shows the front of the plates, and the bottom row shows the back side of the plates. The samples are, from left to right, the as-received, the acetone washed and the silane treated (1 wt%, not rinsed)

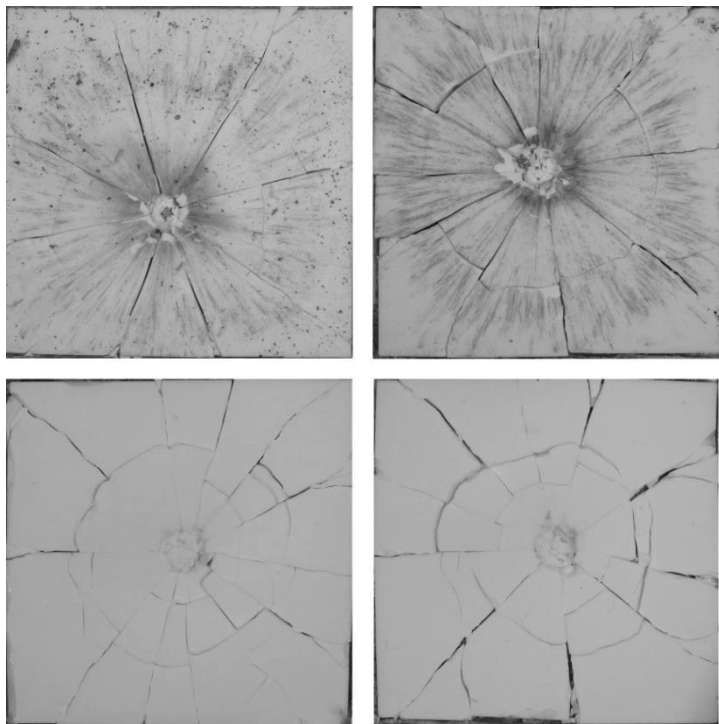


Figure 4.43: The front side of the Teflon wrapped samples. The first sample (top left) was tested with a projectile velocity of 343 m/s, the second (top right) at 481 m/s, the third (bottom left) at 582 m/s, and the fourth at 573 m/s.



*Figure 4.44: The back side of the Teflon wrapped sample from the second set of test samples after the composite has been removed. This sample was tested with a projectile velocity of 481 m/s. (Some of the ceramic pieces have shifted when the composite was removed)*

## 4.4 POSS particles

The results from the peel tests on the samples where POSS-containing interlayer films were placed between the ceramic and the composite, are shown in Figure 4.45 and Figure 4.46. Figure 4.45 shows the results from the acetone washed alumina, and Figure 4.46 shows the results from the silane treated alumina.

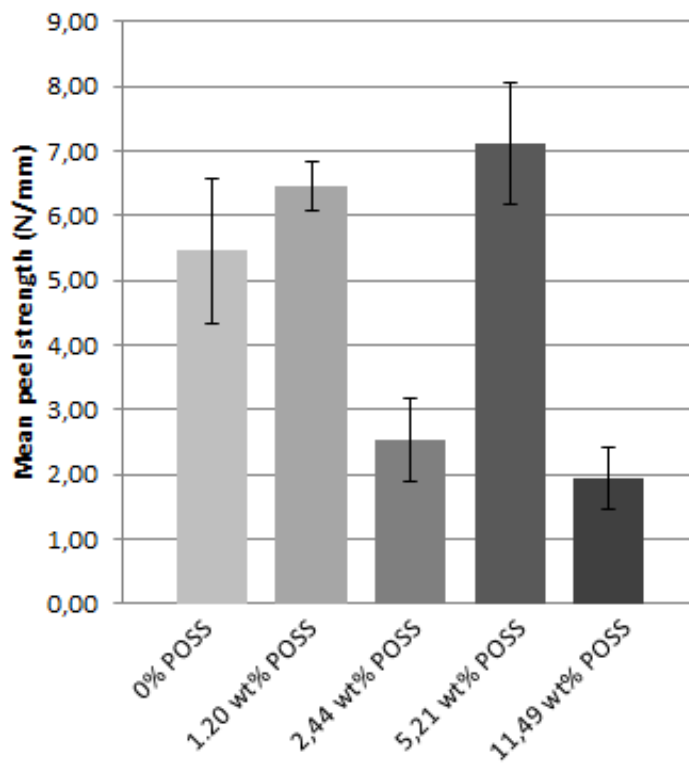


Figure 4.45: Peel test results from the systems where the interlayer films were used in combination with acetone washed ceramic. The percentage of POSS particles is the content in the films which were added between the ceramic and the composite.

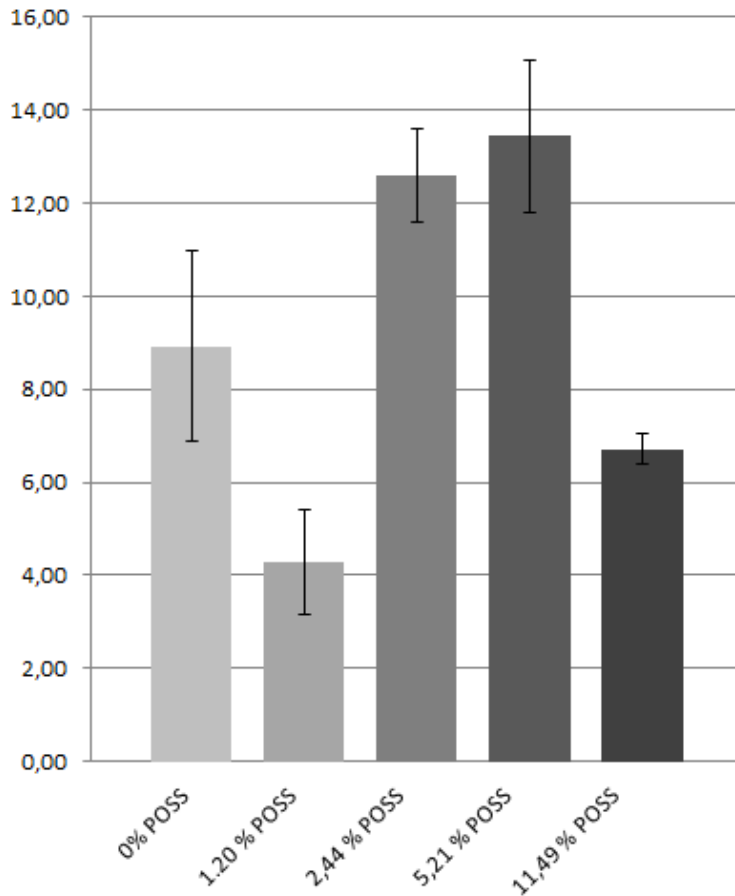


Figure 4.46: Peel test results from the systems where the interlayer films were used in combination with silane treated (0.5 wt%) ceramic. The percentage of POSS particles is the content in the films which were added between the ceramic and the composite.

From the results in Figure 4.45 and Figure 4.46, it is possible to see that the peel strength increases, to a certain point, when the POSS-concentration is increased. After this point, the peel strength decreases again. This decrease in peel strength seems to be due to an increased brittleness of the composite matrix. The peel strengths are generally higher for the silane treated samples, and the relative increase in peel strength when the POSS concentration is increased is also higher. It is also worth mentioning that the reduction in peel strength at high POSS-concentrations is less dramatic for the silane treated samples. A few of the measured peel strengths do not fit into this trend (2.44 wt% POSS on the acetone washed surface, and 1.20 wt% POSS on the silane treated sample). The reasons for these deviations are explained in some more detail later in this section.

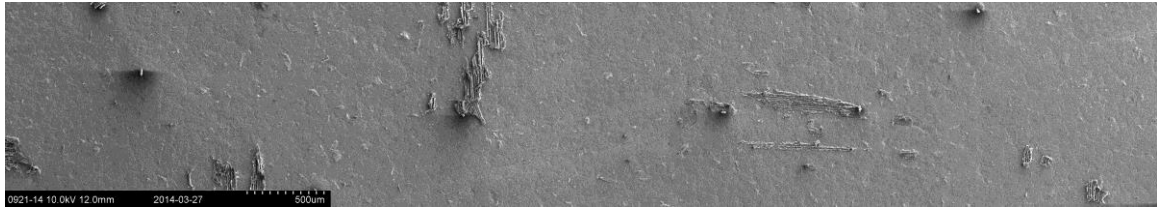
SEM images were again taken of the fracture surface after the peel tests in order to better understand the results from the peel tests. Figure 4.47 show the ceramic side of the fracture surface from the acetone washed samples where interlayer POSS-containing films were used. Note how the fracture shows characteristics of being quite brittle when



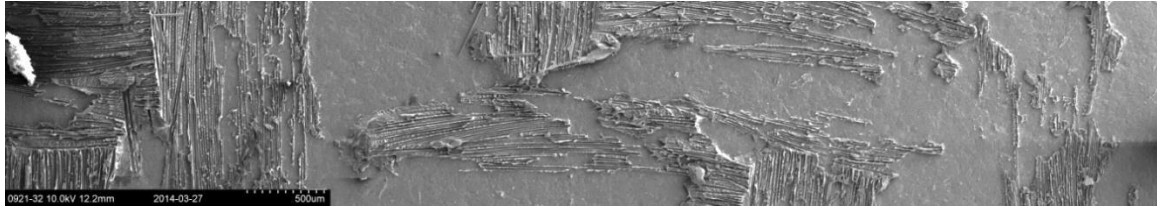
the POSS-concentration is high. The fracture surface becomes smoother, and the amount of cohesive fracture in the composite matrix becomes very high. This corresponds well with the increasing brittleness of the films which was observed during the production of the films as mentioned at the end of Section 3.4, and can explain the reduction in peel strength at high POSS-concentrations. By looking at the SEM images of these fracture surfaces, the amount of adhesive fracture in the composite-ceramic interface can be seen. On the sample where the interlayer film did not contain POSS particles, 90-100 % of the failure occurred in this interface. When the POSS-concentration in the film was 1.20 wt%, approximately 50 % was adhesive fracture in this interface; and on the sample with 2.44 wt% POSS in the film, all of the fracture occurred in this interface. The reason for this is given later in this section. With a POSS-concentration of 5.21 wt%, approximately 40 % of the fracture was in the composite-ceramic interface, and a substantial amount of the fracture is cohesive in the composite matrix instead of in the interface between the composite matrix and the glass fibres. When the concentration is increased to 11.49 wt%, almost 0 % of the fracture was adhesive, and almost all of it was cohesive fracture in the composite matrix. This is probably both because the adhesion between ceramic and composite is increased, and because the cohesive strength of the composite matrix is reduced due to increasing brittleness.

In Figure 4.48, the composite side of the fracture surface is shown. It is clear that with increasing amounts of POSS particles, the composite side of the fracture surface shows less of the imprint of the ceramic, and more exposed glass fibres. When the concentration is too high, the fracture propagates in the composite matrix as can be seen in Figure 4.48 E and to some extent in Figure 4.48 D.

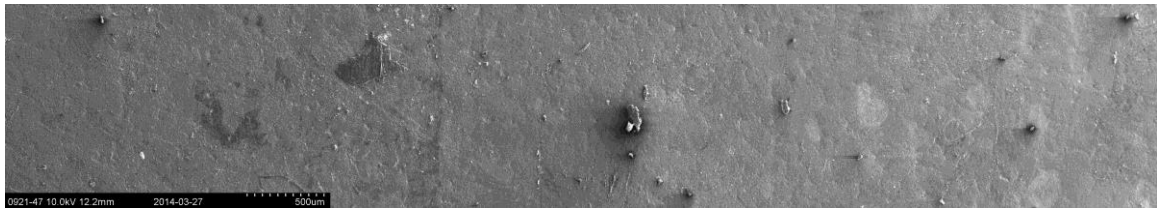
A. 0% POSS



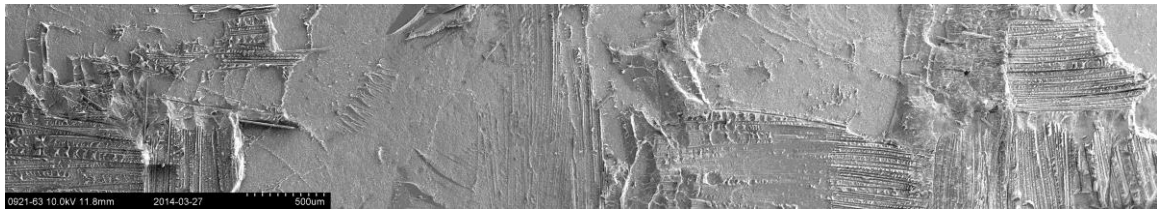
B. 1.20 wt% POSS



C. 2.44 wt% POSS



D. 5.21 wt% POSS

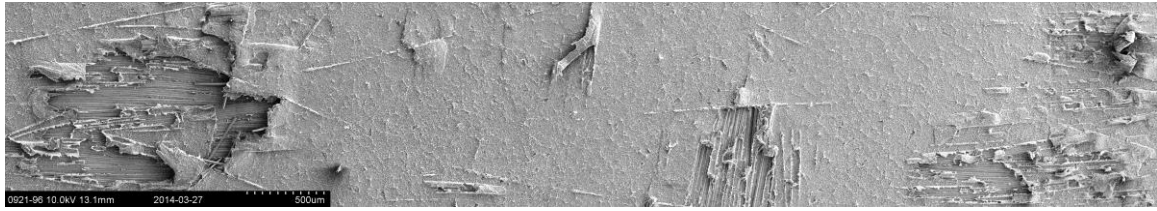


E. 11.4 wt% POSS

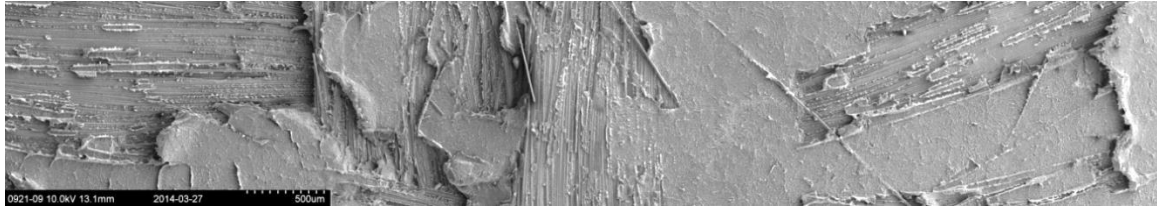


*Figure 4.47: The ceramic side of the fracture surfaces after peel testing on the samples where the interlayer films were used in combination with the acetone washed alumina.*

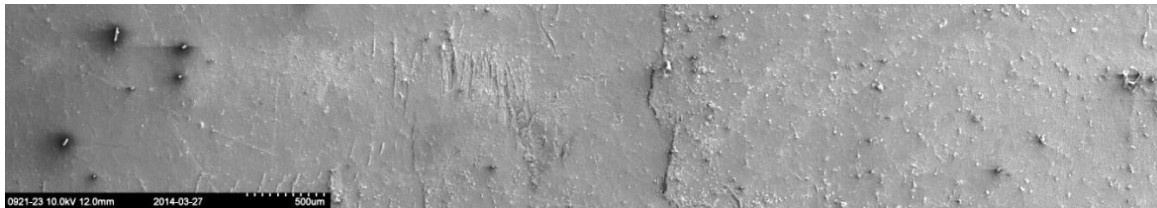
A. 0% POSS



B. 1.20 wt% POSS



C. 2.44 wt% POSS



D. 5.21 wt% POSS



E. 11.49 wt% POSS

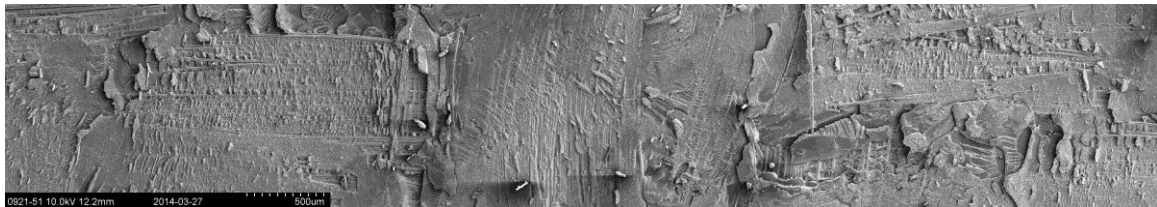


*Figure 4.48: The composite side of the fracture surfaces after peel testing on the samples where the interlayer films were used in combination with the acetone washed alumina.*

Figure 4.47 C and Figure 4.48 C shows the fracture surface of the acetone washed sample where the film contained 2.44% POSS. This sample showed a surprisingly low peel strength, and by the looks of its fracture surface, something seems to have gone wrong in the production or application of the POSS-film. SEM images with high magnifications of this fracture surface can be seen in Figure 4.49, and they seem to indicate that the POSS containing film has not melted properly.

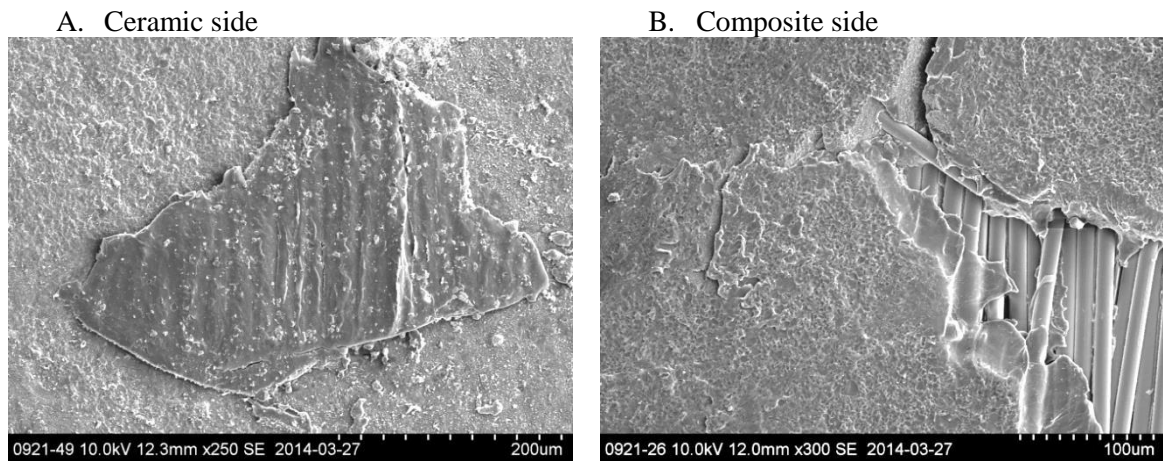
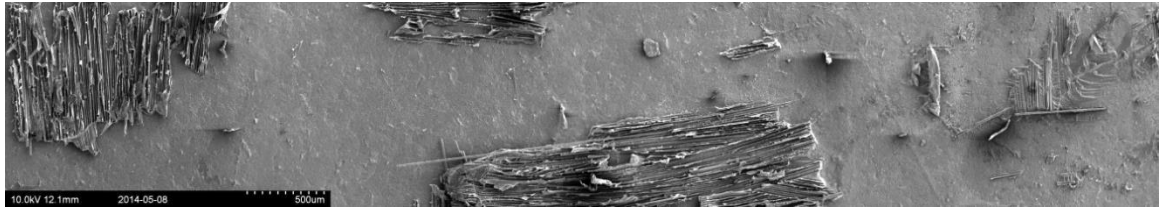


*Figure 4.49: SEM images from, A: the ceramic side and B: the composite side of the fracture surface for the acetone washed sample where the POSS film with 2.44% POSS particles was used.*

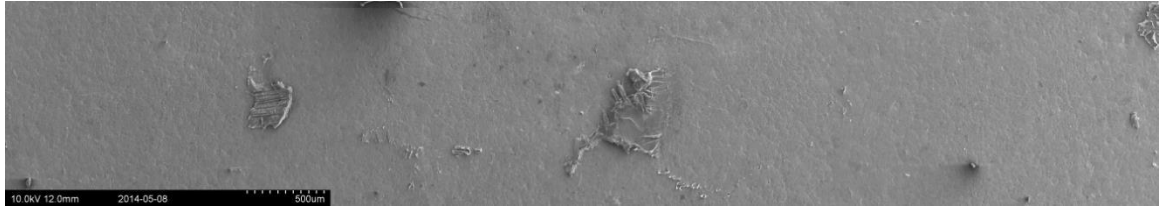
SEM images were also taken from the fracture surface on the silane treated samples with POSS particles. These images can be seen in Figure 4.50 and Figure 4.51. Figure 4.50 shows the ceramic side and Figure 4.51 shows the composite side of the fracture surfaces.

In this series, the sample with 1.20% POSS particles in the film has a very low peel strength, and deviates from the trend which is seen in Figure 4.46. This sample was overheated in the vacuum oven during production which may have caused the LPET to degrade. The fracture surface for this sample can be seen in Figure 4.50 B and Figure 4.51 B, and high magnification SEM images of this fracture surface can be seen in Figure 4.52. (A similar sample with 0 % POSS was also overheated, also resulting in very low peel strength. This sample is not reported here.)

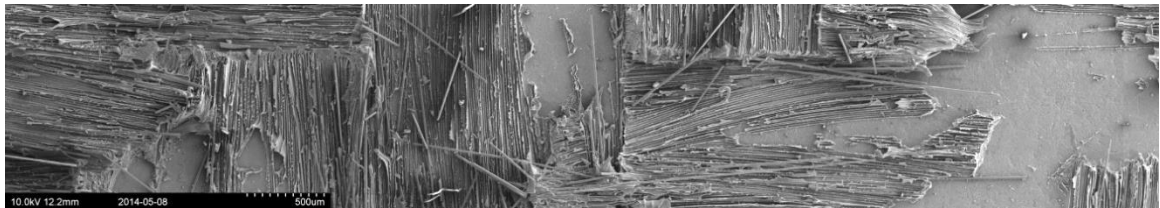
A. 0% POSS



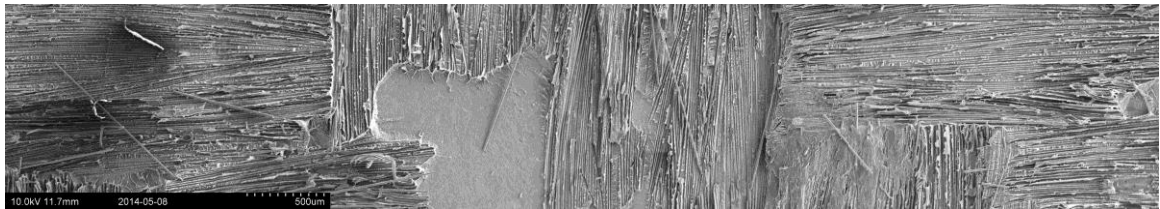
B. 1.20 wt% POSS



C. 2.44 wt% POSS



D. 5.21 wt% POSS



E. 11.49 wt% POSS

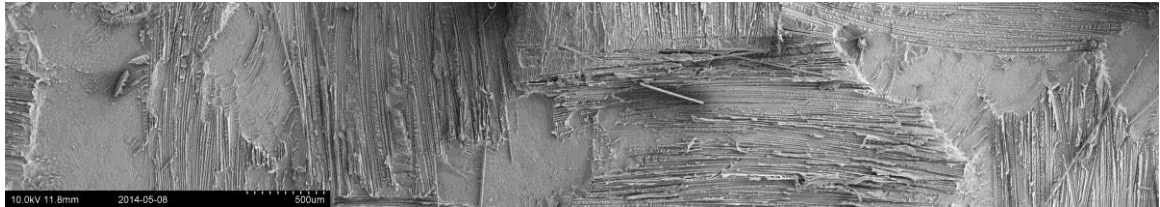
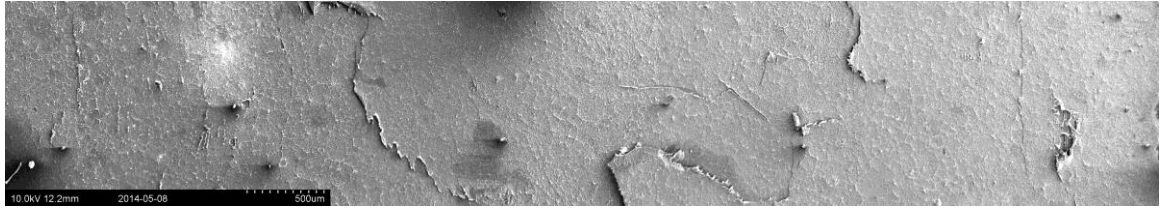


*Figure 4.50: The ceramic side of the fracture surface after peel testing on the silane treated (0.5 wt%) where the POSS-containing interlayer films were used.*

A. 0% POSS



B. 1.20 wt% POSS



C. 2.44 wt% POSS



D. 5.21 wt% POSS



E. 11.49 wt% POSS

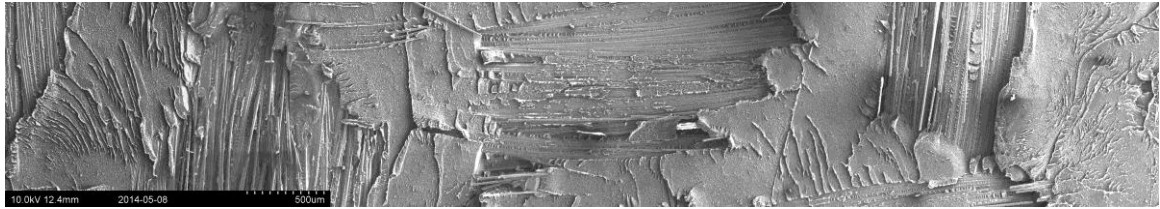
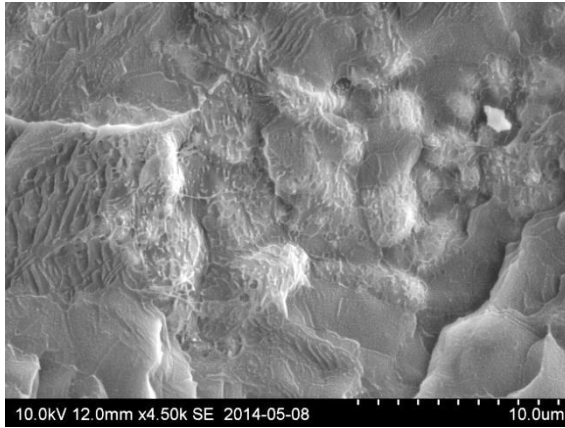


*Figure 4.51: The composite side of the fracture surface after peel testing on the silane treated (0.5 wt%) where the POSS-containing interlayer films were used.*

A. Ceramic side



B. Composite side

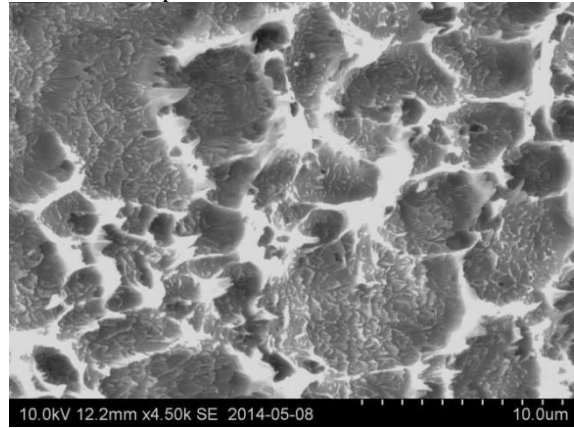


*Figure 4.52: SEM images from, A: the ceramic side and B: the composite side of the fracture surface for the silane treated (0.5 wt%) sample where the POSS film with 1.20% POSS particles was used.*





# 5 Discussion

In the discussion part, the results from the analyses presented in Chapter 4 will be discussed. In Section 5.1, the various surface treatments are discussed. The differences in measured adhesion will be discussed in light of the differences in topology and chemical composition on the surfaces. Section 5.2 will be focused on discussing the results from the ballistic tests which were presented in Section 4.3, and in Section 5.3, the results from the samples where a POSS-containing interlayer film was used, are discussed.

## 5.1 Adhesion

By looking at the results from the contact angle measurements for the different surface treatments corrected for their varying roughness, summarised in Figure 4.14, and the amount of carbon found by XPS on each surface, shown in Figure 4.21 and Table 4.6, it seems that none of the surfaces are completely clean. Some of the surface treatments, such as washing with acetone or chromic sulphuric acid, appear to clean away some of the carbon-based compounds on the surface, but not all of it. In the following, the surface analyses of the different surface treated samples are related to the adhesion found by peel tests. The contact angle measurements will be discussed in more detail in Section 5.1.7.

### 5.1.1 As-received

The results from the peel tests show that the as-received sample is the worst when it comes to adhesion. This is also evident from the SEM images of the fracture surface after the peel test where very little of the composite is left on the ceramic surface, as can be seen in Figure 4.28 A. The composite side Figure 4.29 A is also quite intact. This poor adhesion can be explained by there being a layer of contaminants such as fat and polysaccharides on the surface. Such a contamination layer would result in a weak boundary layer [18;20]. This would result in poor adhesion which would cause the fracture to be dominated by adhesive failure. The SEM images of the fracture surface in Figure 4.28 A and Figure 4.29 A show that this is in fact the case for this sample.

The explanation that there is a significant contamination layer on the as-received sample is in good agreement with the XPS result where this sample shows a higher content of

carbon than the other samples, with exception of the silane treated (1 wt%, not rinsed) sample. As discussed in Section 5.1.7, this contamination layer also agrees well with the results from contact angle measurements.

The carbon peak for the as-received sample is shown in Figure 4.22. This peak is split into three different peaks where peak 1 most likely corresponds to carbon which shares bonds only to other carbon atoms and hydrogen atoms. Based on the chemical shift of 1.527 eV from peak 1 to peak 2 (see Table 4.7), it seems that peak 2 corresponds to carbon bonded to an alcohol group, carbon in an ether group and/or one of the two different carbons in an ester group. Peak 3 is most likely the other carbon in the ester groups (see Appendix A for table values on the chemical shifts). Table 4.7 also summarises the contributions from each of these three peaks. From this table we can see that carbon in simple hydrocarbon chains make up 19.55% of the atoms on the surface, carbon in ester groups make up 2.9 at% and the remaining 6.28 at% from peak 2 corresponds to carbon bonded to an alcohol group and/or carbon in an ether group. This corresponds well with a contamination layer which would be a mixture of fat, containing ester groups and hydrocarbon chains; polysaccharides, containing alcohol groups and possibly ether groups; and other carbon based compounds.

### **5.1.2 Acetone washed**

By washing the ceramic in acetone, the peel strength was increased by almost 50%, compared to the as-received alumina. This increase is most likely because much of the contamination layer which was found on the as-received sample was washed away. This is supported by the XPS results. In Figure 4.22, the carbon peak for the acetone washed sample is compared to the as-received, the silane treated (1 wt%, rinsed) and the chromic sulphuric acid-etched samples. It is clear that the carbon peak is smaller after the sample has been washed in acetone. It is also interesting to see that the composition of the remaining contamination layer after washing with acetone is different from the composition on the as-received sample. This may be because some of the compounds in the contamination layer are more soluble in acetone than the rest. The XPS results also indicate that there may be chemical groups such as OH-groups on the alumina surface. This may also contribute to increasing the adhesion since it can cause a stronger interaction between the materials.

The SEM images of the fracture surface for this sample, shown in Figure 4.28 B and Figure 4.29 B, show that the amount of adhesive fracture in the composite-ceramic interface is decreased compared to the as-received alumina. As mentioned before, a

contamination layer causes a weak boundary layer, which gives high amounts of adhesive fracture. So the fact that the amount of adhesive fracture is decreased for the acetone washed sample supports the statement that a lot of the contaminants have been washed away.

Since all the ceramic tiles were washed in acetone before the various surface treatments, the acetone washed sample should be seen as a control for the other surface treatments.

### **5.1.3 Sandblasted**

From the peel tests it seems that the sandblasted sample may perform slightly worse than the acetone washed sample. In order to understand this, we can look at the XPS results where we see that there may be a small amount of fluorine on the surface. Fluorine is not good with regards to improving adhesion but in this case it is a very small amount, and should not affect the adhesion that much. Another reason for the decreased peel strength can be that the sandblasting crushes the alumina grains, and creates small cracks on the surface of the ceramic. These small cracks enable the crack front in the peel test to propagate through weak areas of the ceramic. This can be seen by the fact that some ceramic grains or crushed ceramic particles are found on the composite side of the fracture surface from the peel test, as shown in Figure 4.34. The cracks and crushed grains created by the sandblasting can also be seen in the cross-section image in Figure 4.11. From this image, it also appears that the LPET from the composite has not penetrated in between the cracks and pores on this surface. This may be because the cracks are too small, and the LPET has a too high viscosity to penetrate into them.

The XPS results for the sandblasted sample shows that it is slightly less clean than the acetone washed sample. This may be because the sand which was used for the sandblasting was polluted.

### **5.1.4 Plasma treated**

The plasma treated sample performs worse than the acetone washed sample in terms of peel strength. Based on the XPS results, it seems that the plasma treatment does not clean away more of the contamination on the surface. The only significant difference in the

XPS results between the plasma treated sample and the acetone washed sample is that the plasma treated sample contains 3.58 at% fluorine on the surface. This fluorine probably comes from pollutions in the plasma chamber, and may to some extent explain the reduced peel strength.

In Figure 4.14, the surface energies of the plasma treated and the acetone washed samples are almost identical, which would suggest that the plasma treatment has had little effect on the ceramic surface. However, these surface energies are corrected for the roughness of the samples. The roughness measurements are quite uncertain, and they suggest a difference in roughness between the plasma treated sample and the acetone washed sample. It can be assumed that the roughness of these two samples is quite similar. If that is the case, the surface energies which are not corrected for roughness in Figure 4.13 should be compared for these samples. This comparison indicates that the surface energy is a little higher for the plasma treated sample.

### **5.1.5 Silane treated**

The silane treatment was conducted in several different ways. Three different concentrations of the silane solution were tested, and at the highest concentration (1 wt%) the procedure was tested in two different ways.

By increasing the concentration of the silane solution, the peel strength increases. When the concentration of the silane solution is 0.25 wt%, the peel strength is the same as for the acetone washed sample, in other words, this does not seem to be enough silane to improve the peel strength significantly. A small increase in the peel strength is measured when the concentration is 0.5 wt%, and a rather large improvement is seen when the concentration is 1 wt%. These results can be seen in Figure 4.30. SEM images of the fracture surfaces are shown in Figure 4.31 and Figure 4.32. The amount of composite matrix left on the ceramic side of the fracture surface increased with increasing concentration of the silane solution. This indicates that the amount of adhesive failure in the composite-ceramic interface decreases which suggests improved adhesion. This agrees well with the measured increase in peel strength.

The sample which was silane treated in the 1 wt% solution (which was not rinsed) showed the highest peel strength of all the tested samples. One of the reasons why this silane treatment gives the best adhesion, may be that the silane molecules form covalent

bonds to the ceramic surface, as illustrated in Figure 3.14, and provide bonding possibilities for the LPET. Another important reason for this good adhesion is that the silane layer is rather thick, filling pores and in between grains on the alumina surface as seen in the SEM images in Figure 4.6 and Figure 4.7. This has made the surface more flat which is confirmed by the profilometer measurements in Table 4.3 in Section 4.1.2. The molten LPET seems to be too viscous to fully penetrate into pores and in between grains on the alumina surface and cause mechanical interlocking, so a more flat surface will improve the adhesion by creating a larger contact area.

The contact angle results for the three samples which were silane treated with different silane-concentrations show that the polar part of the surface energy becomes quite small when the silane-concentration is low. This may be because the distance between each silane molecule on the surface becomes larger allowing the silane molecules to lay flat on the surface and expose their unipolar chains. In the case where more silane is added, they no longer lay flat. Instead the silane molecules stand perpendicular to the surface and expose only the ends of the molecules which have a higher polarity. In addition to this, there may be multiple layers of silane molecules when the concentration of the solution is high enough, this means that both ends of the silane molecule may be exposed.

As mentioned above, the procedure for the silane treatment was tested in two different ways. A rinsing step was added after the sample was taken out of the silane solution and before it was dried in the oven at 93 °C for one hour. The purpose of adding such a step was in order to wash away any silane which was not adhered to the ceramic surface before it was left to dry. However, it seems that this rinsing step washed away almost all of the silane on the surface. The XPS results show that the sample which was not rinsed after silane treatment has a very high carbon content compared to the acetone washed sample while the carbon content of the sample which was rinsed after silane treatment was only slightly higher than the acetone washed sample. The carbon peak from the rinsed silane treated sample is quite similar to the one for the acetone washed sample with a small increase in the contribution from peak 2 (see Figure 4.22). This indicates that the carbon on the surface of the rinsed silane treated sample is mostly the same contamination layer as the one on the acetone washed sample with a small amount of silane left on the surface. Moreover, the carbon peak for the silane treated sample which was not rinsed is completely different from the acetone washed sample, which indicates that this peak is mostly dominated by the carbon in the silane molecules (see Figure 4.23). In addition to this, the surface energy measurements are more similar to the acetone washed sample for the sample which has been rinsed after silane treatment than for the sample which has not been rinsed. However, the polar part of the surface energy for the rinsed silane treated sample is lower than the acetone washed sample. This may be caused by the same effect as for the samples silane treated with a low concentration of silane. The measured peel strengths also shows that the rinsed silane treated sample has almost the same level of

adhesion as the acetone washed sample. Again, this indicates that most of the silane is washed away in the rinsing step.

### **5.1.6 Chromic sulphuric acid etched**

As mentioned in Section 3.2.4, two different chromic sulphuric acid recipes were used. Both were analysed with contact angle measurements, profilometer measurements and XPS, however, only the FPL-etch was used for preparing peel test samples.

The results from the contact angle measurements which are corrected for roughness on the surface (see Figure 4.14) and the XPS results (see Figure 4.21 and Table 4.6) both show that the chromic sulphuric acid cleans the surface better than washing with acetone only. The dispersive part of the surface energy is higher for these samples than for the one washed in acetone which, as discussed in Section 5.1.7, may be because the contamination layer on the surface is thinner after washing. In addition to this, the XPS result show that the amount of carbon on the surface is reduced compared to the acetone washed sample. It is also clear from the results of these tests that the strong chromic sulphuric acid cleans the surface better than the FPL-etch.

The FPL etched samples perform slightly better than the acetone washed samples in the peel test which serves to confirm the idea that better cleaning of the surface provides better adhesion between the ceramic and the composite backing material. This indicates that even better result could have been obtained if the composite also had been rinsed in some way before use.

By comparing the high resolution XPS scans of the carbon peaks of these two samples to the rest, it is clear that the FPL etched sample is quite similar to the as-received and acetone washed samples. The carbon peak splits into three peaks, and the chemical shifts between them are similar to the chemical shifts for the other samples (see Table 4.7). The main difference is the composition of the remaining contamination layer, and the total amount of carbon on the surface. The carbon peak for the sample etched with the strong chromic sulphuric acid also splits into three peaks. However, for this sample the chemical shifts between the peaks are higher. This may for example indicate that the triglycerides in the fat have split into glycerol and fatty acids. Peak 3 would then correspond to the acid group, and the increase in the chemical shift in peak 2 would be due to an increased amount of neighbour effects between carbon atoms bonded to an alcohol group.

### 5.1.7 Contact angle measurements

We can see from the contact angle measurements in Figure 4.14 that the dispersive part of the surface energy increases when the surface is washed. This may be because carbon-based contamination on the surfaces is partly washed away leaving behind a thinner layer which causes the dispersive contribution from the underlying alumina to increase. The polar part of the surface energy is almost unchanged by washing away some of the contaminants. This may be because the contaminants on the surface are mostly located between the grains on the alumina surface, so by washing, the total area of exposed alumina may not have increased dramatically.

Another possible reason why the polar part is mostly unchanged while the dispersive part increases when some of the contaminants are washed away, may be that there is a difference between the polar and the dispersive interactions in the distance dependency between the underlying alumina surface and the liquid drop. The polarity in the alumina is found only in the surface of the material since the dipole moments in the bulk will cancel each other. The dispersive contribution to the surface energy, on the other hand, is also affected by atoms deeper in the material.

In order to get the total force between the alumina surface and the liquid drop, one has to integrate over all the interactions between the surface and the liquid drop. By doing this, one will find that the polar contribution of the surface energy is reduced more quickly with increasing distance between the alumina and the drop than the dispersive contribution where the integration has to be done in three dimensions in order to cover all the interactions. In other words, when the contamination layer becomes thinner and the distance between the alumina surface and the liquid drop becomes smaller, the dispersive part will increase because of the contribution of the alumina, as mentioned above. However, the polar part is not affected since the contamination layer is still too thick for the liquid drop to be affected by the polarity of the underlying alumina. Bain and Whitesides [55] partly confirm this statement by showing that the polar contribution from chemical groups deeper down in the material rapidly decreases when the distance between these groups and the liquid drop increases.

In addition to the explanations above, the relative large increase in the dispersive contribution may be because the contaminants could be partly soluble in the diiodomethane. If this is true, some of the contamination layer may have been dissolved in the diiodomethane which may change the properties of the diiodomethane, and which brings the liquid drop closer to the alumina surface.

In any case, it can be seen that the total surface energy increases when the surface is washed in acetone, and that it increases even further when the ceramic is washed with the chromic sulphuric acid. This increase in surface energy is mostly due to an increase in the dispersive part. It is interesting to note that the dispersive part of the surface energy of the LPET is very large compared to the polar contribution. So by washing the surfaces in acetone or chromic sulphuric acid, the LPET may be more able to wet the surface.

The sandblasted, and silane treated samples differ from the rest of the samples when it comes to the contact angle measurements in Figure 4.14. In these cases, the surface has not only been washed, but also altered in other ways. The surface structure of the sand blasted surface is completely different. It is rougher and has a lot of small cracks on the surface. The roughness has already been corrected for in this bar graph. However, if the liquid in the drop is unable to penetrate the cracks on the surface, the drop may actually be resting on a combination of alumina and air pockets. Such effects may cause the contact angle results from this sample to be different from the rest. If this is the case, it is difficult to compare this sample to the others. The silane treated samples, on the other hand, differ from the others in that there is a layer of silane on the surface. This lowers the polarity of the surface, and increases the dispersive contribution. The decrease in polarity is because the silane itself has a quite low polarity, and the increase in the dispersive part of the surface energy may be because there is a dispersive contribution from the Si-atoms in the silane layer. These Si-atoms are above the contamination layer, and in more direct contact with the liquid drop. This should make their contribution to the dispersive part larger than that of the underlying alumina.

## 5.2 Ballistic properties

By looking at the results from the ballistic tests in Figure 4.39 to Figure 4.44, there are a few differences that are worth mentioning.

The diameter of the damaged area in the ceramic seems to increase with increasing projectile velocity. This diameter does not change much with the changes in the adhesion between the ceramic and the composite. However, what seems to depend on the adhesion is the amount of cracks in the ceramic cone. With increasing adhesion, the amount of cracks in the ceramic cone appears to increase. This can be seen by comparing the images of the backside of the plates, which are shown in the bottom rows of Figure 4.39 to Figure 4.42. This trend is most clear for the first set where the projectile velocity was quite low, and the damage is less extensive. In order to confirm whether this trend is true, the



composite was removed from the backside of the Teflon wrapped sample in the second set. The picture of this can be seen in Figure 4.44. It is clear that the ceramic pieces in the centre of the tile are quite big while in the cases where the adhesion is stronger, this centre area is almost pulverised. This increase in crack formation in the ceramic cone could both be positive and negative. On one hand, the cracking absorbs energy and should leave the rest of the tile relatively intact and ready for a second strike, but on the other hand, if the damage in the ceramic is too concentrated, the energy will be spread on a smaller area and the plate may lose some of its ability to protect against the projectile.

It is also possible to see from the images of the tested plates that there is some delamination between the ceramic and the composite. This delamination will probably reduce the performance when the plate is hit a second time, but no delamination may cause the composite to crack. By comparing the silane treated and acetone washed samples from the third set (see Figure 4.41) to the corresponding samples in the fourth set (see Figure 4.42), it can be seen that the amount of delamination affects the ballistic performance of the plate. The samples with a low amount of delamination (the silane treated sample from the third set and the acetone washed sample from the fourth set) show a larger amount of damage to the composite backing material than the samples with a high amount of delamination (the acetone washed sample from the third set and the silane treated sample from the fourth set). In the two samples with low amounts of delamination, there was a hole through the backing material with ceramic fragments sticking out. In the two other samples, the delamination in the areas around the ceramic cone will have allowed the composite to be stretched instead of being held back and bent when the ceramic cone pushed against it. This may have prevented the composite from breaking since it can endure more in tension than it can in bending, and may be a reason why too high adhesion could have a negative effect.

In the fourth set of samples, the amount of delamination is a little different from what one could expect from the peel test results. The silane treated sample shows a large increase in the amount of delamination with an increase in the projectile velocity while the acetone washed sample shows a reduction in delamination with an increase in the projectile velocity. This may be due to inaccuracies in the sample production or some randomness of the results. However, it may also be due to some unknown effects. More work should be done with a larger set of samples in order to get a clearer view of what causes this delamination, and how it affects the ballistic performance of the plates.

## 5.3 Interlayer film of POSS/LPET

Two series were made with POSS particles, one with acetone washed ceramic tiles and the other with silane treated ceramic tiles. The concentration of the solution used for the silane treatment was 0.5 wt% in order to avoid getting peel strengths that were too high to measure. By adding the LPET film without POSS between the ceramic and the composite, the peel strength decreased drastically. In other words, the method for adding the POSS particles to the bonded system should be reconsidered.

### 5.3.1 Acetone washed ceramic

As mentioned above, the peel strength dropped significantly by adding the films. This may be because the films were contaminated, or because the LPET used in making the films was heated in air and not in vacuum causing it to degrade. However, when POSS particles were added in increasing amount, the peel strength increased a little before it dropped. This trend is seen in the results in Figure 4.45, and is quite similar to the trend seen by Nguyen et al. [49]. However, their results do not drop as dramatically with high concentrations of POSS particles. The reason for this may be a difference in the mechanisms causing the decrease in peel strength. It is clear from the standard deviation in the results in Figure 4.45 that the results are somewhat uncertain, this may for example be because the interlayer films varied a little in thickness.

The results from the sample with 2.44% POSS in the film deviates from the abovementioned trend. This sample gave a surprisingly low value for the peel strength. Based on the SEM images of the fracture surface in Figure 4.47 C and Figure 4.48 C, it is evident that something has gone wrong with the production or application of the POSS film. In Figure 4.49, detail SEM images of this fracture surface are shown. Here it is evident that the POSS film has not melted thoroughly. On the ceramic side, a large portion of the film is still intact, and on the composite side, the imprint from the ceramic is shallower than what is seen for the other samples.

By looking at the SEM images of the ceramic side of the fracture surfaces in Figure 4.47, one can see that an increasing amount of the composite is left on the ceramic surface when the POSS concentration increases. This indicates that the adhesion has increased, and supports the trend described above. At the same time, the fracture shows more and more characteristics of a brittle fracture. The fracture surface becomes smoother, and, in the case of the sample with the highest amount of POSS particles, the fracture propagates

only through the polymer matrix, which is evident from Figure 4.47 E and Figure 4.48 E. Here the entire ceramic surface is covered with LPET, and none of the glass fibres are visible on the composite side of the fracture surface. This brittleness would explain why the peel strength drops significantly when too much POSS particles are added. The fact that the LPET becomes brittle with increasing POSS content was also seen during the production of the films. The films containing 11.49% POSS had a tendency to break into smaller pieces as can be seen in Figure 3.24 in Section 3.4. Nguyen et al. [49] do not find the same increase in the brittleness in the polyethylene they used, and explain the decrease in peel strength with too high concentrations of POSS as an effect of the reduced ability of the mixtures to flow into pores on the surface. This difference in behaviour may explain why the decrease in peel strength at high POSS concentrations is much less dramatic in their case.

### 5.3.2 Silane treated ceramic

When the interlayer films were used in combination with silane treated ceramics, a similar trend as the one described above is seen. The trend is that the peel strength increases with POSS concentration, up to a certain level, whereafter it decreases. The results from these tests are shown in Figure 4.46. The sample with the interlayer film without POSS particles show an increased peel strength compared to the corresponding sample where an acetone washed ceramic tile was used which indicated that the silane treatment has an effect. However, the peel strength for this sample is still lower than the silane treated (0.5 wt%) where no interlayer film was added.

In the bar graph in Figure 4.46, it is clear that the sample with 1.20 wt% POSS particles in the film deviates from the trend. Some technical problems caused this test sample to be overheated in the vacuum oven during production. This overheating seems to have caused the LPET in the composite to degrade to a certain degree which caused the fracture to propagate through the composite matrix close to the ceramic surface. SEM images of the fracture surface from this sample can be seen in Figure 4.50 B and Figure 4.51 B. More detailed images of this fracture surface are shown in Figure 4.52.

As mentioned above, the trends in the two different series with POSS particles are quite similar. By adding POSS particles the peel strength increases to a certain limit where the increased brittleness causes the peel strength to decrease. However, the relative amount by which the peel strength increases is different for the two series. The increase from the sample without POSS particles to the one with 5.21% POSS particles relative to the first sample is approximately 30% in the series with acetone washed ceramic tiles. This same

increase in the silane treated series is approximately 50%. This may indicate that the presence of silane allows the POSS particles to improve the adhesion more than they do on a surface without silane, which again may indicate that more bonds are formed between the silane layer and the POSS particles than between the acetone washed surface and the POSS particles. This could be because the epoxy group in the silane molecule reacts with the amine group in the POSS particles. However, bear in mind that the accuracy of the measurements is not that great, and the number of measurements is quite low, so this difference in relative increase of the peel strength between the two series may not be as large as it seems.

It is also worth mentioning that the sample with the highest amount of POSS particles in combination with the silane treated surface does not appear to be as brittle as the corresponding sample on the acetone washed sample. This can be seen from the SEM images of the fracture surface, and from the fact that the decrease in peel strength is lower in combination with the silane treated ceramic than with the acetone washed ceramic. What causes this sample to be less brittle is not clear, but it may be because of chemical bonds forming between the POSS particles and the silane layer.

## 6 Conclusion

By cleaning the alumina surface of contaminants, the adhesion between the ceramic and the composite is improved. Cleaning with acetone improves the peel strength from 9.6 N/mm for the as-received sample to 13.2 N/mm. By cleaning further with chromic sulphuric acid (FPL, 10 min), the peel strength is increased to 15.7 N/mm. This is because the contaminants on a poorly washed surface cause a weak boundary layer.

The best adhesion was obtained by treating the surface with a silane called 3-glycidyloxypropyl trimethoxysilane (GPS). The silane bonded to the ceramic and filled pores and valleys between grains on the alumina surface, leaving behind a flatter surface. The increased flatness of the surface increased the contact area between the polymer matrix and the ceramic since the polymer was too viscous to otherwise penetrate into pores on the surface. The silane itself also facilitated bonding between the ceramic and the polymer. By conducting this surface treatment, the peel strength was increased to 19.9 N/mm which is more than a doubling compared to the as-received sample.

Adding polyhedral oligomeric silsesquioxanes (POSS) particles to the composite matrix close to the composite-ceramic interface can also increase the adhesion. However, the method for adding POSS to the system lowered the peel strength of the control samples and should be reconsidered. The peel strength increased with increasing POSS concentration up to a certain point where the POSS particles caused the polymer matrix to become increasingly brittle which lowered the peel strength. The relative increase in peel strength from the control sample to the one where 5.21 wt% POSS was added to the interlayer film was 30% when the films were used in combination with the acetone washed surfaces, and 50% when the silane treated ceramic was used. This indicated that POSS particles may be even more effective when used in combination with a silane coupling agent.

Ballistic tests were performed on plates where the ceramic was surface treated in different ways. It is difficult to draw any clear conclusion from these tests, both because relatively few samples were tested and because the projectile velocity varied a little for some of the tests. However, it seems that there may be an ideal amount of adhesion for optimum ballistic performance. Too low adhesion may cause delamination between the composite and the ceramic, which would cause the ballistic performance to be low on the second impact. Too high adhesion, on the other hand, seems to concentrate the damage to a small area, which could reduce the plate's ballistic performance in the first place.



## 7 Future work

There are a lot of things that would be interesting to investigate in addition to the work done in this thesis. In this section, a few of these will be suggested.

- In this thesis, the ceramic tiles were washed in acetone before the various other surface treatments. It would be interesting to try these surface treatments without washing in acetone in order to be able to compare these surface treated samples directly to the acetone washed sample.
- It could be interesting to do a depth profiling with the XPS technique in order to investigate whether there is a difference in thickness of the contamination layer on the samples which are washed in various ways. This is done by etching away part of the material with an ion gun, and taking measurements in different levels in the material. It could also be interesting to use the XPS technique to take 2D images of a larger area on each sample in order to see whether the distribution of the elements is uniform or not. This could also be done on the fracture surfaces in order to see whether the areas where the ceramic seems to be exposed are in fact free of all LPET.
- In order to better understand the effect of adhesion on the ballistic performance of the protection plate, more ballistic test should be performed especially more parallel tests at a rather high projectile velocity in order to see if there is a difference in the amount of delamination. In addition to this, it would be very interesting to do multiple  $V_{50}$  tests on plates with varying levels of adhesion in order to be able to plot the ballistic properties as a function of the adhesion between the materials.
- It would also be interesting to test how well the plates perform when a second projectile is fired into the test sample, and see how that varies with the level of adhesion between the ceramic and the backing material. In order to get good results in that case, many samples of the same type should be made.
- By stabilising the plates with epoxy after the ballistic tests, the composite could be removed without destroying the ceramic tiles. By doing this, it may be possible to get more information out of the tests that have been done. For instance, the

amount of small cracks in the ceramic cone would be easier to see when the composite is removed.

- Some work similar to the work done in this thesis should be done on thinner ceramic tiles. The ceramic tiles used in armour plates today usually are thinner than the 10 mm thick plates which were tested here, and the thickness of the ceramic may affect the importance of the adhesion between the ceramic and the backing material.
- More work should be done in order to find a new technique for adding POSS particles to the composite matrix without degrading the LPET.
- Performing ballistic tests on plates where POSS particles are added to the composite could be interesting. It is possible that the POSS particles not only affect the adhesion between the materials, but also the material properties, such as the impedance, of the composite.



# References

- [1] D. Sherman, "Impact failure mechanisms in alumina tiles on finite thickness support and the effect of confinement," *International Journal of Impact Engineering*, vol. 24, no. 3, pp. 313-328, 2000.
- [2] C. Navarro, M. A. Martinez, R. Cortes, and V. Sanchezgalvez, "Some Observations on the Normal Impact on Ceramic Faced Armors Backed by Composite Plates," *International Journal of Impact Engineering*, vol. 13, no. 1, pp. 145-156, 1993.
- [3] S. Sarva, S. Nemat-Nasser, J. Mcgee, and J. Isaacs, "The effect of thin membrane restraint on the ballistic performance of armor grade ceramic tiles," *International Journal of Impact Engineering*, vol. 34, no. 2, pp. 277-302, 2007.
- [4] J. Wells, N. Rupert, and M. Neal, *Impact Damage Analysis in A Level Iii Flexible Body Armor Vest Using Xct Diagnostics*. WESTERVILLE: AMER CERAMIC SOC, 2010, pp. 171-179.
- [5] R. Zaera, S. Sanchez-Saez, J. L. Perez-Castellanos, and C. Navarro, "Modelling of the adhesive layer in mixed ceramic/metal armours subjected to impact," *Composites Part A-Applied Science and Manufacturing*, vol. 31, no. 8, pp. 823-833, 2000.
- [6] M. L. Wilkins, "Mechanics of Penetration and Perforation," *International Journal of Engineering Science*, vol. 16, no. 11, pp. 793-807, 1978.
- [7] M. Ubeyli, R. O. Yildirim, and B. Ogel, "Investigation on the ballistic behavior of Al(2)O(3)/Al2O24 laminated composites," *Journal of Materials Processing Technology*, vol. 196, no. 1-3, pp. 356-364, 2008.
- [8] M. Grujicic, B. Pandurangan, and B. d'Entremont, "The role of adhesive in the ballistic/structural performance of ceramic/polymer-matrix composite hybrid armor," *Materials & Design*, vol. 41, pp. 380-393, 2012.
- [9] P. J. Hazell, *CERAMIC ARMOUR: Design and Defeat Mechanisms* Agros Press, Canberra, Australia, 2006.
- [10] K. T. Ramesh and J. H. Beatty, "Materials in Extreme Dynamic Environments," [http://www.arl.army.mil/www/pages/1419/1419\\_MEDE%20Overview.pdf](http://www.arl.army.mil/www/pages/1419/1419_MEDE%20Overview.pdf) 29.05.2014.
- [11] J. B. Gao, Y. W. Wang, L. Y. Zhang, G. F. Han, and F. C. Wang, *Study on the Ballistic Performance of Ceramic Composite Armor with Different Adhesive*. STAFA-ZURICH: TRANS TECH PUBLICATIONS LTD, 2011, pp. 308-313.
- [12] National Research Council, "Opportunities in Protection Materials Science and Technology for Future Army Applications," The National Academes Press, Washington, D.C., USA, 2011.

- [13] S. Skriudalen, O. Dullum, S. M. Bergsrud, and E. Wulvik, "Materialer for ballistisk beskyttelse," FFI-rapport 2009/00651, Mar.2009.
- [14] C. Kaufmann, D. Cronin, M. Worswick, G. Pageau, and A. Beth, "Influence of material properties on the ballistic performance of ceramics for personal body armour," *Shock and Vibration*, vol. 10, no. 1, pp. 51-58, 2003.
- [15] M. Grujicic, P. S. Glomski, T. He, G. Arakere, W. C. Bell, and B. A. Cheeseman, "Material Modeling and Ballistic-Resistance Analysis of Armor-Grade Composites Reinforced with High-Performance Fibers," *Journal of Materials Engineering and Performance*, vol. 18, no. 9, pp. 1169-1182, 2009.
- [16] N. K. Naik, P. Shirao, and B. C. K. Reddy, "Ballistic impact behaviour of woven fabric composites: Formulation," *International Journal of Impact Engineering*, vol. 32, no. 9, pp. 1521-1552, Sept.2006.
- [17] M. Guden, U. Yildirim, and I. W. Hall, "Effect of strain rate on the compression behavior of a woven glass fiber/SC-15 composite," *Polymer Testing*, vol. 23, no. 6, pp. 719-725, Sept.2004.
- [18] T.-A. Nguyen, "Polyhedral oligomeric sisesquioxanes: Effects on adhesion, water resistance and water vapour barrier properties of paperboard." Phd Norwegian University of Science and Thecnology (NTNU), 2013.
- [19] Adhesiveandglue.com, "<http://www.adhesiveandglue.com/adhesion-theories.html>," 18.12.2013.
- [20] A. V. Pocius, *Adhesion and Adhesives Technology*. Munich, Vienna, New York: Hanser Publishers, 2013.
- [21] A. J. Harris, B. Vaughan, J. A. Yeomans, P. A. Smith, and S. T. Burnage, "Surface Preparation of silicon carbide for improved adhesive bond strength in armour applications," 2013.
- [22] A. J. Harris, J. A. Yeomans, P. A. Smith, B. Vaughan, and S. T. Burnage, "Surface treatment of alumina and silicon carbide for improved adhesive strength in armour.," 2014.
- [23] M. Madani, F. C. S. Chu, A. V. McDonald, and R. J. Smales, "Effects of surface treatments on shear bond strengths between a resin cement and an alumina core," *Journal of Prosthetic Dentistry*, vol. 83, no. 6, pp. 644-647, 2000.
- [24] A. Della Bona, K. J. Anusavice, and C. Shen, "Microtensile Strength of Composite Bonded to Hot-pressed Ceramics," *The Journal of Adhesive Dentistry*, vol. 2, no. 4, pp. 305-313, Oct.2000.
- [25] B. K. Kim, H. E. K. Bae, J. S. Shim, and K. W. Lee, "The influence of ceramic surface treatments on the tensile bond strength of composite resin to all-ceramic coping materials," *Journal of Prosthetic Dentistry*, vol. 94, no. 4, pp. 357-362, 2005.

- [26] M. Özcan, H. N. Alkumru, and D. Gemalmaz, "The Effect of Surface Treatment on the Shear Bond Strength of Luting Cement to a Glass-Infiltrated Alumina Ceramic," *The international Journal of Prosthodontics*, vol. 14, no. 4, pp. 335-339, 2001.
- [27] L. F. Valandro, A. Della Bona, M. A. Bottino, and M. P. Neisser, "The effect of ceramic surface treatment on bonding to densely sintered alumina ceramic," *Journal of Prosthetic Dentistry*, vol. 93, no. 3, pp. 253-259, 2005.
- [28] B. B. Johnsen, K. Olafsen, and A. Stori, "Reflection-absorption FT-IR studies of the specific interaction of amines and an epoxy adhesive with GPS treated aluminium surfaces," *International Journal of Adhesion and Adhesives*, vol. 23, no. 2, pp. 155-163, 2003.
- [29] D. D. Rodrigues and J. G. Broughton, "Silane surface modification of boron carbide in epoxy composites," *International Journal of Adhesion & Adhesives*, vol. 46, pp. 62-73, 2013.
- [30] M. Tanoglu, S. H. McKnight, G. R. Palmese, and J. W. Gillespie, "Use of silane coupling agents to enhance the performance of adhesively bonded alumina to resin hybrid composites," *International Journal of Adhesion and Adhesives*, vol. 18, no. 6, pp. 431-434, 1998.
- [31] M. A. Sobolewski, J. G. Langan, and B. S. Felker, "Electrical optimization of plasma-enhanced chemical vapor deposition chamber cleaning plasmas," *Journal of Vacuum Science & Technology B*, vol. 16, no. 1, pp. 173-182, 1998.
- [32] H. Asai, N. Iwase, and T. Suga, "Influence of ceramic surface treatment on peel-off strength between aluminum nitride and epoxy-modified polyaminobismaleimide adhesive," *Advanced Packaging, IEEE Transactions on*, vol. 24, no. 1, pp. 104-112, Feb.2001.
- [33] A. A. Bujanda, V. Rodriguez-Santiago, C. C. Ho, B. E. Stein, R. E. Jensen, and D. D. Pappas, "Atmospheric Plasma Treatment of Polymer Films and Alumina Ceramics for Enhanced Adhesive Bonding," 2011.
- [34] F. K. Hansen, "The Measurement of Surface Energy of Polymers by Means of Contact Angles of Liquids on Solid Surfaces," 2004.
- [35] Attension, "<http://www.attension.com/applications/measurements/roughness-1>," 03.02.2014.
- [36] A. M. Paepegaey, M. L. Barker, D. W. Bartlett, M. Mistry, N. X. West, N. Hellin, L. J. Brown, and P. G. Bellamy, "Measuring enamel erosion: A comparative study of contact profilometry, non-contact profilometry and confocal laser scanning microscopy," *Dental Materials*, vol. 29, no. 12, pp. 1265-1272, 2013.
- [37] D. Fridy, "<http://www.opticalprofilometry.com/non-contact-vs-contact-profilometers/>," 03.02.2014.
- [38] Info Web Industrie, "<http://www.infowebindustrie.com/produit-7257/Sensofar-Tech-S-L-/PLu-2300.html>," 03.02.2014.





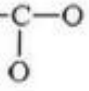
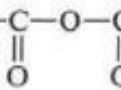

- [39] C. Fadley, "X-ray photoelectron spectroscopy: from origins to future directions," *Elsevier*, 2009.
- [40] F. J. Owens and C. P. Poole Jr, *The physics and chemistry of nanosolids*. Hoboken, New Jersey: Jhon Wiley & Sons, Inc., 2008.
- [41] Laboratoire Léon Brillouin, "[http://www-llb.cea.fr/Phocea/Vie\\_des\\_labos/Ast/ast\\_sstechnique.php?id\\_ast=229](http://www-llb.cea.fr/Phocea/Vie_des_labos/Ast/ast_sstechnique.php?id_ast=229)," 09.12.2013.
- [42] K. Siegbahn, "ELECTRON SPECTROSCOPY AND MOLECULAR STRUCTURE," *Pure & Appl. Chem.*, vol. 48, pp. 77-97, 1976.
- [43] HitachiHitec, "<http://www.hitachi-hitec.com/global/em/fe/su6600.html>," 29.05.2013.
- [44] ExpertsMind, "<http://www.expertsmind.com/topic/looking-at-microbes/transmission-and-scanning-electron-microscopy-92282.aspx>," 10.12.2013.
- [45] D. R. Moore, "An introduction to the special issue on peel testing," *International Journal of Adhesion and Adhesives*, vol. 28, no. 4-5, pp. 153-157, 2008.
- [46] D. R. Moore and J. G. Williams, "A protocol for determination of the adhesive fracture toughness of flexible laminates by peel testing: fixed arm and T-peel methods," 2010.
- [47] V. M. Karbhari and M. Engineer, "Investigation of bond between concrete and composites: Use of a peel test," *Journal of Reinforced Plastics and Composites*, vol. 15, no. 2, pp. 208-227, 1996.
- [48] V. M. Karbhari, M. Engineer, and D. A. Eckel, "On the durability of composite rehabilitation schemes for concrete: Use of a peel test," *Journal of Materials Science*, vol. 32, no. 1, pp. 147-156, 1997.
- [49] N. Tuan-Anh, F. Mannle, and O. W. Gregersen, "Polyethylene/octa-(ethyl octadeca-10,13 dienoamide) silsesquioxane blends and the adhesion strength to paperboard," *International Journal of Adhesion and Adhesives*, vol. 38, pp. 117-124, 2012.
- [50] Comfil, "<http://www.comfil.biz/>," 16.10.2013.
- [51] SigmaAldrich, "<http://www.sigmaaldrich.com/catalog/product/aldrich/440167?lang=en&region=NO>," 14.11.2013.
- [52] Pubchem, "<http://pubchem.ncbi.nlm.nih.gov/summary/summary.cgi?cid=17317#itabs-2d>," 14.11.2013.
- [53] "<http://folk.uio.no/oddsg/metodebok/Oppskrifter.html>," 06.02.2014.

- [54] A. J. Harris, B. Vaughan, J. A. Yeomans, P. A. Smith, and S. T. Burnage, "Surface preparation of alumina for improved adhesive bond strength in armour applications,".
- [55] C. D. Bain and G. M. Whitesides, "Depth Sensitivity of Wetting: Monolayers of  $\omega$ -Mercapto Ethers on Gold," *Journal of the American Chemical Society*, 1988.



# Appendix A XPS tables

Table A-1: Chemical shift (eV) for oxygen functions relative to saturated hydrocarbon.

Functional group	Chemical shift			Number of examples
	Min.	Max.	Mean	
C—O—C	1.13	1.75	1.45	18
C—OH	1.47	1.73	1.55	5
*C—O—C <sup>a</sup> 	1.12	1.98	1.64	21
	—	—	2.02	1
C=O <sup>b</sup>	2.81	2.97	2.90	3
O—C—O	2.83	3.06	2.93	5
C—O—*C <sup>c</sup> 	3.64	4.23	3.99	21
HO—C— 	4.18	4.33	4.26	2
O—C—O 	4.30	4.34	4.32	2
—C—O—C— 	4.36	4.46	4.41	3
—O—C—O— 	5.35	5.44	5.40	2

<sup>a</sup> Neglecting aromatic carboxylic esters, mean of 18 is 1.72, min. 1.48.

<sup>b</sup> PEEK significantly lower: shift = 2.10 (BE referenced to aromatic CH C 1s = 284.70 eV).

<sup>c</sup> Neglecting aromatic carboxylic esters, mean of 18 is 4.05, min. 3.84.

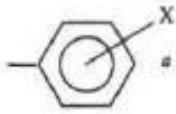
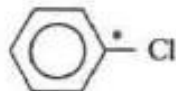
Table A-2: Chemical shift (eV) for nitrogen functions relative to saturated hydrocarbon.

Functional group	Chemical shift			Number of examples
	Min.	Max.	Mean	
$C-NO_2^a$	—	—	0.76	1
$C-N<$	0.56	1.41	0.94	9
$C-N^+<$	0.99	1.22	1.11	2
$*C-C\equiv N$	1.35	1.46	1.41	2
$-C\equiv N$	1.73	1.74	1.74	2
$C-ONO_2$	—	—	2.62	1
$N-C-O$	—	—	2.78	1
$N-C=O$	2.97	3.59	3.11	6
$\begin{array}{c} C-N-C \\    \quad    \\ O \quad O \end{array}$	3.49	3.61	3.55	2
$\begin{array}{c} N-C-N \\    \\ O \end{array}$	—	—	3.84	1
$\begin{array}{c} N-C-O \\    \\ O \end{array}$	—	—	4.60	1

<sup>a</sup> C in phenyl ring.



Table A-3: Chemical shift (eV) for halogen functions and various other functions relative to saturated hydrocarbon.

Functional group	Chemical shift			Number of examples
	Min.	Max.	Mean	
C=C	-0.24	-0.31	-0.27	4
	-0.20	-0.56	-0.34	20
C-Si	-0.61	-0.78	-0.67	3
C-S	0.21 <sup>b</sup>	0.52	0.37	2
C-SO <sub>2</sub>	0.31 <sup>b</sup>	0.64	0.38	2
C-SO <sub>3</sub> <sup>-b</sup>	—	—	0.16	1
C-Br <sup>b</sup>	—	—	0.74	1
	0.99	1.07	1.02	3
C-Cl	2.00	2.03	2.02	2
-CCl <sub>2</sub>	—	—	3.56	1
C-F	—	—	2.91	1
-CF <sub>2</sub>	—	—	5.90	1
-CF <sub>3</sub>	7.65	7.72	7.69	2

<sup>a</sup> Average of C atoms not directly bonded to substituent X.

<sup>b</sup> In this example bonded C atom is in phenyl ring.

Table A-4: Secondary chemical shift (eV) relative to saturated hydrocarbon.

Functional group	Chemical shift	Number of examples
$\text{O}-\text{C}-\overset{*}{\text{C}}$	$\sim 0.2$	6
$\text{F}-\text{C}-\overset{*}{\text{C}}$	$\sim 0.4$	11
$\text{Cl}-\text{C}-\overset{*}{\text{C}}$	$\sim 0.5$	9
$\begin{array}{c} \text{---C---}\overset{*}{\text{C}} \\    \\ \text{O} \end{array}$	$\sim 0.4$	4
$\begin{array}{c} \text{O---C---}\overset{*}{\text{C}} \\    \\ \text{O} \end{array}$	$\sim 0.4$	7
$\begin{array}{c} \text{O---C---}\overset{*}{\text{C}}-\text{CH}_3 \\    \\ \text{O} \end{array}$	$\sim 0.7$	8

# Appendix B XPS survey scans

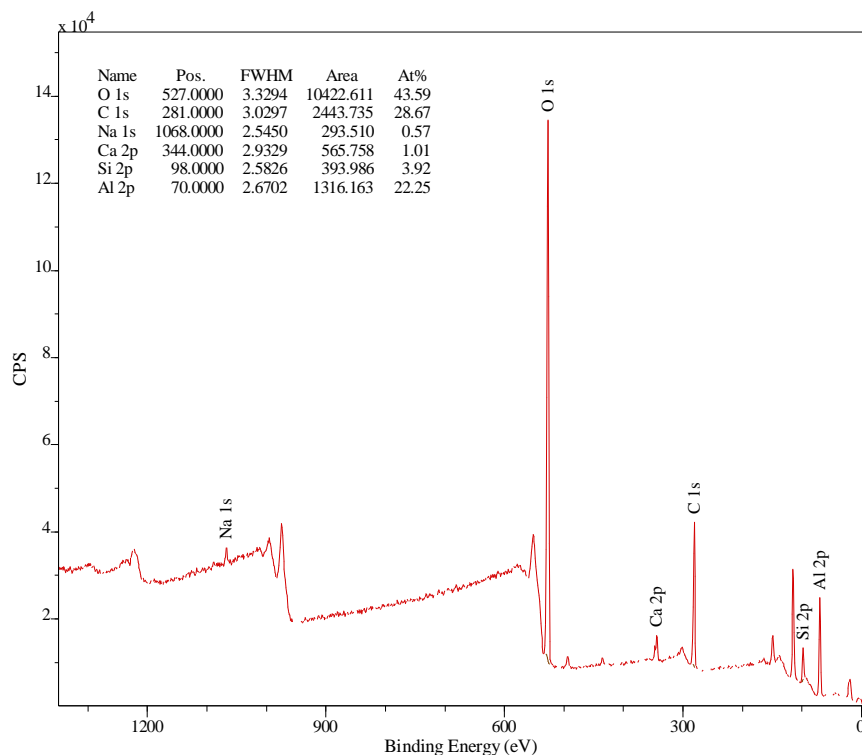


Figure B-1: Survey scan of the as-received sample.

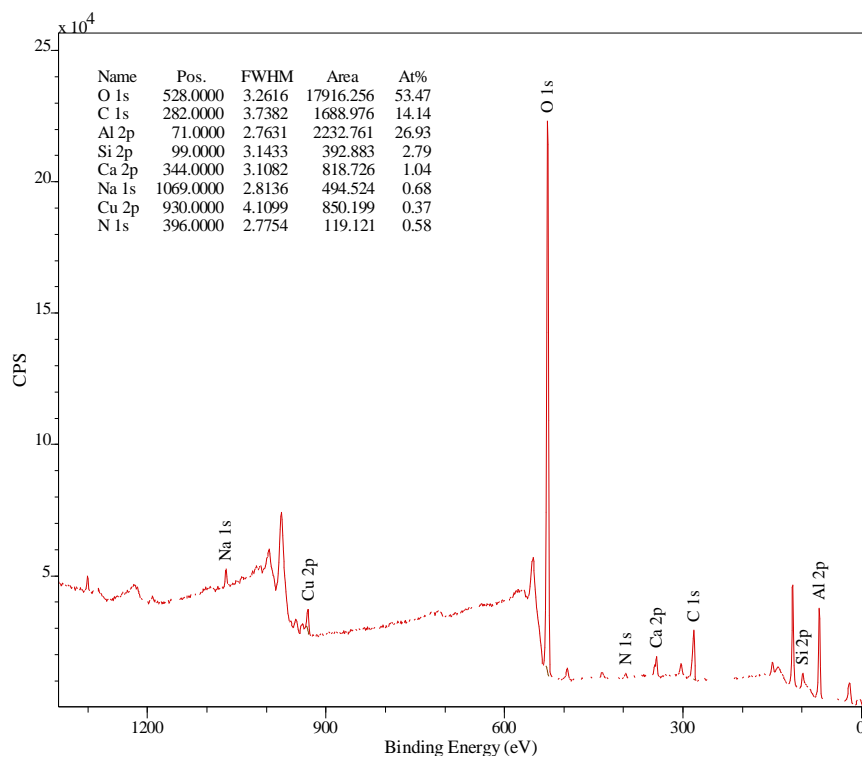


Figure B-2: Survey scan of the acetone washed sample.

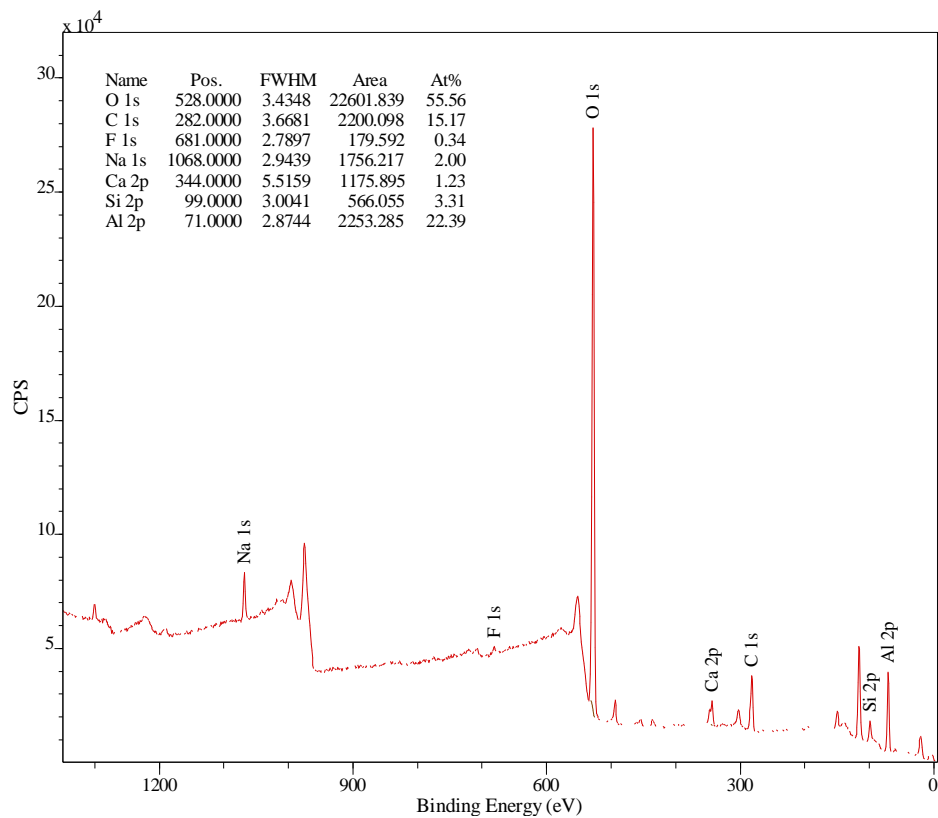


Figure B-3: Survey scan of the sandblasted sample.

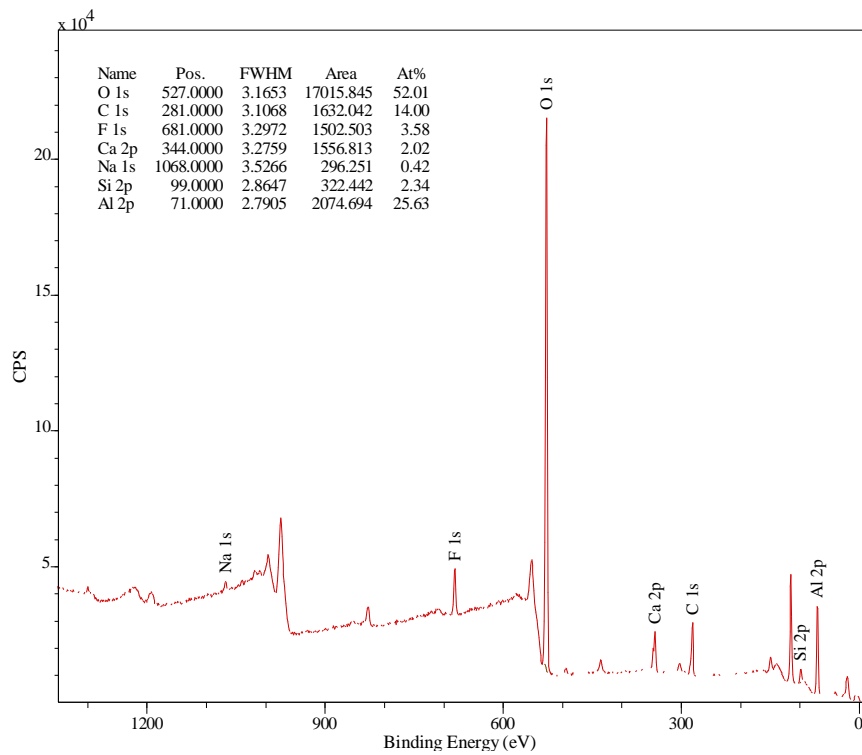


Figure B-4: Survey scan of the plasma treated sample.

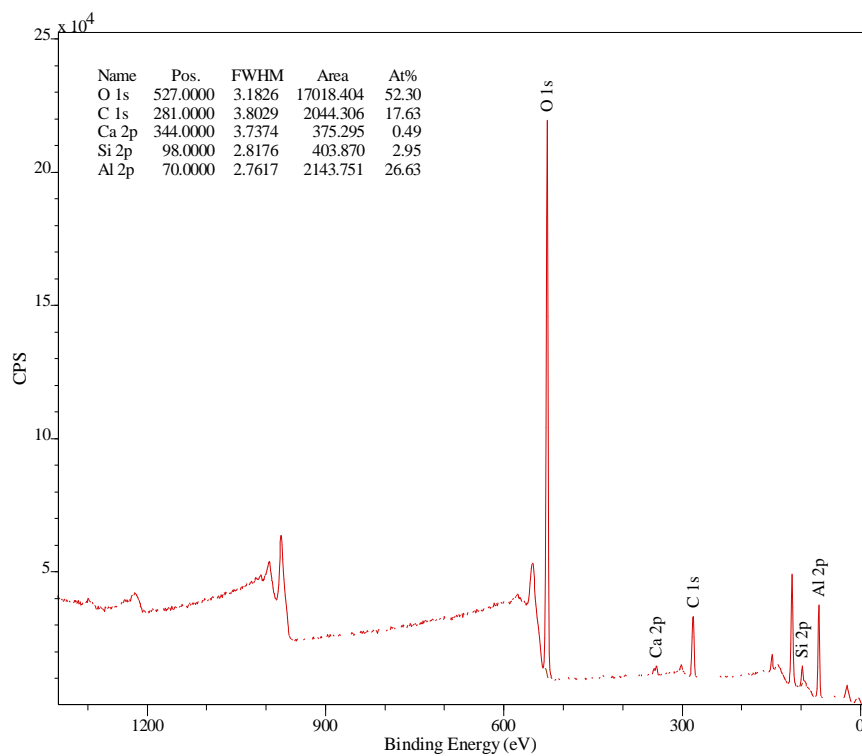


Figure B-5: Survey scan of the silane treated (1 wt%, rinsed) sample.

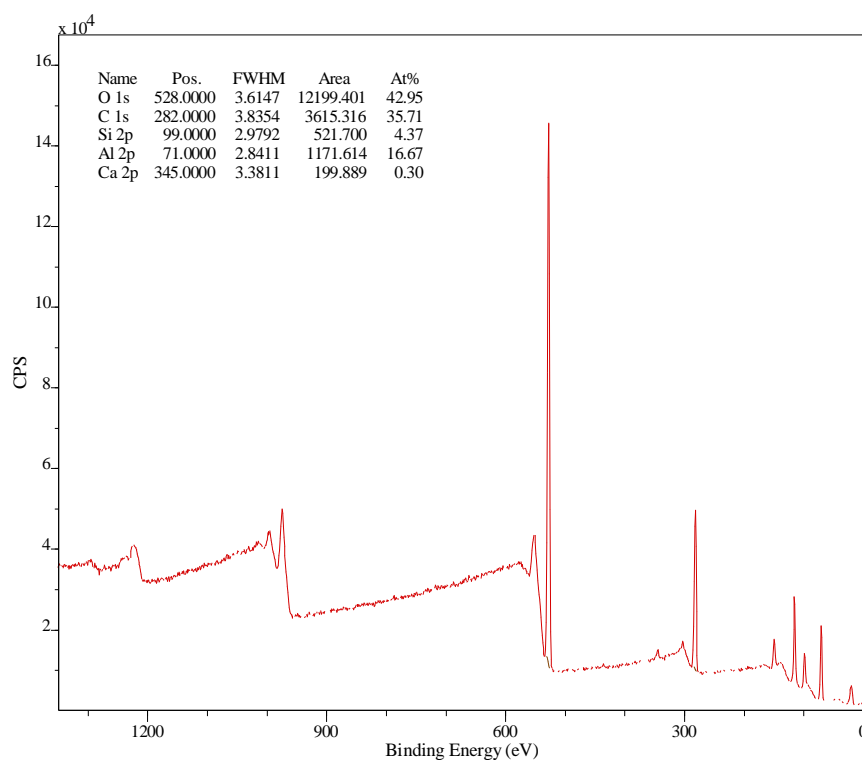


Figure B-6: Survey scan of the silane treated (1 wt%, not rinsed) sample.

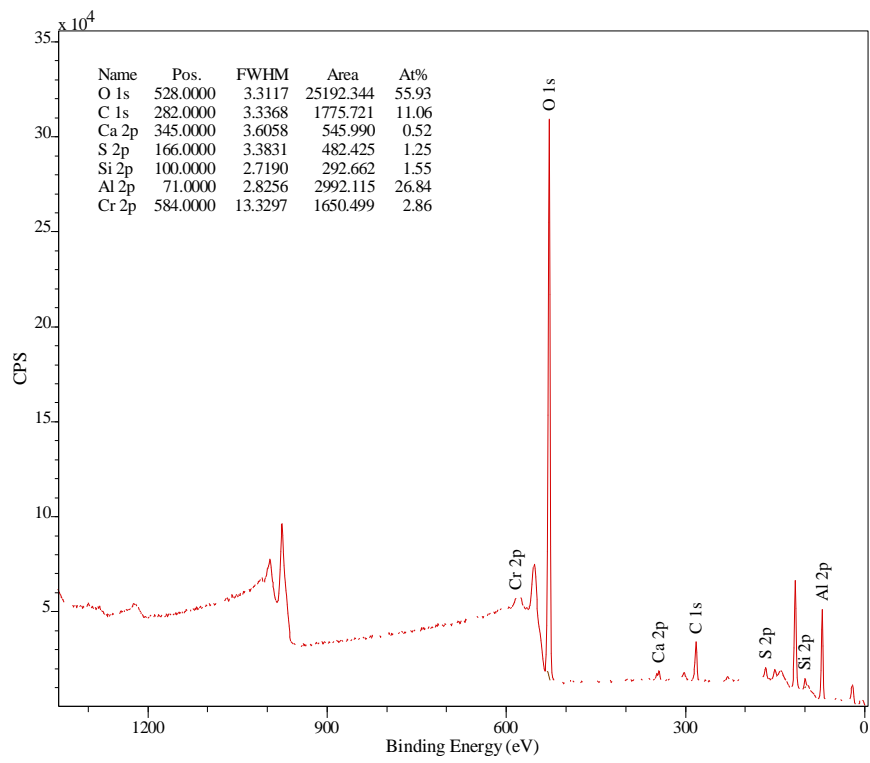


Figure B-7: Survey scan of the FPL etched sample.

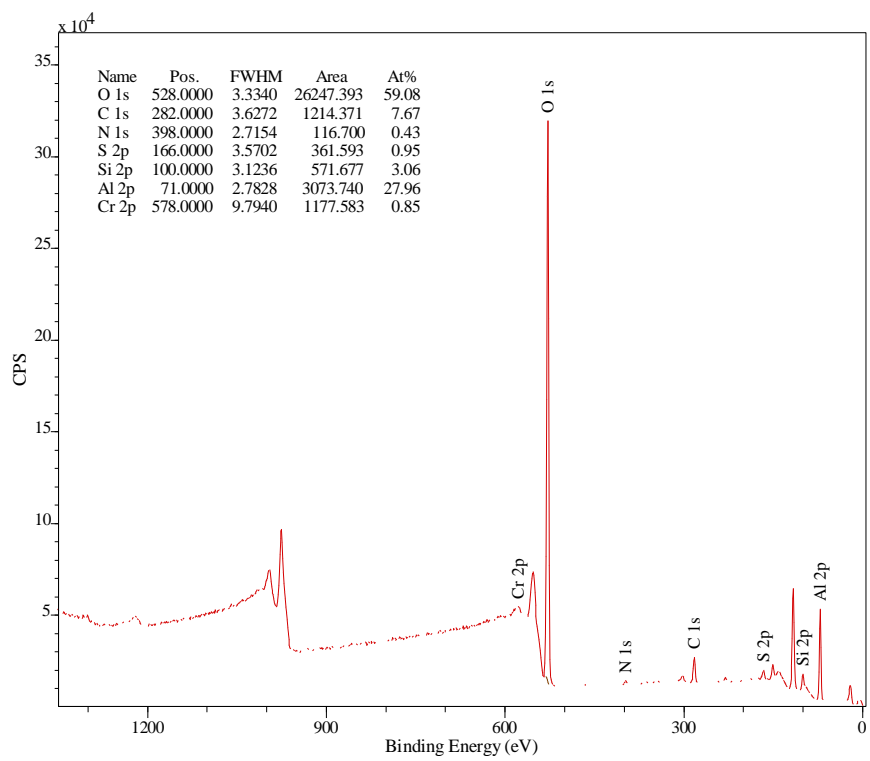


Figure B-8: Survey scan of the strong chromic sulphuric acid etched sample.

## Appendix C Profilometer images

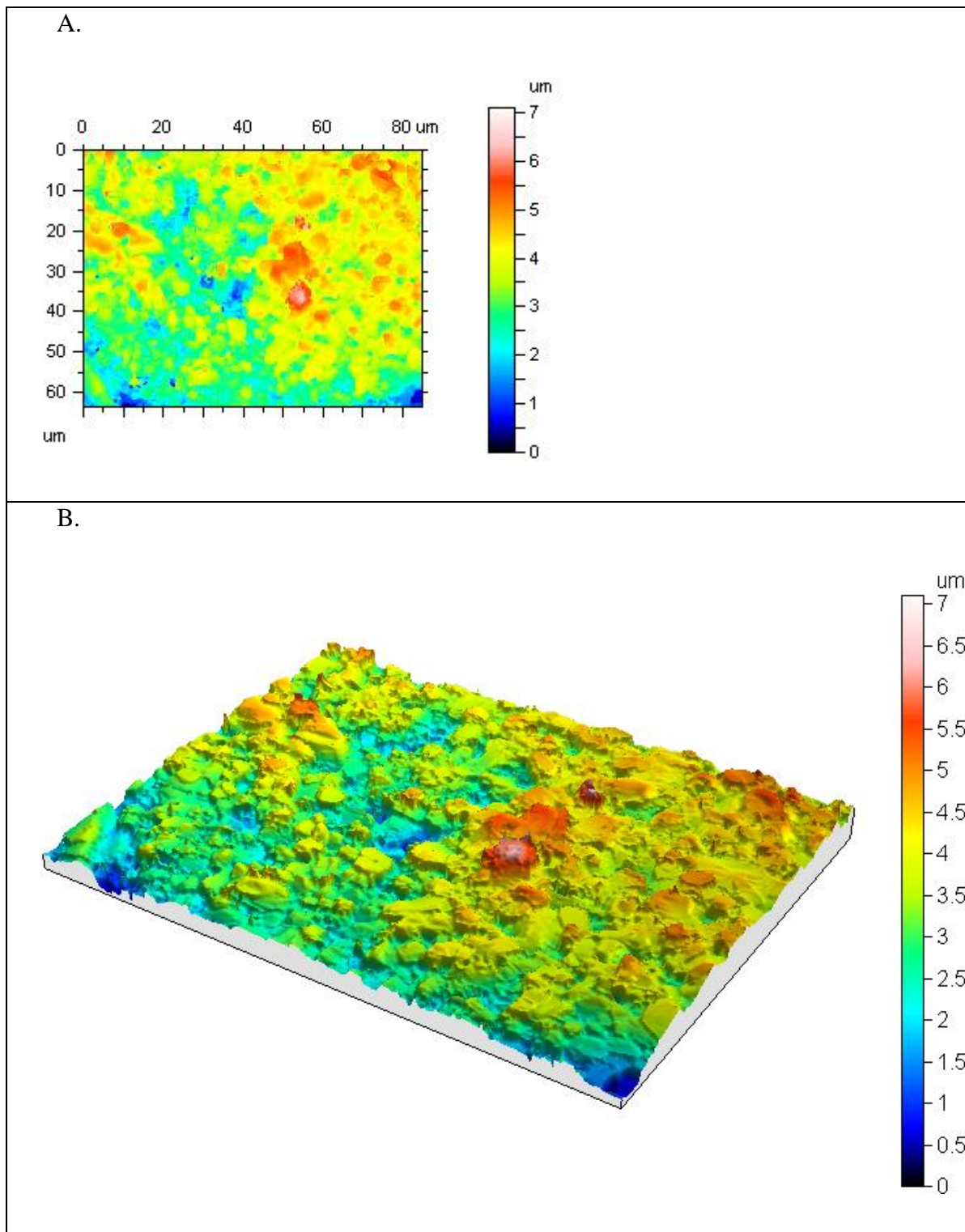


Figure C-1: Profilometer measurements for the acetone washed sample. A is a 2D height map of the surface, and B is the 3D scan of the same surface.

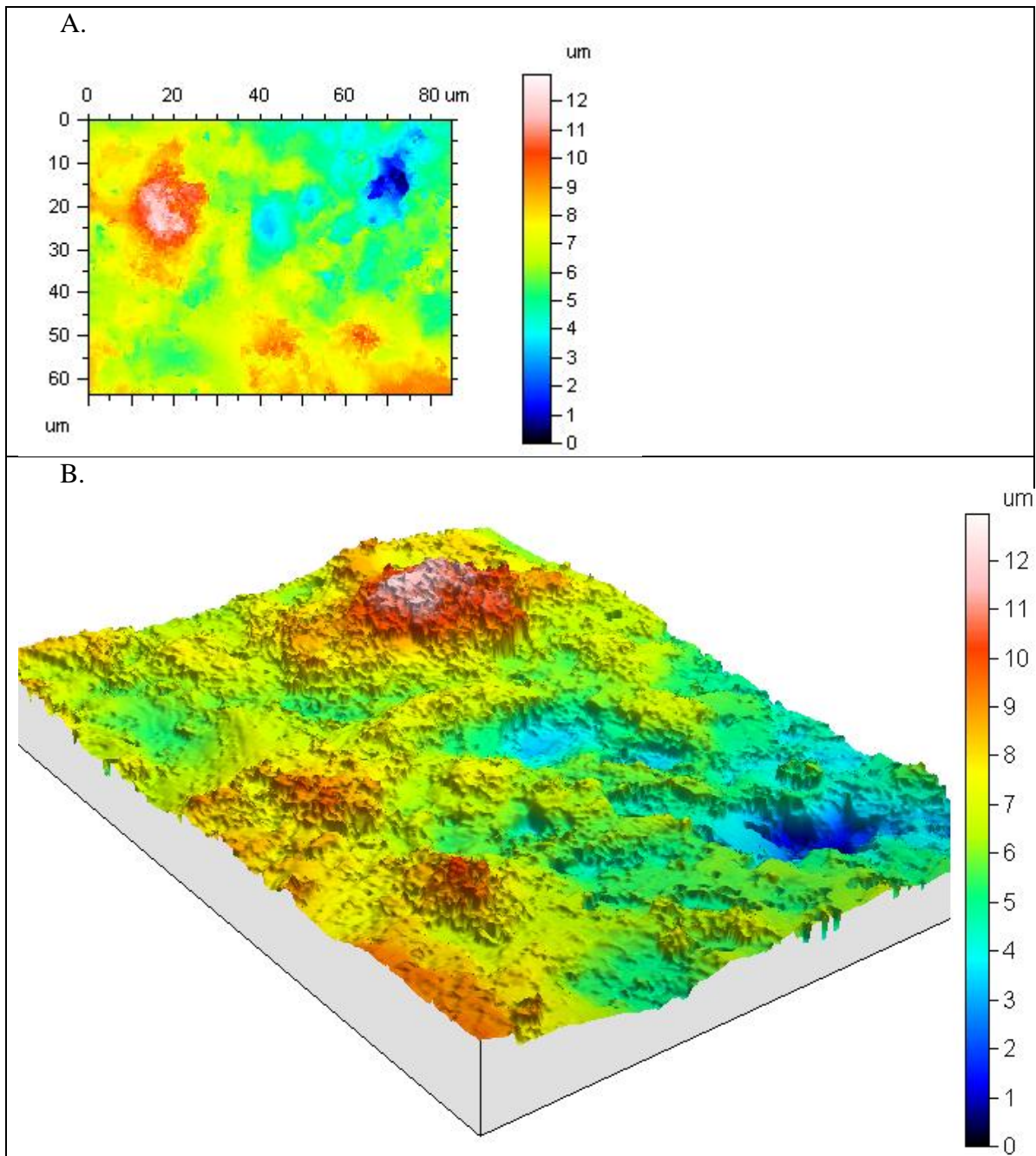
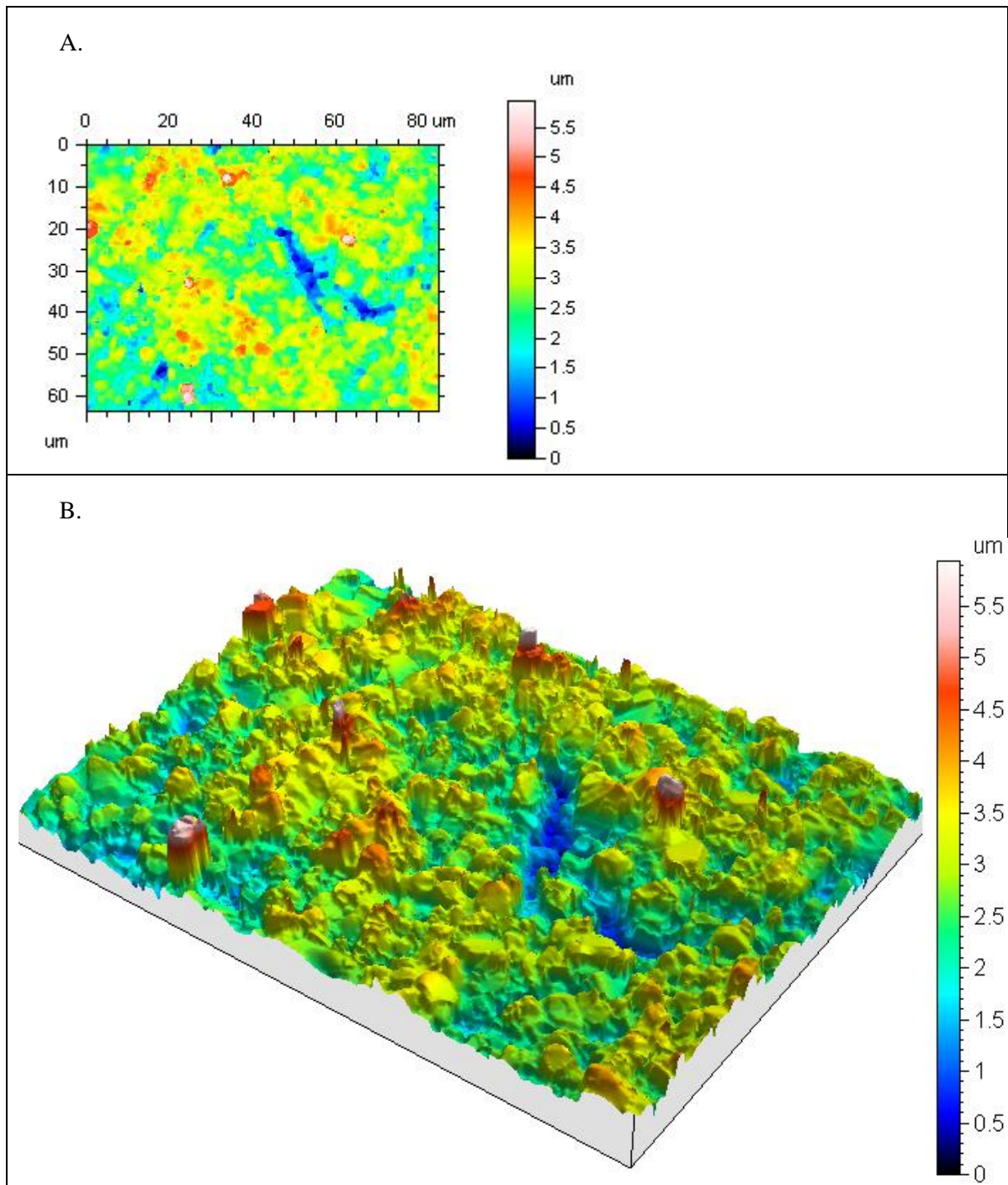


Figure C-2: Profilometer measurements for the sandblasted sample. A is a 2D height map of the surface, and B is the 3D scan of the same surface.





*Figure C-3: Profilometer measurements for the plasma treated sample. A is a 2D height map of the surface, and B is the 3D scan of the same surface.*

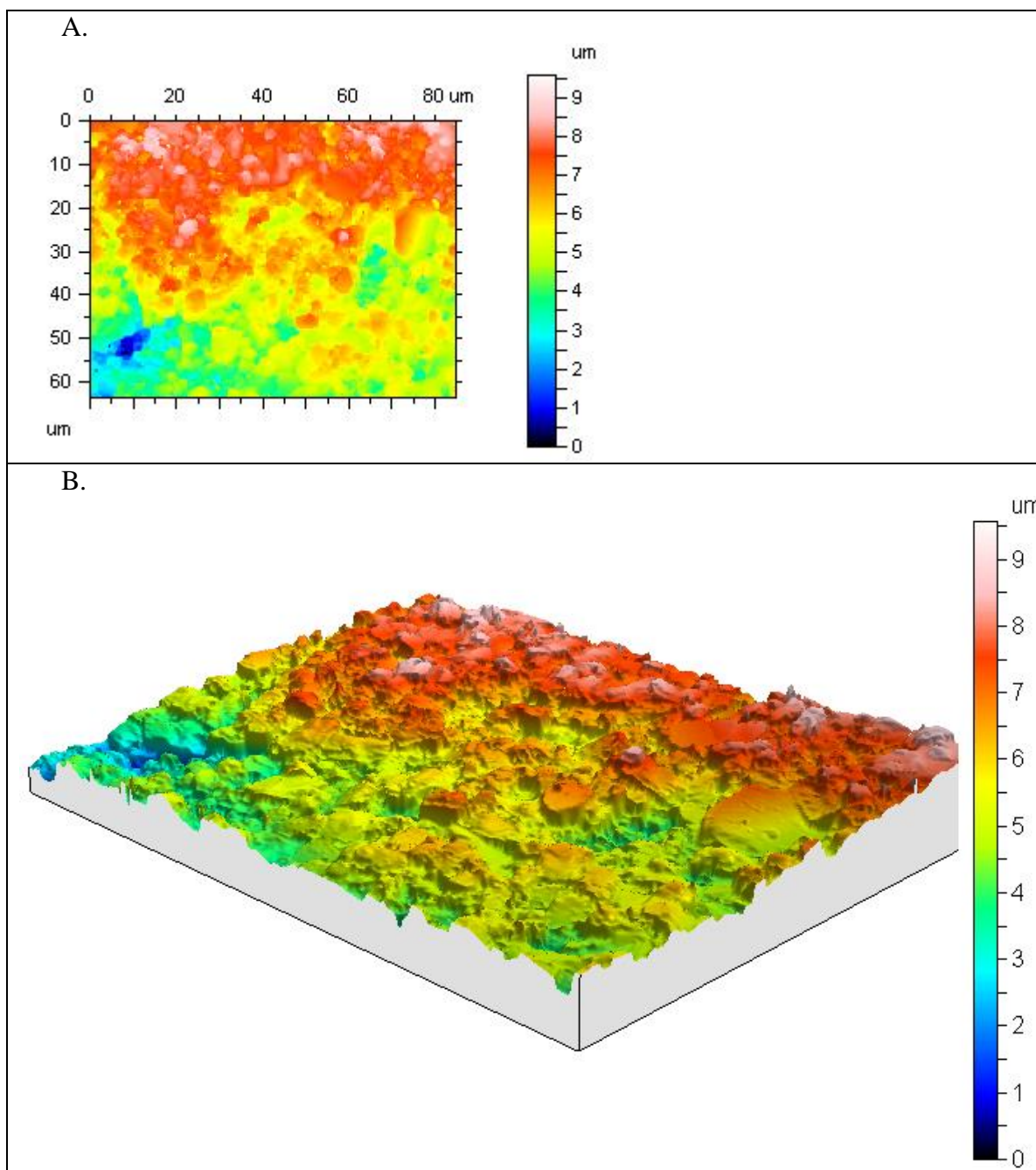


Figure C-4: Profilometer measurements for the silane treated (1 wt%, rinsed) sample. A is a 2D height map of the surface, and B is the 3D scan of the same surface.

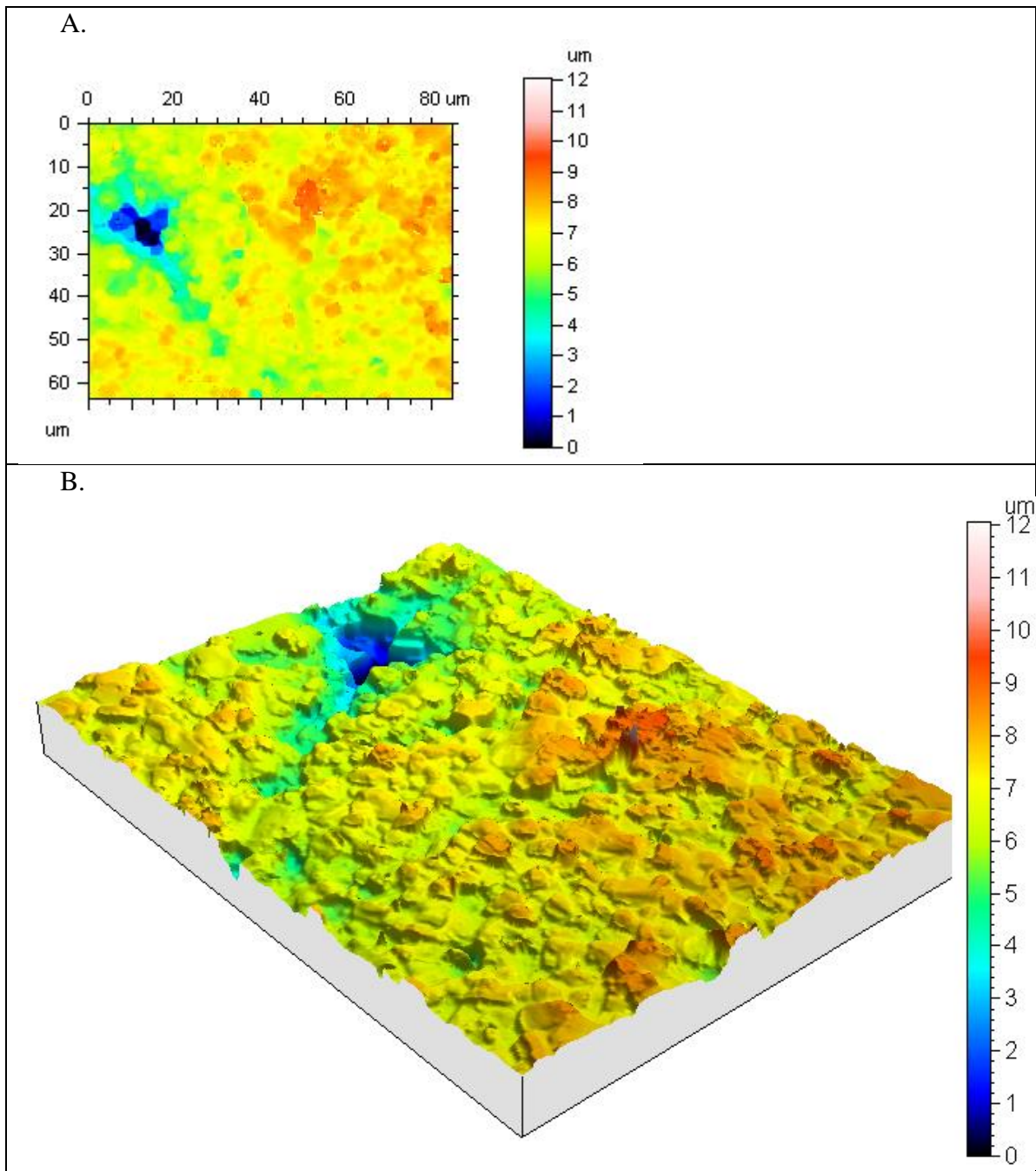
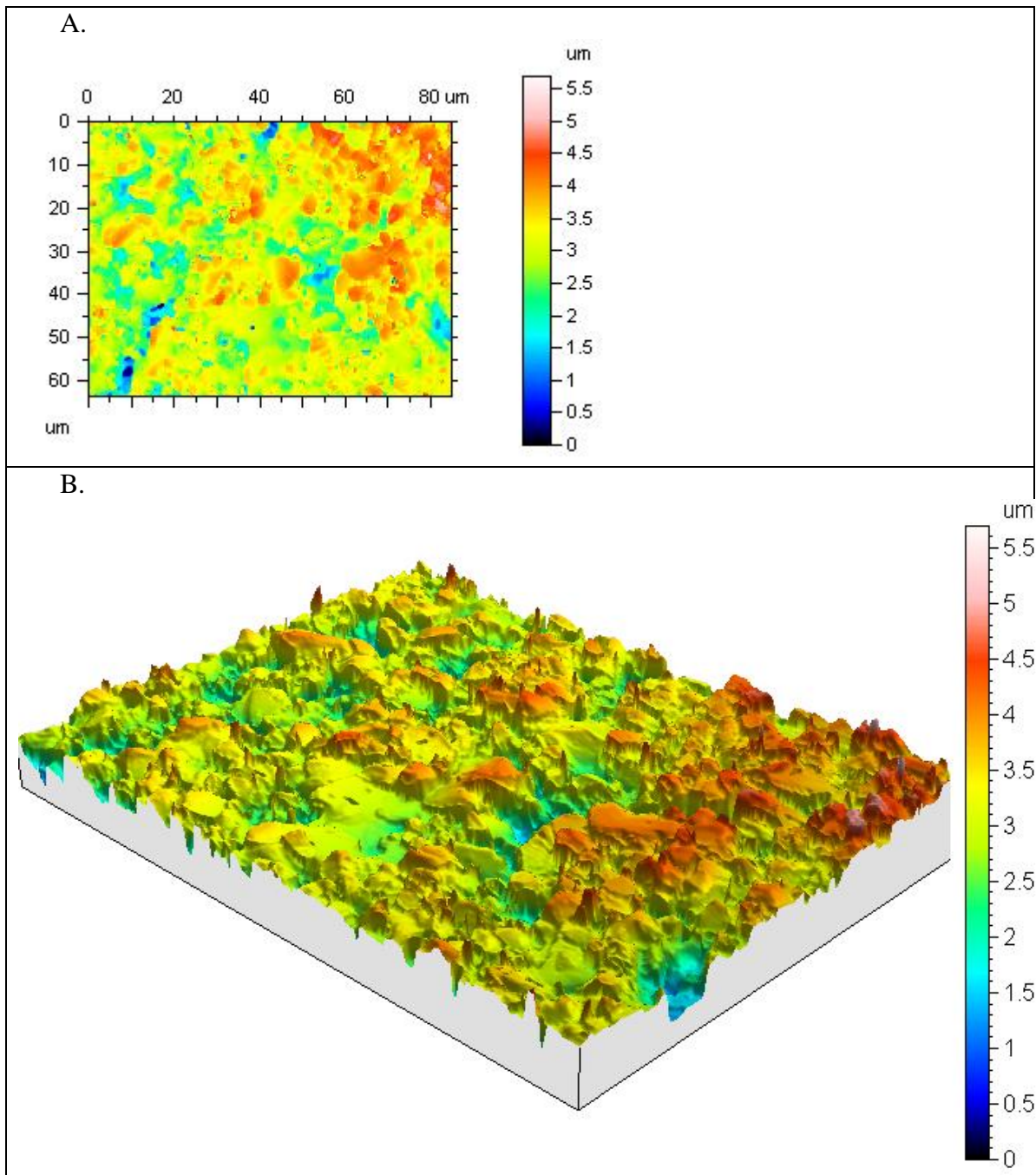


Figure C-5: Profilometer measurements for the silane treated (1 wt%, not rinsed) sample. A is a 2D height map of the surface, and B is the 3D scan of the same surface.



*Figure C-6: Profilometer measurements for the FPL etched (10 min) sample. A is a 2D height map of the surface, and B is the 3D scan of the same surface.*

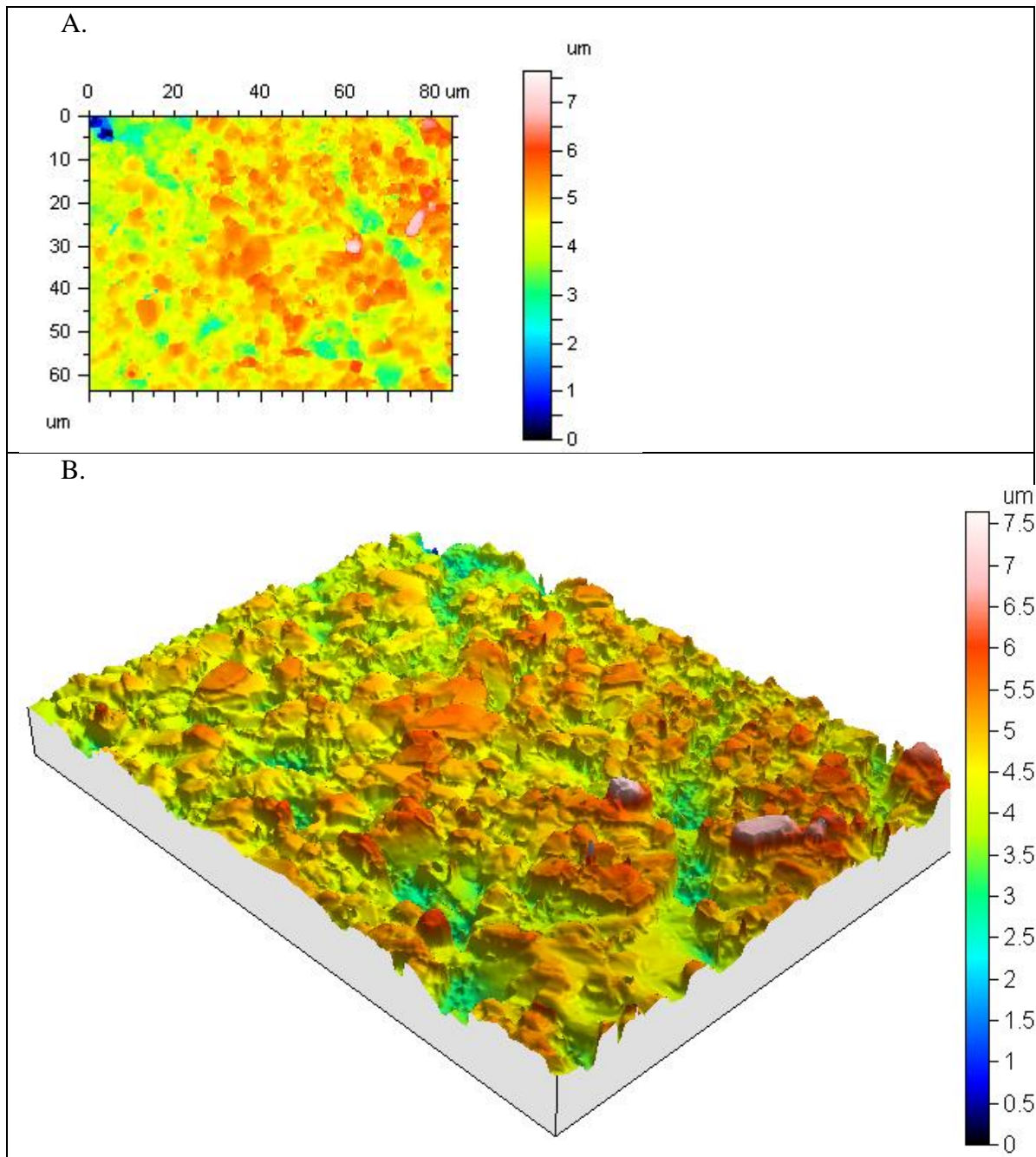
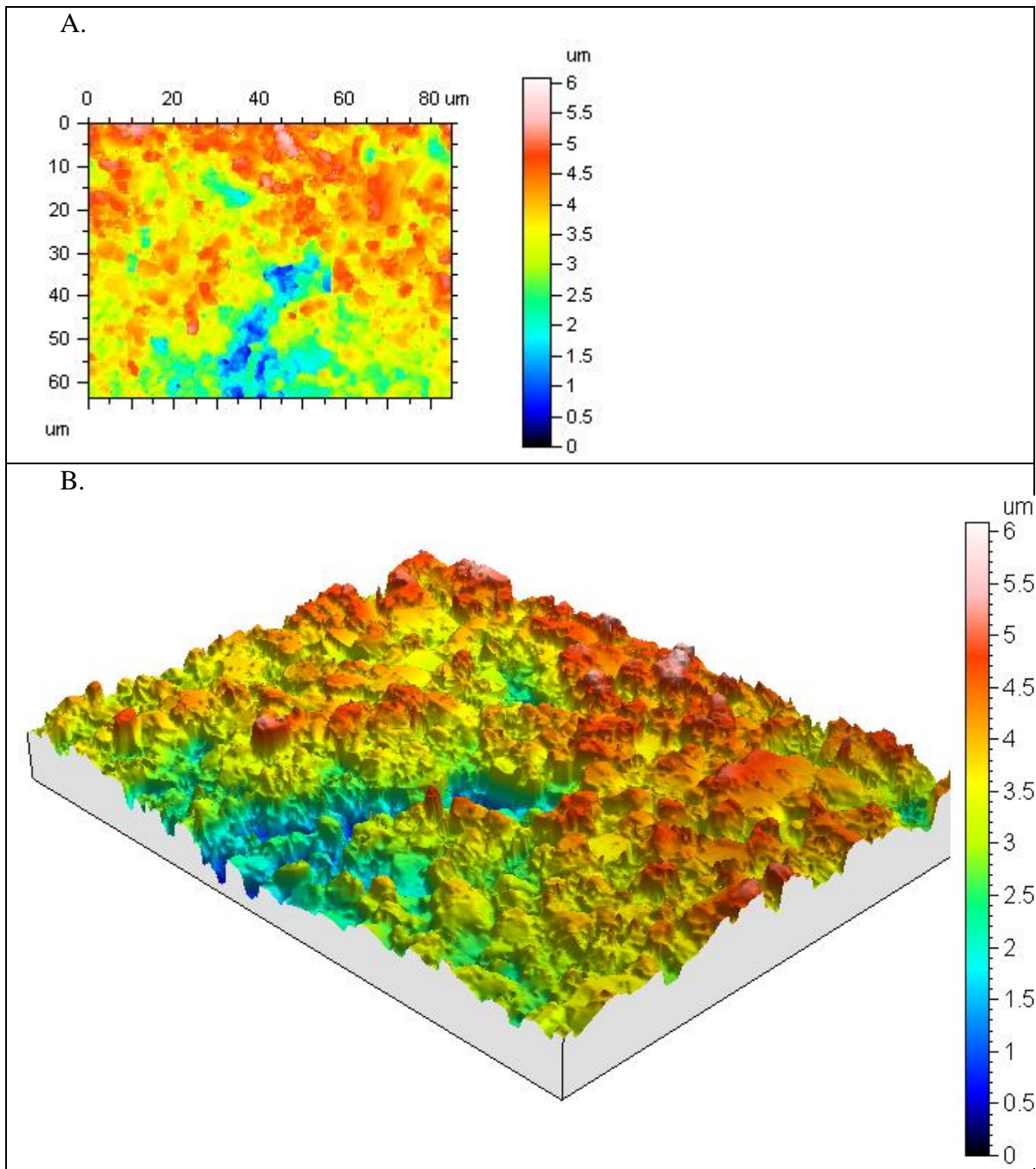
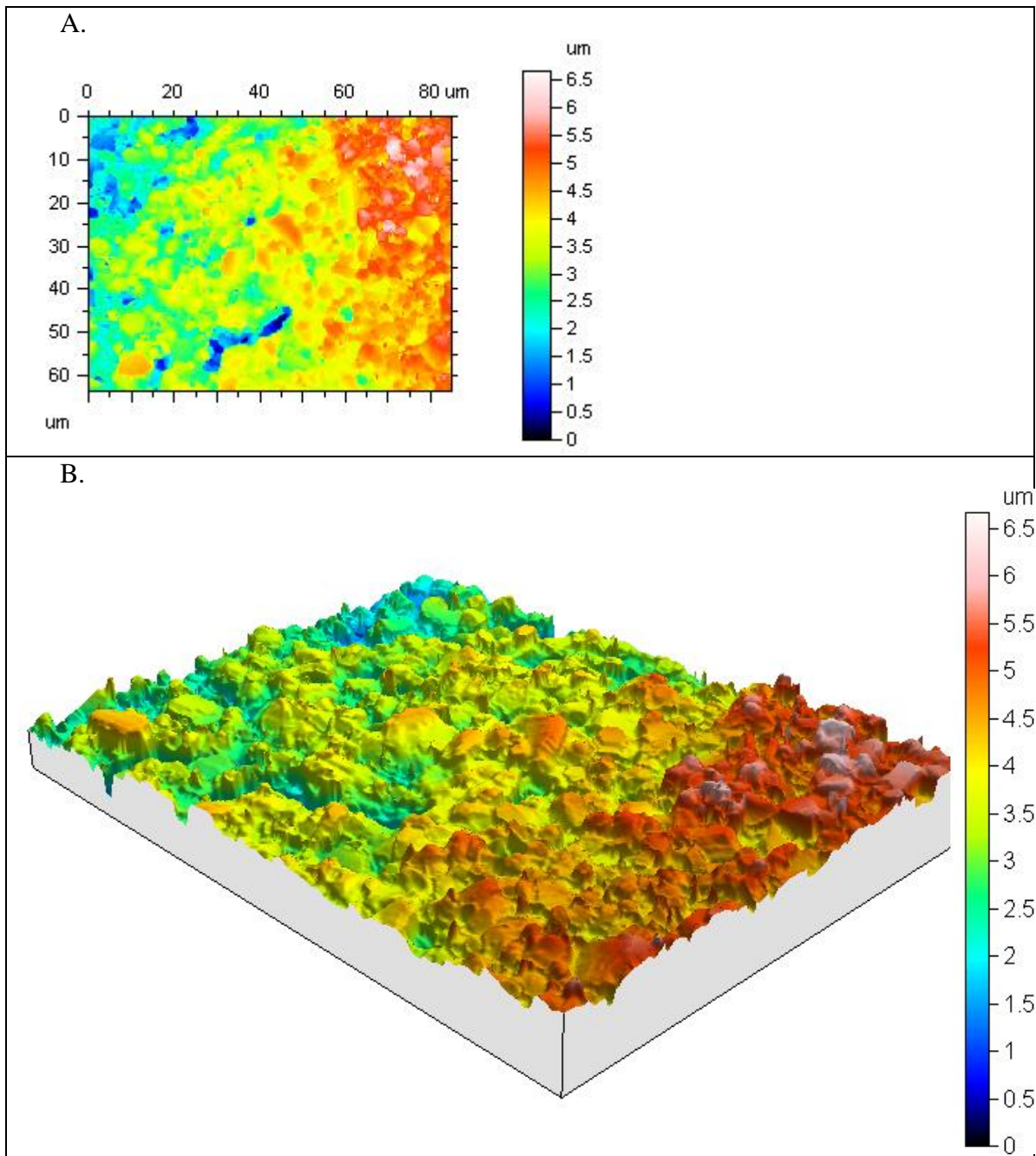


Figure C-7: Profilometer measurements for the FPL etched (60 min) sample. A is a 2D height map of the surface, and B is the 3D scan of the same surface.



*Figure C-8: Profilometer measurements for the strong chromic sulphuric acid etched (10 min) sample. A is a 2D height map of the surface, and B is the 3D scan of the same surface.*



*Figure C-9: Profilometer measurements for the strong chromic sulphuric acid etched (60 min) sample. A is a 2D height map of the surface, and B is the 3D scan of the same surface.*





# Appendix D Peel test results

## As-received

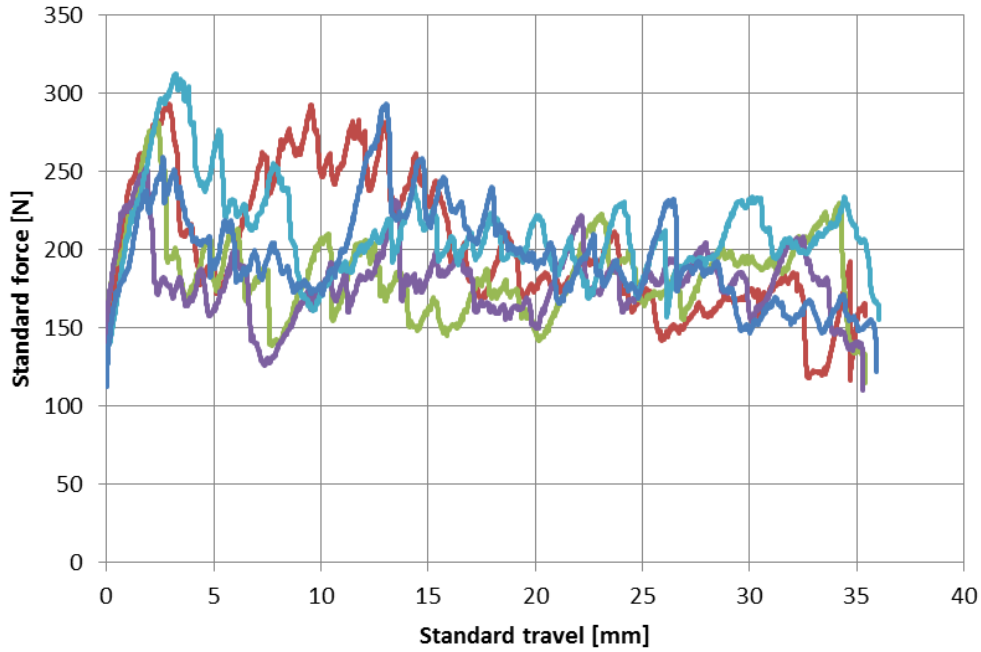


Figure D-1: Peel test results for the as-received sample.

## Acetone washed

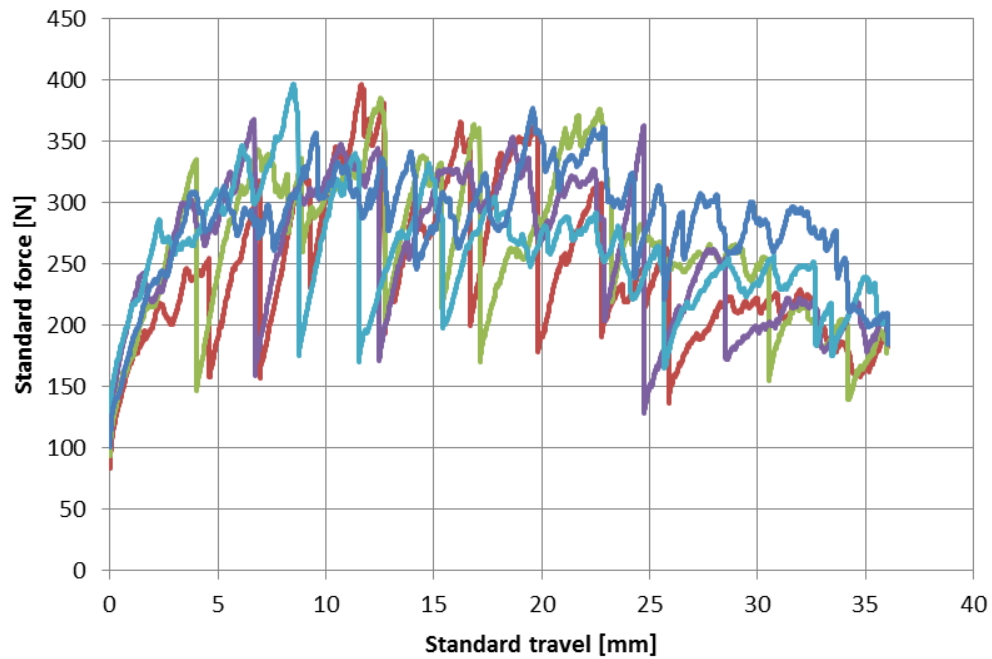


Figure D-2: Peel test results for the acetone washed sample.

### Sandblasted

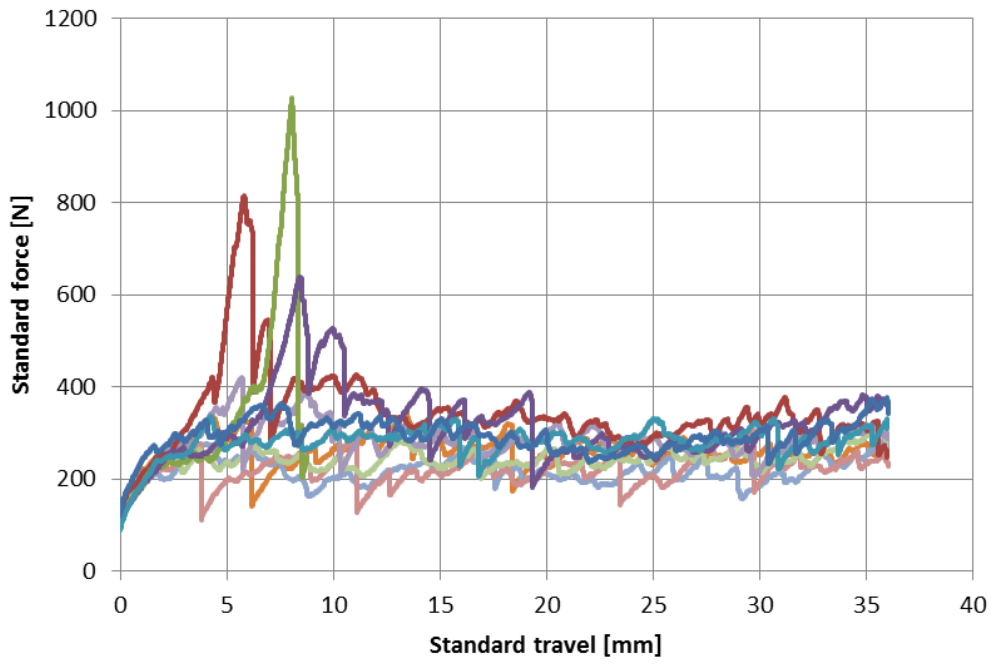


Figure D-3: Peel test results for the sandblasted sample.

### Plasma treated

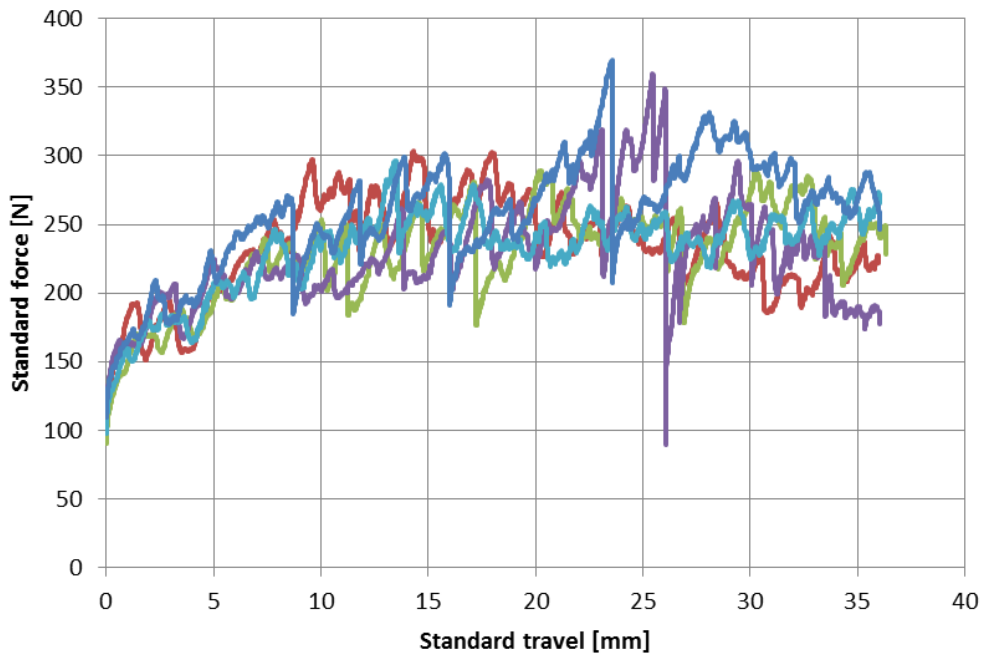


Figure D-4: Peel test results for the plasma treated sample.

### Silane treated (0.25 wt%)

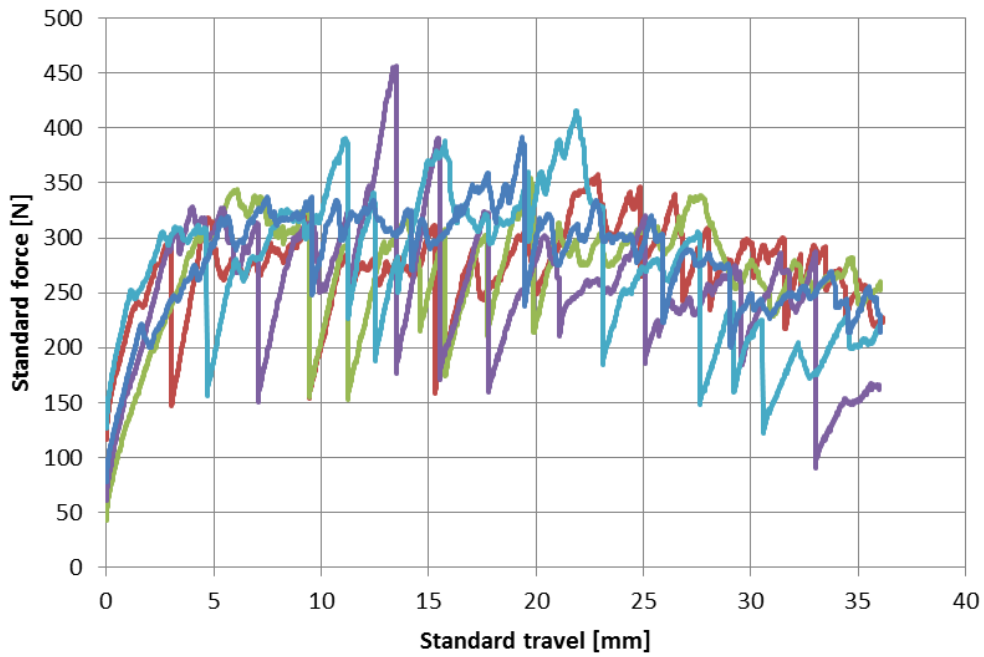


Figure D-5: Peel test results for the silane treated (0.25 wt%) sample.

### Silane treated (0.5 wt%)

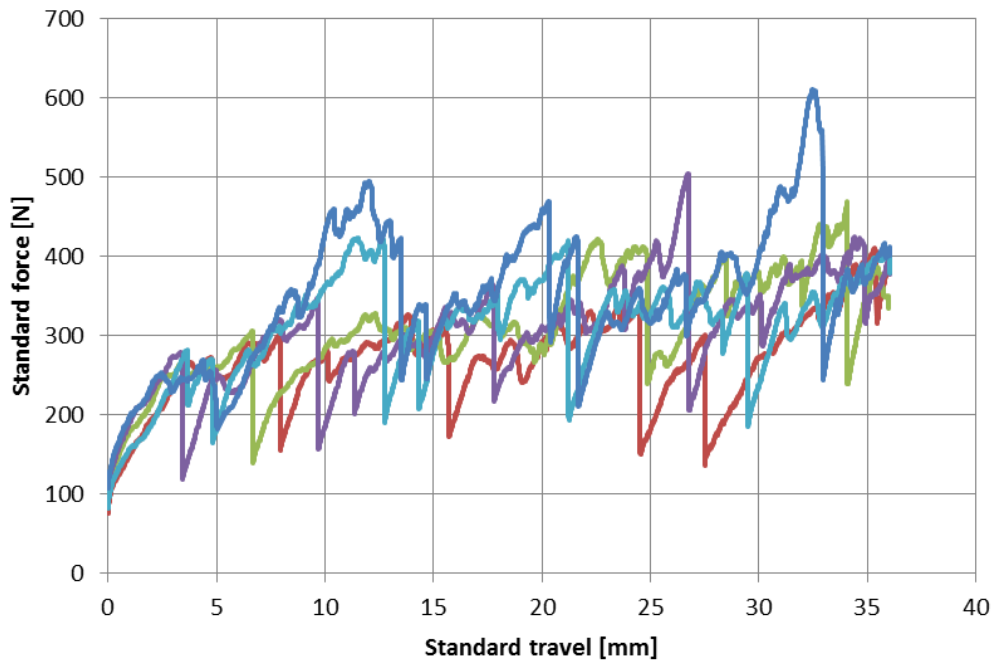


Figure D-6: Peel test results for the silane treated (0.5 wt%) sample.

### Silane treated (1 wt%, rinsed)

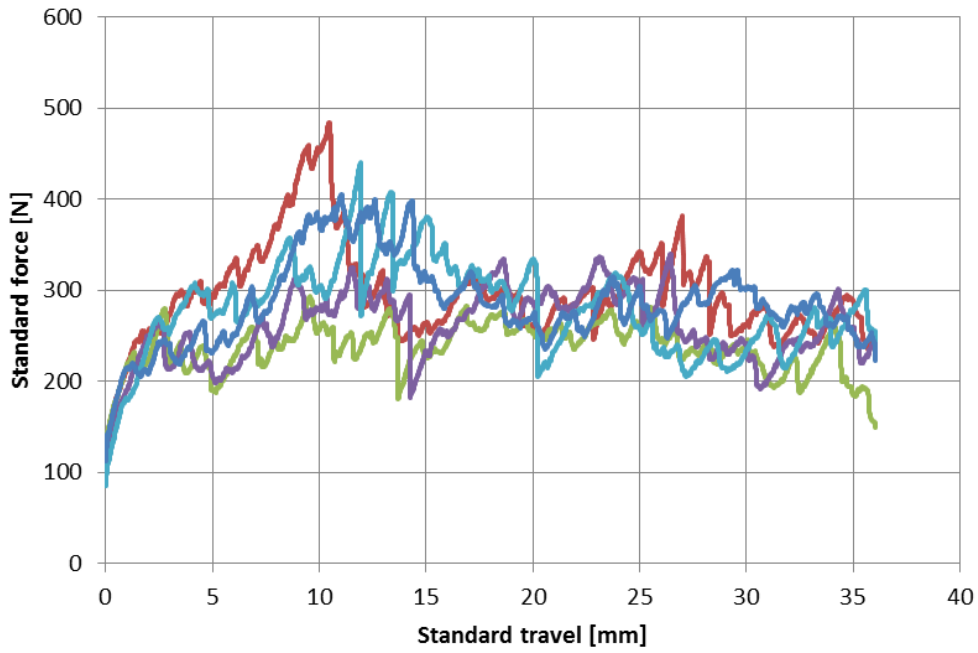


Figure D-7: Peel test results for the silane treated (1 wt%, rinsed) sample.

### Silane treated (1 wt%, not rinsed)

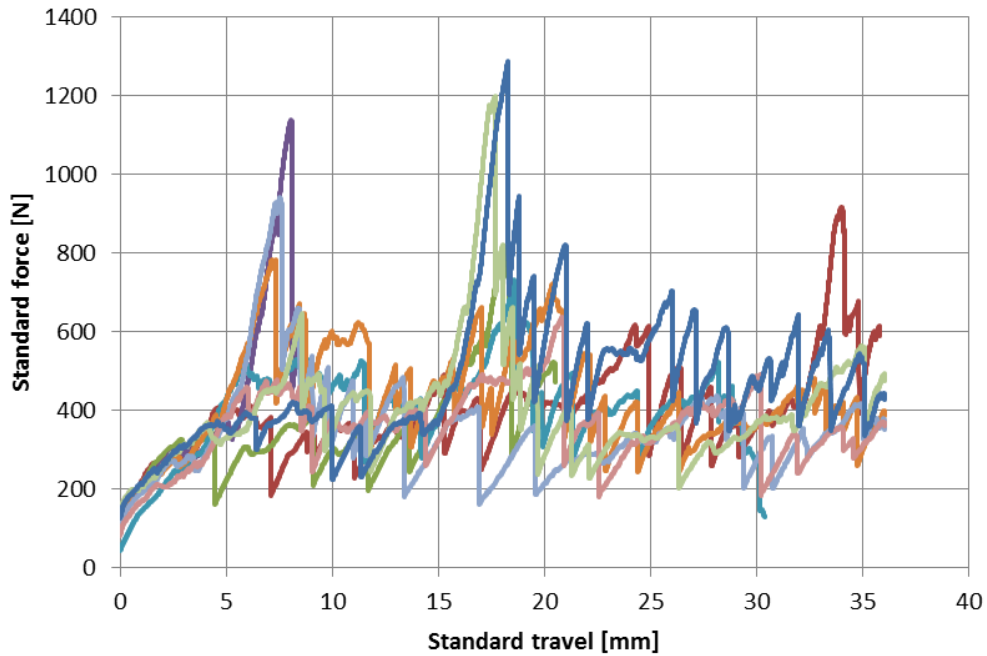


Figure D-8: Peel test results for the silane treated (1 wt%, not rinsed) sample.

### FPL etched

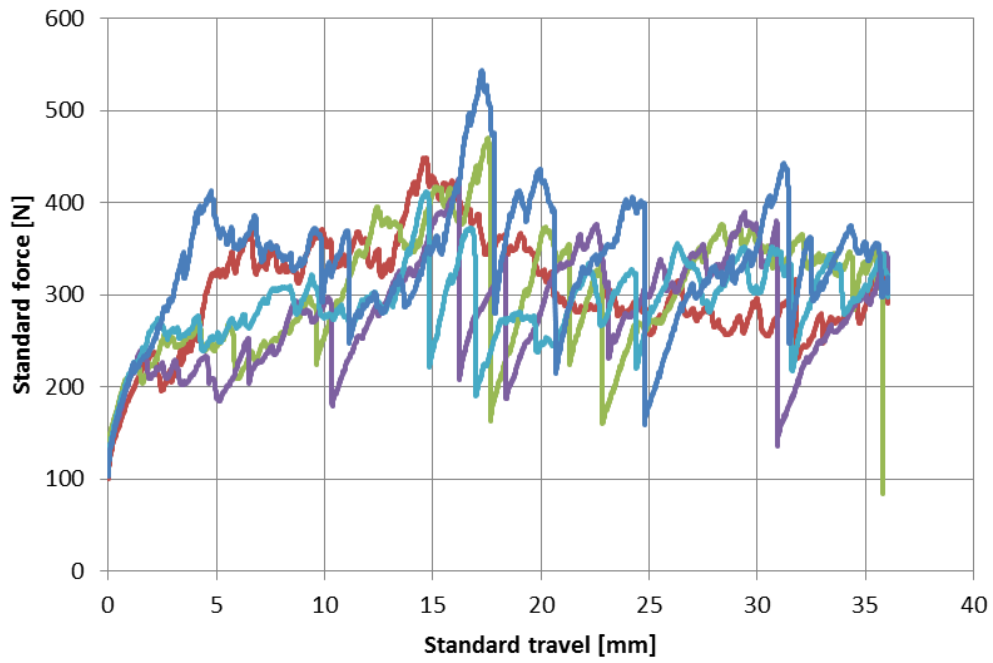


Figure D-9: Peel test results for the FPL etched sample.

### Acetone washed (0 wt% POSS)

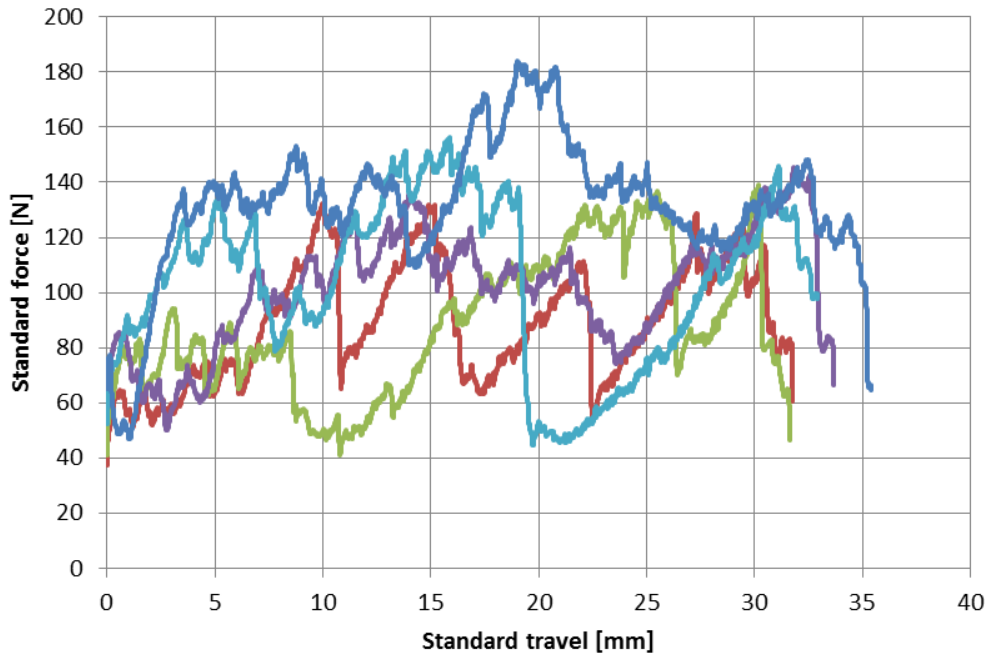


Figure D-10: Peel results from the sample with an interlayer film without POSS particles on the acetone washed surface.

### Acetone washed (1.20 wt% POSS)

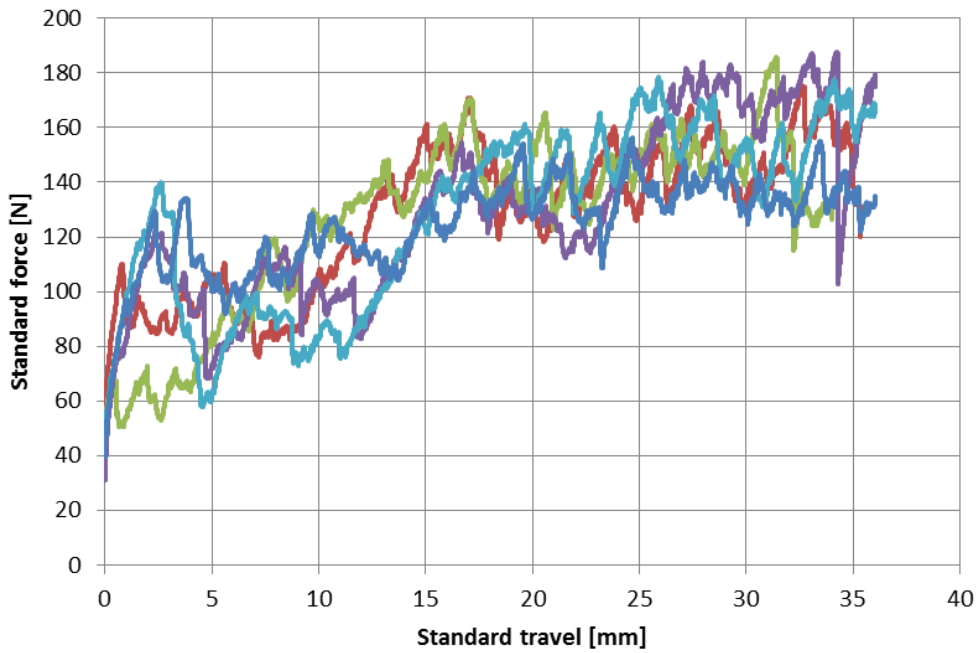


Figure D-11: Peel results from the sample with an interlayer film with 1.20 wt% POSS particles on the acetone washed surface.

### Acetone washed (2.44 wt% POSS)

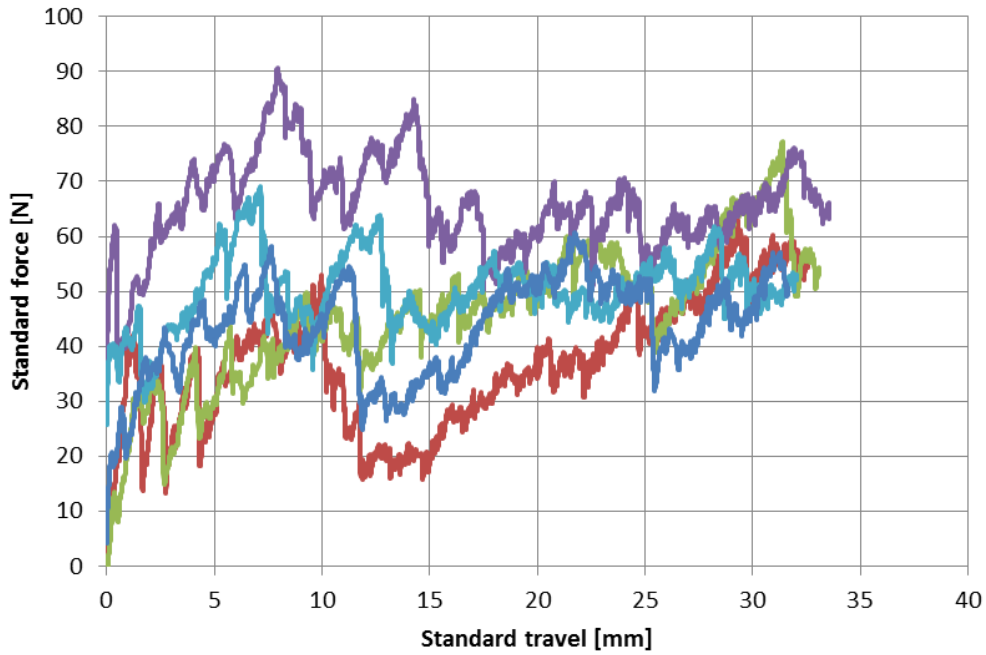


Figure D-12: Peel results from the sample with an interlayer film with 2.44 wt% POSS particles on the acetone washed surface.

### Acetone washed (5.21 wt% POSS)

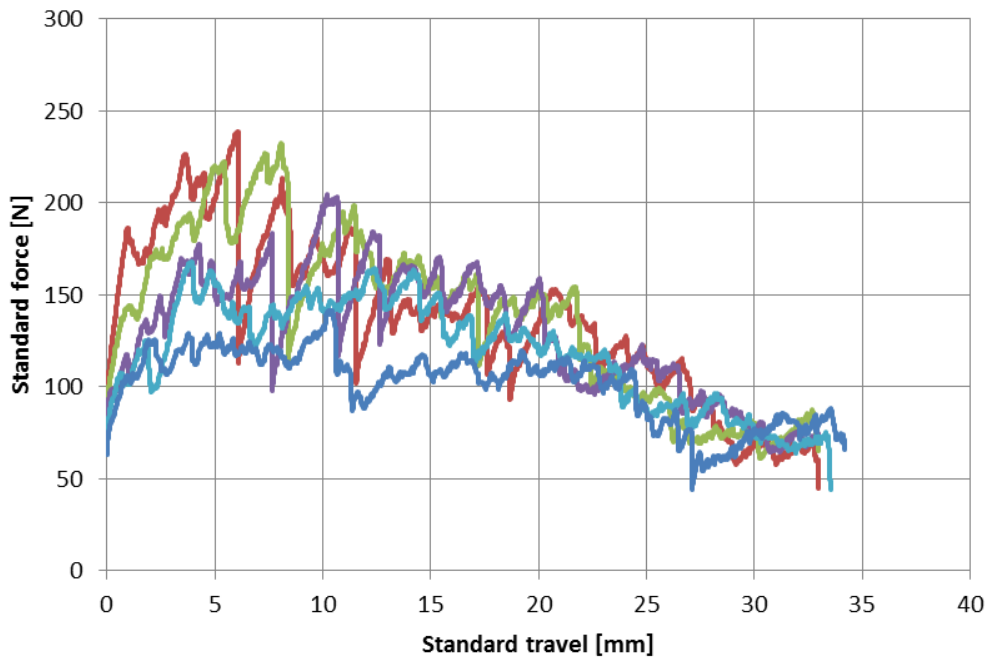


Figure D-13: Peel results from the sample with an interlayer film with 5.21 wt% POSS particles on the acetone washed surface.

### Acetone washed (11.49 wt% POSS)

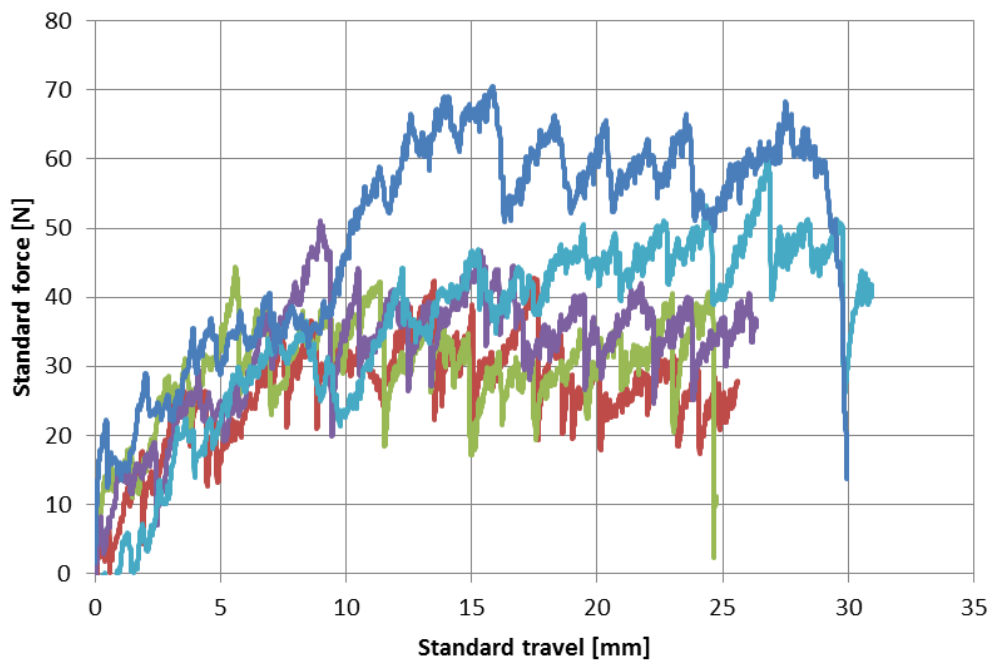


Figure D-14: Peel results from the sample with an interlayer film with 11.49 wt% POSS particles on the acetone washed surface.



### Silane treated (0 wt% POSS)

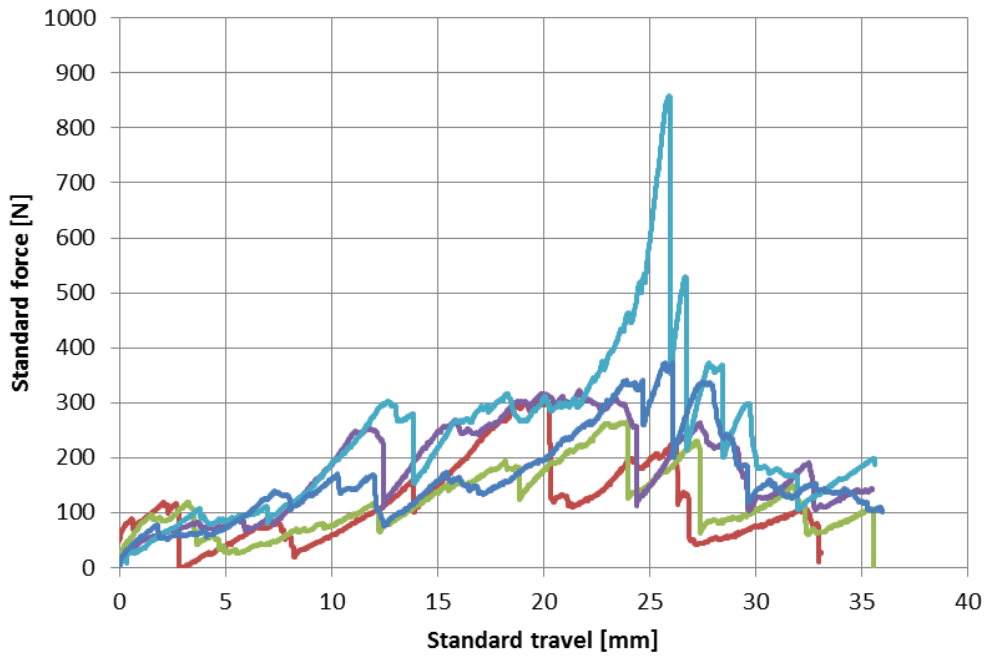


Figure D-15: Peel results from the sample with an interlayer film without POSS particles on the silane treated surface.

### Silane treated (1.20 wt% POSS)

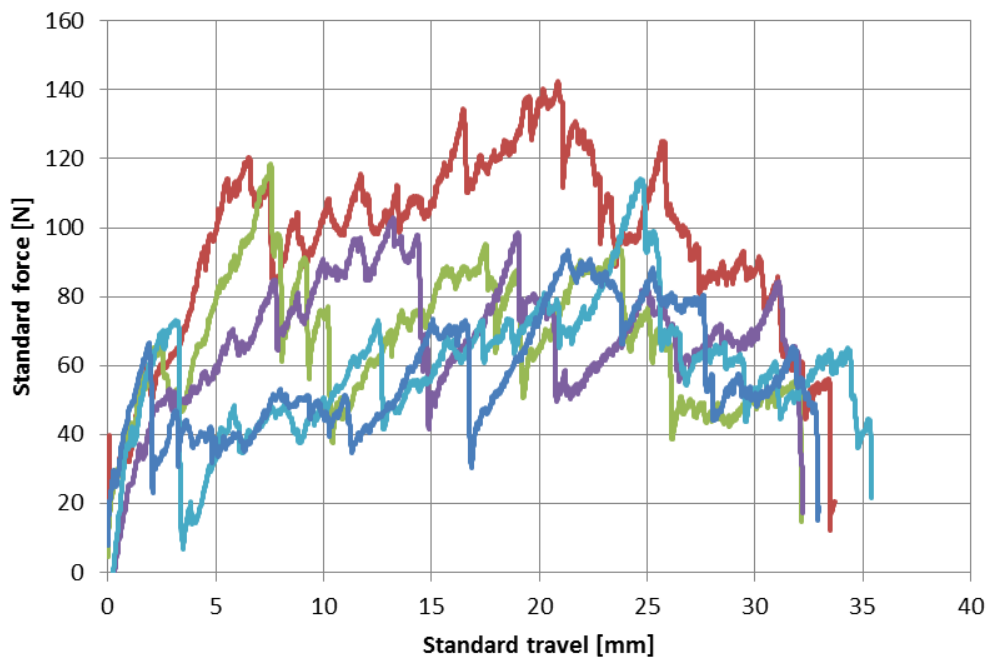


Figure D-16: Peel results from the sample with an interlayer film with 1.20 wt% POSS particles on the silane treated surface.

### Silane treated (2.44 wt% POSS)

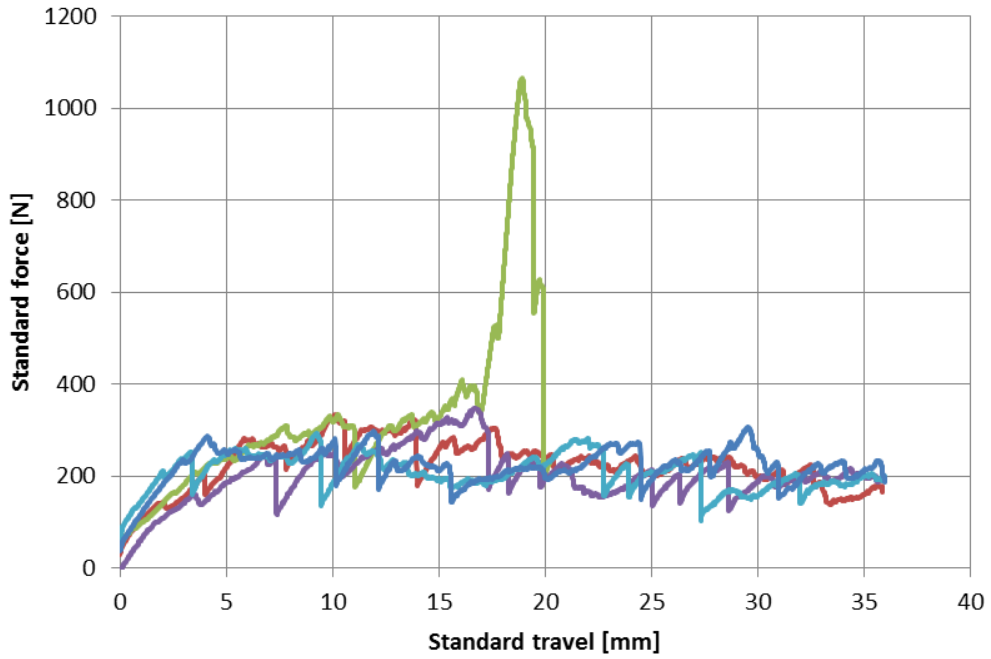


Figure D-17: Peel results from the sample with an interlayer film with 2.44 wt% POSS particles on the silane treated surface.

### Silane treated (5.21 wt% POSS)

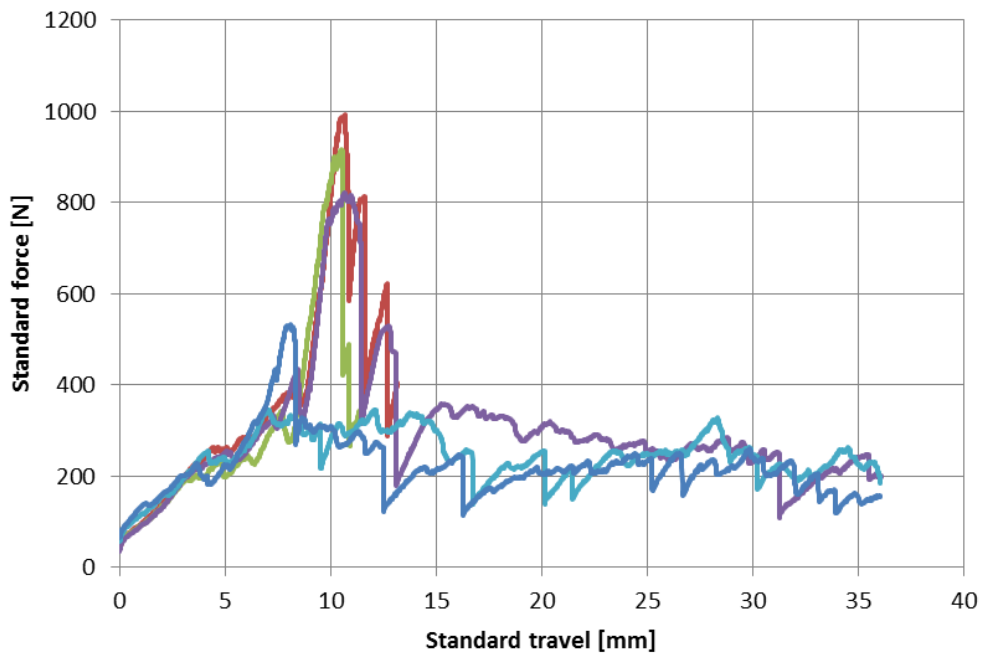


Figure D-18: Peel results from the sample with an interlayer film with 5.21 wt% POSS particles on the silane treated surface.

### Silane treated (11.49 wt% POSS)

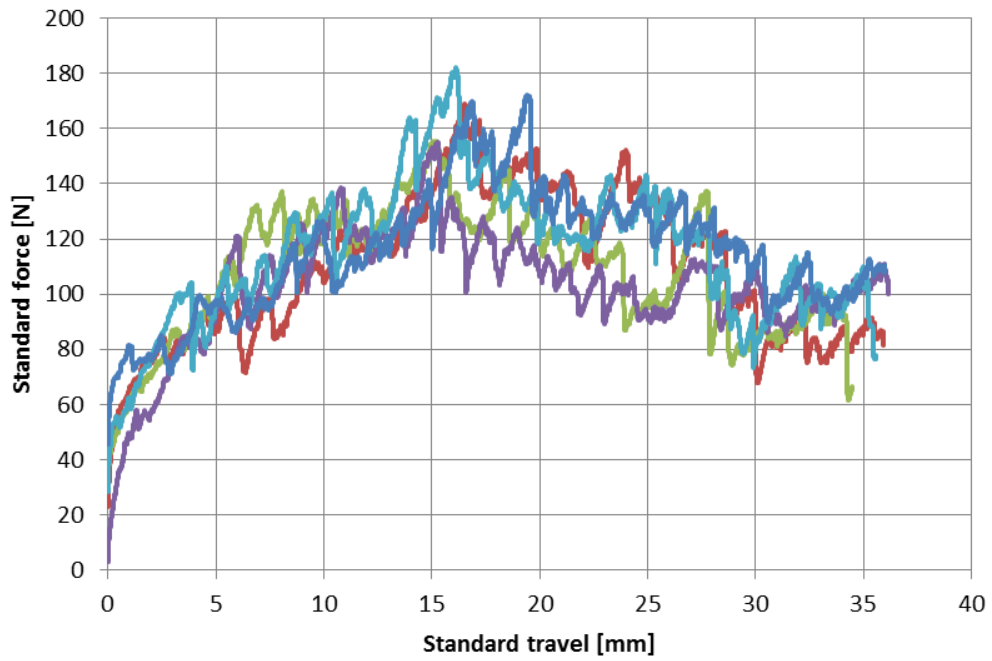


Figure D-19: Peel results from the sample with an interlayer film with 11.49 wt% POSS particles on the silane treated surface.



# Appendix E Composite data sheet

**COMFIL**<sup>®</sup> THERMOPLASTIC COMPOSITES

DATA SHEET

1/9-2010

<b>Product No:</b>	<b>30001-3</b>	<b>WG1-LPET-750</b>
--------------------	----------------	---------------------

## Woven Fabric Glass/LPET Balanced Twill 2/2

Data given is for production over longer time. Standard variation for separate lots will be with less variation.

PROPERTY	MEASURED VALUE	St. Variation	Test
Grammage g/m <sup>2</sup>	750	+/- 2%	ASTM D646
Fiber content %(weight)	57	+/- 1%	-
Fiber content % (volume)	42	+/- 1%	-
Width incl. selvage cm	130 (or tailored)	+/- 1 %	-
Thickness of consolidated fabric mm	0,4	+/- 2%	-
Density of consolidated material g/cm <sup>3</sup>	1,87	+/- 0,03	-
Cardboard tube inside diameter mm	77	+/- 1 mm	-
Length of fabric m	50	+/- 1%	-

HB

COMFIL® are registered trademarks of Comfil ApS. THIS PUBLICATION SHOULD NOT BE CONSTRUED AS ENGINEERING ADVICE. WHILE INFORMATION CONTAINED IN THIS PUBLICATION IS ACCURATE TO THE BEST OF OUR KNOWLEDGE, COMFIL DOES NOT WARRANT ITS ACCURACY OR COMPLETENESS. THE ULTIMATE CUSTOMER AND USER OF THE PRODUCTS SHOULD ASSUME SOLE RESPONSIBILITY FOR THE FINAL DETERMINATION OF THE SUITABILITY OF THE INFORMATION AND THE PRODUCTS FOR THE CONTEMPLATED AND ACTUAL USE. THE ONLY WARRANTY MADE BY COMFIL FOR ITS PRODUCTS IS SET FORTH IN OUR PRODUCT DATA SHEETS FOR THE PRODUCT, OR SUCH OTHER WRITTEN WARRANTY AS MAY BE AGREED BY COMFIL AND INDIVIDUAL CUSTOMERS. COMFIL SPECIFICALLY DISCLAIMS ALL OTHER WARRANTIES, EXPRESS OR IMPLIED, INCLUDING WITHOUT LIMITATION, WARRANTIES OF MERCHANTABILITY OR FITNESS FOR A PARTICULAR PURPOSE, OR ARISING FROM PROVISION OF SAMPLES, A COURSE OF DEALING OR USAGE OF TRADE.

*Comfil ApS*  
Karolinehundsvej 2  
DK 8883 Gjern, Danmark  
Vat no. : DK 26 20 85 80  
☎ +45 87244111 fax: +45 8724 0093  
www.comfil.biz ✉ [info@comfilbiz](mailto:info@comfilbiz)

*Danske Bank*  
Vestergade 3, DK 8600 Silkeborg  
IBAN (€) : DK1230003462858353  
IBAN (DKK) : DK5930003462855761  
SWIFT: DABADKKK



# Appendix F Silane data sheet

**SIGMA-ALDRICH**

[sigma-aldrich.com](http://sigma-aldrich.com)

## SAFETY DATA SHEET

according to Regulation (EC) No. 1907/2006  
Version 5.2 Revision Date 31.10.2013  
Print Date 28.05.2014

GENERIC EU MSDS - NO COUNTRY SPECIFIC DATA - NO OEL DATA

### SECTION 1: Identification of the substance/mixture and of the company/undertaking

#### 1.1 Product identifiers

Product name : (3-Mercaptopropyl)trimethoxysilane

Product Number : 176617  
Brand : Aldrich  
REACH No. : A registration number is not available for this substance as the substance or its uses are exempted from registration, the annual tonnage does not require a registration or the registration is envisaged for a later registration deadline.

CAS-No. : 4420-74-0

#### 1.2 Relevant identified uses of the substance or mixture and uses advised against

Identified uses : Laboratory chemicals, Manufacture of substances

#### 1.3 Details of the supplier of the safety data sheet

Company : Sigma-Aldrich Norway AS  
Filipstad Brygge 1  
N-0252 OSLO

Telephone : +47 23 176000  
Fax : +47 23 176010  
E-mail address : eurtechserv@sial.com

#### 1.4 Emergency telephone number

Emergency Phone # : Giftinformasjonssentralen 22 59 13 00

### SECTION 2: Hazards identification

#### 2.1 Classification of the substance or mixture

Classification according to Regulation (EC) No 1272/2008

Acute toxicity, Oral (Category 4), H302  
Skin sensitisation (Category 1), H317  
Chronic aquatic toxicity (Category 2), H411

For the full text of the H-Statements mentioned in this Section, see Section 16.


Classification according to EU Directives 67/548/EEC or 1999/45/EC

Xn, N Harmful, Dangerous for the environment R22, R43, R51/53

For the full text of the R-phrases mentioned in this Section, see Section 16.

#### 2.2 Label elements

Labelling according Regulation (EC) No 1272/2008

Pictogram 

Signal word : Warning

Hazard statement(s)  
H302 : Harmful if swallowed.  
H317 : May cause an allergic skin reaction.  
H411 : Toxic to aquatic life with long lasting effects.

Precautionary statement(s)  
P273 Avoid release to the environment.  
P280 Wear protective gloves.  
Supplemental Hazard Statements none

**2.3 Other hazards - none**

**SECTION 3: Composition/information on ingredients**

**3.1 Substances**

Formula : C<sub>8</sub>H<sub>16</sub>O<sub>3</sub>SSi  
Molecular Weight : 196,34 g/mol  
CAS-No. : 4420-74-0  
EC-No. : 224-588-5

**Hazardous ingredients according to Regulation (EC) No 1272/2008**

Component	Classification	Concentration
<b>3-Trimethoxysilylpropane-1-thiol</b>		
CAS-No. 4420-74-0 EC-No. 224-588-5	Acute Tox. 4; Skin Sens. 1; Aquatic Chronic 2; H302, H317, H411	<= 100 %

**Hazardous ingredients according to Directive 1999/45/EC**

Component	Classification	Concentration
<b>3-Trimethoxysilylpropane-1-thiol</b>		
CAS-No. 4420-74-0 EC-No. 224-588-5	Xn, N, R22 - R43 - R51/53	<= 100 %

For the full text of the H-Statements and R-Phrases mentioned in this Section, see Section 16

**SECTION 4: First aid measures**

**4.1 Description of first aid measures**

**General advice**

Consult a physician. Show this safety data sheet to the doctor in attendance.

**If inhaled**

If breathed in, move person into fresh air. If not breathing, give artificial respiration. Consult a physician.

**In case of skin contact**

Wash off with soap and plenty of water. Consult a physician.

**In case of eye contact**

Rinse thoroughly with plenty of water for at least 15 minutes and consult a physician.

**If swallowed**

Never give anything by mouth to an unconscious person. Rinse mouth with water. Consult a physician.

**4.2 Most important symptoms and effects, both acute and delayed**

The most important known symptoms and effects are described in the labelling (see section 2.2) and/or in section 11

**4.3 Indication of any immediate medical attention and special treatment needed**

no data available

**SECTION 5: Firefighting measures**

**5.1 Extinguishing media**

**Suitable extinguishing media**

Use water spray, alcohol-resistant foam, dry chemical or carbon dioxide.



# Appendix G Projectile data sheet

## 7.62x51 HC 9.6 g / 148 gr

Lead-free versatile round

MG round for enhanced penetration power on armoured targets

Extended shelf life due to a non-corrosive coating of the bullet

Reduced wear and strain on the barrel maintains accuracy over the weapon's life



### Application

The HC round is specifically designed to NATO standards and produces the perfect tool for Armed Forces that need excellent penetration over a longer range.

The projectile consists of a hardened steel core which makes two-thirds of the bullet weight. This design guarantees excellent penetration on hard targets. The brass-shoe provides optimal spin, minimal barrel wear and allows outstanding accuracy.

The HC round is also available linked in mixed ratios according to the customer's requirements.

### Cartridge

7.62x51 / .308 Win.

projectile	JHC, 9.6 g / 148 gr	
projectile material	hardened steel core; brass-shoe; zinc-coated	
ballistic coefficient C1	0.359 (ICAO)	
primer / propellant	SINOXID / double base powder	
case material	CuZn - alloy	
cartridge weight	24.0 g	

### Performance

term of reference	MCMOPI	
temperature range	-54°C to +52°C	
mean case mouth pressure + 3s	max. 4 450 bar	(21°C)
muzzle velocity	845 m/s (2 772 fps)	562 mm barrel
muzzle energy	3 430 J	
accuracy at 300 m	$s_x ; s_y \leq 85$ mm	

### Packaging

10 rds/cardboard box, 400 rds/M2A1

Technical specification and numerical data are given as an indication only and are not of a contractual nature

**RUAG Ammotec AG**  
Uttigenstrasse 67  
3602 Thun  
Switzerland

Tel. +41 332 282 879  
Fax +41 332 282 644  
sales.ammotec@ruag.com  
www.ruag.com/ammotec

0312

**Together  
ahead. RUAG**

XXXV



# Appendix H Investigation of small particles on the alumina surface

In some of the SEM images of the chromic-sulphuric acid treated alumina there were a lot of small particles in between the grains of the alumina as can be seen from Figure H-1. These particles might affect the adhesion to the composite, so it is important to find out where they come from.

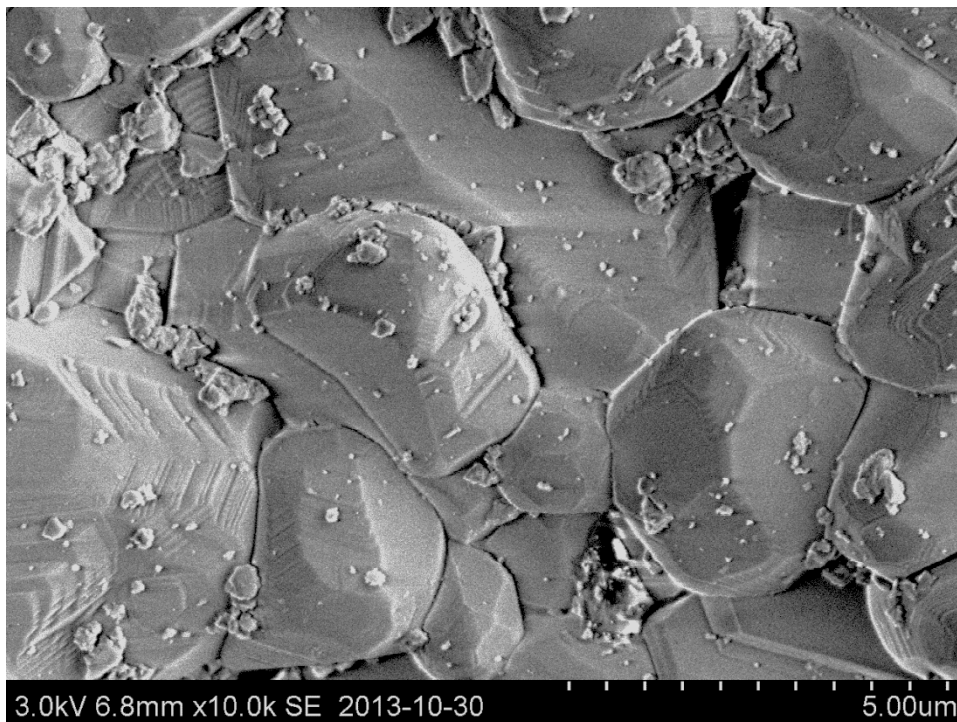


*Figure H-1: SEM-image showing the alumina surface after 10 minutes of the strongest chromic-sulphuric acid. A lot of small particles can be seen in between the grains.*

In order to find out where these particles come from, the following samples were prepared and studied with SEM:

- Sample 1: Plain alumina surface after cutting and washing in acetone
- Sample 2: Alumina surface after cutting and washing on an ultrasonic bath
- Sample 3: Alumina surface after cutting, ultrasonic bath, and strong chromic-sulphuric acid for 10 minutes
- Sample 4: Alumina surface after cutting, ultrasonic bath, and FPL-etch for 60 minutes

Sample 5: Dried sample of the cooling water used while cutting the ceramic

The reason why sample 4 was exposed to the FPL-etch for 60 minutes and sample 3 was exposed to the strong chromic sulphuric acid for 10 minutes is that these are the conditions where the highest amount of particles were observed.

The reason for including sample 5 is that when cutting the ceramic, the cooling water that was used became more and more dirty. The particles that were observed might be crushed ceramic from the cutting. If that was the case, the particles in the cooling water should match in size to the particles found on the alumina surface.

As can be seen from the SEM images in Figure H-2 to Figure H-5, the particles on the surface are there already before surface treatment. An ultrasonic bath seems to be able to clean them away easily. The particles found in the cooling water (see Figure H-6) seem to match the size of the particles found on the alumina surface. In other words, there is reason to believe that the observed particles come from the cutting of the ceramic. In order to prevent getting these particles on our samples, the samples that have been cut into smaller pieces can be washed in an ultrasonic bath. The samples that are not cut into smaller pieces should not have these particles on the surface at all.

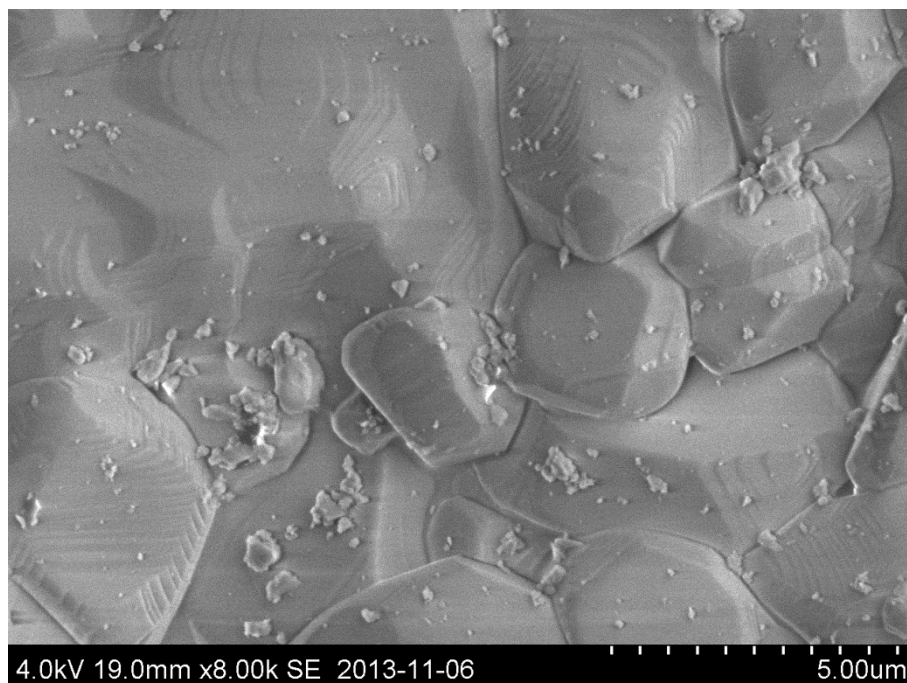


*Figure H-2: SEM-image showing the alumina surface of sample 1. The particles are clearly visible.*

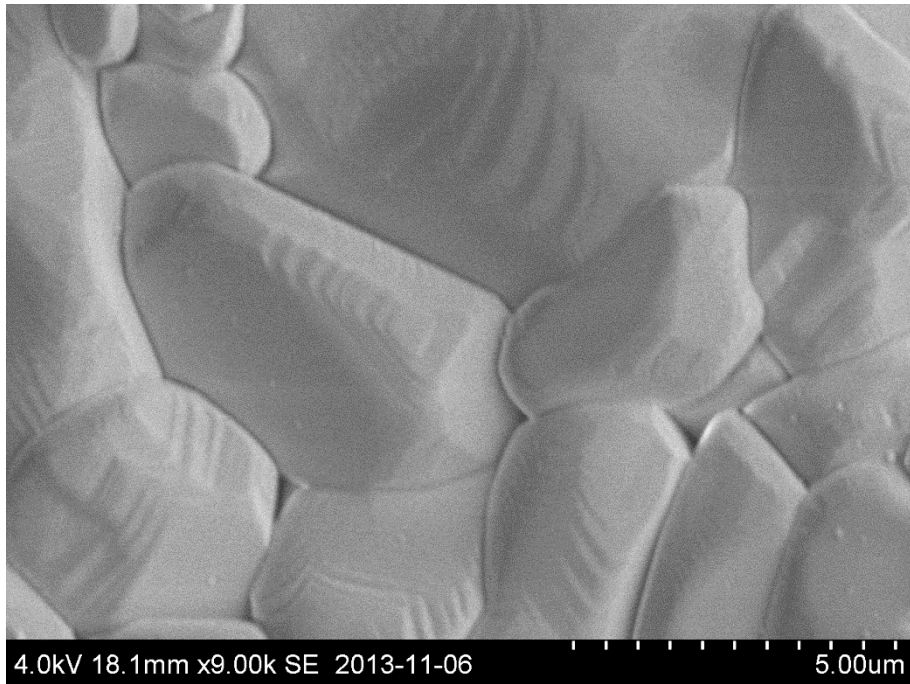


*Figure H-3: SEM-image showing the alumina surface of sample 2. Almost no particles can be seen on the surface.*

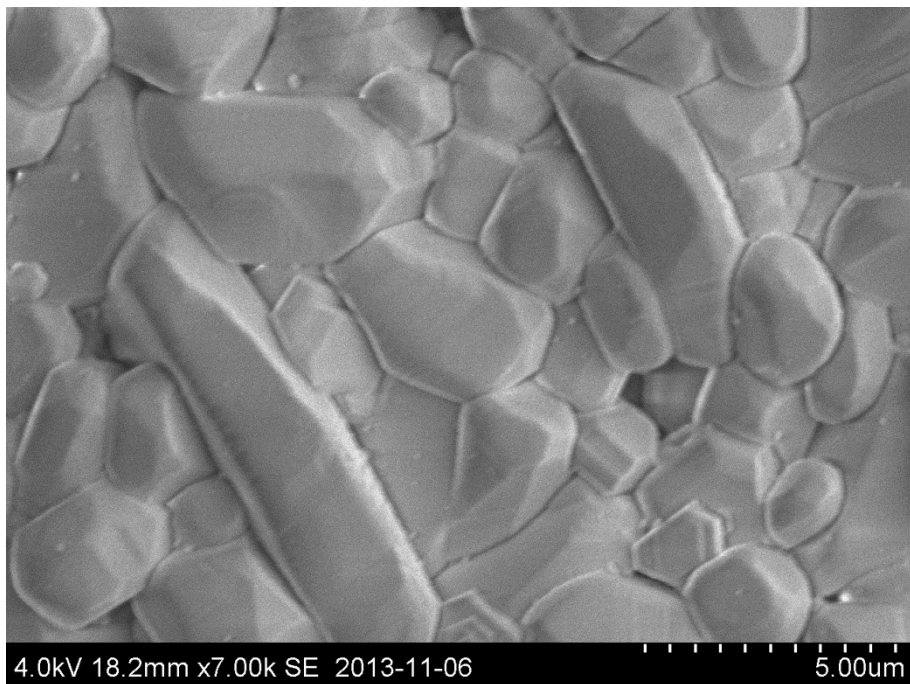


*Figure H-4: SEM-image showing the alumina surface of sample 3. Still almost no particles can be seen.*

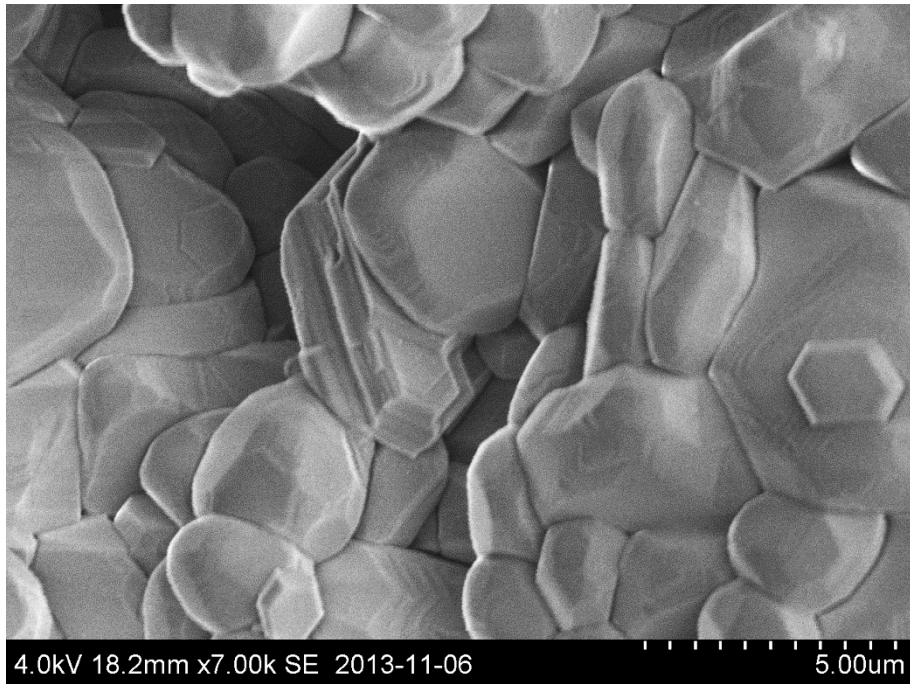


*Figure H-5: SEM-image showing the alumina surface of sample 4. Still almost no particles can be seen.*

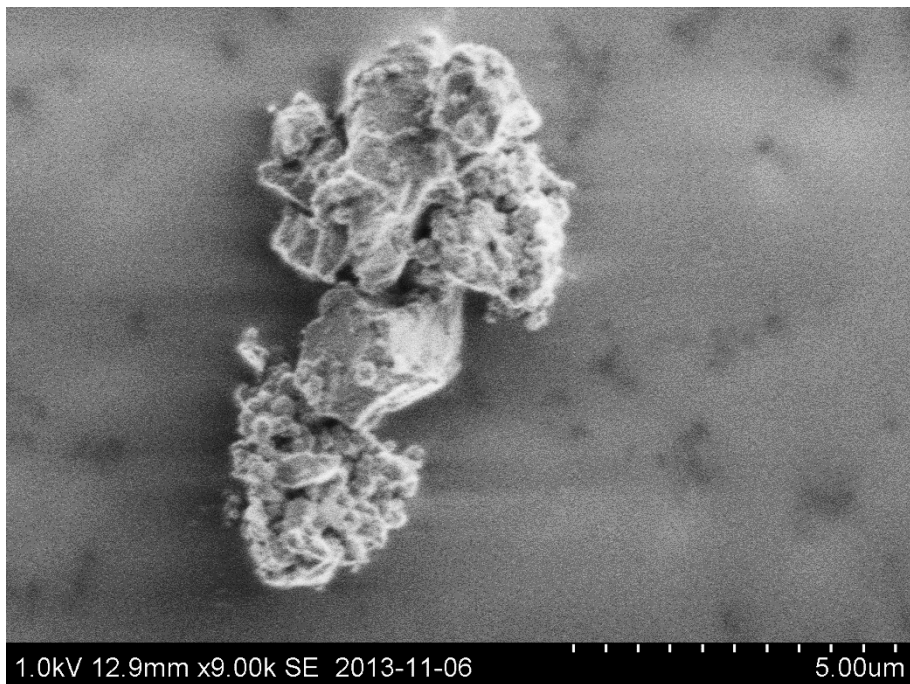


*Figure H-6: SEM-image of sample 5. Many of the particles from the cooling water are in the same size range as the particles found on the alumina surface.*